Flight and Wind-Tunnel Measurements Showing Base Drag Reduction Provided by a Trailing Disk for High Reynolds Number Turbulent Flow for Subsonic and Transonic Mach Numbers

Sheryll Goecke Powers
Dryden Flight Research Facility
Ames Research Center
Edwards, California

Jarrett K. Huffman
and Charles H. Fox, Jr.
Langley Research Center
Hampton, Virginia

SUMMARY

The effectiveness of a trailing disk, or trapped vortex concept, in reducing
the base drag of a large body of revolution, about 20-cm (8-in) diameter, was
studied from measurements made both in flight and in a wind tunnel. Pressure data
were obtained for the flight experiment, and both pressure and force-balance data
were obtained for the wind-tunnel experiment. The flight study also included data
obtained from a hemispherical base. Reynolds number, based on the length of the
body of revolution, ranged from 1.5×10^7 to 2.7×10^7 for the flight data and
from 1.9×10^7 to 4.1×10^7 for the wind-tunnel data. Primary Mach numbers for
the flight data were from 0.70 to 0.93 with a limited amount of data obtained
for Mach 1.20 to 1.60. Mach numbers for the wind-tunnel study ranged from 0.30
to 0.82.

The present experiment demonstrated the significant base drag reduction capa-
bility of the trailing disk to Mach 0.93 and to Reynolds numbers (based on body
length) up to 80 times greater than for the earlier pioneering studies performed
at incompressible speeds. For the trailing disk data from the flight experiment,
the maximum decrease in base drag ranged from 0.08 to 0.07 as Mach number increased
from 0.70 to 0.93. Aircraft angles of attack ranged from 3.9° to 6.6° for the
flight data. For the trailing disk data from the wind-tunnel experiment, the
maximum decrease in base drag and total drag ranged from 0.08 to 0.05 for the
approximately 0° angle-of-attack data as Mach number increased from 0.30 to 0.82.
For the approximately 3° angle-of-attack data, the maximum decrease was 0.07 to
0.06 for the base drag and remained a constant 0.07 for the total drag as Mach
number increased from 0.30 to 0.71. For the flight data, the trailing disk caused
a drag penalty near Mach 1.20, but this penalty decreased rapidly as Mach number
increased to 1.40 and appeared to be eliminated as Mach number increased from 1.40
to 1.60. The hemispherical base had an almost constant drag increase of approxi-
mately 0.01 for data from Mach 0.70 to 0.93 and 1.24.

INTRODUCTION

It has been recognized for many years that the periodic shedding of vortices can
add significantly to the drag of a bluff body. For a shape having a streamlined
forebody, vortex shedding from the blunt base can be the dominant drag component.
Streamlined, axisymmetric shapes are commonly found on aircraft — sometimes as
integral components (such as fin caps, midwing tanks, or wingtip tanks) and some-
times as removable components (such as missiles, external fuel tanks, or other
external stores). Because these shapes commonly occur, it is sometimes desirable
to find ways to reduce the base drag of these bodies without adding the weight
and airloads associated with a conventional boattail afterbody closure.

Two-dimensional studies have shown that interfering with the vortex formation
in the wake can reduce the base drag component caused by vortex shedding (ref. 1).
For example, the incompressible, low Reynolds number, wind-tunnel studies by Roshko
(ref. 2) and Bearman (ref. 3) showed that the effects of vortex formation and hence
the base drag of a two-dimensional configuration could be reduced by placing a
splitter plate in the wake. (A splitter plate is a flat plate placed normal to
the base surface to form a reattachment surface for the impinging separated flow.)

Both the eddy shedding frequency and the location of the vortices were affected by the splitter plate. A quasi-two-dimensional flight study (ref. 4) successfully demonstrated the effectiveness of the splitter plate, or vortex control concept, for Reynolds numbers Re near 10^7 and Mach numbers to 0.90.

Utilization of vortex control with three-dimensional shapes was discussed by Ringleb (ref. 5) and investigated by Migay (ref. 6) in the early 1960's. Incompressible (approximately Mach 0.10), turbulent flow wind-tunnel studies by Mair (ref. 7) and Goodyer (ref. 8) showed that for a blunt base body of revolution (BOR), a rear-mounted disk (the disk mounted parallel to and slightly aft of the base plane) could establish a trapped toroidal vortex. The trapped vortex caused by the trailing disk favorably affected the flow closure pattern around the base region. In effect, the rear-mounted disk caused the flow to behave as though the base region ended in a beneficial boattail closure. Thus, the use of a rear-mounted disk resulted in a substantial reduction in base drag. A more recent wind-tunnel study by Little and Whipkey (ref. 9) for flow conditions similar to those of Mair and Goodyer provides more details about the flow characteristics of rear-mounted disks.

The BOR shape (fin cap) at the top of the F-111 vertical fin provided an opportunity to evaluate the effect of a rear-mounted disk, hereafter referred to as a trailing disk, on the base drag of a larger body. The base diameter of the body was approximately 20 cm (8 in), and Mach numbers and Reynolds numbers are greater than in previous studies of references 7 to 9. Surface pressure data were obtained for a hemispherical base, a blunt base, and a trailing disk configuration for Mach 0.70 to 0.93 and for Reynolds numbers (based on BOR length) of 1.5×10^7 to 2.7×10^7. A limited amount of data was also obtained for Mach 1.20 to 1.60. The trailing disk was tested for two separation distances behind the BOR base.

After the flight tests, full-scale models of the BOR and the trailing disk were built and tested in the NASA Langley High-Speed 7- by 10-Foot Tunnel. (A description of the tunnel is given in ref. 10.) Force-balance and surface pressure measurements were obtained for the BOR with (1) a blunt base, (2) the trailing disk used in the flight study, and (3) the trailing disk built for the wind-tunnel study for Mach 0.30 to 0.82 and for Reynolds numbers (based on BOR length) of 1.9×10^7 to 4.1×10^7. The longer stem, or attachment rod, of the wind-tunnel trailing disk allowed a greater range of separation distances to be studied.

This document presents the results of the flight study, the results of the wind-tunnel study, and a comparison of the data from these studies and the previous wind-tunnel studies. The blunt base configuration for all data is used for the reference (or baseline) condition. The flight study was conducted at the Dryden Flight Research Facility of NASA Ames Research Center (Ames-Dryden); the wind-tunnel study was conducted at Langley Research Center.

NOMENCLATURE

Physical quantities in this document are given in the International System of Units (SI) and parenthetically in U.S. Customary Units. The measurements were taken in Customary Units.

BOR	body of revolution
b	C_p-axis intercept
C_A	axial force coefficient, axial force/qS_b
C_D	drag coefficient
C_{D_b}	base drag coefficient
C_F	turbulent skin friction drag coefficient
C_L	lift coefficient, lift/qS_b
C_M	pitching moment coefficient, pitching moment/$qS_b D$
C_p	pressure coefficient, $(p - p_{ref})/ 0.7M^2 p_{ref}$
$C_p(R)$	linear pressure coefficient function, $mR + b$
D	maximum body diameter (equal to diameter of base for bodies in this study), cm (in)
D_b	base drag, N (lb)
D_s	drag for a given surface, N (lb)
F1101 to F1112	test points for blunt base configuration, flight data, flight 1
F1201 to F1212	test points for hemispherical base configuration, flight data, flight 1
F1301 to F1312	test points for trailing disk configuration, flight data, FLTD, x/D = 0.44, flight 1
F1401 to F1411	test points for trailing disk configuration, flight data, FLTD, x/D = 0.50, flight 1
F2101 to F2114	test points for blunt base configuration, flight data, flight 2
F2201 to F2212	test points for hemispherical base configuration, flight data, flight 2
F2301 to F2310	test points for trailing disk configuration, flight data, FLTD, x/D = 0.44, flight 2
F2401 to F2411	test points for trailing disk configuration, flight data, FLTD, x/D = 0.50, flight 2

3

FC1 to FC19	pressure orifice locations for flight data
FLTD	flight trailing disk
h	geopotential altitude, m (ft)
L	length of BOR, cm (in)
M	local, or reference, Mach number
M_∞	free-stream Mach number
m	slope, cm^{-1} (in^{-1})
p	pressure at a given orifice location, kPa (lb/ft^2)
p_{ref}	local static pressure, kPa (lb/ft^2)
p_∞	free-stream pressure, kPa (lb/ft^2)
q	local dynamic pressure, $0.7M^2p_{ref}$, kPa (lb/ft^2)
R	radius, cm (in)
RB	radius of base, cm (in)
Re	Reynolds number, based on body length
r_{max}	radius to edge of BOR base or to edge of trailing disk, cm (in)
r_{min}	minimum radius value, cm (in); 0 cm (0 in) if stem is not present; 1.3 cm (0.50 in) if stem is present
S	surface (or arc) distance on hemispherical base originating at center of hemisphere, cm (in)
S_b	base area, cm^2 (in^2)
SA	surface distance from center to edge for hemispherical base, 12.0 cm (4.72 in)
TP	test point
W011 to W014	test points for blunt base configuration, $\alpha \approx 0°$, wind-tunnel data
W021 to W024	test points for trailing disk configuration, WTD, x/D = 0.20, $\alpha \approx 0°$, wind-tunnel data

4

W031 to W034	test points for trailing disk configuration, WTD, $x/D = 0.40$, $\alpha \approx 0°$, wind-tunnel data
W041 to W044	test points for trailing disk configuration, WTD, $x/D = 0.45$, $\alpha \approx 0°$, wind-tunnel data
W051 to W054	test points for trailing disk configuration, WTD, $x/D = 0.50$, $\alpha \approx 0°$, wind-tunnel data
W061 to W064	test points for trailing disk configuration, WTD, $x/D = 0.55$, $\alpha \approx 0°$, wind-tunnel data
W071 to W074	test points for trailing disk configuration, WTD, $x/D = 0.60$, $\alpha \approx 0°$, wind-tunnel data
W081 to W084	test points for trailing disk configuration, FLTD, $x/D = 0.44$, $\alpha \approx 0°$, wind-tunnel data
W091 to W094	test points for trailing disk configuration, FLTD, $x/D = 0.50$, $\alpha \approx 0°$, wind-tunnel data
W311 to W313	test points for blunt base configuration, $\alpha \approx 3°$, wind-tunnel data
W341 to W343	test points for trailing disk configuration, WTD, $x/D = 0.45$, $\alpha \approx 3°$, wind-tunnel data
W351 to W353	test points for trailing disk configuration, WTD, $x/D = 0.50$, $\alpha \approx 3°$, wind-tunnel data
W361 to W363	test points for trailing disk configuration, WTD, $x/D = 0.55$, $\alpha \approx 3°$, wind-tunnel data
W381 to W383	test points for trailing disk configuration, FLTD, $x/D = 0.44$, $\alpha \approx 3°$, wind-tunnel data
W391 to W393	test points for trailing disk configuration, FLTD, $x/D = 0.50$, $\alpha \approx 3°$, wind-tunnel data
WC1 to WC139	pressure orifice locations for wind-tunnel data
WTD	wind-tunnel trailing disk
X	distance from nose of BOR, cm (in)
x	distance between base of BOR and upstream surface of trailing disk, cm (in)
α	angle of attack, deg
β	angle of sideslip, deg

ΔC_D difference between C_D of trailing disk configuration and C_D of blunt base configuration

ΔC_{D_b} difference between C_{D_b} of trailing disk or hemispherical configuration and C_{D_b} of blunt base configuration

θ angular orientation with respect to top dead center, deg; 0° at top, increasing in clockwise direction when body is viewed from the rear

DESCRIPTION OF EXPERIMENT

Flight

The BOR (fin cap) at the top of the upper vertical fin of the F-111 aircraft was the location chosen for the experiment. The in-flight photograph (fig. 1) of the BOR shows the location of the trailing disk configuration. The BOR with the hemispherical base and a portion of the vertical tail are shown in figure 2. The precipitation static discharge probes and the navigation light along the trailing edge of the tail were present, as shown in figure 2, for all flights in this study. The vertical tail was designed to have a knife-like edge for the trailing edge; in actuality, the trailing edge thickness approached that of the skin surface material. The 220.0-cm- (86.6-in-) long BOR has an ogive nose followed by a constant-diameter cylindrical centerbody and afterbody of 20.2 cm (7.96 in). The fineness ratio is 10.9. Nominal coordinates for the BOR and vertical tail characteristics are given in table 1. The pitot probe seen in the lower photo in figure 2 was used in determining local, or reference, Mach number (M). The probe opening, which was chamfered internally to a 30.0° included angle, was 71.1 cm (28 in) ahead of the body base, approximately 90.0° left of top dead center, and six support probe diameters ahead of the probe support. The probe centerline was 5.3 cm (2.09 in) from the surface, well beyond the boundary layer. The outside diameter of the probe was 0.5 cm (0.19 in).

The three base shapes investigated — the blunt base, the hemispherical base, and the trailing disk — are shown in figure 3. The blunt base in figure 3(a), as indicated by the name, provided an abrupt right-angle change in the surface contour. The hemispherical base in figure 3(b) was not a full hemisphere, because the subtended angle where the base shape fit into the BOR base was only 121.8°. The chord for the base of this shape was 19.7 cm (7.76 in). However, this base shape, which is the standard base configuration for the fin cap, will be referred to as the hemispherical base. The trailing disk in figure 3(c) was connected from the center of the upstream disk surface to the center of the BOR base by a 2.5-cm- (1-in-) diameter stem. The length of the exposed stem, or the separation distance x between the body base and the upstream disk surface (fig. 4), could be adjusted. The disk was 2.5 cm (1 in) thick and had a diameter of 16.3 cm (6.40 in). The rounded edges of the disk had a nominal 1.3-cm (0.50-in) radius. All joints and openings on the body surface and in the base region were carefully sealed for each of the configurations to insure that base bleed did not exist.

Pressures were measured both on the BOR surface and on the base surface for the blunt base and hemispherical base configurations. The orifices on the body surface were located along two rows (fig. 4). The top row, as viewed from the rear, was 16.9° right of top dead center; the side row, also on the right side, was 90.0° from the top row. The top row of orifices was displaced from top dead center because a ridge extends from near the nose tip to the BOR base. The orifices on the base surfaces were aligned with these two rows.

A surface pressure at the orifice located 71.1 cm (28 in) forward of the base in the top row was measured for all configurations and was used as the local upstream reference pressure. The trailing disk configuration, which had only the local upstream reference pressure orifice on the BOR, had orifices on the BOR base, on the upstream surface of the disk, and on the downstream surface of the disk. The orifice locations for the body surface and each of the base configurations are given in table 2. All orifices were normal to the surface. The edges of the orifices were sharp (that is, free of observable radius) and free of burrs.

A 48-port pressure-scanning valve with a differential pressure transducer referenced to a plenum pressure was used to measure the body and base surface pressures. The transducer for the pressure-scanning valve was referenced to itself and thus measured an in-flight zero, or tare, with each complete cycle. The local upstream reference pressure and a pressure on the base were measured by individual differential pressure transducers, referenced to the plenum pressure, to provide checks for the pressure-scanning valve transducer. The pitot probe pressure was measured by an individual differential pressure transducer referenced to the plenum pressure. Because the pitot probe pressure was much greater than the surface pressures, the pitot probe was not included in the pressure-scanning valve pressure measurements. The plenum pressure source was a static orifice located on the wing upper surface near the fuselage, ahead of the test BOR. The plenum pressure was measured by a high-resolution, absolute pressure transducer, which was kept in a carefully controlled temperature environment. Air data quantities, such as free-stream impact and static pressures, were obtained from sensors on the aircraft nose boom.

Chromel-Alumel (Hoskins Manufacturing Company) thermocouples were used to monitor the temperature environment of the absolute transducer and the temperature environment in the BOR near the pressure-scanning valve transducer. This verified that these transducers remained within acceptable temperature limits during flight.

All data obtained for the flight study were recorded on magnetic tape using a pulse-code modulation system. All records were synchronized by a time-code generator.

Wind-Tunnel Model

A full-scale model of the BOR was constructed from an aircraft loft drawing of the F-111 fin cap; thus, differences between the flight and wind-tunnel BOR shapes are minimal. The diameter of the constant-diameter cylindrical centerbody and afterbody was 20.3 cm (8 in). Figure 5(a) is a photograph of the BOR mounted in the wind tunnel with the wind-tunnel trailing disk (WTD) attached. Figures 5(b) to 5(d) show the rear of the body during the flow visualization (kerosene smoke) tests. No pitot probe was mounted on the wind-tunnel BOR. The nominal coordinates for the

BOR and the characteristics of the mounting strut are given in table 1. All joints and openings on the body surface and in the base region were carefully sealed to insure that base bleed did not exist.

The only significant difference between the BOR configuration that was tested in flight and the one that was tested in the wind-tunnel was the method of mounting. The mounting structure for the flight tests was the vertical tail of the aircraft. The mounting surface extended from the nose to the BOR base (figs. 1 and 2); the BOR was the fin cap for the vertical tail. The mounting structure for the wind-tunnel model was a strut, as shown in figure 5(a), with a 17.8-cm (7-in) chord at the body. The trailing edge of the strut was 82.8 cm (32.6 in) ahead of the body base.

The base shapes investigated in the wind-tunnel study were the blunt base, the flight trailing disk (FLTD), and the WTD. The WTD was constructed to the dimensions of the FLTD but had a longer stem. The longer stem enabled a wider range of separation distances to be studied. There were three major differences between the FLTD and the WTD. First, the FLTD was constructed from sheet metal (and therefore was hollow), while the WTD was machined from a solid piece of metal. Second, the FLTD had a smoother transition from the flat portion of the disk to the curved edge than did the WTD. Third, the orifices for the FLTD were closer to the edge than for the WTD. There was also an orifice on the edge of the FLTD that the WTD did not have.

Force data were obtained from an electrical strain gage. Pressure-scanning valves with differential pressure transducers were used for the pressure measurements. The angle of attack α was determined from an accelerometer mounted in the model.

Pressures were measured on the BOR surface and on each of the bases. The BOR and the base shapes built for the wind-tunnel study had both more rows of orifices and more orifices in each row than the corresponding shapes of the flight study. The blunt base and each surface of the wind-tunnel trailing disk configuration had a radial array of orifices at four different angular locations. The angular locations were 90.0° apart, with the top orifice row having the same orientation with respect to top dead center (16.9° to the right of top dead center, as viewed from the rear) as the FLTD (fig. 4). The orifice locations for the BOR surface and for the wind-tunnel base shapes are presented in table 2.

The surface pressures were measured using pressure-scanning valves with differential pressure transducers referenced to the tunnel free-stream static pressure. The pressure-scanning valves and their transducers were mounted in the BOR.

TEST PROCEDURES

Flight

Four base configurations were tested in the flight study: the blunt base; the hemispherical base, which is the standard base configuration for the fin cap for this F-111 aircraft; and the flight trailing disk configurations, at x/D values of 0.44 and 0.50 (designated the x/D = 0.44 and x/D = 0.50 configurations, respectively). The x/D values (the separation distance divided by the diameter at the

BOR base) were chosen on the basis of previous wind-tunnel data (refs. 7 and 8). The effectiveness of the trailing disk in reducing the base drag was the criterion used in selecting the x/D values.

Data were obtained for a 60-sec period for each test point, beginning after the aircraft had been established at steady-state flight conditions (that is, flight conditions for which the altitude and airspeed were essentially constant). A 15-sec time period was chosen from the steadiest portion of each 60-sec period, and several samples were averaged. The averaged data from that period were then analyzed.

The same nominal Mach numbers of 0.70, 0.80, 0.90, and 0.93 and their respective dynamic pressures were obtained for each configuration. Data were obtained at additional Mach numbers within this nominal Mach number range for the hemispherical base configuration. Some data for each of the configurations were obtained at supersonic Mach numbers. Such data were not always obtained for a given configuration, because the range of the differential pressure transducer was optimized for data for Mach numbers less than Mach 1 and because obtaining these data was a higher priority. If any pressures on a base surface were outside the range of the transducers for any supersonic test point, the base data were not included in this study.

Aircraft, or free-stream, angle-of-attack values ranged from $\alpha = 3.9°$ to $6.6°$. Aircraft, or free-stream, sideslip angles β, except for a few that were near $-1.0°$, were $\pm 0.5°$. The rudder (fig. 2) was in the zero, or null, position for all periods of data collection. It was assumed that turbulent flow began at the nose of the BOR. The body was long enough so that incidental changes in transition location did not affect the data. Turbulent flow Reynolds number based on the body length ranged from 1.5×10^7 to 2.7×10^7. Pressure coefficients and related flight conditions are given in table 3.

Wind-Tunnel Model

Nine base configurations were tested in the wind-tunnel study. These consisted of the blunt base; the WTD configuration at x/D values of 0.20, 0.40, 0.45, 0.50, 0.55, and 0.60; and the FLTD configuration at x/D values of 0.44 and 0.50. For brevity, a trailing disk configuration is sometimes referred to by its x/D value, for example, the x/D = 0.20 configuration.

Nominal Mach numbers of 0.30, 0.50, 0.71, and 0.82 and their respective dynamic pressures were repeated for each configuration for a local $\alpha \approx 0°$. The WTD at x/D values of 0.45, 0.50, and 0.55 and the FLTD at x/D values of 0.44 and 0.50 were also tested for a local $\alpha \approx 3°$ for all but the highest Mach number. No data were obtained at Mach 0.82 for the higher angle-of-attack data, because the forces would have exceeded the range of the force balance system. All data were obtained for a local sideslip angle of $0°$.

A boundary-layer transition strip, 0.08 cm (0.03 in) wide and composed of a band of 150-grit Carborundum grains set in a plastic adhesive, was located 3.6 cm (1.40 in) aft of the nose tip. (Boundary-layer transition strip requirements are discussed in ref. 11.) Thus, turbulent flow was assumed to begin at the nose of the body. Turbulent flow Reynolds number based on body length ranged from 1.9×10^7

9

at Mach 0.30 to 4.1 × 10⁷ at Mach 0.82. Pressure coefficients and related wind-tunnel conditions are given in table 4.

Jet boundary and blockage corrections were applied to the force data based on references 12 and 13, respectively. The balance chamber pressure was measured, and the balance readings were adjusted to a condition of free-stream static pressure acting over the cutout of the strut.

DRAG COEFFICIENT ANALYSIS

An average base drag coefficient C_{D_b} was obtained for each base configuration of the flight and wind-tunnel tests by assuming that the pressure coefficient varied linearly between each pair of adjacent orifices. The drag for the blunt base and each surface of the trailing disk configuration was determined from

$$D_s = 2\pi q \int_{r_{min}}^{r_{max}} R C_p(R) \, dR \qquad (1)$$

where D_s is the drag for a given surface; q is the local dynamic pressure; R is the radius; $C_p(R) = mR + b$, m is a slope, and b is the C_p-axis intercept; r_{max} is the radius to the edge of the BOR base or to the edge of the trailing disk; and r_{min} is zero if the stem is not present and 1.27 cm (0.50 in) if the stem is present.

The disk surfaces were assumed to be normal to the free-stream flow from the center to the disk edge. This equation gave the base drag directly for the blunt base. However, for the trailing disk configuration, this equation gave the drag for each of the base surfaces. Thus, the base drag for the trailing disk configuration required the algebraic summation of the individual drags and was obtained by subtracting the upstream surface drag from the sum of the body base and the downstream surface drags. The base drag coefficient was then calculated using the following equation:

$$C_{D_b} = D_b/(qS_b) \qquad (2)$$

where D_b is the base drag and S_b is the base area. The drag equation used for the hemispherical base accounted for the surface curvature. Consequently, the base area used to calculate the base drag coefficient also accounted for the surface curvature.

Only the FLTD configuration had a measured pressure coefficient value at the edge. Edge conditions for all the other base configurations were assumed as follows. For the WTD configuration, the edge conditions chosen were dependent on the x/D value. A study of the data near and on the edge of the flight disk indicated that an assigned pressure coefficient value of zero would be a reasonable edge value for both surfaces of the WTD configurations with x/D values from 0.40 to 0.60. The average of the surface pressure coefficients closest to the edge on the upstream surface and closest to the edge on the downstream surface was used as the edge condition for the x/D = 0.20 disk configuration. The pressure coefficient closest to

the edge was assumed to be the edge pressure coefficient value for (1) the hemispherical base configuration, (2) for both flight and wind-tunnel blunt base configurations, and (3) for the body base for both FLTD and WTD configurations.

A local upstream Mach number, obtained from the pitot probe pressure and the local upstream reference pressure, was used for the flight data calculations. For Mach < 1, both the local upstream Mach number and local upstream reference pressure were close to the calibrated free-stream values of aircraft Mach number and static pressure. These parameters are included in table 3.

The effectiveness of the trailing disk configuration was evaluated in terms of drag increment from the blunt base configuration. The standard deviation for the base drag increments was estimated to be ±0.006 for both the flight and wind-tunnel measurements. The standard deviation for the total drag increment was estimated to be smaller than that for the base drag increment. Considerations used in obtaining this value for the standard deviation were the repeatability of the data and the fact that the pressure-scanning valves provide a zero with each revolution.

RESULTS AND DISCUSSION

Pressure data were obtained in the base region and on the body surface for both the flight and the wind-tunnel studies. Force-balance data were also obtained for the wind-tunnel study. The pressure data for the base region and the force-balance data are presented in the following discussion.

The flight body surface data were obtained during flights with the blunt base and the hemispherical base. The wind-tunnel body surface pressures were obtained for all configurations. The pressure orifice locations for both sets of data are given in table 2. Examples of the pressure coefficients obtained for the body surface for both flight and wind-tunnel data are presented in the appendix. The pressure coefficients for the wind-tunnel data show that the pressures immediately forward of the base are dependent on the x/D configuration.

Flight Data

Base surfaces. — The pressure coefficient on the different base surfaces is shown as a function of the ratio of radial position to the base radius, R/RB (figs. 6 to 9 and table 3). The center pressure, where R/RB = 0 (for example, see fig. 6), was arbitrarily plotted with the symbol for the 16.9° row; the edge pressure for the trailing disk (figs. 8 and 9) was arbitrarily plotted with the symbol for the downstream surface. The pressure coefficients on the base surfaces were, not unexpectedly, affected by the base configuration, Mach number, radial position, and angular location. The aircraft angle-of-attack range for this study was small, and no angle-of-attack effect could be defined.

The effect of base configuration was defined by two general pressure distributions, one for the blunt and hemispherical base configurations and the other for the trailing disk configurations. For the blunt and hemispherical bases (figs. 6 and 7), the pressure coefficients along the 106.9° location had an almost constant negative value as radial distance increased from the center. The pressure coefficients for the 16.9° location became less negative as the radial distance increased

11

from the center. The pressure coefficients along the radials at 16.9° and 106.9° were in closer agreement for Mach > 1 and had almost constant negative values.

The two trailing disk configurations (figs. 8 and 9) had similar pressure coefficient distributions. The pressure coefficients for the downstream surface of the disk for Mach numbers less than Mach 1, indicated in figures 8(a) to 8(d) and 9(a) to 9(d), were positive and almost constant with respect to radial distance. For the upstream disk surface and for the BOR base (the two surfaces forming the cavity), the pressure coefficients were negative and similarly nonlinear with respect to radial distance. The least negative value was in the region near the supporting stem (R/RB ≈ 0.20). The pressure coefficients reached a most negative value near an R/RB ≈ 0.70. The pressure coefficients became less negative as the edges of the disk or the body base were approached, as indicated in figures 8(a) to 8(d) and 9(a) to 9(d). As the edge of the disk was neared, the gradient for the upstream pressure coefficient became steep and the value of the coefficient rapidly approached the value of the downstream pressure coefficients.

A slowly recirculating flow pattern was expected for a blunt base region, but as shown for the blunt base configuration of this study and the downstream surface of the disk, the pressure coefficient gradient across the surface was usually linear and almost constant. This was not necessarily true for the cavity formed by the trailing disk configurations. Instead, the pressure coefficient distributions over the two surfaces forming the cavity appeared to depend on a toroidal vortex that was trapped within the cavity. (Such a trapped vortex flow is discussed in references 7 and 8 and is shown in photographs in reference 9.)

At the conclusion of the wind-tunnel force-balance tests of the present study, sufficient scheduled tunnel time remained so that a limited number of flow visualization studies could be performed. Smoke was generated by a handheld kerosene smoke wand, at very low wind-tunnel speeds, for both the FLTD and WTD configurations. The vortex images were visibly discernible. However, these images were difficult to photograph, and no time was available to obtain quality photographs of the flow for the different separation distances.

Examples of the observed toroidal vortices and the flow field are shown in figures 5(b) to 5(d). In figure 5(b), the toroidal vortices are clearly visible. The relative density of the vortices (the top vortex appears more dense than the bottom vortex) was caused by the position of the smoke wand and the position of the lighting. In figure 5(c), the outer stream lines can be observed, and the flow behind the disk appears to be forming a boattail. The top and bottom vortices did not photograph as clearly as in figure 5(b). The boattail shape was more apparent when photographed from a greater distance as in figure 5(d); however, only the top vortex can be seen in this photograph. The separation distance, or cavity size, appeared to affect both the strength and the core location of the vortex.

The pressure distributions in the cavity region remained nonlinear as speeds increased above Mach 1, as indicated in figures 8(e) to 8(g) and 9(e) to 9(f). However, unlike the pressure coefficients at the lower speeds, those on the BOR base were not appreciably less negative as the edge was approached. The pressure coefficients for the downstream disk surface were positive or nearly zero for the data near Mach 1.20, as shown in figures 8(e) and 9(e). However, they approached negative levels of the cavity region as Mach number increased to almost 1.60, as shown in figures 8(f), 8(g), and 9(f). Thus, it was not readily apparent from the

pressure distribution that the trailing disk would provide any base drag reduction for Mach > 1.

The general agreement between the pressure coefficients on the surfaces forming the cavity meant that the net drag resulting from the upstream disk surface and the corresponding area on the BOR base was close to zero. Therefore, the base drag due to the trailing disk configuration was mainly dependent on the pressure coefficients on the downstream disk surface and on the pressure coefficients on the remaining surface area (the annular area beyond or outside the shadow of the disk) of the BOR base. Thus, when the pressure coefficients on the downstream surface were positive by about the same amount as the pressure coefficients near the edge of the body base were negative, the trailing disk configuration probably had a lower net base drag than the blunt base configuration. However, if the pressure coefficients on the downstream surface were close to zero or negative, the relationship between the base drag for the trailing disk and for the blunt base was not readily apparent. Because the pressure distributions over the cavity surfaces tended to cancel each other, the positive pressure coefficients on the downstream disk for the subsonic Mach number data provided a relative thrust effect, as indicated in figures 8(a) to 8(d) and 9(a) to 9(d).

Base drag coefficients. — The base drag coefficient as a function of Mach number for each of the configurations is shown in figures 10 to 12. The data for the blunt base configuration (fig. 10) are considered to be the baseline from which the incremental drag changes, caused by the trailing disk or hemispherical base, will be derived. For subsonic Mach numbers, the blunt base drag coefficient decreased slightly as Mach number increased. Typical supersonic base drag coefficients were not evident until about Mach 1.40. The base drag data were obtained from two flights at two nominal dynamic pressures of 14.4 and 23.9 kPa (300 and 500 lb/ft^2) and for a significant range of Reynolds numbers (1.5×10^7 to 2.7×10^7). Although limited for Mach > 1, the data provided results that were repeatable and consistent.

The magnitude of the subsonic base drag coefficients for the blunt base (fig. 10) was lower than those usually obtained for nonboattailed BORs. These relatively low values for the subsonic base drag coefficient (and the low values near Mach 1.20) were believed to be caused by the recompression region on the aft portions of the vertical tail that was the support structure for the BOR. This supposition was borne out by a theoretical wing-body analysis based on a version of the Woodward-Carmichael method. (See ref. 14 for other examples of this method.) Comparisons of corresponding body surface pressure distributions for the flight and wind-tunnel data indicated the influence of different mounting structures. These effects are discussed in the appendix.

The base drag coefficients obtained for the hemispherical base configuration are presented in figure 11. The magnitude over the subsonic speed range was slightly greater than for the blunt base, but the variation with Mach number for the subsonic speeds was similar.

The base drag coefficients for trailing disk configurations x/D = 0.44 and x/D = 0.50 are shown in figures 12(a) and 12(b), respectively. The subsonic base drag coefficients for both of these configurations were negative. If the increment between the base drag coefficients for a trailing disk configuration and a blunt base was assumed to be independent of the initial blunt base drag coefficient, these negative coefficients were probably the result of the unusually low base drag

coefficients for the present blunt base configuration. Because of the low values for the blunt base drag coefficients, percentages of base drag reduction are not discussed in this document. Instead, increments of base drag coefficient from the blunt base values are presented.

The subsonic base drag coefficients for the x/D = 0.44 configuration were almost constant as Mach number increased. However, the subsonic base drag coefficients for the x/D = 0.50 configuration increased in magnitude (became more negative) as Mach number increased. The supersonic base drag coefficients were positive for both x/D configurations and increased with increasing Mach number.

The base drag coefficients were averaged for each of the four configurations, and the average was compared as a function of Mach number, as shown in figure 13(a). These data are shown as incremental differences in figure 13(b) with the blunt base data used as the baseline reference condition. A positive difference means that the test configuration (either the hemispherical or one of the trailing disk configurations) had a larger base drag coefficient than the blunt base. Thus, when compared to the blunt base, a positive difference represents a base drag increase and a negative difference represents a base drag decrease. The hemispherical base had an almost constant base drag increase of approximately 0.01 for Mach 0.70 to 0.93 and Mach 1.24. Both trailing disk configurations had a significant base drag decrease for the range of Mach 0.70 to 0.93. The base drag decreases ranged from 0.08 to 0.07 for the x/D = 0.50 configuration and from 0.08 to 0.06 for the x/D = 0.44 configuration. These decreases in base drag coefficient became smaller as Mach number increased from Mach 0.70 to 0.93.

The trailing disk configurations caused a drag penalty at the lower supersonic speeds. As Mach increased from 1.20 to 1.60, the drag penalty decreased rapidly. By M = 1.60, the trailing disk base drag and the blunt base drag were approximately equal. Benefits were not expected at supersonic speeds, and the data were limited; consequently, the supersonic data are not further discussed.

Wind-Tunnel Data for Full-Scale Model

Base surfaces. — The pressure coefficient distributions for the α ≈ 0° data are shown in figures 14 to 22 and for the α ≈ 3° data in figures 23 to 28. Similar to those for the flight data, the pressure coefficients on the base surfaces were affected by the base configuration, the Mach number, the radial position, and the angular location. An angle-of-attack effect could also be observed. The pressure for the center orifice was arbitrarily plotted with the symbol for the 16.9° row, and the edge pressure for the FLTD was arbitrarily plotted with the symbol for the downstream disk surface.

The effect of base configuration on the pressure coefficients for the α ≈ 0° data was defined by two general pressure distributions. One was exhibited by the blunt base and the WTD configuration with x/D = 0.20 (figs. 14 and 15), and the other was exhibited by the remaining trailing disk configurations (figs. 16 to 22). For the blunt base and the x/D = 0.20 configurations (figs. 14 and 15, respectively), the pressure distributions at a given angular location had a nearly linear, relatively constant value as radial distance increased. The downstream disk surface

showed the most variation with respect to increasing radial distance. Some variation with respect to angular orientation could be seen on the blunt base surface and on the downstream disk surface. The similarities between the blunt base and the x/D = 0.20 configuration indicated that the disk was having a minimal effect on the free shear layer that was being shed from the BOR base. That is, the free shear layer from the BOR base was passing clear of the disk.

The pressure distribution data for the WTD configurations for x/D = 0.40, 0.45, 0.50, 0.55, and 0.60 (figs. 16 to 20) and the FLTD configurations for x/D = 0.44 and 0.50 (figs. 21 and 22) were nonlinear with respect to radial distance for both the base of the BOR and the upstream surface of the disk. This nonlinear variation of pressure coefficient with respect to radial location was the same as that observed in the flight data (figs. 8 and 9). The effect of angular location was minimal for x/D = 0.40 (fig. 16). The effect of angular location became more noticeable with increasing x/D. Depending on the x/D value, the pressure coefficients on the downstream surface varied from slightly negative to slightly positive.

The α ≈ 3° data are shown in figure 23 for the blunt base, in figures 24 to 26 for the WTD configurations x/D = 0.45, 0.50, and 0.55, and in figures 27 and 28 for the FLTD configurations x/D = 0.44 and 0.50. The main difference between the surface pressure distributions for the α ≈ 0° and α ≈ 3° data concerned the pressure coefficients along the 196.9° row for the blunt base and the downstream disk surfaces. For these surfaces for the α ≈ 0° data (figs. 14 to 20), the relationship between the pressure coefficient and radial location was the same for each angular location. However, for the α ≈ 3° data (figs. 23 to 26), the relationship between pressure coefficient and radial location was different for the 196.9° row than for the other rows. The FLTD data are not included in this discussion because there was no orifice array along the 196.9° row. The pressure coefficients along the row at 196.9° became less negative (and in some cases more positive) as R/RB increased. The pressure coefficients along the other rows were relatively constant as R/RB increased. The less negative pressure coefficients along the row at 196.9° may have been caused by the influence of the model support strut (angular orientation of 180.0°).

Base drag and total drag coefficients. — The base drag coefficient (from the pressure data) and the total drag coefficient (from the force data) are each plotted as a function of Mach number for each configuration in figure 29. Both the α ≈ 0° and α ≈ 3° data are shown. The general and not unexpected result for each configuration was that the base drag and total drag coefficients increased as Mach number increased.

In figure 30, the total drag coefficient is compared with the sum of the corresponding base drag coefficient and a predicted turbulent flow skin friction drag coefficient. The predicted skin friction drag coefficient was calculated for turbulent flow conditions and adjusted for compressibility effects using information from reference 15. An adjustment for three-dimensional effects was calculated using equation 32 from chapter 2 of reference 1. This summed (or predicted total drag) value was in good to excellent agreement with the measured total drag coefficient for the majority of the data. The largest differences between the two values, which occurred for the WTD configuration x/D = 0.60 in figure 30(k), was 10 percent or less. As expected for these low (0° and 3°) angle-of-attack data,

this indicated that the total drag coefficient was composed primarily of the base drag and skin friction drag coefficients.

Figure 31 shows the base drag and total drag coefficients for both the $\alpha \approx 0°$ and $\alpha \approx 3°$ data as a function of x/D for each Mach number. The blunt base coefficient values are indicated by a dashed line. The effective drag reducing configurations for the $\alpha \approx 0°$ data, that is, those that had base drag or total drag coefficients lower than the blunt base for all Mach numbers studied, were the x/D = 0.44 to 0.60 configurations. The base drag and total drag coefficients for the configurations tested at $\alpha \approx 3°$, x/D = 0.44 to 0.55, were also lower than the corresponding blunt base coefficients.

The difference between the base drag or total drag coefficient for a given trailing disk configuration and the corresponding blunt base coefficient is shown in figure 32. A negative increment meant that the configuration had a lower coefficient, and hence less drag, than the blunt base. The effective drag reducing configurations were the primary interest in this study; thus, the following comments are only concerned with the x/D = 0.44 to 0.60 configurations for the $\alpha \approx 0°$ data and the x/D = 0.44 to 0.55 configurations for the $\alpha \approx 3°$ data. The maximum decrease, or improvement, from the blunt base configuration is presented below.

	M	c_D		c_{D_b}	
		Decrease	Percent	Decrease	Percent
$\alpha \approx 0°$	0.30	0.08	30	0.08	52
	0.50	0.08	31	0.07	45
	0.71	0.06	23	0.06	33
	0.82	0.05	18	0.05	29
$\alpha \approx 3°$	0.30	0.07	27	0.07	39
	0.50	0.07	27	0.07	37
	0.71	0.07	27	0.06	32

The maximum decrease in base drag and total drag increments ranged from 0.08 to 0.05 for the $\alpha \approx 0°$ data as Mach number increased from 0.30 to 0.82. For the $\alpha \approx 3°$ data, the maximum decrease was 0.07 to 0.06 for the base drag and remained a constant 0.07 for the total drag from Mach 0.30 to 0.71. The effect of Mach number on the maximum decrement appeared to be more noticeable for the $\alpha \approx 0°$ data than for the $\alpha \approx 3°$ data.

Body moment coefficient. — The body moment coefficient data obtained for the full-scale wind-tunnel data of the present study were limited. However, comparison of data for the blunt base and the trailing disk configurations indicated that the trailing disk configurations would not degrade the stability of the BOR. The changes in the moment coefficient for the trailing disk configurations appeared to be in the direction of increasing stability. This increase in stability was consistent with the concept that the flow field for the trailing disk configurations behaved as if the body had been lengthened by a boattail extension. Hence, the neutral point for the trailing disk configuration would be farther from the nose than for the blunt body configuration.

16

Comparisons of Flight and Wind-Tunnel Model Data

The only significant difference between the BOR configuration tested in flight and the one tested in the wind tunnel was the method of mounting. However, as discussed in the appendix, these different mounting structures caused a substantial difference in the pressure field of the body. Thus, the blunt base drag coefficients for the flight data and the wind-tunnel data were not in agreement. Because of the large disagreements in the data, comparisons between the trailing disk configurations of the flight and wind-tunnel data are in terms of differences from their respective blunt base configurations. These differences are plotted with x/D in figure 33(a) and with Mach number in figure 33(b). Only the wind-tunnel x/D values near those of the flight data are shown. The aircraft angle of attack, not the BOR angle of attack, is given for the flight data. The data for the trailing disk in flight had a larger decrease in the base drag coefficient than did the trailing disk data from the wind-tunnel study. However, both the present flight experiment and the full-scale wind-tunnel model experiment demonstrated the significant base drag reduction capability of the trailing disk concept at low transonic speeds.

Figure 34 shows the maximum difference in the base drag and the total drag coefficients (for each set of experimental data, irrespective of x/D) as a function of Mach number. The total drag and base drag reductions obtained for the data for nonzero angle of attack were relatively insensitive to changes in Mach number. Data from references 7 to 9 are also shown in figure 34. These data are for $\alpha = 0°$ and approximately Mach 0.10. In general, the trailing disk data of the present study had larger reductions in the base drag and total drag coefficients than did the low Reynolds number, incompressible data of the previous studies. Although the magnitudes were different, all data of previous studies and the present study showed substantial reductions in both the base drag and total drag coefficients.

The differences between the present study and previous studies could be due to a number of factors. In addition to differences in the mounting structures, differences in Mach numbers and Reynolds numbers were significant. A Reynolds number comparison for the present experiment, as well as the earlier small-scale studies at incompressible speeds, is shown in figure 35. The Reynolds numbers for the present flight experiment and the full-scale wind-tunnel experiment were up to 50 to 80 times greater, respectively, than for the previous small-scale studies.

CONCLUSIONS

The effectiveness of a trailing disk in reducing the base drag of a large body of revolution, 20.3-cm (8-in) diameter, was studied both in flight and in the wind tunnel. Pressure data were obtained for the flight experiment, and both pressure and force-balance data were obtained for the wind-tunnel experiment. The flight study also included data obtained from a hemispherical base. Reynolds number, based on the length of the body of revolution, ranged from 1.5×10^7 to 2.7×10^7 for the flight data and from 1.9×10^7 to 4.1×10^7 for the wind-tunnel data. Primary Mach numbers for the flight data were from 0.70 to 0.93 with some data obtained for Mach 1.20 to 1.60. Aircraft angles of attack ranged from 3.9° to 6.6° for the flight data. Mach numbers for the wind-tunnel study were from 0.30

to 0.82 for the approximately 0° angle-of-attack data and from 0.30 to 0.71 for the approximately 3° angle-of-attack data. The data were analyzed using the blunt base for a reference, or baseline, configuration and were compared with other wind-tunnel data. The analysis led to the following conclusions:

1. The present flight and full-scale wind-tunnel model experiments demonstrated the significant base drag reduction capability of the trailing disk concept at low transonic speeds. The Reynolds numbers for the present flight experiment and the full-scale wind-tunnel experiment were up to 50 to 80 times greater, respectively, than for the earlier pioneering studies performed at incompressible speeds.

2. For the trailing disk data from the flight experiment, the maximum decrease in base drag increments ranged from 0.08 to 0.07 as Mach number increased from 0.70 to 0.93. The trailing disk configurations caused a drag penalty at the lower supersonic speeds. However, the limited data indicated that this penalty decreased rapidly as Mach number increased to 1.40, and the penalty appeared to be eliminated as Mach number increased from 1.40 to 1.60. The hemispherical base had an almost constant drag increase of approximately 0.01 for data from Mach 0.70 to 0.93 and 1.24.

3. For the trailing disk data from the full-scale wind-tunnel model experiment, the maximum decrease in base drag and total drag increments ranged from 0.08 to 0.05 for the 0° angle-of-attack data as Mach number increased from 0.30 to 0.82. For the 3° angle-of-attack data, the maximum decrease was 0.07 to 0.06 for the base drag and remained a constant 0.07 for the total drag as Mach number increased from 0.30 to 0.71.

4. The base drag coefficient for the blunt base configuration was lower for the flight data than for the wind-tunnel data. Moreover, the base drag reduction due to the trailing disk was larger for the flight data than for the wind-tunnel data. These differences observed between the flight and wind-tunnel tests were probably due to the different mounting structures. The body surface pressure coefficients for the flight and wind-tunnel data were also affected by the difference in mounting structures. The pressure coefficients for the wind-tunnel data show that the pressures immediately forward of the base are dependent on the trailing disk configuration.

5. In general, the trailing disk data of the present study had larger reductions in the base drag and total drag coefficients than did the low Reynolds number, incompressible data of previous studies. In addition to differences in the mounting structure, Mach numbers and Reynolds number were also significantly different between the data in the present study and those in previous studies.

6. The pressure coefficients for the downstream surface of the trailing disk were positive for some of the conditions that were tested. Thus, this surface was exerting a thrust load on the base of the body of revolution.

National Aeronautics and Space Administration
Ames Research Center
Dryden Flight Research Facility
Edwards, California, December 11, 1984

APPENDIX - BODY SURFACE PRESSURE COEFFICIENTS

Flight Data

Typical pressure coefficients for the BOR surface for the blunt and hemispherical base configurations are shown in figures 36 and 37, respectively. A pressure coefficient from the base surface is also shown. Body surface pressure coefficients were obtained for only these two configurations. The pressure distributions and the levels of the pressure coefficients for the two configurations were essentially the same for the subsonic Mach numbers, and the differences in the pressure coefficients for the two angular locations $\theta = 16.9°$ and $106.9°$ were small. The effect of the lower pressure from the base of the body could be seen propagating upstream, or forward, of the base. As the flow approached the base, the effect on the surface pressure coefficient was first seen as a compression followed by an expansion that rapidly approached the level of the base pressure coefficient.

The agreement between the two angular locations for the supersonic Mach number data was not as close for either configuration. The trends for the pressure coefficients immediately ahead of the base also differed between the two angular locations. The difference in the pressure coefficient levels could be most easily observed by comparing the values of the pressure coefficient at $X/L = 0.68$ (where X/L is the ratio of distance from the nose to body length) for the two angular locations shown. The reference pressure location was at $X/L = 0.68$ and $\theta = 16.9°$ (where the pressure coefficient was zero); therefore, the pressure coefficient at $X/L = 0.68$ and $\theta = 106.9°$ also needed to be zero for perfect agreement. The differences between the two angular locations could have been caused by the presence of the vertical tail ($\theta = 180°$). The probable effect of the vertical tail is discussed in more detail later in this appendix.

Wind-Tunnel Data for Full-Scale Model

The surface pressure coefficient data for the BOR in the blunt base configuration are shown in figure 38 for the $\alpha \approx 0°$ data and in figure 39 for the $\alpha \approx 3°$ data. In figures 38(a) and 39(a), the surface pressure coefficient is plotted as a function of X/L; in figures 38(b) and 39(b), the surface pressure coefficient is plotted as a function of θ. A pressure coefficient from the base surface is also shown. As expected, the surface pressure data were affected by the location, the angle of attack, and the Mach number. The effects due to the location and the angle of attack were observable but were not pertinent to the evaluation of the trailing disk and therefore are not discussed here. Both the $\alpha \approx 0°$ and the $\alpha \approx 3°$ pressure coefficient data, except for the most forward location ($X/L = 0.283$), showed that pressure coefficients became more negative as Mach number increased.

The effect of the lower pressure from the body base could be seen propagating upstream, or forward, of the base, as indicated in figures 38(a) and 39(a). As the flow approached the base, this effect on the pressure distribution was first seen as a slight compression followed by an expansion that rapidly approached the base pressure. The effect of this lower base pressure was observed within 15.2 cm (6 in), $x/(D/2) = 1.3$, of the base. When expressed in terms of radial distance, the effect was less than that seen in quasi-two-dimensional flow (refs. 16 and 17) where the

effect was usually expressed in terms of step height (or half of the base width). For the step heights of 1.3 cm (0.50 in) or less, studied in references 16 and 17, the effect of the lower pressures on the base was propagated upstream for approximately four step heights ahead of the base. However, if the effect was considered as a distance ahead of the base instead of in terms of step height, the actual distance forward of the base that was affected by the lower base pressure was greater for the three-dimensional configuration than for the quasi-two-dimensional configuration. It was reasonable to expect that the effect of a disturbance would be more widely and rapidly communicated in a three-dimensional flow than in a two-dimensional flow.

The body surface pressure coefficients for the other base configurations followed the same trend as the blunt configuration. However, the pressure coefficient levels, especially near the base region, were different. To observe more easily the effect of the different base configurations on the body surface pressure coefficients near the base region, the data were presented as the difference between a given x/D trailing disk configuration and the blunt base configuration for the same Mach number and angle-of-attack conditions. The surface pressure coefficient values were negative for all configurations. Hence, a negative difference, as plotted, meant that the surface pressure coefficients for the trailing disk configurations were more negative than for the corresponding blunt base configuration. This difference as a function of separation distance, x/D ratio, is shown in figure 40 for the surface pressure location of X/L = 0.99 and θ = 315°. The magnitude of the difference was primarily affected by Mach number and the x/D value. As Mach number increased, the magnitude of the differences also increased. The differences decreased in magnitude as x/D increased from 0.40 to 0.60 for the $\alpha \approx 0°$ data and 0.44 to 0.55 for the $\alpha \approx 3°$ data.

Similar plots of surface pressure coefficient as a function of x/D for other X/L locations (not presented here) showed that, as expected, the influence of the lower pressures in the base region decreased with increasing distance forward of the base. By X/L = 0.88, 25.4 cm (10 in) ahead of the base, the effect of x/D on the surface pressures was negligible. The differences in surface pressures between the blunt and trailing disk configurations for the remaining body surface locations were small. Again, as for the locations near the base, the differences became larger as Mach number increased.

Comparison of Flight and Wind-Tunnel Model Data

As mentioned in the description of the wind-tunnel model, the only significant difference between the flight-tested and wind-tunnel-tested BOR configurations was the method of mounting, as shown in figures 2 and 5(a). The effect of these different mounting structures on the pressures of the blunt base configurations of the flight and wind-tunnel data of the present study could be observed for both the body surface pressure coefficients and the base drag coefficients. The surface pressure coefficients along the top row of the BOR (the 16.9° row for the flight data and the 45.0° row for the wind-tunnel data) for Mach numbers near 0.80 are presented in figure 41. Surface pressure coefficients for the other Mach numbers behaved similarly and, therefore, are not shown. The location for the reference pressure used in the flight data calculations is indicated in figure 41. The difference in the level of the surface pressure coefficient between the two sets of data was believed to be caused by the different mounting structures.

The theoretical effect of the different mounting structures was more easily observed from the comparison in figure 42 for $\alpha \approx 0°$, $\theta = 45°$, and Mach 0.82. The theoretical wing-body program is based on a version of the Woodward-Carmichael method. (See ref. 14 for examples of this method.) Three configurations are shown in figure 42: the BOR alone, the BOR with the vertical tail, and the BOR with the wind-tunnel strut. It is interesting to observe that as X/L increased from 0.69 to the base, the surface pressure coefficients for the body alone were essentially constant. However, the coefficients for the body with the vertical tail became significantly more positive (compression effect), and the coefficients for the body with the wind-tunnel strut became less positive (expansion effect). These last two trends were upheld by both the flight and the wind-tunnel data, shown in figures 37(a) and 38(a), respectively. The absolute values of these theoretical coefficients were different from both the flight and wind-tunnel data of the present study. However, the purpose of this theoretical comparison was to observe the effects of different mounting structures. No attempt was made to account for the effects of such factors as Reynolds number, the navigation light, and the precipitation static discharge probes.

The differences in level between the body surface pressure coefficients ahead of the base for the flight and wind-tunnel data suggested that the blunt base drag coefficients would also differ between these two sets of data. Earlier studies for Mach 0.70 to 1.30 (ref. 18), Mach 1.50 and 2.00 (ref. 19), and the examples discussed in reference 1 indicated that the base pressures could be affected by the flow disturbance created by a strut or vertical tail shape. In reference 18, a higher base drag coefficient was observed for a body alone than for one with stabilizing fins. In reference 19, the differences in base drag coefficient between a BOR alone and the same BOR with tail surfaces showed that tail surfaces could cause a lower base drag coefficient than for the BOR alone. The data shown and the examples discussed in reference 1 also indicated that a vertical tail, or fin, could cause a lower base drag coefficient than for a body alone. Thus, the observed differences between the base drag coefficients for the blunt base configurations of the flight data and the wind-tunnel data were not unexpected.

Theoretical surface pressure coefficients were also calculated for supersonic Mach numbers of 1.20 and 1.53 from the same theoretical wing-body program that was used for the subsonic calculations. No attempt was made to account for the effect of such factors as Reynolds number, the navigation light, and the precipitation static discharge probes. The surface pressure coefficients were calculated for two configurations: the BOR alone and the BOR with the vertical tail (fig. 43). Two angular locations, $\theta = 15°$ and $105°$, are shown in figure 43 for the BOR with the vertical tail. The presence of the vertical tail affected the surface pressure coefficient in both magnitude and variation. The effect of angular location was mainly noticeable toward the rear of the body for Mach 1.20 pressures and toward the front of the body for Mach 1.50 pressures. On the basis of the theoretical pressures, the effect of the vertical tail on the angular pressure variation immediately ahead of the base should have decreased as Mach number increased. This agreed with the surface pressure coefficients in this region for the blunt base flight data in figure 36(b).

REFERENCES

1. Hoerner, Sighard F.: Fluid-Dynamic Drag. Second ed. (Published by the author) 148 Busteed Drive, Midland Park, N.J., 1965.

2. Roshko, Anatol: On the Drag and Shedding Frequency of Two-Dimensional Bluff Bodies. NACA TN-3169, 1954.

3. Bearman, P.W.: Investigation of the Flow Behind a Two-Dimensional Model With a Blunt Trailing Edge and Fitted With Splitter Plates. J. Fluid Mech., vol. 21, part 2, Feb. 1965, pp. 241-256.

4. Saltzman, Edwin J.; and Hintz, John: Flight Evaluation of Splitter-Plate Effectiveness in Reducing Base Drag at Mach Numbers From 0.65 to 0.90. NASA TM X-1376, 1967.

5. Ringleb, Friedrich O.: Separation Control by Trapped Vortices. Boundary Layer and Flow Control, G.V. Lachmann, ed., Pergamon Press, 1961, pp. 265-294.

6. Migay, V.K. (Translation Div., Foreign Technology Div., Wright-Patterson AFB): Investigating Finned Diffusers. Available from DDC as AD-402582, 1963. (Primary source — Teploenergetika, Nr. 10, Oct. 1962, pp. 55-59, in Russian.)

7. Mair, W.A.: The Effect of a Rear-Mounted Disc on the Drag of a Blunt-Based Body of Revolution. Aeronaut. Quarterly, Nov. 1965, pp. 350-360.

8. Goodyer, M.J.: Some Experimental Investigations Into the Drag Effects of Modifications to the Blunt Base of a Body of Revolution. Rep. 150, Inst. of Sound and Vibration, 1966.

9. Little, B.H., Jr.; and Whipkey, R.R.: Locked Vortex Afterbodies. AIAA-78-1179, 1978.

10. Fox, Charles H., Jr.; and Huffman, Jarrett K.: Calibration and Test Capabilities of the Langley 7- by 10-Foot High Speed Tunnel. NASA TM X-74027, 1977.

11. Braslow, Albert L.; Hicks, Raymond M.; and Harris, Roy V., Jr.: Use of Grit-Type Boundary-Layer-Transition Trips on Wind-Tunnel Models. NASA TN D-3579, 1966.

12. Gillis, Clarence L.; Polhamus, Edward C.; and Gray, Joseph L., Jr.: Charts for Determining Jet-Boundary Corrections for Complete Models in 7- by 10-Foot Closed Rectangular Wind Tunnels. NACA WR-L-123, 1945. (Primary source — originally issued as ARR No. L5G31, 1945.)

13. Herriot, John G,: Blockage Corrections for Three-Dimensional-Flow Closed-Throat Wind Tunnels, With Consideration of the Effect of Compressibility. NACA TR-995, 1950.

14. Curry, Robert E.: Utilization of the Wing-Body Aerodynamic Analysis Program. NASA TM-72856, 1978.

15. Peterson, John B., Jr.: A Comparison of Experimental and Theoretical Results for the Compressible Turbulent-Boundary-Layer Skin Friction With Zero Pressure Gradient. NASA TN D-1795, 1963.

16. Goecke, Sheryll A.: Flight-Measured Base Pressure Coefficients for Thick Boundary-Layer Flow Over an Aft-Facing Step for Mach Numbers from 0.4 to 2.5. NASA TN D-7202, 1973.

17. Powers, Sheryll Goecke: Flight-Measured Pressure Characteristics of Aft-Facing Steps in Thick Boundary Layer Flow for Transonic and Supersonic Mach Numbers. NASA CP-2054, 1978.

18. Hart, Roger G.: Effects of Stabilizing Fins and a Rear-Support Sting on the Base Pressures of a Body of Revolution in Free Flight at Mach Numbers From 0.7 to 1.3. NACA RM-L52E06, 1952.

19. Spahr, Richard J.; and Dickey, Robert R.: Effect of Tail Surfaces on the Base Drag of a Body of Revolution at Mach Numbers of 1.5 and 2.0. NACA TN-2360, 1951.

20. Abbott, Ira H.; Von Doenhoff, Albert E.; and Stivers, Louis S., Jr.: Summary of Airfoil Data. NACA TR-824, 1945.

TABLE 1. — MODEL CHARACTERISTICS

(a) Nominal coordinates for BOR

X/L	R/RB	X/L	R/RB	X/L	R/RB
0	0	0.137	0.455	0.303	0.820
0.013	0.050	0.149	0.490	0.324	0.850
0.022	0.085	0.160	0.518	0.354	0.890
0.034	0.125	0.172	0.545	0.368	0.908
0.045	0.165	0.183	0.575	0.405	0.945
0.057	0.205	0.195	0.605	0.432	0.965
0.068	0.245	0.207	0.630	0.455	0.979
0.080	0.280	0.218	0.655	0.483	0.993
0.091	0.318	0.230	0.680	0.497	0.995
0.103	0.350	0.241	0.705	0.531	1.000
0.114	0.388	0.253	0.728	1.000	1.000
0.126	0.423	0.301	0.815		

(b) Vertical tail characteristics (mount for flight BOR)

Span, m (ft) 2.71 (8.9)
Root chord, m (ft) 5.42 (17.8)
Tip chord, m (ft) 2.23 (7.3)
Airfoil section
  At root, percent biconvex 3.2
  At tip, percent biconvex 3.0
Leading edge sweep, deg 55

(c) Strut characteristics (mount for wind-tunnel BOR)

Span, cm (in) 96.3 (37.9)
Chord from body to 22.1 cm (8.7 in), cm (in) . . . 17.8 (7)
Chord at 93.7 cm (36.9 in), cm (in) 50.8 (20)
Airfoil section . . . . NACA 64-010
                                       (ref. 20)
X/L of strut centerline 0.581

Notes:

1. X and R measurements are to ± 0.025 cm (± 0.010 in).
2. For the the flight experiment, L = 220.0 cm (86.6 in), R = 10.11 cm (3.98 in).
3. For the wind-tunnel experiment, L = 218.8 cm (86.1 in), R = 10.16 cm (4.00 in).
4. A ridge 0.48 cm (0.19 in) high and 1.91 cm (0.75 in) wide extended along the top centerline from an X/L of 0.038 for the flight BOR and an X/L of 0.035 for the wind-tunnel BOR to the BOR base.

TABLE 2. — LOCATIONS OF ORIFICES ON BOR AND BASE SURFACES

(a) Flight experiment, blunt base configuration

BOR base				BOR surface			
$\theta = 16.9°$		$\theta = 106.9°$		$\theta = 16.9°$		$\theta = 106.9°$	
R/RB	Orifice	R/RB	Orifice	X/L	Orifice	X/L	Orifice
0	FC1	0	FC1	0.108	FC6	0.108	FC13
0.410	FC2	0.224	FC4	0.450	FC7	0.450	FC14
0.909	FC3	0.724	FC5	0.681	FC8	0.681	FC15
				0.958	FC9	0.959	FC16
				0.969	FC10	0.970	FC17
				0.981	FC11	0.981	FC18
				0.993	FC12	0.993	FC19

(b) Flight experiment, hemispherical base configuration

BOR base				BOR surface
$\theta = 16.9°$		$\theta = 106.9°$		Same as for blunt base configuration
S/SA	Orifice	S/SA	Orifice	
0	FC1	0	FC1	
0.377	FC2	0.371	FC4	
0.695	FC3	0.689	FC5	

(c) Flight experiment, FLTD configurations

BOR base				BOR surface
$\theta = 16.9°$		$\theta = 106.9°$		P_{ref} at X/L = 0.681, θ = 16.9°
R/RB	Orifice	R/RB	Orifice	
0.410	FC1	0.224	FC3	
0.909	FC2	0.724	FC4	

Disk, upstream surface				Disk, downstream surface			
$\theta = 16.9°$		$\theta = 106.9°$		$\theta = 16.9°$		$\theta = 106.9°$	
R/RB	Orifice	R/RB	Orifice	R/RB	Orifice	R/RB	Orifice
0.196	FC5	0.302	FC10	0	FC12	0	FC12
0.394	FC6	0.701	FC11	0.113	FC13	0.201	FC17
0.595	FC7			0.314	FC14	0.402	FC18
0.751	FC8			0.513	FC15	0.756	FC19
0.804	FC9[a]			0.714	FC16		
				0.804	FC9[a]		

[a]Pressure orifice FC9 is located on the disk edge.

TABLE 2. — Continued

(d) Wind-tunnel experiment, blunt base configuration[b]

BOR base

θ = 16.0°		θ = 106.0°			θ = 196.9°		θ = 286.9°	
R/RB	Orifice	R/RB	Orifice		R/RB	Orifice	R/RB	Orifice
0	WC1	0	WC1		0	WC1	0	WC1
0.150	WC2	0.185	WC8		0.220	WC13	0.255	WC18
0.290	WC3	0.325	WC9		0.360	WC14	0.395	WC19
0.430	WC4	0.465	WC10		0.640	WC15	0.535	WC20
0.570	WC5	0.605	WC11		0.780	WC16	0.675	WC21
0.710	WC6	0.885	WC12		0.920	WC17	0.815	WC22
0.850	WC7						0.955	WC23

BOR surface

	Circumferential locations			Longitudinal locations		
θ, deg	X/L = 0.283	X/L = 0.803	X/L = 0.988	X/L	θ = 45.0°	θ = 315.0°
	Orifice	Orifice	Orifice		Orifice	Orifice
15.0	WC55	WC78	WC101	0.283	WC57	WC75
30.0	WC56	WC79	WC102	0.570	WC124	WC132
45.0	WC57	WC80	WC103	0.617	WC125	WC133
60.0	WC58	WC81	WC104	0.663	WC126	WC134
75.0	WC59	WC82	WC105	0.710	WC127	WC135
90.0	WC60	WC83	WC106	0.756	WC128	WC136
105.0	WC61	WC84	WC107	0.803	WC80	WC98
120.0	WC62	WC85	WC108	0.849	WC129	WC137
135.0	WC63	WC86	WC109	0.896	WC130	WC138
150.0	WC64	WC87	WC110	0.942	WC131	WC139
165.0	WC65	WC88	WC111	0.988	WC103	WC121
180.0	WC66	WC89	WC112			
195.0	WC67	WC90	WC113			
210.0	WC68	WC91	WC114			
225.0	WC69	WC92	WC115			
240.0	WC70	WC93	WC116			
255.0	WC71	WC94	WC117			
270.0	WC72	WC95	WC118			
285.0	WC73	WC96	WC119			
300.0	WC74	WC97	WC120			
315.0	WC75	WC98	WC121			
330.0	WC76	WC99	WC122			
345.0	WC77	WC100	WC123			

[b]Pressure orifices WC24 to WC54 are reserved for the WTD and FLTD surfaces.

TABLE 2. - Concluded

(e) Wind-tunnel experiment, WTD configurations[c]

BOR base							
$\theta = 16.9°$		$\theta = 106.9°$		$\theta = 196.9°$		$\theta = 286.9°$	
R/RB	Orifice	R/RB	Orifice	R/RB	Orifice	R/RB	Orifice
0.150	WC1	0.185	WC7	0.220	WC12	0.255	WC17
0.290	WC2	0.325	WC8	0.360	WC13	0.395	WC18
0.430	WC3	0.465	WC9	0.640	WC14	0.535	WC19
0.570	WC4	0.605	WC10	0.780	WC15	0.675	WC20
0.710	WC5	0.885	WC11	0.920	WC16	0.815	WC21
0.850	WC6					0.955	WC22
Disk, upstream surface							
0.150	WC23	0.325	WC27	0.220	WC30	0.255	WC34
0.290	WC24	0.465	WC28	0.360	WC31	0.395	WC35
0.430	WC25	0.605	WC29	0.500	WC32	0.535	WC36
0.570	WC26			0.640	WC33	0.675	WC37
Disk, downstream surface							
0	WC38	0	WC38	0	WC38	0	WC38
0.150	WC39	0.185	WC43	0.220	WC47	0.255	WC51
0.290	WC40	0.325	WC44	0.360	WC48	0.395	WC52
0.430	WC41	0.465	WC45	0.500	WC49	0.535	WC53
0.570	WC42	0.605	WC46	0.640	WC50	0.675	WC54

[c]BOR surface orifice locations are the same as for the wind-tunnel blunt base configuration.

(f) Wind-tunnel experiment, FLTD configurations[d]

Disk, upstream surface				Disk, downstream surface			
$\theta = 16.9°$		$\theta = 106.9°$		$\theta = 16.9°$		$\theta = 106.9°$	
R/RB	Orifice	R/RB	Orifice	R/RB	Orifice	R/RB	Orifice
0.195	WC23	0.300	WC28	0	WC31	0	WC31
0.393	WC24	0.500	WC29	0.113	WC32	0.200	WC36
0.593	WC25	0.698	WC30	0.313	WC33	0.400	WC37
0.748	WC26			0.510	WC34	0.593	WC38
0.800	WC27[e]			0.710	WC35	0.753	WC39
				0.800	WC27[e]		

[d]BOR base orifice locations for the FLTD configuration are the same as for the WTD configuration; BOR surface orifice locations are the same as for the wind-tunnel blunt base configuration.

[e]Pressure orifice WC27 is located on the disk edge.

TABLE 3. — PRESSURE COEFFICIENTS AND RELATED PARAMETERS FOR FLIGHT EXPERIMENT
(Refer to NOMENCLATURE for definitions of flight and configuration test point designations such as F1101, F1102, and F1103.)

(a) Blunt base configuration

TP	F1101	F1102	F1103	F1104	F1105	F1106
M	0.70	0.70	0.70	0.79	0.88	0.89
α, deg	5.70	4.20	6.50	5.20	5.30	6.10
β, deg	0.18	0.04	0.10	-0.04	-0.28	-0.14
C_{D_b}	0.0504	0.0555	0.0506	0.0363	0.0419	0.0329
Re $\times$ 10^{-6}	18.34	26.44	26.42	17.16	16.36	23.29
P_{ref}, kPa	41.959	69.837	69.602	32.334	25.192	41.991
(lb/ft^2)	(876.3)	(1458.6)	(1453.7)	(675.3)	(526.1)	(877.0)
M_∞	0.70	0.71	0.71	0.80	0.90	0.90
p_∞, kPa	42.145	69.618	69.471	32.304	24.987	41.668
(lb/ft^2)	(880.2)	(1454.0)	(1450.9)	(674.7)	(521.9)	(870.3)
h, m	6814	3055	3072	8666	10,366	6896
(ft)	(22,357)	(10,024)	(10,078)	(28,430)	(34,010)	(22,624)
C_p at						
FC1	-0.0682	-0.0683	-0.0617	-0.0549	-0.0597	-0.0475
FC2	-0.0463	-0.0530	-0.0410	-0.0341	-0.0378	-0.0295
FC3	-0.0277	-0.0334	-0.0367	-0.0130	-0.0189	-0.0129
FC4	-0.0726	-0.0743	-0.0680	-0.0554	-0.0628	-0.0520
FC5	-0.0690	-0.0734	-0.0658	-0.0548	-0.0609	-0.0492
FC6	0.0263	0.0279	0.0161	0.0142	0.0045	-0.0011
FC7	-0.0746	-0.0761	-0.0808	-0.0903	-0.1063	-0.1113
FC8	0	0	0	0	0	0
FC9	0.0085	0.0091	0.0098	0.0153	0.0266	0.0316
FC10	0.0084	0.0098	0.0110	0.0138	0.0252	0.0344
FC11	-0.0015	-0.0020	-0.0008	-0.0006	0.0135	0.0224
FC12	-0.0124	-0.0144	-0.0170	-0.0142	-0.0083	0.0011
FC13	0.0255	0.0214	0.0156	0.0102	-0.0008	-0.0093
FC14	-0.0805	-0.0820	-0.0880	-0.0952	-0.1096	-0.1135
FC15	-0.0142	-0.0166	-0.0185	-0.0212	-0.0181	-0.0147
FC16	0.0120	0.0087	0.0081	0.0131	0.0299	0.0370
FC17	0.0148	0.0110	0.0114	0.0169	0.0360	0.0429
FC18	0.0030	0.0003	0.0021	0.0052	0.0219	0.0306
FC19	-0.0302	-0.0332	-0.0326	-0.0291	-0.0146	-0.0065

TABLE 3. — Continued

(a) Continued

TP	F1107	F1108	F1109	F1110	F1111
M	0.89	0.92	0.93	1.25	1.40
α, deg	4.20	6.10	5.90	5.60	5.10
β, deg	0.04	0.01	0.13	-0.24	0.03
C_{D_b}	0.0389	0.0394	0.0283	0.0567	0.1797
Re $\times$ 10^{-6}	23.28	15.97	22.53	21.89	20.21
p_{ref}, kPa	42.023	22.719	37.851	23.801	17.666
(lb/ft^2)	(877.7)	(474.5)	(790.5)	(497.1)	(369.0)
M_∞	0.90	0.95	0.95	1.10	1.31
p_∞, kPa	41.708	22.300	37.124	28.723	20.064
(lb/ft^2)	(871.1)	(465.8)	(775.4)	(599.9)	(419.1)
h, m	6889	11,094	7709	9454	11,764
(ft)	(22,600)	(36,397)	(25,292)	(31,016)	(38,595)
C_p at					
FC1	-0.0580	-0.0517	-0.0415	-0.0653	-0.1855
FC2	-0.0391	-0.0323	-0.0258	-0.0571	-0.1791
FC3	-0.0161	-0.0231	-0.0100	-0.0447	-0.1719
FC4	-0.0606	-0.0570	-0.0444	-0.0670	-0.1859
FC5	-0.0546	-0.0551	-0.0433	-0.0651	-0.1858
FC6	0.0056	0.0100	-0.0155	0.1889	0.1618
FC7	-0.1088	-0.1099	-0.1278	-0.0031	-0.0055
FC8	0	0	0	0	0
FC9	0.0296	0.0282	0.0393	0.0565	-0.0331
FC10	0.0337	0.0296	0.0438	0.0465	-0.0412
FC11	0.0196	0.0123	0.0299	0.0411	-0.0317
FC12	-0.0037	-0.0092	0.0042	0.0321	-0.0130
FC13	-0.0053	0.0081	-0.0238	0.1916	0.1871
FC14	-0.1129	-0.1166	-0.1316	-0.0329	-0.0138
FC15	-0.0151	-0.0175	-0.0127	-0.0566	-0.0401
FC16	0.0337	0.0324	0.0440	-0.0256	-0.0598
FC17	0.0396	0.0379	0.0504	-0.0211	-0.0634
FC18	0.0262	-0.0238	0.0386	-0.0261	-0.0653
FC19	-0.0120	-0.0135	0.0019	-0.0357	-0.0799

TABLE 3. — Continued

(a) Continued

TP	F1112	F2101	F2102	F2103	F2104
M	1.55	0.69	0.70	0.70	0.78
α, deg	4.20	5.60	4.20	6.60	5.20
β, deg	-0.07	0.04	-0.17	0.01	-0.12
C_{D_b}		0.0652	0.0505	0.0580	0.0511
Re $\times$ 10^{-6}	17.67	18.67	27.02	26.61	17.56
P_{ref}, kPa	13.734	42.483	69.834	69.523	32.410
(lb/ft^2)	(286.8)	(887.3)	(1458.5)	(1452.0)	(676.9)
M_∞	1.49	0.70	0.71	0.71	0.80
P_∞, kPa	15.248	42.476	69.683	69.431	32.366
(lb/ft^2)	(318.5)	(887.1)	(1455.4)	(1450.1)	(676.0)
h, m	13,505	6759	3048	3076	8652
(ft)	(44,306)	(22,174)	(10,000)	(10,093)	(28,387)
C_p at					
FC1		-0.0834	-0.0697	-0.0602	-0.0657
FC2		-0.0573	-0.0495	-0.0567	-0.0498
FC3		-0.0455	-0.0351	-0.0451	-0.0291
FC4		-0.0839	-0.0691	-0.0698	-0.0710
FC5		-0.0842	-0.0605	-0.0685	-0.0678
FC6	0.1180	0.0154	0.0269	0.0154	0.0193
FC7	-0.0109	-0.0851	-0.0754	-0.0790	-0.0853
FC8	0	0	0	0	0
FC9	-0.0326	0.0042	0.0091	0.0091	0.0152
FC10	-0.0461	-0.0057	0.0091	0.0094	0.0166
FC11	-0.0452	-0.0151	-0.0029	-0.0019	0.0030
FC12	-0.0271	-0.0258	-0.0033	-0.0162	-0.0090
FC13	0.1271	0.0134	0.0188	0.0148	0.0130
FC14	-0.0153	-0.0927	-0.0811	-0.0876	-0.0897
FC15	-0.0290	-0.0253	-0.0156	-0.0176	-0.0151
FC16	-0.0763	0.0008	0.0099	0.0085	0.0180
FC17	-0.0758	0.0028	0.0116	0.0113	0.0225
FC18	-0.0699	-0.0088	0.0028	-0.0006	0.0100
FC19	-0.0883	-0.0423	-0.0317	-0.0320	-0.0251

TABLE 3. — Continued

TP	F2105	F2106	F2107	F2108	F2109
M	0.88	0.89	0.89	0.92	0.94
α, deg	5.30	6.20	4.20	6.20	6.00
β, deg	-0.38	-0.16	-0.33	-0.21	-0.24
C_{D_b}	0.0437	0.0341	0.0404	0.0415	0.0288
Re × 10^{-6}	16.27	23.63	23.71	15.58	23.03
p_{ref}, kPa	25.463	41.885	42.030	22.826	37.636
(lb/ft^2)	(531.8)	(874.8)	(877.8)	(476.7)	(786.0)
M_∞	0.90	0.90	0.90	0.95	0.96
p_∞, kPa	25.213	41.558	41.748	22.461	36.868
(lb/ft^2)	(526.6)	(868.0)	(871.9)	(469.1)	(770.0)
h, m	10,308	6914	6882	11,048	7757
(ft)	(33,819)	(22,685)	(22,578)	(36,247)	(25,450)
C_p at					
FC1	-0.0574	-0.0463	-0.0559	-0.0478	-0.0413
FC2	-0.0380	-0.0296	-0.0385	-0.0335	-0.0230
FC3	-0.0254	-0.0161	-0.0179	-0.0308	-0.0134
FC4	-0.0584	-0.0513	-0.0593	-0.0533	-0.0444
FC5	-0.0609	-0.0499	-0.0582	-0.0541	-0.0432
FC6	0.0025	-0.0043	0.0037	0.0167	-0.0193
FC7	-0.1066	-0.1109	-0.1088	-0.1038	-0.1286
FC8	0	0	0	0	0
FC9	0.0251	0.0317	0.0294	0.0267	0.0395
FC10	0.0265	0.0348	0.0334	0.0289	0.0444
FC11	0.0137	0.0216	0.0192	0.0146	0.0300
FC12	-0.0036	0.0024	-0.0025	-0.0067	0.0050
FC13	-0.0030	-0.0127	-0.0088	0.0143	-0.0304
FC14	-0.1060	-0.1155	-0.1108	-0.1091	-0.1299
FC15	-0.0149	-0.0165	-0.0124	-0.0093	-0.0086
FC16	0.0306	0.0354	0.0340	0.0375	0.0469
FC17	0.0348	0.0427	0.0391	0.0430	0.0533
FC18	0.0243	0.0303	0.0241	0.0284	0.0389
FC19	-0.0149	-0.0064	-0.0107	-0.0082	0.0038

TABLE 3. — Continued

(a) Concluded

TP	F2110	F2111	F2112	F2113	F2114
M	1.20	1.23	1.39	1.57	1.57
α, deg	5.90	5.80	5.30	5.20	5.70
β, deg	-0.27	-0.28	0.07	0.05	-0.08
c_{D_b}	0.0981	0.0706	0.1822	0.2127	
Re × 10^{-6}	22.06	22.13	19.25	17.18	16.33
p_{ref}, kPa	25.159	24.324	17.852	13.569	13.594
(lb/ft^2)	(525.5)	(508.0)	(372.8)	(283.4)	(283.9)
M_∞	1.10	1.10	1.31	1.51	1.51
p_∞, kPa	28.759	28.759	20.137	14.939	14.930
(lb/ft^2)	(600.6)	(600.6)	(420.6)	(312.0)	(311.8)
h, m	9446	9446	11,741	13,634	13,638
(ft)	(30,990)	(30,990)	(38,520)	(44,732)	(44,745)
c_p at					
FC1	-0.1056	-0.0763	-0.1917	-0.2190	
FC2	-0.0992	-0.0698	-0.1816	-0.2095	
FC3	-0.0866	-0.0584	-0.1750	-0.2042	
FC4	-0.1032	-0.0779	-0.1891	-0.2232	
FC5	-0.1072	-0.0809	-0.1874	-0.2202	
FC6	0.1424	0.1726	0.1680	0.1093	0.0993
FC7	-0.0365	-0.0109	-0.0066	-0.0064	-0.0091
FC8	0	0	0	0	0
FC9	-0.0057	0.0347	-0.0244	-0.0333	-0.0326
FC10	-0.0187	0.0237	-0.0366	-0.0456	-0.0424
FC11	-0.0223	0.0189	-0.0298	-0.0430	-0.0420
FC12	-0.0254	0.0113	-0.0158	-0.0223	-0.0224
FC13	0.1439	0.1738	0.1872	0.1145	0.0973
FC14	-0.0317	-0.0078	-0.0087	-0.0134	-0.0164
FC15	-0.0680	-0.0469	-0.0427	-0.0280	-0.0307
FC16	-0.0828	-0.0443	-0.0688	-0.0675	-0.0675
FC17	-0.0801	-0.0406	-0.0704	-0.0685	-0.0676
FC18	-0.0862	-0.0459	-0.0704	-0.0625	-0.0595
FC19	-0.0949	-0.0550	-0.0875	-0.0804	-0.0763

TABLE 3. — Continued

(b) Hemispherical base configuration

TP	F1201	F1202	F1203	F1204	F1205	F1206
M	0.66	0.74	0.79	0.84	0.86	0.87
α, deg	6.30	4.90	4.50	4.10	5.10	3.90
β, deg	0.50	0.42	0.43	0.36	0.50	0.31
c_{D_b}	0.0575	0.0611	0.0561	0.0560	0.0521	0.0559
Re $\times$ 10^{-6}	14.79	17.10	17.82	19.32	20.28	20.17
p_{ref}, kPa	37.643	37.297	37.109	36.869	37.384	36.784
(lb/ft^2)	(786.2)	(779.0)	(775.0)	(770.0)	(780.8)	(768.2)
M_∞	0.61	0.71	0.76	0.81	0.84	0.85
p_∞, kPa	37.705	37.350	37.102	36.755	37.432	36.607
(lb/ft^2)	(787.5)	(780.1)	(774.9)	(767.7)	(781.8)	(764.6)
h, m	7601	7667	7713	7779	7651	7807
(ft)	(24,936)	(25,154)	(25,305)	(25,521)	(25,103)	(25,612)
c_p at						
FC1	-0.0430	-0.0433	-0.0348	-0.0348	-0.0371	-0.0420
FC2	-0.0506	-0.0543	-0.0539	-0.0539	-0.0486	-0.0545
FC3	-0.0635	-0.0707	-0.0707	-0.0707	-0.0617	-0.0648
FC4	-0.0686	-0.0738	-0.0698	-0.0698	-0.0604	-0.0633
FC5	-0.0709	-0.0779	-0.0726	-0.0726	-0.0697	-0.0709
FC6	0.0095	0.0166	0.0179	0.0171	0.0096	0.0128
FC7	-0.0627	-0.0679	-0.0723	-0.0809	-0.0820	-0.0886
FC8	0	0	0	0	0	0
FC9	0.0026	0.0065	0.0089	0.0146	0.0166	0.0188
FC10	0.0019	0.0073	0.0099	0.0158	0.0178	0.0216
FC11	-0.0040	-0.0015	0.0011	0.0070	0.0079	0.0117
FC12	-0.0126	-0.0111	-0.0105	-0.0083	-0.0045	-0.0056
FC13	0.0217	0.0213	0.0187	0.0158	0.0106	0.0101
FC14	-0.0654	-0.0735	-0.0785	-0.0859	-0.0881	-0.0936
FC15	-0.0162	-0.0165	-0.0175	-0.0168	-0.0194	-0.0179
FC16	-0.0009	0.0049	0.0076	0.0146	0.0184	0.0195
FC17	0.0034	0.0090	0.0120	0.0201	0.0229	0.0260
FC18	-0.0056	-0.0016	0.0021	0.0080	0.0106	0.0150
FC19	-0.0298	-0.0305	-0.0266	-0.0234	-0.0148	-0.0176

TABLE 3. — Continued

(b) Continued

TP	F1207	F1208	F1209	F1210	F1211	F2201
M	0.87	0.88	0.91	0.93	0.95	0.70
α, deg	5.00	4.80	4.70	4.80	4.90	5.40
β, deg	0.40	0.41	0.37	0.27	0.39	-0.03
C_{D_b}	0.0520	0.0474	0.0478	0.0457	0.0438	0.0717
$Re \times 10^{-6}$	20.20	20.64	21.25	21.77	22.47	17.81
P_{ref}, kPa	36.991	37.242	37.135	36.901	37.017	42.233
(lb/ft^2)	(772.6)	(777.8)	(775.6)	(770.7)	(773.1)	(882.1)
M_∞	0.85	0.86	0.89	0.91	0.95	0.70
p_∞, kPa	36.786	37.289	37.132	36.934	36.701	42.262
(lb/ft^2)	(768.3)	(778.8)	(775.5)	(771.4)	(766.5)	(882.7)
h, m	7773	7678	7708	7745	7789	6795
(ft)	(25,501)	(25,191)	(25,288)	(25,409)	(25,554)	(22,292)
C_p at						
FC1	-0.0348	-0.0348	-0.0345	-0.0295	-0.0266	-0.0553
FC2	-0.0494	-0.0410	-0.0393	-0.0446	-0.0408	-0.0661
FC3	-0.0599	-0.0562	-0.0555	-0.0508	-0.0535	-0.0774
FC4	-0.0628	-0.0557	-0.0583	-0.0572	-0.0547	-0.0830
FC5	-0.0691	-0.0617	-0.0610	-0.0578	-0.0604	-0.0890
FC6	0.0102	0.0057	0.0071	0.0013	-0.0130	0.0182
FC7	-0.0875	-0.0845	-0.0896	-0.0979	-0.1131	-0.0787
FC8	0	0	0	0	0	0
FC9	0.0190	0.0187	0.0226	0.0286	0.0327	0.0084
FC10	0.0200	0.0196	0.0249	0.0314	0.0378	0.0048
FC11	0.0106	0.0101	0.0125	0.0203	0.0270	-0.0093
FC12	-0.0026	-0.0035	0.0004	0.0041	0.0043	-0.0176
FC13	0.0095	0.0078	0.0037	-0.0039	-0.0195	0.0180
FC14	-0.0933	-0.0903	-0.0957	-0.1045	-0.1188	-0.0842
FC15	-0.0187	-0.0194	-0.0185	-0.0174	-0.0134	-0.0216
FC16	0.0205	0.0216	0.0271	0.0322	0.0380	0.0026
FC17	0.0258	0.0256	0.0313	0.0385	0.0450	0.0056
FC18	0.0143	0.0151	0.0202	0.0270	0.0330	-0.0072
FC19	-0.0150	-0.0143	-0.0084	-0.0076	-0.0018	-0.0367

TABLE 3. — Continued

(b) Continued

TP	F2202	F2203	F2204	F2205	F2206	F2207
M	0.71	0.71	0.71	0.79	0.88	0.89
α, deg	4.10	6.30	6.20	5.00	4.90	5.90
β, deg	0.12	0.16	0.17	-0.02	-0.16	-0.22
C_{D_b}	0.0680	0.0635	0.0660	0.0686	0.0519	0.0488
Re × 10^{-6}	25.70	25.85	25.68	16.72	15.89	22.51
p_{ref}, kPa	69.307	69.158	69.175	32.731	25.689	42.185
(lb/ft^2)	(1447.5)	(1444.4)	(1444.8)	(683.6)	(536.5)	(881.1)
M_∞	0.71	0.71	0.71	0.80	0.90	0.90
p_∞, kPa	69.729	69.645	69.667	32.449	25.134	41.875
(lb/ft^2)	(1456.3)	(1454.6)	(1455.0)	(677.7)	(524.9)	(874.6)
h, m	3043	3052	3050	8635	10,329	6861
(ft)	(9983)	(10,014)	(10,006)	(28,330)	(33,886)	(22,508)
C_p at						
FC1	-0.0518	-0.0476	-0.0499	-0.0509	-0.0357	-0.0359
FC2	-0.0596	-0.0558	-0.0579	-0.0633	-0.0473	-0.0432
FC3	-0.0771	-0.0718	-0.0721	-0.0797	-0.0615	-0.0602
FC4	-0.0800	-0.0736	-0.0783	-0.0805	-0.0622	-0.0561
FC5	-0.0839	-0.0839	-0.0823	-0.0855	-0.0688	-0.0649
FC6	0.0281	0.0159	0.0162	0.0148	0.0060	-0.0009
FC7	-0.0736	-0.0789	-0.0785	-0.0863	-0.0999	-0.1061
FC8	0	0	0	0	0	0
FC9	0.0091	0.0103	0.0100	0.0144	0.0252	0.0288
FC10	0.0087	0.0103	0.0102	0.0113	0.0258	0.0312
FC11	-0.0010	0.0026	0.0007	-0.0033	0.0144	0.0197
FC12	-0.0118	-0.0099	-0.0089	-0.0146	-0.0015	0.0020
FC13	0.0238	0.0199	0.0196	0.0124	0.0009	-0.0083
FC14	-0.0797	-0.0860	-0.0857	-0.0910	-0.1017	-0.1098
FC15	-0.0171	-0.0184	-0.0179	-0.0214	-0.0163	-0.0151
FC16	0.0067	0.0068	0.0066	0.0111	0.0294	0.0332
FC17	0.0091	0.0110	0.0102	0.0160	0.0344	0.0398
FC18	-0.0020	-0.0005	-0.0002	0.0015	0.0207	0.0265
FC19	-0.0349	-0.0329	-0.0328	-0.0307	-0.0126	-0.0093

TABLE 3. — Continued

(b) Concluded

TP	F2208	F2209	F2210	F2211	F2212
M	0.90	0.92	0.93	1.23	1.53
α, deg	4.10	5.90	5.70	5.00	5.20
β, deg	-0.21	-0.24	-0.06	0.02	-0.14
C_{D_b}	0.0527	0.0478	0.0441	0.0678	
Re $\times 10^{-6}$	22.55	15.63	21.84	21.29	17.43
P_{ref}, kPa	41.889	23.187	38.008	24.248	14.190
(lb/ft^2)	(874.9)	(484.3)	(793.8)	(506.4)	(296.4)
M_∞	0.90	0.95	0.95	1.10	1.49
p_∞, kPa	41.580	22.425	37.267	28.853	15.079
(lb/ft^2)	(868.4)	(468.4)	(778.3)	(602.6)	(314.9)
h, m	6911	11,059	7682	9424	13,575
(ft)	(22,673)	(36,281)	(25,204)	(30,919)	(44,538)
C_p at					
FC1	-0.0351	-0.0351	-0.0296	-0.0611	
FC2	-0.0464	-0.0397	-0.0368	-0.0668	
FC3	-0.0640	-0.0551	-0.0552	-0.0735	
FC4	-0.0645	-0.0576	-0.0543	-0.0729	
FC5	-0.0703	-0.0610	-0.0583	-0.0710	
FC6	0.0431	0.0178	-0.0099	0.1854	0.1132
FC7	-0.1052	-0.0988	-0.1188	-0.0130	-0.0065
FC8	0	0	0	0	0
FC9	0.0277	0.0272	0.0356	0.0640	-0.0328
FC10	0.0322	0.0289	0.0390	0.0587	-0.0435
FC11	0.0191	0.0172	0.0262	0.0514	-0.0436
FC12	-0.0020	-0.0014	0.0047	0.0451	-0.0210
FC13	0.0411	0.0142	-0.0180	0.1882	0.1109
FC14	-0.1079	-0.1041	-0.1215	0.0142	-0.0137
FC15	-0.0138	-0.0092	-0.0100	-0.0424	-0.0263
FC16	0.0328	0.0384	0.0440	-0.0232	-0.0695
FC17	0.0387	0.0442	0.0504	-0.0157	-0.0695
FC18	0.0251	0.0287	0.0366	-0.0215	-0.0650
FC19	-0.0105	-0.0044	0.0002	-0.0262	-0.0791

TABLE 3. — Continued

(c) Trailing disk configuration, flight disk, x/D = 0.44

TP	F1301	F1302	F1303	F1304	F1305	F1306
M	0.70	0.71	0.70	0.79	0.89	0.89
α, deg	5.50	4.00	6.60	5.10	5.10	6.10
β, deg	-0.12	-0.13	-0.11	-0.08	-0.46	-0.24
C_{D_b}	-0.0225	-0.0207	-0.0325	-0.0250	-0.0226	-0.0305
$Re \times 10^{-6}$	18.47	26.77	26.76	17.56	15.62	23.45
p_{ref}, kPa	42.037	69.654	69.564	32.254	25.160	42.070
(lb/ft^2)	(878.0)	(1454.8)	(1452.9)	(673.6)	(525.5)	(878.7)
M_∞	0.71	0.71	0.71	0.80	0.90	0.90
p_∞, kPa	42.208	69.534	69.462	32.315	25.070	41.762
(lb/ft^2)	(881.5)	(1452.2)	(1450.8)	(674.9)	(523.6)	(872.2)
h, m	6804	3065	3073	8663	10,345	6880
(ft)	(22,322)	(10,055)	(10,081)	(28,420)	(33,940)	(22,571)
C_p at						
FC1	-0.1268	-0.1330	-0.1240	-0.1273	-0.1278	-0.1309
FC2	-0.1117	-0.1165	-0.1065	-0.1138	-0.1160	-0.1130
FC3	-0.0609	-0.0477	-0.0637	-0.0735	-0.0834	-0.0819
FC4	-0.2019	-0.2132	-0.1884	-0.1904	-0.1850	-0.1919
FC5	-0.1199	-0.1226	-0.1112	-0.1214	-0.1243	-0.1268
FC6	-0.1393	-0.1314	-0.1337	-0.1312	-0.1300	-0.1386
FC7	-0.2033	-0.2060	-0.1981	-0.1881	-0.1772	-0.1880
FC8	-0.1511	-0.1498	-0.1561	-0.1581	-0.1706	-0.1803
FC9	0.0867	0.0867	0.0933	0.0889	0.0850	0.0941
FC10	-0.1053	-0.1028	-0.1050	-0.1097	-0.1127	-0.1125
FC11	-0.2641	-0.2657	-0.2525	-0.2461	-0.2370	-0.2390
FC12	0.0885	0.0952	0.1039	0.0942	0.0975	0.1083
FC13	0.0954	0.0948	0.1041	0.0995	0.0987	0.1052
FC14	0.0906	0.1036	0.1080	0.1026	0.1059	0.1153
FC15	0.0981	0.1085	0.1099	0.1090	0.1125	0.1228
FC16	0.1056	0.1105	0.1115	0.1130	0.1068	0.1140
FC17	0.0874	0.0936	0.0982	0.0936	0.0918	0.1017
FC18	0.0835	0.0932	0.0960	0.0940	0.0905	0.1022
FC19	0.0849	0.0843	0.0916	0.0892	0.0854	0.0967

TABLE 3. — Continued

(c) Continued

TP	F1307	F1308	F1309	F1310	F1311	F1312
M	0.89	0.92	0.93	1.24	1.40	1.57
α, deg	4.10	6.10	5.80	5.50	5.10	5.00
β, deg	-0.46	-0.59	-0.32	-0.35	-0.13	0.11
C_{D_b}	-0.0251	-0.0220	-0.0327	0.1182	0.1916	0.2130
Re $\times$ 10^{-6}	23.34	14.88	22.96	21.58	18.49	16.60
p_{ref}, kPa	41.852	22.697	37.941	24.005	17.594	13.399
(lb/ft^2)	(874.1)	(474.0)	(792.4)	(501.4)	(367.5)	(279.9)
M_∞	0.90	0.95	0.95	1.10	1.31	1.51
p_∞, kPa	41.643	22.355	38.016	28.705	20.013	14.876
(lb/ft^2)	(869.7)	(466.9)	(794.0)	(599.5)	(418.0)	(310.7)
h, m	6900	11,078	7690	9458	11,780	13,661
(ft)	(22,638)	(36,345)	(25,229)	(31,030)	(38,648)	(44,820)
C_p at						
FC1	-0.1315	-0.1203	-0.1265	-0.2535	-0.2473	-0.2369
FC2	-0.1144	-0.1094	-0.1102	-0.2560	-0.2316	-0.2372
FC3	-0.0800	-0.0995	-0.0830	-0.1943	-0.2043	-0.2019
FC4	-0.1943	-0.1949	-0.1867	-0.2880	-0.2693	-0.2367
FC5	-0.1263	-0.0983	-0.1200	-0.1823	-0.1829	-0.2089
FC6	-0.1413	-0.1321	-0.1308	-0.2386	-0.2552	-0.2379
FC7	-0.1870	-0.1776	-0.1803	-0.2851	-0.2632	-0.2166
FC8	-0.1797	-0.1907	-0.1842	-0.0530	0.0041	-0.1030
FC9	0.0872	0.0887	0.0955	-0.0310	-0.1059	-0.1297
FC10	-0.1153	-0.1125	-0.1116	-0.2173	-0.2412	-0.2127
FC11	-0.2393	-0.2341	-0.2326	-0.2709	-0.1773	-0.2128
FC12	0.0997	0.1005	0.1096	-0.0018	-0.1265	-0.1782
FC13	0.0988	0.1038	0.1146	0.0021	-0.1240	-0.1754
FC14	0.1064	0.1061	0.1171	0.0077	-0.1175	-0.1702
FC15	0.1147	0.1178	0.1255	0.0276	-0.0987	-0.1642
FC16	0.1064	0.1046	0.1181	0.0033	-0.1146	-0.1596
FC17	0.0950	0.0913	0.1057	0.0013	-0.1167	-0.1797
FC18	0.0949	0.0857	0.1000	0.0004	-0.1231	-0.1835
FC19	0.0924	0.0798	0.0998	-0.0154	-0.1291	-0.1900

TABLE 3. — Continued

(c) Continued

TP	F2301	F2302	F2303	F2304	F2305
M	0.70	0.70	0.70	0.80	0.90
α, deg	5.40	4.10	6.40	5.00	5.10
β, deg	-0.81	0.05	0.04	-1.03	-1.42
C_{D_b}	-0.0147	-0.0154	-0.0241	-0.0186	-0.0172
Re × 10^{-6}	18.57	26.43	26.60	17.65	15.51
p_{ref}, kPa	41.878	69.861	69.717	32.088	25.216
(lb/ft^2)	(874.6)	(1459.1)	(1456.1)	(670.2)	(526.6)
M_∞	0.71	0.70	0.70	0.80	0.90
p_∞, kPa	42.255	69.633	69.659	32.286	25.214
(lb/ft^2)	(882.5)	(1454.3)	(1454.9)	(674.3)	(526.6)
h, m	6796	3054	3051	8669	10,308
(ft)	(22,296)	(10,018)	(10,009)	(28,442)	(33,818)
C_p at					
FC1	-0.1289	-0.1360	-0.1246	-0.1225	-0.1162
FC2	-0.1223	-0.1255	-0.1085	-0.1167	-0.1103
FC3	-0.0596	-0.0683	-0.0683	-0.0551	-0.0726
FC4	-0.1713	-0.2172	-0.2110	-0.1686	-0.1468
FC5	-0.1139	-0.1302	-0.1114	-0.1186	-0.1012
FC6	-0.1267	-0.1404	-0.1268	-0.1321	-0.1086
FC7	-0.1824	-0.2191	-0.2022	-0.1797	-0.1547
FC8	-0.0982	-0.1484	-0.1394	-0.1207	-0.1053
FC9	0.0917	0.0865	0.0990	0.0931	0.0878
FC10	-0.0968	-0.1171	-0.1042	-0.0937	-0.0938
FC11	-0.2323	-0.2726	-0.2520	-0.2190	-0.2073
FC12	0.0897	0.0871	0.1045	0.0867	0.0904
FC13	0.0940	0.0915	0.1073	0.0896	0.0889
FC14	0.0944	0.0924	0.1123	0.0907	0.0902
FC15	0.0976	0.1032	0.1139	0.1004	0.1032
FC16	0.0999	0.1033	0.1144	0.0955	0.0969
FC17	0.0862	0.0867	0.1016	0.0848	0.0832
FC18	0.0851	0.0860	0.0994	0.0828	0.0806
FC19	0.0836	0.0845	0.0946	0.0774	0.0674

TABLE 3. — Continued

(c) Concluded

TP	F2306	F2307	F2308	F2309	F2310
M	0.90	0.93	0.93	1.18	1.23
α, deg	4.20	6.10	5.80	5.50	5.60
β, deg	-0.98	-1.05	-1.06	-0.77	-0.77
C_{D_b}	-0.0211	-0.0176	-0.0260	0.1223	0.1382
Re $\times$ 10^{-6}	23.39	14.74	22.90	20.97	21.35
p_{ref}, kPa	41.778	22.645	37.713	25.613	24.492
(lb/ft^2)	(872.6)	(473.0)	(787.7)	(534.9)	(511.5)
M_∞	0.90	0.95	0.95	1.09	1.10
p_∞, kPa	41.629	22.448	37.162	28.863	28.844
(lb/ft^2)	(869.4)	(468.8)	(776.2)	(602.8)	(602.4)
h, m	6903	11,052	7702	9422	9426
(ft)	(22,646)	(36,259)	(25,268)	(30,911)	(30,925)
C_p at					
FC1	-0.1232	-0.1132	-0.1157	-0.2802	-0.2791
FC2	-0.1183	-0.1049	-0.1109	-0.2658	-0.2741
FC3	-0.0675	-0.0881	-0.0678	-0.2285	-0.1960
FC4	-0.1602	-0.1693	-0.1439	-0.3002	-0.2977
FC5	-0.1131	-0.1085	-0.1000	-0.2250	-0.1886
FC6	-0.1217	-0.1092	-0.1082	-0.2697	-0.2558
FC7	-0.1729	-0.1568	-0.1564	-0.3054	-0.2916
FC8	-0.1181	-0.1438	-0.1089	-0.1409	-0.0361
FC9	0.0916	0.0847	0.0982	-0.0430	-0.0421
FC10	-0.0995	-0.0981	-0.0927	-0.2968	-0.2358
FC11	-0.2294	-0.2210	-0.2124	-0.3406	-0.2964
FC12	0.0932	0.0965	0.1008	-0.0201	-0.0183
FC13	0.0940	0.0954	0.1016	-0.0197	-0.0099
FC14	0.0946	0.0972	0.1036	-0.0123	-0.0064
FC15	0.1079	0.1052	0.1160	-0.0082	0.0055
FC16	0.1005	0.0959	0.1044	-0.0192	-0.0152
FC17	0.0883	0.0888	0.0938	-0.0125	-0.0120
FC18	0.0861	0.0843	0.0925	-0.0161	-0.0075
FC19	0.0783	0.0687	0.0770	-0.0553	-0.0403

TABLE 3. — Continued

(d) Trailing disk configuration, flight disk, x/D = 0.50

TP	F1401	F1402	F1403	F1404	F1405	F1406
M	0.69	0.71	0.70	0.79	0.90	0.89
α, deg	5.60	4.00	6.50	5.20	5.20	6.00
β, deg	0.01	-0.29	-0.17	-0.23	-0.77	-0.24
C_{D_b}	-0.0223	-0.0217	-0.0317	-0.0304	-0.0393	-0.0419
Re × 10^{-6}	18.21	26.42	26.37	17.18	16.53	23.11
p_{ref}, kPa	42.186	69.809	69.803	32.387	25.025	41.835
(lb/ft^2)	(881.1)	(1458.0)	(1457.9)	(676.4)	(522.7)	(873.8)
M_∞	0.70	0.71	0.71	0.79	0.90	0.90
p_∞, kPa	42.266	69.543	69.652	32.450	24.988	41.510
(lb/ft^2)	(882.8)	(1452.4)	(1454.7)	(677.7)	(521.9)	(867.0)
h, m	6794	3064	3051	8635	10,366	6923
(ft)	(22,290)	(10,052)	(10,011)	(28,329)	(34,010)	(22,712)
C_p at						
FC1	-0.0891	-0.0866	-0.0779	-0.0799	-0.0698	-0.0767
FC2	-0.0767	-0.0722	-0.0713	-0.0701	-0.0582	-0.0720
FC3	-0.0560	-0.0356	-0.0452	-0.0515	-0.0448	-0.0590
FC4	-0.1475	-0.1487	-0.1409	-0.1403	-0.1582	-0.1459
FC5	-0.0890	-0.0771	-0.0706	-0.0845	-0.0788	-0.0825
FC6	-0.1056	-0.1044	-0.0952	-0.0989	-0.1291	-0.0974
FC7	-0.1638	-0.1657	-0.1585	-0.1302	-0.1451	-0.1560
FC8	-0.0794	-0.0770	-0.0634	-0.0912	-0.1431	-0.0964
FC9	0.0677	0.0645	0.0800	0.0855	0.0683	0.0930
FC10	-0.0652	-0.0555	-0.0588	-0.0652	-0.0566	-0.0715
FC11	-0.1962	-0.1873	-0.1927	-0.1814	-0.1454	-0.1802
FC12	0.0660	0.0769	0.0813	0.0787	0.0842	0.0929
FC13	0.0692	0.0781	0.0869	0.0840	0.0908	0.0975
FC14	0.0792	0.0742	0.0906	0.0924	0.0966	0.1038
FC15	0.0855	0.0820	0.0940	0.1024	0.1071	0.1229
FC16	0.0852	0.0813	0.0946	0.0977	0.0971	0.1089
FC17	0.0651	0.0636	0.0801	0.0786	0.0837	0.0945
FC18	0.0602	0.0584	0.0762	0.0742	0.0789	0.0882
FC19	0.0566	0.0500	0.0707	0.0693	0.0773	0.0844

TABLE 3. — Continued

(d) Continued

TP	F1407	F1408	F1409	F1410	F1411	F2401
M	0.90	0.92	0.93	1.23	1.40	0.71
α, deg	4.10	6.20	5.80	5.60	5.10	5.40
β, deg	-0.31	-0.29	-0.18	-0.53	-0.21	0.26
C_{D_b}	-0.0376	-0.0304	-0.0497	0.1180	0.2027	-0.0327
Re $\times$ 10^{-6}	23.12	16.11	22.61	21.93	20.51	18.21
P_{ref}, kPa	41.885	22.765	37.892	24.324	17.575	41.667
(lb/ft^2)	(874.8)	(475.5)	(791.4)	(508.0)	(367.1)	(870.2)
M_∞	0.90	0.95	0.95	1.10	1.31	0.71
p_∞, kPa	41.659	22.345	37.265	28.837	19.970	41.979
(lb/ft^2)	(870.1)	(466.7)	(778.3)	(602.3)	(417.1)	(876.8)
h, m	6897	11,081	7683	9427	11,793	6843
(ft)	(22,629)	(36,355)	(25,205)	(30,927)	(38,692)	(22,450)
C_p at						
FC1	-0.0808	-0.0786	-0.0719	-0.2598	-0.2296	-0.0826
FC2	-0.0745	-0.0753	-0.0629	-0.2297	-0.2334	-0.0687
FC3	-0.0603	-0.0738	-0.0514	-0.1162	-0.1633	-0.0574
FC4	-0.1405	-0.1378	-0.1448	-0.2283	-0.2697	-0.1335
FC5	-0.0870	-0.0874	-0.0782	-0.0966	-0.1174	-0.0873
FC6	-0.1020	-0.1015	-0.1215	-0.1844	-0.1968	-0.0999
FC7	-0.1594	-0.1479	-0.1515	-0.2134	-0.2334	-0.1595
FC8	-0.0953	-0.0973	-0.1269	0.0679	0.0098	-0.0756
FC9	0.0847	0.0829	0.0913	-0.0494	-0.1139	0.0750
FC10	-0.0679	-0.0742	-0.0642	-0.1790	-0.1782	-0.0561
FC11	-0.1794	-0.1727	-0.1485	-0.2455	-0.2343	-0.1922
FC12	0.0853	0.0847	0.0966	0.0061	-0.1334	0.0753
FC13	0.0888	0.0877	0.1004	0.0119	-0.1295	0.0793
FC14	0.0967	0.0909	0.1067	0.0233	-0.1229	0.0866
FC15	0.1158	0.1019	0.1265	0.0309	-0.1143	0.0944
FC16	0.0991	0.0937	0.1114	0.0185	-0.1098	0.0927
FC17	0.0856	0.0787	0.0960	0.0057	-0.1209	0.0735
FC18	0.0804	0.0722	0.0922	-0.0010	-0.1307	0.0671
FC19	0.0713	0.0663	0.0896	-0.0280	-0.1448	0.0594

TABLE 3. — Continued

(d)   Continued

TP	F2402	F2403	F2404	F2405	F2406
M	0.70	0.71	0.79	0.89	0.89
α, deg	4.00	6.40	5.10	5.20	6.10
β, deg	0.26	0.28	0.15	-0.24	-0.05
C_{D_b}	-0.0248	-0.0347	-0.0302	-0.0381	-0.0439
Re $\times$ 10^{-6}	26.23	26.28	17.12	16.41	22.83
p_{ref}, kPa	69.439	69.590	32.282	25.105	42.146
(lb/ft^2)	(1450.3)	(1453.4)	(674.2)	(524.3)	(880.2)
M_∞	0.71	0.71	0.80	0.90	0.89
p_∞, kPa	69.336	69.508	32.402	25.029	41.822
(lb/ft^2)	(1448.1)	(1451.7)	(676.7)	(522.8)	(873.5)
h, m	3087	3068	8645	10,355	6869
(ft)	(10,128)	(10,064)	(28,362)	(33,974)	(22,537)
C_p at					
FC1	-0.0885	-0.0802	-0.0805	-0.0784	-0.0764
FC2	-0.0708	-0.0682	-0.0699	-0.0721	-0.0741
FC3	-0.0480	-0.0563	-0.0553	-0.0580	-0.0541
FC4	-0.1409	-0.1390	-0.1390	-0.1405	-0.1421
FC5	-0.0857	-0.0740	-0.0869	-0.0875	-0.0855
FC6	-0.1038	-0.0965	-0.1008	-0.1007	-0.0976
FC7	-0.1614	-0.1603	-0.1574	-0.1535	-0.1570
FC8	-0.0657	-0.0716	-0.0923	-0.1062	-0.1022
FC9	0.0642	0.0819	0.0698	0.0873	0.0940
FC10	-0.0581	-0.0594	-0.0684	-0.0724	-0.0724
FC11	-0.1987	-0.1987	-0.1870	-0.1767	-0.1886
FC12	0.0701	0.0822	0.0728	0.0844	0.0964
FC13	0.0728	0.0879	0.0738	0.0883	0.0971
FC14	0.0787	0.0932	0.0817	0.0949	0.1041
FC15	0.0859	0.0979	0.0939	0.1100	0.1204
FC16	0.0821	0.0953	0.0875	0.1023	0.1059
FC17	0.0721	0.0806	0.0689	0.0831	0.0933
FC18	0.0594	0.0776	0.0648	0.0767	0.0887
FC19	0.0510	0.0677	0.0536	0.0753	0.0852

TABLE 3. — Concluded

(d) Concluded

TP	F2407	F2408	F2409	F2410	F2411
M	0.90	0.89	0.94	1.24	1.40
α, deg	4.10	5.20	5.90	5.10	5.20
β, deg	-0.27	-0.24	-0.21	0.03	0.09
C_{D_b}	-0.0407	-0.0381	-0.0468	0.1012	0.2127
$Re \times 10^{-6}$	22.95	16.41	22.43	21.93	20.59
p_{ref}, kPa	41.767	25.105	37.686	23.910	17.728
(lb/ft^2)	(872.3)	(524.3)	(787.1)	(499.4)	(370.3)
M_∞	0.90	0.90	0.95	1.10	1.32
p_∞, kPa	41.487	25.029	36.980	28.804	20.075
(lb/ft^2)	(866.5)	(522.8)	(772.3)	(601.6)	(419.3)
h, m	6927	10,355	7736	9435	11,761
(ft)	(22,725)	(33,974)	(25,381)	(30,955)	(38,584)
C_p at					
FC1	-0.0826	-0.0784	-0.0722	-0.2034	-0.2064
FC2	-0.0752	-0.0721	-0.0686	-0.2141	-0.2368
FC3	-0.0574	-0.0580	-0.0573	-0.1320	-0.2109
FC4	-0.1418	-0.1405	-0.1383	-0.2636	-0.2895
FC5	-0.0889	-0.0875	-0.0874	-0.0960	-0.1498
FC6	-0.1070	-0.1007	-0.0969	-0.1823	-0.2140
FC7	-0.1635	-0.1535	-0.1519	-0.2449	-0.2722
FC8	-0.1086	-0.1062	-0.1086	0.0747	-0.0131
FC9	0.0873	0.0873	0.0967	-0.0536	-0.1112
FC10	-0.0730	-0.0724	-0.0694	-0.1573	-0.2021
FC11	-0.1862	-0.1767	-0.1684	-0.2165	-0.2020
FC12	0.0867	0.0844	0.0962	0.0284	-0.1505
FC13	0.0892	0.0883	0.1003	0.0322	-0.1454
FC14	0.0968	0.0949	0.1075	0.0384	-0.1416
FC15	0.1153	0.1100	0.1252	0.0429	-0.1373
FC16	0.1004	0.1023	0.1107	0.0348	-0.1352
FC17	0.0858	0.0831	0.0941	0.0313	-0.1437
FC18	0.0823	0.0767	0.0909	0.0246	-0.1565
FC19	0.0732	0.0753	0.0823	0.0101	-0.1568

TABLE 4. — PRESSURE COEFFICIENTS AND RELATED PARAMETERS FOR
WIND-TUNNEL EXPERIMENT

(Refer to NOMENCLATURE for definitions of wind-tunnel configuration
test point designations such as W011, W012, and W013.)

(a) Blunt base configuration

TP	W011	W012	W013	W014	W311	W312	W313
M	0.30	0.50	0.71	0.82	0.30	0.50	0.71
α, deg	0.17	0.19	0.23	0.30	3.21	3.27	3.38
C_{D_b}	0.1531	0.1576	0.1615	0.1720	0.1789	0.1852	0.1989
C_D	0.2480	0.2436	0.2449	0.2569	0.2748	0.2699	0.2788
$Re \times 10^{-6}$	20.02	30.57	37.48	40.17	20.03	30.73	37.90
q, kPa	6.085	15.262	25.639	30.727	6.154	15.335	25.823
(lb/ft^2)	(127.1)	(318.7)	(535.5)	(641.8)	(128.5)	(320.3)	(539.3)
C_A	0.2479	0.2425	0.2439	0.2562	0.2658	0.2609	0.2696
C_M	0.0011	0.0028	0.0097	0.0187	0.0243	0.0284	0.0347
C_L	0.0553	0.0532	0.0322	0.0250	0.1520	0.1508	0.1470
C_p at							
WC1	-0.1430	-0.1669	-0.1627	-0.1706	-0.1573	-0.1743	-0.1923
WC2	-0.1867	-0.1901	-0.1903	-0.1904	-0.2000	-0.2036	-0.2194
WC3	-0.1936	-0.1938	-0.1934	-0.1907	-0.2038	-0.2057	-0.2198
WC4	-0.1926	-0.1951	-0.1920	-0.1912	-0.2034	-0.2058	-0.2183
WC5	-0.1880	-0.1914	-0.1878	-0.1902	-0.1994	-0.2029	-0.2152
WC6	-0.1785	-0.1810	-0.1846	-0.1835	-0.1939	-0.1980	-0.2097
WC7	-0.1658	-0.1685	-0.1715	-0.1743	-0.1919	-0.1937	-0.2066
WC8	-0.1869	-0.1906	-0.1890	-0.1776	-0.1932	-0.1911	-0.2151
WC9	-0.1897	-0.1931	-0.1920	-0.1699	-0.1892	-0.1970	-0.2135
WC10	-0.1919	-0.1947	-0.1862	-0.1628	-0.1914	-0.1968	-0.2125
WC11	-0.1822	-0.1866	-0.1800	-0.1518	-0.1898	-0.1945	-0.2118
WC12	-0.1600	-0.1644	-0.1672	-0.1428	-0.1807	-0.1865	-0.2018
WC13	-0.1536	-0.1642	-0.1739	-0.1867	-0.1833	-0.1889	-0.2045
WC14	-0.1447	-0.1548	-0.1670	-0.1845	-0.1743	-0.1814	-0.1945
WC15	-0.1293	-0.1367	-0.1632	-0.1763	-0.1532	-0.1606	-0.1717
WC16	-0.1227	-0.1329	-0.1534	-0.1702	-0.1359	-0.1481	-0.1589
WC17	-0.1170	-0.1229	-0.1447	-0.1588	-0.1246	-0.1379	-0.1523
WC18	-0.1565	-0.1629	-0.1596	-0.1953	-0.1929	-0.1983	-0.2142
WC19	-0.1509	-0.1561	-0.1549	-0.1941	-0.1952	-0.1998	-0.2148
WC20	-0.1481	-0.1455	-0.1401	-0.1846	-0.1911	-0.2001	-0.2110
WC21	-0.1384	-0.1412	-0.1436	-0.1732	-0.1898	-0.1956	-0.2107
WC22	-0.1325	-0.1377	-0.1344	-0.1679	-0.1864	-0.1911	-0.2060
WC23	-0.1251	-0.1292	-0.1294	-0.1615	-0.1789	-0.1851	-0.1981
WC55	-0.0244	-0.0243	-0.0238	-0.0145	-0.0381	-0.0403	-0.0421
WC56	-0.0215	-0.0215	-0.0209	-0.0107	-0.0356	-0.0393	-0.0420
WC57	-0.0288	-0.0301	-0.0286	-0.0188	-0.0402	-0.0440	-0.0466
WC58	-0.0285	-0.0296	-0.0293	-0.0190	-0.0395	-0.0450	-0.0469

TABLE 4. — Continued

TP	W011	W012	W013	W014	W311	W312	W313
M	0.30	0.50	0.71	0.82	0.30	0.50	0.71
α, deg	0.17	0.19	0.23	0.30	3.21	3.27	3.38
C_{D_b}	0.1531	0.1576	0.1615	0.1720	0.1789	0.1852	0.1989
C_D	0.2480	0.2436	0.2449	0.2569	0.2748	0.2699	0.2788
Re $\times$ 10^{-6}	20.02	30.57	37.48	40.17	20.03	30.73	37.90
q, kPa	6.085	15.262	25.639	30.727	6.154	15.335	25.823
(lb/ft^2)	(127.1)	(318.7)	(535.5)	(641.8)	(128.5)	(320.3)	(539.3)
C_A	0.2479	0.2425	0.2439	0.2562	0.2658	0.2609	0.2696
C_M	0.0011	0.0028	0.0097	0.0187	0.0243	0.0284	0.0347
C_L	0.0553	0.0532	0.0322	0.0250	0.1520	0.1508	0.1470
C_p at							
WC59	-0.0198	-0.0208	-0.0180	-0.0075	-0.0306	-0.0344	-0.0354
WC60	-0.0170	-0.0183	-0.0156	-0.0055	-0.0263	-0.0288	-0.0299
WC61	-0.0118	-0.0133	-0.0086	-0.0002	-0.0154	-0.0158	-0.0162
WC62	-0.0177	-0.0199	-0.0160	-0.0073	-0.0159	-0.0174	-0.0169
WC63	-0.0152	-0.0168	-0.0129	-0.0048	-0.0070	-0.0071	-0.0056
WC64	-0.0158	-0.0178	-0.0141	-0.0046	-0.0010	-0.0017	0.0020
WC65	-0.0067	-0.0075	-0.0033	0.0069	0.0156	0.0158	0.0204
WC66	-0.0051	-0.0064	-0.0025	0.0077	0.0173	0.0186	0.0225
WC67	-0.0140	-0.0141	-0.0120	-0.0022	0.0084	0.0075	0.0128
WC68	-0.0247	-0.0266	-0.0242	-0.0147	-0.0074	-0.0099	-0.0054
WC69	-0.0198	-0.0206	-0.0182	-0.0077	-0.0075	-0.0091	-0.0046
WC70	-0.0168	-0.0177	-0.0141	-0.0038	-0.0130	-0.0143	-0.0113
WC71	-0.0085	-0.0088	-0.0052	0.0061	-0.0105	-0.0113	-0.0078
WC72	-0.0129	-0.0136	-0.0111	-0.0021	-0.0238	-0.0257	-0.0238
WC73	-0.0127	-0.0126	-0.0114	-0.0018	-0.0263	-0.0280	-0.0291
WC74	-0.0127	-0.0129	-0.0122	-0.0034	-0.0303	-0.0320	-0.0335
WC75	-0.0162	-0.0169	-0.0140	-0.0069	-0.0339	-0.0373	-0.0387
WC76	-0.0219	-0.0230	-0.0216	-0.0140	-0.0392	-0.0420	-0.0429
WC77	-0.0297	-0.0310	-0.0308	-0.0223	-0.0443	-0.0484	-0.0495
WC78	-0.0502	-0.0550	-0.0627	-0.0681	-0.0458	-0.0526	-0.0623
WC79	-0.0434	-0.0474	-0.0552	-0.0617	-0.0440	-0.0508	-0.0604
WC80	-0.0452	-0.0493	-0.0561	-0.0613	-0.0473	-0.0539	-0.0625
WC81	-0.0442	-0.0481	-0.0543	-0.0592	-0.0516	-0.0582	-0.0671
WC82	-0.0261	-0.0264	-0.0319	-0.0355	-0.0374	-0.0404	-0.0483
WC83	-0.0421	-0.0462	-0.0534	-0.0565	-0.0575	-0.0647	-0.0727
WC84	-0.0324	-0.0346	-0.0395	-0.0394	-0.0462	-0.0501	-0.0564
WC85	-0.0325	-0.0347	-0.0406	-0.0397	-0.0482	-0.0529	-0.0587

TABLE 4. — Continued

TP	W011	W012	W013	W014	W311	W312	W313
M	0.30	0.50	0.71	0.82	0.30	0.50	0.71
α, deg	0.17	0.19	0.23	0.30	3.21	3.27	3.38
C_{D_b}	0.1531	0.1576	0.1615	0.1720	0.1789	0.1852	0.1989
C_D	0.2480	0.2436	0.2449	0.2569	0.2748	0.2699	0.2788
Re × 10^{-6}	20.02	30.57	37.48	40.17	20.03	30.73	37.90
q, kPa	6.085	15.262	25.639	30.727	6.154	15.335	25.823
(lb/ft^2)	(127.1)	(318.7)	(535.5)	(641.8)	(128.5)	(320.3)	(539.3)
C_A	0.2479	0.2425	0.2439	0.2562	0.2658	0.2609	0.2696
C_M	0.0011	0.0028	0.0097	0.0187	0.0243	0.0284	0.0347
C_L	0.0553	0.0532	0.0322	0.0250	0.1520	0.1508	0.1470
C_p at							
WC86	-0.0301	-0.0323	-0.0364	-0.0339	-0.0403	-0.0434	-0.0495
WC87	-0.0290	-0.0311	-0.0360	-0.0321	-0.0312	-0.0325	-0.0374
WC88	-0.0460	-0.0516	-0.0547	-0.0483	-0.0427	-0.0469	-0.0544
WC89	-0.0488	-0.0538	-0.0583	-0.0513	-0.0425	-0.0484	-0.0551
WC90	-0.0441	-0.0500	-0.0565	-0.0483	-0.0396	-0.0461	-0.0528
WC91	-0.0427	-0.0481	-0.0572	-0.0533	-0.0461	-0.0523	-0.0569
WC92	-0.0422	-0.0486	-0.0544	-0.0517	-0.0484	-0.0553	-0.0602
WC93	-0.0195	-0.0212	-0.0266	-0.0275	-0.0250	-0.0264	-0.0301
WC94	-0.0280	-0.0298	-0.0352	-0.0381	-0.0394	-0.0415	-0.0467
WC95	-0.0332	-0.0351	-0.0425	-0.0467	-0.0474	-0.0506	-0.0571
WC96	-0.0422	-0.0476	-0.0540	-0.0604	-0.0540	-0.0613	-0.0700
WC97	-0.0320	-0.0351	-0.0419	-0.0478	-0.0424	-0.0470	-0.0565
WC98	-0.0230	-0.0254	-0.0319	-0.0382	-0.0332	-0.0365	-0.0460
WC99	-0.0308	-0.0342	-0.0401	-0.0443	-0.0371	-0.0422	-0.0525
WC100	-0.0469	-0.0529	-0.0594	-0.0674	-0.0467	-0.0537	-0.0642
WC101	-0.1137	-0.1176	-0.1203	-0.1240	-0.1300	-0.1355	-0.1462
WC102	-0.1132	-0.1142	-0.1174	-0.1170	-0.1272	-0.1326	-0.1444
WC103	-0.1207	-0.1238	-0.1270	-0.1231	-0.1303	-0.1380	-0.1516
WC104	-0.1140	-0.1162	-0.1179	-0.1133	-0.1293	-0.1346	-0.1469
WC105	-0.1187	-0.1219	-0.1258	-0.1186	-0.1334	-0.1418	-0.1535
WC106	-0.1156	-0.1198	-0.1208	-0.1145	-0.1331	-0.1407	-0.1531
WC107	-0.1126	-0.1167	-0.1186	-0.1117	-0.1279	-0.1313	-0.1437
WC108	-0.1076	-0.1134	-0.1178	-0.1115	-0.1216	-0.1270	-0.1389
WC109	-0.1016	-0.1069	-0.1114	-0.1042	-0.1068	-0.1106	-0.1225
WC110	-0.1047	-0.1120	-0.1173	-0.1181	-0.1084	-0.1134	-0.1263
WC111	-0.0996	-0.1088	-0.1148	-0.1177	-0.0997	-0.1072	-0.1190
WC112	-0.0543	-0.0601	-0.0553	-0.0621	-0.0565	-0.0662	-0.0724

TABLE 4. — Continued

(a) Concluded

TP	W011	W012	W013	W014	W311	W312	W313
M	0.30	0.50	0.71	0.82	0.30	0.50	0.71
α, deg	0.17	0.19	0.23	0.30	3.21	3.27	3.38
C_{D_b}	0.1531	0.1576	0.1615	0.1720	0.1789	0.1852	0.1989
C_D	0.2480	0.2436	0.2449	0.2569	0.2748	0.2699	0.2788
$Re \times 10^{-6}$	20.02	30.57	37.48	40.17	20.03	30.73	37.90
q, kPa	6.085	15.262	25.639	30.727	6.154	15.335	25.823
(lb/ft^2)	(127.1)	(318.7)	(535.5)	(641.8)	(128.5)	(320.3)	(539.3)
C_A	0.2479	0.2425	0.2439	0.2562	0.2658	0.2609	0.2696
C_M	0.0011	0.0028	0.0097	0.0187	0.0243	0.0284	0.0347
C_L	0.0553	0.0532	0.0322	0.0250	0.1520	0.1508	0.1470
C_p at							
WC113	-0.0932	-0.0995	-0.1117	-0.1222	-0.0963	-0.1049	-0.1164
WC114	-0.0875	-0.0914	-0.1061	-0.1188	-0.0955	-0.1039	-0.1125
WC115	-0.0944	-0.1018	-0.1151	-0.1300	-0.1131	-0.1229	-0.1298
WC116	-0.0879	-0.0923	-0.1038	-0.1203	-0.1126	-0.1205	-0.1286
WC117	-0.0901	-0.0946	-0.1039	-0.1186	-0.1215	-0.1291	-0.1372
WC118	-0.0905	-0.0963	-0.1032	-0.1173	-0.1237	-0.1311	-0.1404
WC119	-0.0958	-0.1005	-0.1042	-0.1191	-0.1271	-0.1344	-0.1446
WC120	-0.0845	-0.0818	-0.0847	-0.0962	-0.1106	-0.1124	-0.1220
WC121	-0.1117	-0.1136	-0.1167	-0.1267	-0.1307	-0.1366	-0.1483
WC122	-0.0989	-0.0975	-0.0986	-0.1084	-0.1176	-0.1209	-0.1321
WC123	-0.1164	-0.1215	-0.1232	-0.1292	-0.1305	-0.1390	-0.1493
WC124	-0.0551	-0.0634	-0.0804	-0.0929	-0.0507	-0.0609	-0.0815
WC125	-0.0427	-0.0495	-0.0677	-0.0932	-0.0532	-0.0649	-0.0875
WC126	-0.0467	-0.0524	-0.0680	-0.0943	-0.0494	-0.0586	-0.0770
WC127	-0.0399	-0.0443	-0.0527	-0.0594	-0.0422	-0.0494	-0.0620
WC128	-0.0409	-0.0457	-0.0522	-0.0553	-0.0445	-0.0517	-0.0626
WC129	-0.0432	-0.0462	-0.0520	-0.0549	-0.0471	-0.0527	-0.0609
WC130	-0.0501	-0.0533	-0.0596	-0.0624	-0.0550	-0.0607	-0.0684
WC131	-0.0612	-0.0639	-0.0680	-0.0677	-0.0697	-0.0746	-0.0819
WC132	-0.0419	-0.0477	-0.0622	-0.0836	-0.0516	-0.0620	-0.0816
WC133	-0.0413	-0.0481	-0.0641	-0.0977	-0.0528	-0.0635	-0.0856
WC134	-0.0451	-0.0516	-0.0661	-0.0967	-0.0535	-0.0635	-0.0810
WC135	-0.0350	-0.0409	-0.0512	-0.0703	-0.0448	-0.0509	-0.0647
WC136	-0.0396	-0.0449	-0.0535	-0.0648	-0.0474	-0.0524	-0.0643
WC137	-0.0443	-0.0494	-0.0564	-0.0585	-0.0507	-0.0563	-0.0659
WC138	-0.0232	-0.0235	-0.0276	-0.0314	-0.0404	-0.0424	-0.0491
WC139	-0.0534	-0.0576	-0.0612	-0.0636	-0.0656	-0.0699	-0.0764

TABLE 4. — Continued

(b) Trailing disk configuration,
wind-tunnel disk, x/D = 0.20

TP	W021	W022	W023	W024
M	0.30	0.50	0.71	0.82
α, deg	0.36	0.37	0.42	0.49
c_{D_b}	0.1501	0.1643	0.1712	0.1841
c_D	0.2462	0.2510	0.2548	0.2734
Re $\times$ 10^{-6}	19.93	30.30	37.68	39.90
q, kPa	6.085	15.189	25.620	30.692
(lb/ft^2)	(127.1)	(317.2)	(535.1)	(641.0)
c_A	0.2459	0.2506	0.2546	0.2733
c_M	0.0044	0.0041	0.0157	0.0278
c_L	0.0568	0.0535	0.0349	0.0101
c_p at				
WC1	-0.1661	-0.1914	-0.1857	-0.2016
WC2	-0.1666	-0.1932	-0.1850	-0.2030
WC3	-0.1681	-0.1906	-0.1860	-0.1999
WC4	-0.1676	-0.1921	-0.1862	-0.2030
WC5	-0.1639	-0.1919	-0.1845	-0.1996
WC6	-0.1639	-0.1884	-0.1845	-0.1947
WC7	-0.1661	-0.1939	-0.1843	-0.1997
WC8	-0.1662	-0.1907	-0.1860	-0.2026
WC9	-0.1695	-0.1929	-0.1870	-0.2031
WC10	-0.1678	-0.1919	-0.1873	-0.2013
WC11	-0.1593	-0.1880	-0.1809	-0.1994
WC12	-0.1657	-0.1912	-0.1848	-0.1999
WC13	-0.1666	-0.1920	-0.1856	-0.2021
WC14	-0.1701	-0.1921	-0.1880	-0.2023
WC15	-0.1665	-0.1879	-0.1818	-0.1999
WC16	-0.1623	-0.1843	-0.1767	-0.1925
WC17	-0.1644	-0.1918	-0.1868	-0.2026
WC18	-0.1683	-0.1953	-0.1871	-0.2036
WC19	-0.1677	-0.1928	-0.1886	-0.2037
WC20	-0.1667	-0.1910	-0.1844	-0.2028
WC21	-0.1669	-0.1852	-0.1817	-0.1929
WC22	-0.1582	-0.1838	-0.1777	-0.1892
WC23	-0.1662	-0.1900	-0.1851	-0.2026
WC24	-0.1666	-0.1912	-0.1854	-0.2027
WC25	-0.1674	-0.1926	-0.1864	-0.2030
WC26	-0.1677	-0.1918	-0.1875	-0.2040
WC27	-0.1659	-0.1902	-0.1856	-0.2014
WC28	-0.1663	-0.1916	-0.1860	-0.2002

TABLE 4. — Continued

(b)   Continued

TP	W021	W022	W023	W024
M	0.30	0.50	0.71	0.82
α, deg	0.36	0.37	0.42	0.49
C_{D_b}	0.1501	0.1643	0.1712	0.1841
C_D	0.2462	0.2510	0.2548	0.2734
Re $\times$ 10^{-6}	19.93	30.30	37.68	39.90
q, kPa	6.085	15.189	25.620	30.692
(lb/ft^2)	(127.1)	(317.2)	(535.1)	(641.0)
C_A	0.2459	0.2506	0.2546	0.2733
C_M	0.0044	0.0041	0.0157	0.0278
C_L	0.0568	0.0535	0.0349	0.0101
C_p at				
WC29	-0.1680	-0.1931	-0.1886	-0.2003
WC30	-0.1651	-0.1909	-0.1865	-0.2047
WC31	-0.1672	-0.1924	-0.1863	-0.2026
WC32	-0.1655	-0.1939	-0.1881	-0.2050
WC33	-0.1700	-0.1963	-0.1904	-0.2064
WC34	-0.1663	-0.1902	-0.1864	-0.2011
WC35	-0.1659	-0.1922	-0.1868	-0.2050
WC36	-0.1670	-0.1935	-0.1877	-0.2060
WC37	-0.1700	-0.1966	-0.1906	-0.2084
WC38	-0.1075	-0.1064	-0.1293	-0.1501
WC39	-0.1227	-0.1227	-0.1432	-0.1610
WC40	-0.1341	-0.1445	-0.1575	-0.1756
WC41	-0.1494	-0.1616	-0.1751	-0.1904
WC42	-0.1610	-0.1814	-0.1896	-0.2012
WC43	-0.1126	-0.1246	-0.1378	-0.1629
WC44	-0.1232	-0.1425	-0.1506	-0.1805
WC45	-0.1347	-0.1620	-0.1653	-0.1929
WC46	-0.1466	-0.1737	-0.1779	-0.2021
WC47	-0.1099	-0.1080	-0.1297	-0.1481
WC48	-0.1204	-0.1169	-0.1388	-0.1564
WC49	-0.1335	-0.1286	-0.1541	-0.1674
WC50	-0.1422	-0.1465	-0.1672	-0.1767
WC51	-0.1139	-0.1152	-0.1403	-0.1475
WC52	-0.1306	-0.1240	-0.1567	-0.1530
WC53	-0.1429	-0.1393	-0.1638	-0.1655
WC54	-0.1588	-0.1606	-0.1836	-0.1875
WC55	-0.0226	-0.0259	-0.0233	-0.0192
WC56	-0.0193	-0.0226	-0.0200	-0.0152

50

TABLE 4. — Continued

(b) Continued

TP	W021	W022	W023	W024
M	0.30	0.50	0.71	0.82
α, deg	0.36	0.37	0.42	0.49
C_{D_b}	0.1501	0.1643	0.1712	0.1841
C_D	0.2462	0.2510	0.2548	0.2734
Re $\times$ 10^{-6}	19.93	30.30	37.68	39.90
q, kPa	6.085	15.189	25.620	30.692
(lb/ft^2)	(127.1)	(317.2)	(535.1)	(641.0)
C_A	0.2459	0.2506	0.2546	0.2733
C_M	0.0044	0.0041	0.0157	0.0278
C_L	0.0568	0.0535	0.0349	0.0101
C_p at				
WC57	-0.0264	-0.0307	-0.0265	-0.0224
WC58	-0.0267	-0.0302	-0.0270	-0.0222
WC59	-0.0184	-0.0207	-0.0168	-0.0116
WC60	-0.0163	-0.0188	-0.0135	-0.0069
WC61	-0.0112	-0.0118	-0.0057	0.0007
WC62	-0.0160	-0.0176	-0.0124	-0.0056
WC63	-0.0142	-0.0138	-0.0087	-0.0017
WC64	-0.0147	-0.0150	-0.0096	-0.0021
WC65	-0.0036	-0.0031	0.0031	0.0103
WC66	-0.0021	-0.0017	0.0037	0.0111
WC67	-0.0098	-0.0102	-0.0063	0.0015
WC68	-0.0210	-0.0226	-0.0194	-0.0120
WC69	-0.0159	-0.0169	-0.0133	-0.0058
WC70	-0.0140	-0.0143	-0.0110	-0.0035
WC71	-0.0059	-0.0058	-0.0031	0.0046
WC72	-0.0110	-0.0122	-0.0107	-0.0037
WC73	-0.0117	-0.0112	-0.0116	-0.0038
WC74	-0.0122	-0.0125	-0.0127	-0.0054
WC75	-0.0163	-0.0176	-0.0178	-0.0107
WC76	-0.0214	-0.0230	-0.0239	-0.0170
WC77	-0.0287	-0.0313	-0.0320	-0.0244
WC78	-0.0454	-0.0529	-0.0644	-0.0788
WC79	-0.0410	-0.0476	-0.0598	-0.0723
WC80	-0.0427	-0.0489	-0.0608	-0.0731
WC81	-0.0416	-0.0472	-0.0591	-0.0713
WC82	-0.0244	-0.0274	-0.0373	-0.0495
WC83	-0.0399	-0.0459	-0.0586	-0.0678
WC84	-0.0298	-0.0330	-0.0432	-0.0523

TABLE 4. — Continued

(b) Continued

TP	W021	W022	W023	W024
M	0.30	0.50	0.71	0.82
α, deg	0.36	0.37	0.42	0.49
C_{D_b}	0.1501	0.1643	0.1712	0.1841
C_D	0.2462	0.2510	0.2548	0.2734
$Re \times 10^{-6}$	19.93	30.30	37.68	39.90
q, kPa	6.085	15.189	25.620	30.692
(lb/ft^2)	(127.1)	(317.2)	(535.1)	(641.0)
C_A	0.2459	0.2506	0.2546	0.2733
C_M	0.0044	0.0041	0.0157	0.0278
C_L	0.0568	0.0535	0.0349	0.0101
C_p at				
WC85	-0.0298	-0.0345	-0.0455	-0.0559
WC86	-0.0254	-0.0290	-0.0415	-0.0520
WC87	-0.0207	-0.0248	-0.0340	-0.0432
WC88	-0.0396	-0.0468	-0.0557	-0.0598
WC89	-0.0425	-0.0497	-0.0615	-0.0589
WC90	-0.0400	-0.0480	-0.0590	-0.0578
WC91	-0.0440	-0.0467	-0.0588	-0.0636
WC92	-0.0431	-0.0452	-0.0573	-0.0620
WC93	-0.0202	-0.0209	-0.0323	-0.0369
WC94	-0.0279	-0.0294	-0.0395	-0.0466
WC95	-0.0352	-0.0381	-0.0481	-0.0582
WC96	-0.0415	-0.0474	-0.0592	-0.0695
WC97	-0.0320	-0.0357	-0.0464	-0.0573
WC98	-0.0242	-0.0278	-0.0392	-0.0493
WC99	-0.0308	-0.0346	-0.0464	-0.0572
WC100	-0.0456	-0.0523	-0.0642	-0.0773
WC101	-0.1158	-0.1294	-0.1343	-0.1462
WC102	-0.1117	-0.1271	-0.1295	-0.1448
WC103	-0.1184	-0.1349	-0.1384	-0.1527
WC104	-0.1124	-0.1289	-0.1296	-0.1442
WC105	-0.1171	-0.1337	-0.1371	-0.1525
WC106	-0.1151	-0.1315	-0.1341	-0.1510
WC107	-0.1131	-0.1288	-0.1306	-0.1462
WC108	-0.1093	-0.1248	-0.1273	-0.1433
WC109	-0.1015	-0.1165	-0.1175	-0.1322
WC110	-0.1109	-0.1259	-0.1272	-0.1414
WC111	-0.1089	-0.1231	-0.1274	-0.1392
WC112	-0.0572	-0.0582	-0.0618	-0.0698

TABLE 4. — Continued

(b) Concluded

TP	W021	W022	W023	W024
M	0.30	0.50	0.71	0.82
α, deg	0.36	0.37	0.42	0.49
c_{D_b}	0.1501	0.1643	0.1712	0.1841
c_D	0.2462	0.2510	0.2548	0.2734
Re $\times$ 10^{-6}	19.93	30.30	37.68	39.90
q, kPa	6.085	15.189	25.620	30.692
(lb/ft^2)	(127.1)	(317.2)	(535.1)	(641.0)
c_A	0.2459	0.2506	0.2546	0.2733
c_M	0.0044	0.0041	0.0157	0.0278
c_L	0.0568	0.0535	0.0349	0.0101
c_p at				
WC113	-0.1149	-0.1248	-0.1291	-0.1395
WC114	-0.1100	-0.1219	-0.1263	-0.1358
WC115	-0.1214	-0.1335	-0.1390	-0.1502
WC116	-0.1132	-0.1251	-0.1293	-0.1403
WC117	-0.1147	-0.1277	-0.1315	-0.1426
WC118	-0.1112	-0.1250	-0.1301	-0.1410
WC119	-0.1120	-0.1264	-0.1314	-0.1433
WC120	-0.0959	-0.1039	-0.1076	-0.1183
WC121	-0.1175	-0.1327	-0.1376	-0.1492
WC122	-0.1033	-0.1136	-0.1177	-0.1303
WC123	-0.1162	-0.1315	-0.1373	-0.1468
WC124	-0.0539	-0.0683	-0.0857	-0.1064
WC125	-0.0472	-0.0621	-0.0833	-0.1222
WC126	-0.0452	-0.0546	-0.0748	-0.1129
WC127	-0.0362	-0.0435	-0.0602	-0.0854
WC128	-0.0381	-0.0444	-0.0587	-0.0757
WC129	-0.0414	-0.0467	-0.0572	-0.0680
WC130	-0.0482	-0.0543	-0.0649	-0.0741
WC131	-0.0597	-0.0660	-0.0742	-0.0833
WC132	-0.0420	-0.0495	-0.0761	-0.0940
WC133	-0.0440	-0.0511	-0.0826	-0.1193
WC134	-0.0439	-0.0513	-0.0780	-0.1144
WC135	-0.0354	-0.0417	-0.0612	-0.0848
WC136	-0.0372	-0.0433	-0.0595	-0.0752
WC137	-0.0437	-0.0507	-0.0608	-0.0700
WC138	-0.0247	-0.0266	-0.0333	-0.0436
WC139	-0.0563	-0.0617	-0.0686	-0.0768

TABLE 4. — Continued

(c) Trailing disk configuration,
wind-tunnel disk, x/D = 0.40

TP	W031	W032	W033	W034
M	0.30	0.50	0.71	0.82
α, deg	0.34	0.37	0.43	0.50
C_{D_b}	0.1261	0.1496	0.1794	0.1912
C_D	0.2265	0.2431	0.2626	0.2681
Re $\times$ 10^{-6}	19.67	30.00	36.93	38.93
q, kPa	6.086	15.161	25.563	30.658
(lb/ft^2)	(127.1)	(316.6)	(533.9)	(640.3)
C_A	0.2262	0.2429	0.2623	0.2679
C_M	0.0112	0.0140	0.0188	0.0253
C_L	0.0415	0.0361	0.0289	0.0196
C_p at				
WC1	-0.1341	-0.1615	-0.2152	-0.2709
WC2	-0.1581	-0.1843	-0.2270	-0.2813
WC3	-0.2628	-0.2861	-0.3173	-0.3510
WC4	-0.3498	-0.3674	-0.3909	-0.4053
WC5	-0.3735	-0.3869	-0.4085	-0.4194
WC6	-0.2728	-0.2897	-0.3216	-0.3528
WC7	-0.1114	-0.1312	-0.1866	-0.2446
WC8	-0.1845	-0.2024	-0.2405	-0.2996
WC9	-0.2804	-0.3019	-0.3367	-0.3737
WC10	-0.3514	-0.3718	-0.4000	-0.4309
WC11	-0.2484	-0.2666	-0.2983	-0.3526
WC12	-0.1212	-0.1491	-0.2059	-0.2700
WC13	-0.2262	-0.2497	-0.2930	-0.3352
WC14	-0.3665	-0.3901	-0.4151	-0.4317
WC15	-0.3342	-0.3532	-0.3748	-0.4013
WC16	-0.2438	-0.2665	-0.3026	-0.3477
WC17	-0.1410	-0.1634	-0.2109	-0.2741
WC18	-0.2295	-0.2505	-0.2861	-0.3280
WC19	-0.3086	-0.3333	-0.3569	-0.3849
WC20	-0.3488	-0.3751	-0.3967	-0.4191
WC21	-0.3014	-0.3242	-0.3522	-0.3824
WC22	-0.2335	-0.2589	-0.2981	-0.3378
WC23	-0.1740	-0.1972	-0.2596	-0.3092
WC24	-0.2041	-0.2265	-0.2718	-0.3327
WC25	-0.2508	-0.2714	-0.3096	-0.3506
WC26	-0.3262	-0.3479	-0.3759	-0.4049
WC27	-0.2077	-0.2369	-0.2632	-0.3069
WC28	-0.2636	-0.2850	-0.3194	-0.3619

TABLE 4. — Continued

(c) Continued

TP	W031	W032	W033	W034
M	0.30	0.50	0.71	0.82
α, deg	0.34	0.37	0.43	0.50
C_{D_b}	0.1261	0.1496	0.1794	0.1912
C_D	0.2265	0.2431	0.2626	0.2681
Re $\times$ 10^{-6}	19.67	30.00	36.93	38.93
q, kPa	6.086	15.161	25.563	30.658
(lb/ft^2)	(127.1)	(316.6)	(533.9)	(640.3)
C_A	0.2262	0.2429	0.2623	0.2679
C_M	0.0112	0.0140	0.0188	0.0253
C_L	0.0415	0.0361	0.0289	0.0196
C_p at				
WC29	-0.3436	-0.3657	-0.3899	-0.4169
WC30	-0.1701	-0.1922	-0.2436	-0.3029
WC31	-0.2190	-0.2456	-0.2867	-0.3345
WC32	-0.3043	-0.3283	-0.3594	-0.3936
WC33	-0.3659	-0.3884	-0.4144	-0.4410
WC34	-0.2078	-0.2248	-0.2676	-0.3243
WC35	-0.2284	-0.2507	-0.2884	-0.3409
WC36	-0.3073	-0.3267	-0.3563	-0.3890
WC37	-0.4617	-0.4821	-0.5060	-0.5149
WC38	-0.0781	-0.1114	-0.1235	-0.1004
WC39	-0.0337	-0.0666	-0.1273	-0.0869
WC40	-0.0400	-0.0641	-0.1181	-0.1058
WC41	-0.0237	-0.0538	-0.1008	-0.0827
WC42	-0.0383	-0.0601	-0.0779	-0.0790
WC43	0.0019	-0.0685	-0.1225	-0.0960
WC44	-0.0606	-0.0706	-0.0856	-0.0839
WC45	-0.0498	-0.0696	-0.0792	-0.0831
WC46	-0.0176	-0.0671	-0.0909	-0.0770
WC47	-0.0511	-0.0963	-0.0922	-0.0951
WC48	-0.0516	-0.0664	-0.1052	-0.1014
WC49	-0.0479	-0.0822	-0.1061	-0.0946
WC50	-0.0069	-0.0484	-0.0781	-0.0649
WC51	-0.0357	-0.0894	-0.1137	-0.0808
WC52	-0.0425	-0.0580	-0.1031	-0.0824
WC53	-0.0393	-0.0467	-0.0720	-0.0724
WC54	-0.0072	-0.0177	-0.0463	-0.0498
WC55	-0.0239	-0.0259	-0.0241	-0.0189
WC56	-0.0202	-0.0224	-0.0206	-0.0145

TABLE 4. — Continued

(c) Continued

TP	W031	W032	W033	W034
M	0.30	0.50	0.71	0.82
α, deg	0.34	0.37	0.43	0.50
c_{D_b}	0.1261	0.1496	0.1794	0.1912
c_D	0.2265	0.2431	0.2626	0.2681
$Re \times 10^{-6}$	19.67	30.00	36.93	38.93
q, kPa	6.086	15.161	25.563	30.658
(lb/ft^2)	(127.1)	(316.6)	(533.9)	(640.3)
c_A	0.2262	0.2429	0.2623	0.2679
c_M	0.0112	0.0140	0.0188	0.0253
c_L	0.0415	0.0361	0.0289	0.0196
c_p at				
WC57	-0.0271	-0.0297	-0.0284	-0.0223
WC58	-0.0272	-0.0293	-0.0282	-0.0216
WC59	-0.0183	-0.0196	-0.0173	-0.0111
WC60	-0.0162	-0.0181	-0.0142	-0.0078
WC61	-0.0109	-0.0110	-0.0070	0.0010
WC62	-0.0164	-0.0175	-0.0140	-0.0052
WC63	-0.0132	-0.0135	-0.0102	-0.0016
WC64	-0.0146	-0.0143	-0.0117	-0.0026
WC65	-0.0038	-0.0024	0.0010	0.0112
WC66	-0.0027	-0.0013	0.0032	0.0114
WC67	-0.0108	-0.0106	-0.0064	0.0021
WC68	-0.0217	-0.0228	-0.0204	-0.0103
WC69	-0.0167	-0.0176	-0.0140	-0.0051
WC70	-0.0146	-0.0148	-0.0111	-0.0023
WC71	-0.0074	-0.0072	-0.0013	0.0069
WC72	-0.0131	-0.0127	-0.0076	-0.0014
WC73	-0.0129	-0.0126	-0.0091	-0.0031
WC74	-0.0128	-0.0139	-0.0102	-0.0043
WC75	-0.0155	-0.0179	-0.0145	-0.0079
WC76	-0.0223	-0.0239	-0.0218	-0.0162
WC77	-0.0306	-0.0318	-0.0281	-0.0203
WC78	-0.0498	-0.0556	-0.0630	-0.0767
WC79	-0.0457	-0.0511	-0.0586	-0.0707
WC80	-0.0468	-0.0522	-0.0588	-0.0721
WC81	-0.0470	-0.0524	-0.0581	-0.0698
WC82	-0.0290	-0.0313	-0.0373	-0.0475
WC83	-0.0451	-0.0510	-0.0578	-0.0637
WC84	-0.0352	-0.0391	-0.0440	-0.0515

TABLE 4. — Continued

(c) Continued

TP	W031	W032	W033	W034
M	0.30	0.50	0.71	0.82
α, deg	0.34	0.37	0.43	0.50
c_{D_b}	0.1261	0.1496	0.1794	0.1912
c_D	0.2265	0.2431	0.2626	0.2681
Re × 10^{-6}	19.67	30.00	36.93	38.93
q, kPa	6.086	15.161	25.563	30.658
(lb/ft^2)	(127.1)	(316.6)	(533.9)	(640.3)
c_A	0.2262	0.2429	0.2623	0.2679
c_M	0.0112	0.0140	0.0188	0.0253
c_L	0.0415	0.0361	0.0289	0.0196
c_p at				
WC85	-0.0365	-0.0413	-0.0473	-0.0539
WC86	-0.0357	-0.0392	-0.0459	-0.0517
WC87	-0.0291	-0.0326	-0.0377	-0.0420
WC88	-0.0446	-0.0492	-0.0556	-0.0582
WC89	-0.0489	-0.0550	-0.0586	-0.0582
WC90	-0.0464	-0.0535	-0.0561	-0.0580
WC91	-0.0492	-0.0548	-0.0600	-0.0627
WC92	-0.0472	-0.0539	-0.0587	-0.0609
WC93	-0.0257	-0.0278	-0.0317	-0.0366
WC94	-0.0331	-0.0344	-0.0392	-0.0456
WC95	-0.0403	-0.0422	-0.0493	-0.0558
WC96	-0.0473	-0.0523	-0.0611	-0.0675
WC97	-0.0372	-0.0403	-0.0488	-0.0558
WC98	-0.0280	-0.0313	-0.0404	-0.0502
WC99	-0.0359	-0.0405	-0.0485	-0.0580
WC100	-0.0512	-0.0573	-0.0662	-0.0746
WC101	-0.1572	-0.1706	-0.1895	-0.2037
WC102	-0.1537	-0.1660	-0.1815	-0.1977
WC103	-0.1631	-0.1752	-0.1907	-0.2079
WC104	-0.1574	-0.1672	-0.1836	-0.1999
WC105	-0.1635	-0.1733	-0.1882	-0.2079
WC106	-0.1584	-0.1698	-0.1875	-0.2062
WC107	-0.1572	-0.1693	-0.1852	-0.2055
WC108	-0.1527	-0.1644	-0.1804	-0.2014
WC109	-0.1433	-0.1536	-0.1689	-0.1875
WC110	-0.1516	-0.1625	-0.1832	-0.1986
WC111	-0.1525	-0.1625	-0.1812	-0.1958
WC112	-0.0822	-0.0940	-0.1037	-0.1025

TABLE 4. — Continued

(c)   Concluded

TP	W031	W032	W033	W034
M	0.30	0.50	0.71	0.82
α, deg	0.34	0.37	0.43	0.50
C_{D_b}	0.1261	0.1496	0.1794	0.1912
C_D	0.2265	0.2431	0.2626	0.2681
Re $\times$ 10^{-6}	19.67	30.00	36.93	38.93
q, kPa	6.086	15.161	25.563	30.658
(lb/ft^2)	(127.1)	(316.6)	(533.9)	(640.3)
C_A	0.2262	0.2429	0.2623	0.2679
C_M	0.0112	0.0140	0.0188	0.0253
C_L	0.0415	0.0361	0.0289	0.0196
C_p at				
WC113	-0.1565	-0.1673	-0.1823	-0.1944
WC114	-0.1551	-0.1659	-0.1800	-0.1886
WC115	-0.1677	-0.1787	-0.1963	-0.2031
WC116	-0.1579	-0.1699	-0.1843	-0.1934
WC117	-0.1595	-0.1711	-0.1854	-0.1954
WC118	-0.1553	-0.1686	-0.1827	-0.1949
WC119	-0.1535	-0.1678	-0.1810	-0.1969
WC120	-0.1358	-0.1426	-0.1568	-0.1714
WC121	-0.1590	-0.1718	-0.1886	-0.2050
WC122	-0.1410	-0.1506	-0.1670	-0.1839
WC123	-0.1536	-0.1693	-0.1857	-0.2026
WC124	-0.0537	-0.0625	-0.0771	-0.1015
WC125	-0.0487	-0.0583	-0.0767	-0.1165
WC126	-0.0479	-0.0554	-0.0718	-0.1091
WC127	-0.0403	-0.0465	-0.0574	-0.0828
WC128	-0.0431	-0.0495	-0.0571	-0.0734
WC129	-0.0469	-0.0523	-0.0582	-0.0670
WC130	-0.0563	-0.0615	-0.0683	-0.0741
WC131	-0.0749	-0.0805	-0.0870	-0.0951
WC132	-0.0465	-0.0552	-0.0700	-0.0915
WC133	-0.0496	-0.0591	-0.0793	-0.1169
WC134	-0.0511	-0.0605	-0.0772	-0.1095
WC135	-0.0412	-0.0477	-0.0602	-0.0818
WC136	-0.0447	-0.0501	-0.0590	-0.0736
WC137	-0.0499	-0.0562	-0.0614	-0.0714
WC138	-0.0326	-0.0332	-0.0386	-0.0472
WC139	-0.0707	-0.0763	-0.0823	-0.0888

TABLE 4. — Continued

(d) Trailing disk configuration, wind-tunnel disk, x/D = 0.45

TP	W041	W042	W043	W044	W341	W342	W343
M	0.30	0.50	0.71	0.82	0.30	0.50	0.71
α, deg	0.37	0.40	0.46	0.53	3.38	3.44	3.55
c_{D_b}	0.0736	0.0910	0.1213	0.1560	0.1087	0.1168	0.1379
c_D	0.1740	0.1786	0.2017	0.2322	0.2054	0.2011	0.2135
Re $\times$ 10^{-6}	20.00	30.47	37.50	39.70	19.93	30.47	37.53
q, kPa	6.092	15.172	25.599	30.693	6.125	15.275	25.748
(lb/ft^2)	(127.2)	(316.9)	(534.6)	(641.0)	(127.9)	(319.0)	(537.8)
c_A	0.1737	0.1783	0.2014	0.2318	0.1960	0.1913	0.2034
c_M	0.0109	0.0139	0.0187	0.0251	0.0285	0.0312	0.0357
c_L	0.0453	0.0413	0.0351	0.0437	0.1539	0.1568	0.1566
c_p at							
WC1	-0.1201	-0.1531	-0.2043	-0.2486	-0.0956	-0.1308	-0.1960
WC2	-0.1272	-0.1708	-0.2086	-0.2483	-0.1490	-0.1825	-0.2476
WC3	-0.2335	-0.2679	-0.2946	-0.3174	-0.2362	-0.2613	-0.3465
WC4	-0.3199	-0.3386	-0.3691	-0.3705	-0.3022	-0.3281	-0.3994
WC5	-0.3391	-0.3597	-0.3780	-0.3835	-0.3295	-0.3499	-0.3928
WC6	-0.2321	-0.2535	-0.2887	-0.3149	-0.2656	-0.2822	-0.3174
WC7	-0.0983	-0.1241	-0.1758	-0.2361	-0.1265	-0.1461	-0.1825
WC8	-0.1238	-0.1536	-0.2058	-0.2691	-0.1775	-0.1969	-0.2327
WC9	-0.2233	-0.2395	-0.2909	-0.3475	-0.2626	-0.2742	-0.2945
WC10	-0.3003	-0.3071	-0.3508	-0.4033	-0.3225	-0.3321	-0.3350
WC11	-0.2029	-0.2276	-0.2701	-0.3179	-0.2353	-0.2537	-0.2801
WC12	-0.1082	-0.1496	-0.1932	-0.2484	-0.1743	-0.1976	-0.2312
WC13	-0.2060	-0.2449	-0.2710	-0.3070	-0.2229	-0.2442	-0.2893
WC14	-0.3650	-0.3822	-0.3993	-0.4032	-0.3029	-0.3254	-0.3808
WC15	-0.3121	-0.3258	-0.3528	-0.3724	-0.2591	-0.2794	-0.3230
WC16	-0.2168	-0.2495	-0.2849	-0.3190	-0.1984	-0.2228	-0.2714
WC17	-0.1092	-0.1390	-0.1891	-0.2426	-0.1336	-0.1629	-0.2198
WC18	-0.1731	-0.1930	-0.2452	-0.2947	-0.2307	-0.2498	-0.2837
WC19	-0.2454	-0.2632	-0.3079	-0.3546	-0.2984	-0.3100	-0.3234
WC20	-0.2960	-0.3033	-0.3507	-0.3856	-0.3292	-0.3410	-0.3422
WC21	-0.2513	-0.2709	-0.3082	-0.3471	-0.2888	-0.3080	-0.3267
WC22	-0.1831	-0.2078	-0.2558	-0.3049	-0.2386	-0.2658	-0.3003
WC23	-0.1200	-0.1474	-0.2039	-0.2661	-0.0881	-0.1177	-0.1665
WC24	-0.1439	-0.1699	-0.2269	-0.2930	-0.1330	-0.1615	-0.2041
WC25	-0.2039	-0.2404	-0.2767	-0.3092	-0.2108	-0.2411	-0.2799
WC26	-0.2813	-0.3010	-0.3379	-0.3708	-0.2879	-0.3110	-0.3324
WC27	-0.1541	-0.1844	-0.2260	-0.2734	-0.1619	-0.1845	-0.2238
WC28	-0.2147	-0.2397	-0.2837	-0.3264	-0.2352	-0.2559	-0.2842

TABLE 4. — Continued

(d) Continued

TP	W041	W042	W043	W044	W341	W342	W343
M	0.30	0.50	0.71	0.82	0.30	0.50	0.71
α, deg	0.37	0.40	0.46	0.53	3.38	3.44	3.55
C_{D_b}	0.0736	0.0910	0.1213	0.1560	0.1087	0.1168	0.1379
C_D	0.1740	0.1786	0.2017	0.2322	0.2054	0.2011	0.2135
$Re \times 10^{-6}$	20.00	30.47	37.50	39.70	19.93	30.47	37.53
q, kPa	6.092	15.172	25.599	30.693	6.125	15.275	25.748
(lb/ft^2)	(127.2)	(316.9)	(534.6)	(641.0)	(127.9)	(319.0)	(537.8)
C_A	0.1737	0.1783	0.2014	0.2318	0.1960	0.1913	0.2034
C_M	0.0109	0.0139	0.0187	0.0251	0.0285	0.0312	0.0357
C_L	0.0453	0.0413	0.0351	0.0437	0.1539	0.1568	0.1566
C_p at							
WC29	-0.3095	-0.3301	-0.3602	-0.3811	-0.2936	-0.3140	-0.3599
WC30	-0.1146	-0.1360	-0.1956	-0.2603	-0.1827	-0.2047	-0.2155
WC31	-0.1807	-0.2164	-0.2606	-0.3035	-0.2238	-0.2451	-0.2719
WC32	-0.2671	-0.2942	-0.3310	-0.3602	-0.2934	-0.3156	-0.3421
WC33	-0.3003	-0.3180	-0.3629	-0.4082	-0.3435	-0.3576	-0.3690
WC34	-0.1702	-0.2005	-0.2410	-0.2797	-0.1668	-0.1920	-0.2498
WC35	-0.1934	-0.2319	-0.2636	-0.3031	-0.2218	-0.2441	-0.2932
WC36	-0.2590	-0.2786	-0.3183	-0.3574	-0.2766	-0.2942	-0.3191
WC37	-0.4301	-0.4417	-0.4653	-0.4717	-0.3821	-0.4012	-0.4569
WC38	0.0447	0.0229	-0.0032	-0.0469	0.0133	0.0120	0.0008
WC39	0.0394	0.0171	-0.0121	-0.0364	0.0164	0.0110	-0.0010
WC40	0.0328	0.0198	-0.0142	-0.0588	0.0088	0.0064	-0.0055
WC41	0.0268	0.0218	0.0004	-0.0335	-0.0031	-0.0032	-0.0156
WC42	0.0291	0.0157	0.0019	-0.0363	-0.0056	-0.0069	-0.0216
WC43	0.0377	0.0316	-0.0277	-0.0458	-0.0005	-0.0016	-0.0052
WC44	0.0359	0.0129	-0.0207	-0.0454	-0.0098	-0.0072	-0.0112
WC45	0.0329	0.0069	-0.0034	-0.0514	-0.0088	-0.0059	-0.0121
WC46	0.0337	0.0320	-0.0056	-0.0389	-0.0020	-0.0012	-0.0120
WC47	0.0433	0.0291	-0.0111	-0.0445	0.0143	0.0138	0.0060
WC48	0.0481	0.0241	-0.0058	-0.0372	0.0199	0.0192	0.0103
WC49	0.0464	0.0332	0.0051	-0.0380	0.0279	0.0246	0.0119
WC50	0.0485	0.0336	0.0042	-0.0214	0.0376	0.0354	0.0146
WC51	0.0381	0.0153	-0.0126	-0.0352	-0.0142	-0.0077	-0.0064
WC52	0.0317	0.0256	-0.0036	-0.0310	-0.0182	-0.0154	-0.0136
WC53	0.0351	0.0229	0.0002	-0.0284	-0.0170	-0.0120	-0.0151
WC54	0.0414	0.0252	0.0176	-0.0124	-0.0124	-0.0085	-0.0157
WC55	-0.0244	-0.0252	-0.0257	-0.0186	-0.0405	-0.0403	-0.0432
WC56	-0.0215	-0.0218	-0.0220	-0.0145	-0.0382	-0.0397	-0.0422

TABLE 4. — Continued

(d)   Continued

TP	W041	W042	W043	W044	W341	W342	W343
M	0.30	0.50	0.71	0.82	0.30	0.50	0.71
α, deg	0.37	0.40	0.46	0.53	3.38	3.44	3.55
C_{D_b}	0.0736	0.0910	0.1213	0.1560	0.1087	0.1168	0.1379
C_D	0.1740	0.1786	0.2017	0.2322	0.2054	0.2011	0.2135
Re $\times$ 10^{-6}	20.00	30.47	37.50	39.70	19.93	30.47	37.53
q, kPa	6.092	15.172	25.599	30.693	6.125	15.275	25.748
(lb/ft^2)	(127.2)	(316.9)	(534.6)	(641.0)	(127.9)	(319.0)	(537.8)
C_A	0.1737	0.1783	0.2014	0.2318	0.1960	0.1913	0.2034
C_M	0.0109	0.0139	0.0187	0.0251	0.0285	0.0312	0.0357
C_L	0.0453	0.0413	0.0351	0.0437	0.1539	0.1568	0.1566
C_p at							
WC57	-0.0278	-0.0292	-0.0285	-0.0216	-0.0435	-0.0461	-0.0486
WC58	-0.0284	-0.0313	-0.0294	-0.0216	-0.0431	-0.0471	-0.0480
WC59	-0.0195	-0.0207	-0.0185	-0.0094	-0.0341	-0.0366	-0.0369
WC60	-0.0170	-0.0186	-0.0159	-0.0062	-0.0281	-0.0317	-0.0318
WC61	-0.0107	-0.0112	-0.0086	0.0022	-0.0166	-0.0186	-0.0166
WC62	-0.0161	-0.0180	-0.0147	-0.0046	-0.0170	-0.0194	-0.0175
WC63	-0.0135	-0.0128	-0.0112	-0.0010	-0.0067	-0.0082	-0.0060
WC64	-0.0142	-0.0129	-0.0127	-0.0017	-0.0005	-0.0029	0.0017
WC65	-0.0039	-0.0015	0.0003	0.0113	0.0151	0.0155	0.0212
WC66	-0.0037	-0.0026	0.0009	0.0117	0.0177	0.0177	0.0231
WC67	-0.0114	-0.0114	-0.0071	0.0027	0.0086	0.0081	0.0133
WC68	-0.0222	-0.0243	-0.0205	-0.0123	-0.0078	-0.0095	-0.0054
WC69	-0.0164	-0.0185	-0.0145	-0.0049	-0.0078	-0.0091	-0.0055
WC70	-0.0148	-0.0165	-0.0122	-0.0013	-0.0132	-0.0157	-0.0116
WC71	-0.0074	-0.0066	-0.0032	0.0058	-0.0114	-0.0124	-0.0070
WC72	-0.0137	-0.0140	-0.0097	-0.0036	-0.0246	-0.0280	-0.0239
WC73	-0.0136	-0.0142	-0.0117	-0.0041	-0.0272	-0.0309	-0.0293
WC74	-0.0143	-0.0150	-0.0123	-0.0055	-0.0307	-0.0344	-0.0348
WC75	-0.0157	-0.0180	-0.0169	-0.0087	-0.0349	-0.0397	-0.0401
WC76	-0.0233	-0.0255	-0.0247	-0.0176	-0.0396	-0.0441	-0.0451
WC77	-0.0305	-0.0325	-0.0320	-0.0254	-0.0456	-0.0498	-0.0519
WC78	-0.0498	-0.0562	-0.0661	-0.0762	-0.0476	-0.0556	-0.0666
WC79	-0.0461	-0.0525	-0.0611	-0.0720	-0.0467	-0.0537	-0.0652
WC80	-0.0475	-0.0534	-0.0612	-0.0733	-0.0495	-0.0568	-0.0677
WC81	-0.0472	-0.0536	-0.0610	-0.0727	-0.0545	-0.0615	-0.0713
WC82	-0.0292	-0.0320	-0.0389	-0.0504	-0.0397	-0.0428	-0.0518
WC83	-0.0456	-0.0520	-0.0586	-0.0690	-0.0603	-0.0673	-0.0770
WC84	-0.0356	-0.0401	-0.0464	-0.0543	-0.0487	-0.0533	-0.0615

TABLE 4. — Continued

(d) Continued

TP	W041	W042	W043	W044	W341	W342	W343
M	0.30	0.50	0.71	0.82	0.30	0.50	0.71
α, deg	0.37	0.40	0.46	0.53	3.38	3.44	3.55
C_{D_b}	0.0736	0.0910	0.1213	0.1560	0.1087	0.1168	0.1379
C_D	0.1740	0.1786	0.2017	0.2322	0.2054	0.2011	0.2135
Re × 10^{-6}	20.00	30.47	37.50	39.70	19.93	30.47	37.53
q, kPa	6.092	15.172	25.599	30.693	6.125	15.275	25.748
(lb/ft^2)	(127.2)	(316.9)	(534.6)	(641.0)	(127.9)	(319.0)	(537.8)
C_A	0.1737	0.1783	0.2014	0.2318	0.1960	0.1913	0.2034
C_M	0.0109	0.0139	0.0187	0.0251	0.0285	0.0312	0.0357
C_L	0.0453	0.0413	0.0351	0.0437	0.1539	0.1568	0.1566
C_p at							
WC85	-0.0379	-0.0425	-0.0481	-0.0555	-0.0506	-0.0554	-0.0625
WC86	-0.0376	-0.0411	-0.0467	-0.0526	-0.0420	-0.0454	-0.0534
WC87	-0.0313	-0.0344	-0.0388	-0.0441	-0.0318	-0.0348	-0.0413
WC88	-0.0457	-0.0500	-0.0552	-0.0599	-0.0432	-0.0487	-0.0567
WC89	-0.0468	-0.0542	-0.0582	-0.0568	-0.0434	-0.0499	-0.0568
WC90	-0.0461	-0.0522	-0.0560	-0.0572	-0.0409	-0.0479	-0.0542
WC91	-0.0474	-0.0541	-0.0590	-0.0625	-0.0471	-0.0537	-0.0605
WC92	-0.0457	-0.0522	-0.0575	-0.0618	-0.0498	-0.0573	-0.0640
WC93	-0.0242	-0.0267	-0.0311	-0.0352	-0.0272	-0.0288	-0.0333
WC94	-0.0321	-0.0349	-0.0401	-0.0466	-0.0414	-0.0430	-0.0503
WC95	-0.0380	-0.0419	-0.0471	-0.0559	-0.0503	-0.0533	-0.0620
WC96	-0.0461	-0.0530	-0.0583	-0.0690	-0.0575	-0.0640	-0.0739
WC97	-0.0364	-0.0413	-0.0471	-0.0583	-0.0449	-0.0497	-0.0591
WC98	-0.0278	-0.0324	-0.0375	-0.0493	-0.0356	-0.0393	-0.0486
WC99	-0.0358	-0.0407	-0.0475	-0.0599	-0.0400	-0.0438	-0.0528
WC100	-0.0507	-0.0574	-0.0659	-0.0767	-0.0494	-0.0558	-0.0647
WC101	-0.1434	-0.1587	-0.1780	-0.1922	-0.1544	-0.1677	-0.1906
WC102	-0.1398	-0.1520	-0.1733	-0.1863	-0.1492	-0.1621	-0.1866
WC103	-0.1464	-0.1605	-0.1823	-0.1963	-0.1513	-0.1659	-0.1884
WC104	-0.1397	-0.1523	-0.1728	-0.1881	-0.1499	-0.1627	-0.1833
WC105	-0.1434	-0.1594	-0.1793	-0.1963	-0.1574	-0.1710	-0.1882
WC106	-0.1414	-0.1543	-0.1773	-0.1932	-0.1599	-0.1727	-0.1886
WC107	-0.1420	-0.1551	-0.1761	-0.1937	-0.1576	-0.1674	-0.1829
WC108	-0.1402	-0.1542	-0.1739	-0.1903	-0.1541	-0.1665	-0.1807
WC109	-0.1332	-0.1463	-0.1637	-0.1801	-0.1417	-0.1528	-0.1665
WC110	-0.1427	-0.1560	-0.1762	-0.1911	-0.1454	-0.1589	-0.1745
WC111	-0.1430	-0.1560	-0.1759	-0.1875	-0.1393	-0.1547	-0.1700
WC112	-0.0867	-0.0992	-0.1092	-0.1072	-0.0706	-0.0856	-0.0952

TABLE 4. — Continued

(d) Concluded

TP	W041	W042	W043	W044	W341	W342	W343
M	0.30	0.50	0.71	0.82	0.30	0.50	0.71
α, deg	0.37	0.40	0.46	0.53	3.38	3.44	3.55
c_{D_b}	0.0736	0.0910	0.1213	0.1560	0.1087	0.1168	0.1379
c_D	0.1740	0.1786	0.2017	0.2322	0.2054	0.2011	0.2135
$Re \times 10^{-6}$	20.00	30.47	37.50	39.70	19.93	30.47	37.53
q, kPa	6.092	15.172	25.599	30.693	6.125	15.275	25.748
(lb/ft^2)	(127.2)	(316.9)	(534.6)	(641.0)	(127.9)	(319.0)	(537.8)
c_A	0.1737	0.1783	0.2014	0.2318	0.1960	0.1913	0.2034
c_M	0.0109	0.0139	0.0187	0.0251	0.0285	0.0312	0.0357
c_L	0.0453	0.0413	0.0351	0.0437	0.1539	0.1568	0.1566
c_p at							
WC113	-0.1477	-0.1620	-0.1789	-0.1868	-0.1336	-0.1480	-0.1652
WC114	-0.1449	-0.1582	-0.1732	-0.1797	-0.1288	-0.1419	-0.1587
WC115	-0.1527	-0.1697	-0.1863	-0.1965	-0.1456	-0.1601	-0.1752
WC116	-0.1446	-0.1587	-0.1750	-0.1849	-0.1449	-0.1566	-0.1705
WC117	-0.1415	-0.1562	-0.1744	-0.1839	-0.1557	-0.1683	-0.1796
WC118	-0.1373	-0.1507	-0.1716	-0.1857	-0.1584	-0.1729	-0.1836
WC119	-0.1371	-0.1505	-0.1704	-0.1888	-0.1609	-0.1768	-0.1900
WC120	-0.1184	-0.1263	-0.1460	-0.1627	-0.1410	-0.1521	-0.1681
WC121	-0.1420	-0.1570	-0.1789	-0.1966	-0.1604	-0.1768	-0.1991
WC122	-0.1251	-0.1370	-0.1584	-0.1743	-0.1446	-0.1584	-0.1810
WC123	-0.1414	-0.1602	-0.1801	-0.1925	-0.1613	-0.1796	-0.2034
WC124	-0.0520	-0.0606	-0.0771	-0.1010	-0.0519	-0.0622	-0.0840
WC125	-0.0479	-0.0575	-0.0782	-0.1139	-0.0546	-0.0670	-0.0908
WC126	-0.0483	-0.0568	-0.0745	-0.1099	-0.0516	-0.0606	-0.0807
WC127	-0.0406	-0.0472	-0.0593	-0.0832	-0.0434	-0.0512	-0.0661
WC128	-0.0435	-0.0507	-0.0600	-0.0760	-0.0467	-0.0542	-0.0659
WC129	-0.0465	-0.0522	-0.0594	-0.0696	-0.0500	-0.0563	-0.0659
WC130	-0.0552	-0.0611	-0.0681	-0.0786	-0.0596	-0.0655	-0.0760
WC131	-0.0716	-0.0787	-0.0875	-0.0966	-0.0780	-0.0855	-0.0969
WC132	-0.0460	-0.0550	-0.0698	-0.0944	-0.0525	-0.0626	-0.0841
WC133	-0.0486	-0.0585	-0.0781	-0.1162	-0.0530	-0.0640	-0.0886
WC134	-0.0511	-0.0608	-0.0762	-0.1092	-0.0533	-0.0643	-0.0841
WC135	-0.0405	-0.0472	-0.0584	-0.0821	-0.0450	-0.0525	-0.0673
WC136	-0.0458	-0.0522	-0.0604	-0.0742	-0.0485	-0.0542	-0.0662
WC137	-0.0493	-0.0547	-0.0611	-0.0700	-0.0535	-0.0600	-0.0693
WC138	-0.0314	-0.0327	-0.0376	-0.0463	-0.0448	-0.0481	-0.0572
WC139	-0.0670	-0.0725	-0.0800	-0.0877	-0.0750	-0.0815	-0.0917

TABLE 4. — Continued

(e) Trailing disk configuration, wind-tunnel disk, x/D = 0.50

TP	W051	W052	W053	W054	W351	W352	W353
M	0.30	0.50	0.71	0.82	0.30	0.50	0.71
α, deg	0.35	0.39	0.46	0.52	3.37	3.44	3.55
C_{D_b}	0.0824	0.0923	0.1171	0.1435	0.1136	0.1225	0.1416
C_D	0.1837	0.1815	0.1975	0.2270	0.2139	0.2097	0.2249
$Re \times 10^{-6}$	19.17	29.23	36.07	38.03	20.24	31.23	38.53
q, kPa	6.089	15.149	25.513	30.582	6.127	15.301	25.771
(lb/ft^2)	(127.2)	(316.4)	(532.9)	(638.7)	(128.0)	(319.6)	(538.2)
C_A	0.1836	0.1813	0.1973	0.2265	0.2041	0.1997	0.2146
C_M	0.0139	0.0162	0.0212	0.0272	0.0274	0.0296	0.0343
C_L	0.0169	0.0329	0.0354	0.0493	0.1600	0.1604	0.1600
C_p at							
WC1	-0.1324	-0.1543	-0.1797	-0.2201	-0.0854	-0.1435	-0.2085
WC2	-0.1430	-0.1664	-0.1929	-0.2265	-0.1420	-0.1904	-0.2634
WC3	-0.2185	-0.2388	-0.2584	-0.2822	-0.2131	-0.2752	-0.3459
WC4	-0.2823	-0.2894	-0.3168	-0.3297	-0.2686	-0.3151	-0.3769
WC5	-0.2822	-0.2934	-0.3150	-0.3307	-0.2914	-0.3200	-0.3594
WC6	-0.2005	-0.2219	-0.2538	-0.2829	-0.2502	-0.2700	-0.2969
WC7	-0.1032	-0.1379	-0.1853	-0.2378	-0.1123	-0.1266	-0.1537
WC8	-0.1411	-0.1761	-0.2335	-0.2707	-0.1769	-0.1928	-0.2122
WC9	-0.2111	-0.2434	-0.3018	-0.3409	-0.2666	-0.2668	-0.2773
WC10	-0.2581	-0.2757	-0.3386	-0.3705	-0.3159	-0.3097	-0.3118
WC11	-0.2019	-0.2243	-0.2664	-0.3012	-0.2140	-0.2293	-0.2630
WC12	-0.1398	-0.1687	-0.2008	-0.2346	-0.1451	-0.1682	-0.2084
WC13	-0.2357	-0.2552	-0.2670	-0.2979	-0.1779	-0.2052	-0.2545
WC14	-0.3177	-0.3248	-0.3358	-0.3537	-0.2438	-0.2716	-0.3249
WC15	-0.2726	-0.2840	-0.3118	-0.3379	-0.2234	-0.2476	-0.2850
WC16	-0.2179	-0.2355	-0.2669	-0.2982	-0.1707	-0.1986	-0.2379
WC17	-0.1185	-0.1361	-0.1783	-0.2298	-0.1606	-0.1868	-0.2077
WC18	-0.1766	-0.1921	-0.2327	-0.2740	-0.2481	-0.2578	-0.2647
WC19	-0.2237	-0.2505	-0.2861	-0.3241	-0.2996	-0.2985	-0.2960
WC20	-0.2466	-0.2718	-0.3068	-0.3413	-0.3045	-0.3074	-0.3120
WC21	-0.2239	-0.2425	-0.2668	-0.3040	-0.2636	-0.2851	-0.2970
WC22	-0.1816	-0.1984	-0.2320	-0.2725	-0.2237	-0.2518	-0.2732
WC23	-0.1133	-0.1316	-0.1712	-0.2247	-0.0627	-0.0985	-0.1299
WC24	-0.1392	-0.1625	-0.1966	-0.2481	-0.1102	-0.1458	-0.1721
WC25	-0.1908	-0.2079	-0.2382	-0.2780	-0.1942	-0.2315	-0.2456
WC26	-0.2408	-0.2588	-0.2881	-0.3248	-0.2630	-0.2861	-0.2825
WC27	-0.1494	-0.1675	-0.1955	-0.2429	-0.1449	-0.1703	-0.2004
WC28	-0.2017	-0.2238	-0.2577	-0.2951	-0.2079	-0.2259	-0.2467

TABLE 4. — Continued

TP	W051	W052	W053	W054	W351	W352	W353
M	0.30	0.50	0.71	0.82	0.30	0.50	0.71
α, deg	0.35	0.39	0.46	0.52	3.37	3.44	3.55
C_{D_b}	0.0824	0.0923	0.1171	0.1435	0.1136	0.1225	0.1416
C_D	0.1837	0.1815	0.1975	0.2270	0.2139	0.2097	0.2249
Re $\times$ 10^{-6}	19.17	29.23	36.07	38.03	20.24	31.23	38.53
q, kPa	6.089	15.149	25.513	30.582	6.127	15.301	25.771
(lb/ft^2)	(127.2)	(316.4)	(532.9)	(638.7)	(128.0)	(319.6)	(538.2)
C_A	0.1836	0.1813	0.1973	0.2265	0.2041	0.1997	0.2146
C_M	0.0139	0.0162	0.0212	0.0272	0.0274	0.0296	0.0343
C_L	0.0169	0.0329	0.0354	0.0493	0.1600	0.1604	0.1600
C_p at							
WC29	-0.2658	-0.2888	-0.3200	-0.3376	-0.2435	-0.2714	-0.3225
WC30	-0.1020	-0.1161	-0.1649	-0.2215	-0.1594	-0.1685	-0.1885
WC31	-0.1758	-0.1977	-0.2334	-0.2716	-0.2052	-0.2084	-0.2310
WC32	-0.2376	-0.2584	-0.2964	-0.3254	-0.2649	-0.2802	-0.3009
WC33	-0.2516	-0.2759	-0.3228	-0.3633	-0.3210	-0.3212	-0.3289
WC34	-0.1593	-0.1783	-0.1856	-0.2353	-0.1403	-0.1666	-0.2093
WC35	-0.1856	-0.2033	-0.2236	-0.2680	-0.2090	-0.2305	-0.2646
WC36	-0.2336	-0.2514	-0.2803	-0.3125	-0.2498	-0.2698	-0.2861
WC37	-0.3564	-0.3726	-0.3947	-0.4121	-0.3124	-0.3528	-0.3994
WC38	0.0274	0.0266	0.0046	-0.0321	-0.0032	-0.0065	-0.0084
WC39	0.0254	0.0159	-0.0030	-0.0494	-0.0047	-0.0075	-0.0130
WC40	0.0196	0.0192	-0.0019	-0.0408	-0.0104	-0.0119	-0.0183
WC41	0.0141	0.0090	-0.0005	-0.0241	-0.0199	-0.0213	-0.0290
WC42	0.0123	0.0129	0.0029	-0.0163	-0.0219	-0.0253	-0.0368
WC43	0.0230	0.0223	0.0003	-0.0208	-0.0148	-0.0170	-0.0243
WC44	0.0181	0.0133	-0.0026	-0.0389	-0.0211	-0.0205	-0.0310
WC45	0.0139	0.0120	-0.0031	-0.0272	-0.0186	-0.0197	-0.0297
WC46	0.0176	0.0154	-0.0054	-0.0338	-0.0144	-0.0150	-0.0269
WC47	0.0261	0.0241	0.0011	-0.0188	0.0022	-0.0004	-0.0050
WC48	0.0164	0.0209	0.0058	-0.0333	0.0084	0.0046	0.0008
WC49	0.0238	0.0170	0.0041	-0.0195	0.0153	0.0105	0.0028
WC50	0.0290	0.0270	0.0044	-0.0173	0.0226	0.0191	0.0033
WC51	0.0233	0.0225	0.0154	-0.0143	-0.0193	-0.0174	-0.0156
WC52	0.0174	0.0170	0.0011	-0.0283	-0.0270	-0.0236	-0.0261
WC53	0.0207	0.0157	-0.0075	-0.0211	-0.0250	-0.0217	-0.0306
WC54	0.0232	0.0193	0.0099	-0.0042	-0.0191	-0.0174	-0.0301
WC55	-0.0243	-0.0260	-0.0258	-0.0206	-0.0398	-0.0419	-0.0441
WC56	-0.0210	-0.0227	-0.0223	-0.0164	-0.0373	-0.0413	-0.0431

TABLE 4. — Continued

(e)   Continued

TP	W051	W052	W053	W054	W351	W352	W353
M	0.30	0.50	0.71	0.82	0.30	0.50	0.71
α, deg	0.35	0.39	0.46	0.52	3.37	3.44	3.55
C_{D_b}	0.0824	0.0923	0.1171	0.1435	0.1136	0.1225	0.1416
C_D	0.1837	0.1815	0.1975	0.2270	0.2139	0.2097	0.2249
$Re \times 10^{-6}$	19.17	29.23	36.07	38.03	20.24	31.23	38.53
q, kPa	6.089	15.149	25.513	30.582	6.127	15.301	25.771
(lb/ft^2)	(127.2)	(316.4)	(532.9)	(638.7)	(128.0)	(319.6)	(538.2)
C_A	0.1836	0.1813	0.1973	0.2265	0.2041	0.1997	0.2146
C_M	0.0139	0.0162	0.0212	0.0272	0.0274	0.0296	0.0343
C_L	0.0169	0.0329	0.0354	0.0493	0.1600	0.1604	0.1600
C_p at							
WC57	-0.0274	-0.0295	-0.0286	-0.0230	-0.0428	-0.0466	-0.0486
WC58	-0.0278	-0.0302	-0.0280	-0.0239	-0.0429	-0.0467	-0.0476
WC59	-0.0188	-0.0200	-0.0175	-0.0117	-0.0337	-0.0361	-0.0364
WC60	-0.0171	-0.0180	-0.0153	-0.0089	-0.0298	-0.0316	-0.0304
WC61	-0.0109	-0.0109	-0.0082	-0.0007	-0.0181	-0.0172	-0.0177
WC62	-0.0168	-0.0175	-0.0137	-0.0059	-0.0183	-0.0191	-0.0173
WC63	-0.0146	-0.0138	-0.0101	-0.0030	-0.0079	-0.0080	-0.0056
WC64	-0.0150	-0.0152	-0.0114	-0.0043	-0.0020	-0.0024	0.0013
WC65	-0.0043	-0.0028	0.0011	0.0095	0.0145	0.0147	0.0200
WC66	-0.0035	-0.0024	0.0024	0.0104	0.0174	0.0170	0.0230
WC67	-0.0120	-0.0109	-0.0062	0.0020	0.0084	0.0070	0.0130
WC68	-0.0233	-0.0235	-0.0209	-0.0112	-0.0077	-0.0103	-0.0051
WC69	-0.0176	-0.0176	-0.0154	-0.0054	-0.0084	-0.0098	-0.0058
WC70	-0.0155	-0.0151	-0.0122	-0.0038	-0.0146	-0.0159	-0.0113
WC71	-0.0078	-0.0063	-0.0029	0.0042	-0.0131	-0.0129	-0.0095
WC72	-0.0137	-0.0125	-0.0105	-0.0029	-0.0267	-0.0287	-0.0269
WC73	-0.0125	-0.0134	-0.0112	-0.0048	-0.0293	-0.0307	-0.0289
WC74	-0.0137	-0.0139	-0.0123	-0.0081	-0.0324	-0.0346	-0.0340
WC75	-0.0160	-0.0177	-0.0161	-0.0106	-0.0362	-0.0407	-0.0413
WC76	-0.0230	-0.0243	-0.0234	-0.0176	-0.0411	-0.0454	-0.0463
WC77	-0.0299	-0.0323	-0.0290	-0.0212	-0.0463	-0.0512	-0.0511
WC78	-0.0493	-0.0557	-0.0648	-0.0777	-0.0482	-0.0555	-0.0661
WC79	-0.0452	-0.0515	-0.0607	-0.0717	-0.0471	-0.0532	-0.0639
WC80	-0.0459	-0.0527	-0.0605	-0.0720	-0.0506	-0.0570	-0.0684
WC81	-0.0459	-0.0519	-0.0603	-0.0713	-0.0554	-0.0613	-0.0712
WC82	-0.0288	-0.0306	-0.0387	-0.0495	-0.0403	-0.0434	-0.0512
WC83	-0.0446	-0.0508	-0.0589	-0.0662	-0.0609	-0.0683	-0.0769
WC84	-0.0352	-0.0390	-0.0461	-0.0529	-0.0496	-0.0537	-0.0601

TABLE 4. — Continued

(e)   Continued

TP	W051	W052	W053	W054	W351	W352	W353
M	0.30	0.50	0.71	0.82	0.30	0.50	0.71
α, deg	0.35	0.39	0.46	0.52	3.37	3.44	3.55
c_{D_b}	0.0824	0.0923	0.1171	0.1435	0.1136	0.1225	0.1416
c_D	0.1837	0.1815	0.1975	0.2270	0.2139	0.2097	0.2249
Re × 10^{-6}	19.17	29.23	36.07	38.03	20.24	31.23	38.53
q, kPa	6.089	15.149	25.513	30.582	6.127	15.301	25.771
(lb/ft^2)	(127.2)	(316.4)	(532.9)	(638.7)	(128.0)	(319.6)	(538.2)
c_A	0.1836	0.1813	0.1973	0.2265	0.2041	0.1997	0.2146
c_M	0.0139	0.0162	0.0212	0.0272	0.0274	0.0296	0.0343
c_L	0.0169	0.0329	0.0354	0.0493	0.1600	0.1604	0.1600
c_p at							
WC85	-0.0359	-0.0414	-0.0485	-0.0561	-0.0511	-0.0561	-0.0638
WC86	-0.0357	-0.0393	-0.0468	-0.0521	-0.0423	-0.0450	-0.0518
WC87	-0.0290	-0.0329	-0.0390	-0.0442	-0.0315	-0.0333	-0.0397
WC88	-0.0437	-0.0489	-0.0560	-0.0600	-0.0424	-0.0483	-0.0556
WC89	-0.0471	-0.0540	-0.0583	-0.0588	-0.0431	-0.0511	-0.0566
WC90	-0.0459	-0.0522	-0.0566	-0.0571	-0.0405	-0.0481	-0.0530
WC91	-0.0483	-0.0553	-0.0598	-0.0626	-0.0471	-0.0535	-0.0597
WC92	-0.0458	-0.0533	-0.0585	-0.0618	-0.0504	-0.0572	-0.0638
WC93	-0.0238	-0.0268	-0.0313	-0.0356	-0.0272	-0.0280	-0.0337
WC94	-0.0311	-0.0341	-0.0401	-0.0450	-0.0422	-0.0434	-0.0511
WC95	-0.0383	-0.0424	-0.0487	-0.0573	-0.0501	-0.0533	-0.0619
WC96	-0.0447	-0.0513	-0.0589	-0.0680	-0.0575	-0.0646	-0.0741
WC97	-0.0350	-0.0401	-0.0478	-0.0582	-0.0447	-0.0502	-0.0595
WC98	-0.0272	-0.0321	-0.0401	-0.0507	-0.0353	-0.0396	-0.0489
WC99	-0.0342	-0.0413	-0.0481	-0.0602	-0.0396	-0.0437	-0.0539
WC100	-0.0489	-0.0576	-0.0649	-0.0772	-0.0486	-0.0555	-0.0655
WC101	-0.1286	-0.1436	-0.1610	-0.1803	-0.1456	-0.1605	-0.1815
WC102	-0.1282	-0.1395	-0.1567	-0.1750	-0.1402	-0.1572	-0.1803
WC103	-0.1342	-0.1468	-0.1662	-0.1850	-0.1424	-0.1596	-0.1829
WC104	-0.1292	-0.1407	-0.1589	-0.1790	-0.1420	-0.1563	-0.1772
WC105	-0.1358	-0.1498	-0.1650	-0.1886	-0.1506	-0.1638	-0.1815
WC106	-0.1345	-0.1480	-0.1660	-0.1876	-0.1517	-0.1642	-0.1816
WC107	-0.1361	-0.1472	-0.1667	-0.1869	-0.1496	-0.1574	-0.1724
WC108	-0.1338	-0.1461	-0.1661	-0.1841	-0.1445	-0.1530	-0.1712
WC109	-0.1282	-0.1378	-0.1550	-0.1727	-0.1313	-0.1397	-0.1543
WC110	-0.1379	-0.1483	-0.1662	-0.1832	-0.1351	-0.1463	-0.1608
WC111	-0.1378	-0.1498	-0.1658	-0.1806	-0.1287	-0.1423	-0.1576
WC112	-0.0743	-0.0880	-0.0968	-0.0939	-0.0658	-0.0815	-0.0906

TABLE 4. — Continued

(e) Concluded

TP	W051	W052	W053	W054	W351	W352	W353
M	0.30	0.50	0.71	0.82	0.30	0.50	0.71
α, deg	0.35	0.39	0.46	0.52	3.37	3.44	3.55
C_{D_b}	0.0824	0.0923	0.1171	0.1435	0.1136	0.1225	0.1416
C_D	0.1837	0.1815	0.1975	0.2270	0.2139	0.2097	0.2249
Re $\times$ 10^{-6}	19.17	29.23	36.07	38.03	20.24	31.23	38.53
q, kPa	6.089	15.149	25.513	30.582	6.127	15.301	25.771
(lb/ft^2)	(127.2)	(316.4)	(532.9)	(638.7)	(128.0)	(319.6)	(538.2)
C_A	0.1836	0.1813	0.1973	0.2265	0.2041	0.1997	0.2146
C_M	0.0139	0.0162	0.0212	0.0272	0.0274	0.0296	0.0343
C_L	0.0169	0.0329	0.0354	0.0493	0.1600	0.1604	0.1600
C_p at							
WC113	-0.1427	-0.1530	-0.1662	-0.1780	-0.1235	-0.1389	-0.1527
WC114	-0.1403	-0.1485	-0.1605	-0.1719	-0.1203	-0.1348	-0.1476
WC115	-0.1498	-0.1605	-0.1729	-0.1864	-0.1374	-0.1519	-0.1639
WC116	-0.1394	-0.1483	-0.1610	-0.1748	-0.1370	-0.1481	-0.1598
WC117	-0.1380	-0.1469	-0.1600	-0.1757	-0.1479	-0.1599	-0.1694
WC118	-0.1318	-0.1426	-0.1574	-0.1743	-0.1519	-0.1641	-0.1756
WC119	-0.1308	-0.1415	-0.1585	-0.1769	-0.1549	-0.1694	-0.1823
WC120	-0.1103	-0.1195	-0.1345	-0.1534	-0.1349	-0.1450	-0.1574
WC121	-0.1327	-0.1464	-0.1664	-0.1852	-0.1543	-0.1697	-0.1885
WC122	-0.1157	-0.1256	-0.1448	-0.1633	-0.1377	-0.1516	-0.1724
WC123	-0.1278	-0.1453	-0.1641	-0.1798	-0.1557	-0.1735	-0.1969
WC124	-0.0529	-0.0628	-0.0763	-0.1048	-0.0525	-0.0636	-0.0826
WC125	-0.0478	-0.0577	-0.0775	-0.1156	-0.0551	-0.0672	-0.0905
WC126	-0.0478	-0.0560	-0.0741	-0.1093	-0.0517	-0.0606	-0.0794
WC127	-0.0399	-0.0473	-0.0594	-0.0825	-0.0444	-0.0514	-0.0664
WC128	-0.0424	-0.0492	-0.0592	-0.0748	-0.0477	-0.0544	-0.0661
WC129	-0.0459	-0.0507	-0.0590	-0.0683	-0.0506	-0.0571	-0.0652
WC130	-0.0540	-0.0596	-0.0678	-0.0755	-0.0590	-0.0657	-0.0746
WC131	-0.0689	-0.0750	-0.0843	-0.0923	-0.0767	-0.0843	-0.0937
WC132	-0.0467	-0.0559	-0.0721	-0.0951	-0.0532	-0.0636	-0.0851
WC133	-0.0492	-0.0595	-0.0804	-0.1171	-0.0538	-0.0645	-0.0871
WC134	-0.0508	-0.0607	-0.0781	-0.1114	-0.0535	-0.0640	-0.0822
WC135	-0.0410	-0.0479	-0.0607	-0.0835	-0.0439	-0.0514	-0.0649
WC136	-0.0441	-0.0498	-0.0593	-0.0734	-0.0479	-0.0548	-0.0656
WC137	-0.0486	-0.0547	-0.0618	-0.0700	-0.0525	-0.0595	-0.0680
WC138	-0.0305	-0.0326	-0.0371	-0.0466	-0.0436	-0.0468	-0.0553
WC139	-0.0641	-0.0707	-0.0782	-0.0858	-0.0730	-0.0794	-0.0890

TABLE 4. — Continued

(f) Trailing disk configuration, wind-tunnel disk, x/D = 0.55

TP	W061	W062	W063	W064	W361	W362	W363
M	0.30	0.50	0.71	0.82	0.30	0.50	0.71
α, deg	0.34	0.39	0.46	0.52	3.37	3.45	3.56
C_{D_b}	0.0891	0.0996	0.1108	0.1223	0.1173	0.1254	0.1397
C_D	0.1917	0.1866	0.1954	0.2119	0.2225	0.2188	0.2311
Re $\times$ 10^{-6}	19.77	30.37	37.53	39.70	20.17	30.70	37.87
q, kPa	6.101	15.207	25.600	30.728	6.126	15.257	25.724
(lb/ft^2)	(127.4)	(317.6)	(534.7)	(641.8)	(127.9)	(318.7)	(537.3)
C_A	0.1920	0.1868	0.1955	0.2119	0.2127	0.2088	0.2207
C_M	0.0129	0.0161	0.0209	0.0272	0.0270	0.0291	0.0340
C_L	-0.0566	-0.0319	-0.0079	-0.0110	0.1597	0.1602	0.1597
C_p at							
WC1	-0.1285	-0.1474	-0.1722	-0.2005	-0.0797	-0.1283	-0.1895
WC2	-0.1297	-0.1565	-0.1859	-0.2126	-0.1243	-0.1792	-0.2408
WC3	-0.1906	-0.2107	-0.2553	-0.2870	-0.1972	-0.2468	-0.3173
WC4	-0.2363	-0.2480	-0.3004	-0.3236	-0.2357	-0.2798	-0.3411
WC5	-0.2333	-0.2499	-0.2891	-0.3123	-0.2580	-0.2867	-0.3276
WC6	-0.1830	-0.2015	-0.2278	-0.2553	-0.2259	-0.2520	-0.2756
WC7	-0.1095	-0.1247	-0.1444	-0.1919	-0.1071	-0.1145	-0.1284
WC8	-0.1707	-0.1733	-0.1974	-0.2354	-0.1677	-0.1793	-0.1915
WC9	-0.2315	-0.2429	-0.2612	-0.2889	-0.2595	-0.2604	-0.2625
WC10	-0.2501	-0.2577	-0.2862	-0.3199	-0.2915	-0.2930	-0.2968
WC11	-0.1994	-0.2140	-0.2441	-0.2797	-0.1971	-0.2102	-0.2433
WC12	-0.1299	-0.1609	-0.1955	-0.2275	-0.1294	-0.1496	-0.1868
WC13	-0.2135	-0.2435	-0.2718	-0.2936	-0.1479	-0.1730	-0.2157
WC14	-0.2659	-0.2901	-0.3234	-0.3359	-0.2106	-0.2335	-0.2739
WC15	-0.2414	-0.2575	-0.2836	-0.3095	-0.1962	-0.2173	-0.2443
WC16	-0.1975	-0.2179	-0.2444	-0.2750	-0.1545	-0.1762	-0.2044
WC17	-0.1209	-0.1400	-0.1536	-0.1864	-0.1316	-0.1865	-0.1911
WC18	-0.1805	-0.2001	-0.2010	-0.2255	-0.2336	-0.2558	-0.2443
WC19	-0.2205	-0.2395	-0.2537	-0.2531	-0.2761	-0.2832	-0.2738
WC20	-0.2299	-0.2522	-0.2499	-0.2707	-0.2805	-0.2861	-0.2875
WC21	-0.2046	-0.2229	-0.2358	-0.2569	-0.2306	-0.2521	-0.2716
WC22	-0.1683	-0.1887	-0.2088	-0.2284	-0.1974	-0.2221	-0.2465
WC23	-0.1054	-0.1248	-0.1517	-0.1965	-0.0195	-0.0472	-0.0796
WC24	-0.1293	-0.1458	-0.1742	-0.2074	-0.0754	-0.1144	-0.1294
WC25	-0.1740	-0.1941	-0.2126	-0.2442	-0.1461	-0.1966	-0.2100
WC26	-0.2202	-0.2330	-0.2514	-0.2778	-0.2095	-0.2429	-0.2413
WC27	-0.1159	-0.1359	-0.1609	-0.1937	-0.1372	-0.1570	-0.1796
WC28	-0.1763	-0.1958	-0.2211	-0.2490	-0.1868	-0.2000	-0.2200

TABLE 4. — Continued

(f) Continued

TP	W061	W062	W063	W064	W361	W362	W363
M	0.30	0.50	0.71	0.82	0.30	0.50	0.71
α, deg	0.34	0.39	0.46	0.52	3.37	3.45	3.56
c_{D_b}	0.0891	0.0996	0.1108	0.1223	0.1173	0.1254	0.1397
c_D	0.1917	0.1866	0.1954	0.2119	0.2225	0.2188	0.2311
Re $\times$ 10^{-6}	19.77	30.37	37.53	39.70	20.17	30.70	37.87
q, kPa	6.101	15.207	25.600	30.728	6.126	15.257	25.724
(lb/ft^2)	(127.4)	(317.6)	(534.7)	(641.8)	(127.9)	(318.7)	(537.3)
c_A	0.1920	0.1868	0.1955	0.2119	0.2127	0.2088	0.2207
c_M	0.0129	0.0161	0.0209	0.0272	0.0270	0.0291	0.0340
c_L	-0.0566	-0.0319	-0.0079	-0.0110	0.1597	0.1602	0.1597
c_p at							
WC29	-0.2199	-0.2379	-0.2747	-0.2947	-0.2109	-0.2316	-0.2700
WC30	-0.0801	-0.0963	-0.1280	-0.1709	-0.1477	-0.1493	-0.1752
WC31	-0.1490	-0.1654	-0.2008	-0.2375	-0.2103	-0.1973	-0.2044
WC32	-0.2024	-0.2212	-0.2555	-0.2918	-0.2328	-0.2525	-0.2760
WC33	-0.2163	-0.2332	-0.2629	-0.3027	-0.2879	-0.2949	-0.3034
WC34	-0.1392	-0.1555	-0.1776	-0.2156	-0.1211	-0.1372	-0.1879
WC35	-0.1798	-0.1911	-0.2066	-0.2403	-0.1721	-0.2031	-0.2322
WC36	-0.2169	-0.2308	-0.2512	-0.2737	-0.2118	-0.2425	-0.2589
WC37	-0.3051	-0.3138	-0.3523	-0.3794	-0.2569	-0.2987	-0.3512
WC38	0.0157	0.0201	0.0120	0.0025	-0.0178	-0.0188	-0.0197
WC39	0.0095	0.0148	0.0072	-0.0031	-0.0213	-0.0240	-0.0250
WC40	0.0044	0.0042	0.0005	-0.0093	-0.0292	-0.0288	-0.0305
WC41	-0.0036	-0.0037	-0.0038	-0.0136	-0.0384	-0.0357	-0.0414
WC42	-0.0062	-0.0034	-0.0091	-0.0167	-0.0393	-0.0401	-0.0457
WC43	0.0103	0.0092	0.0008	-0.0086	-0.0288	-0.0321	-0.0324
WC44	-0.0008	-0.0007	-0.0067	-0.0165	-0.0342	-0.0352	-0.0375
WC45	-0.0038	-0.0070	-0.0128	-0.0207	-0.0314	-0.0318	-0.0377
WC46	0.0017	-0.0016	-0.0077	-0.0189	-0.0276	-0.0274	-0.0360
WC47	0.0171	0.0146	0.0122	0.0008	-0.0128	-0.0132	-0.0164
WC48	0.0131	0.0073	0.0069	-0.0016	-0.0069	-0.0077	-0.0104
WC49	0.0075	0.0059	0.0005	-0.0049	-0.0014	-0.0010	-0.0078
WC50	0.0154	0.0139	0.0062	-0.0010	0.0052	0.0049	-0.0066
WC51	0.0143	0.0137	0.0153	0.0078	-0.0312	-0.0277	-0.0279
WC52	0.0076	0.0051	0.0081	0.0054	-0.0355	-0.0345	-0.0390
WC53	0.0048	0.0031	0.0045	0.0031	-0.0344	-0.0357	-0.0447
WC54	0.0127	0.0102	0.0048	0.0001	-0.0305	-0.0316	-0.0451
WC55	-0.0245	-0.0272	-0.0262	-0.0214	-0.0401	-0.0418	-0.0415
WC56	-0.0217	-0.0240	-0.0229	-0.0174	-0.0382	-0.0407	-0.0413

TABLE 4. — Continued

(f) Continued

TP	W061	W062	W063	W064	W361	W362	W363
M	0.30	0.50	0.71	0.82	0.30	0.50	0.71
α, deg	0.34	0.39	0.46	0.52	3.37	3.45	3.56
c_{D_b}	0.0891	0.0996	0.1108	0.1223	0.1173	0.1254	0.1397
c_D	0.1917	0.1866	0.1954	0.2119	0.2225	0.2188	0.2311
$Re \times 10^{-6}$	19.77	30.37	37.53	39.70	20.17	30.70	37.87
q, kPa	6.101	15.207	25.600	30.728	6.126	15.257	25.724
(lb/ft^2)	(127.4)	(317.6)	(534.7)	(641.8)	(127.9)	(318.7)	(537.3)
c_A	0.1920	0.1868	0.1955	0.2119	0.2127	0.2088	0.2207
c_M	0.0129	0.0161	0.0209	0.0272	0.0270	0.0291	0.0340
c_L	-0.0566	-0.0319	-0.0079	-0.0110	0.1597	0.1602	0.1597
c_p at							
WC57	-0.0280	-0.0308	-0.0289	-0.0253	-0.0429	-0.0460	-0.0471
WC58	-0.0287	-0.0314	-0.0300	-0.0242	-0.0428	-0.0460	-0.0478
WC59	-0.0198	-0.0216	-0.0193	-0.0117	-0.0338	-0.0357	-0.0365
WC60	-0.0170	-0.0195	-0.0159	-0.0085	-0.0291	-0.0309	-0.0305
WC61	-0.0114	-0.0121	-0.0085	-0.0006	-0.0172	-0.0179	-0.0164
WC62	-0.0173	-0.0191	-0.0153	-0.0073	-0.0172	-0.0186	-0.0169
WC63	-0.0146	-0.0148	-0.0114	-0.0028	-0.0073	-0.0078	-0.0049
WC64	-0.0154	-0.0153	-0.0121	-0.0041	-0.0015	-0.0008	0.0020
WC65	-0.0051	-0.0044	-0.0002	0.0091	0.0147	0.0166	0.0207
WC66	-0.0037	-0.0030	0.0011	0.0102	0.0166	0.0191	0.0244
WC67	-0.0119	-0.0117	-0.0021	0.0004	0.0081	0.0082	0.0139
WC68	-0.0229	-0.0248	-0.0215	-0.0131	-0.0086	-0.0092	-0.0049
WC69	-0.0173	-0.0182	-0.0142	-0.0053	-0.0083	-0.0092	-0.0040
WC70	-0.0149	-0.0155	-0.0124	-0.0044	-0.0139	-0.0155	-0.0115
WC71	-0.0084	-0.0066	-0.0036	0.0041	-0.0119	-0.0120	-0.0099
WC72	-0.0139	-0.0131	-0.0109	-0.0037	-0.0272	-0.0250	-0.0260
WC73	-0.0142	-0.0143	-0.0116	-0.0049	-0.0289	-0.0297	-0.0301
WC74	-0.0148	-0.0150	-0.0131	-0.0078	-0.0321	-0.0344	-0.0344
WC75	-0.0164	-0.0185	-0.0163	-0.0121	-0.0364	-0.0373	-0.0416
WC76	-0.0234	-0.0261	-0.0241	-0.0200	-0.0416	-0.0426	-0.0464
WC77	-0.0305	-0.0331	-0.0317	-0.0269	-0.0467	-0.0502	-0.0509
WC78	-0.0491	-0.0567	-0.0641	-0.0768	-0.0478	-0.0555	-0.0650
WC79	-0.0450	-0.0503	-0.0602	-0.0707	-0.0462	-0.0519	-0.0623
WC80	-0.0459	-0.0512	-0.0606	-0.0701	-0.0505	-0.0570	-0.0660
WC81	-0.0471	-0.0508	-0.0594	-0.0698	-0.0552	-0.0617	-0.0697
WC82	-0.0287	-0.0301	-0.0380	-0.0470	-0.0403	-0.0439	-0.0511
WC83	-0.0458	-0.0506	-0.0592	-0.0654	-0.0608	-0.0677	-0.0754
WC84	-0.0366	-0.0381	-0.0456	-0.0499	-0.0494	-0.0523	-0.0592

TABLE 4. — Continued

(f) Continued

TP	W061	W062	W063	W064	W361	W362	W363
M	0.30	0.50	0.71	0.82	0.30	0.50	0.71
α, deg	0.34	0.39	0.46	0.52	3.37	3.45	3.56
c_{D_b}	0.0891	0.0996	0.1108	0.1223	0.1173	0.1254	0.1397
c_D	0.1917	0.1866	0.1954	0.2119	0.2225	0.2188	0.2311
$Re \times 10^{-6}$	19.77	30.37	37.53	39.70	20.17	30.70	37.87
q, kPa	6.101	15.207	25.600	30.728	6.126	15.257	25.724
(lb/ft^2)	(127.4)	(317.6)	(534.7)	(641.8)	(127.9)	(318.7)	(537.3)
c_A	0.1920	0.1868	0.1955	0.2119	0.2127	0.2088	0.2207
c_M	0.0129	0.0161	0.0209	0.0272	0.0270	0.0291	0.0340
c_L	-0.0566	-0.0319	-0.0079	-0.0110	0.1597	0.1602	0.1597
c_p at							
WC85	-0.0379	-0.0407	-0.0480	-0.0524	-0.0507	-0.0559	-0.0623
WC86	-0.0386	-0.0402	-0.0457	-0.0515	-0.0419	-0.0451	-0.0512
WC87	-0.0323	-0.0332	-0.0388	-0.0431	-0.0323	-0.0316	-0.0390
WC88	-0.0462	-0.0492	-0.0551	-0.0585	-0.0436	-0.0487	-0.0553
WC89	-0.0465	-0.0534	-0.0573	-0.0571	-0.0450	-0.0506	-0.0560
WC90	-0.0453	-0.0534	-0.0561	-0.0566	-0.0415	-0.0483	-0.0527
WC91	-0.0469	-0.0545	-0.0588	-0.0610	-0.0481	-0.0541	-0.0593
WC92	-0.0450	-0.0532	-0.0574	-0.0599	-0.0518	-0.0577	-0.0649
WC93	-0.0238	-0.0283	-0.0312	-0.0354	-0.0283	-0.0293	-0.0328
WC94	-0.0309	-0.0362	-0.0389	-0.0444	-0.0423	-0.0442	-0.0495
WC95	-0.0375	-0.0437	-0.0471	-0.0540	-0.0511	-0.0535	-0.0611
WC96	-0.0447	-0.0547	-0.0585	-0.0678	-0.0577	-0.0637	-0.0727
WC97	-0.0357	-0.0433	-0.0470	-0.0554	-0.0449	-0.0498	-0.0581
WC98	-0.0264	-0.0330	-0.0382	-0.0481	-0.0360	-0.0389	-0.0484
WC99	-0.0346	-0.0417	-0.0475	-0.0564	-0.0391	-0.0434	-0.0535
WC100	-0.0497	-0.0578	-0.0664	-0.0755	-0.0492	-0.0564	-0.0658
WC101	-0.1221	-0.1343	-0.1520	-0.1666	-0.1387	-0.1539	-0.1735
WC102	-0.1206	-0.1313	-0.1475	-0.1652	-0.1359	-0.1503	-0.1696
WC103	-0.1302	-0.1418	-0.1588	-0.1763	-0.1414	-0.1535	-0.1736
WC104	-0.1270	-0.1368	-0.1511	-0.1715	-0.1393	-0.1508	-0.1695
WC105	-0.1335	-0.1446	-0.1590	-0.1776	-0.1465	-0.1571	-0.1757
WC106	-0.1329	-0.1446	-0.1590	-0.1763	-0.1456	-0.1569	-0.1750
WC107	-0.1337	-0.1432	-0.1579	-0.1762	-0.1403	-0.1479	-0.1644
WC108	-0.1310	-0.1413	-0.1567	-0.1739	-0.1349	-0.1440	-0.1599
WC109	-0.1235	-0.1327	-0.1472	-0.1642	-0.1208	-0.1284	-0.1429
WC110	-0.1313	-0.1419	-0.1573	-0.1741	-0.1221	-0.1340	-0.1479
WC111	-0.1318	-0.1422	-0.1583	-0.1724	-0.1167	-0.1282	-0.1440
WC112	-0.0772	-0.0907	-0.0975	-0.0968	-0.0607	-0.0735	-0.0824

TABLE 4. — Continued

(f) Concluded

TP	W061	W062	W063	W064	W361	W362	W363
M	0.30	0.50	0.71	0.82	0.30	0.50	0.71
α, deg	0.34	0.39	0.46	0.52	3.37	3.45	3.56
c_{D_b}	0.0891	0.0996	0.1108	0.1223	0.1173	0.1254	0.1397
c_D	0.1917	0.1866	0.1954	0.2119	0.2225	0.2188	0.2311
Re $\times$ 10^{-6}	19.77	30.37	37.53	39.70	20.17	30.70	37.87
q, kPa	6.101	15.207	25.600	30.728	6.126	15.257	25.724
(lb/ft^2)	(127.4)	(317.6)	(534.7)	(641.8)	(127.9)	(318.7)	(537.3)
c_A	0.1920	0.1868	0.1955	0.2119	0.2127	0.2088	0.2207
c_M	0.0129	0.0161	0.0209	0.0272	0.0270	0.0291	0.0340
c_L	-0.0566	-0.0319	-0.0079	-0.0110	0.1597	0.1602	0.1597
c_p at							
WC113	-0.1338	-0.1457	-0.1586	-0.1685	-0.1157	-0.1268	-0.1404
WC114	-0.1318	-0.1423	-0.1553	-0.1648	-0.1136	-0.1245	-0.1359
WC115	-0.1403	-0.1543	-0.1670	-0.1769	-0.1298	-0.1418	-0.1531
WC116	-0.1307	-0.1429	-0.1540	-0.1638	-0.1272	-0.1390	-0.1482
WC117	-0.1299	-0.1409	-0.1528	-0.1641	-0.1354	-0.1490	-0.1595
WC118	-0.1249	-0.1364	-0.1491	-0.1618	-0.1361	-0.1517	-0.1653
WC119	-0.1234	-0.1342	-0.1480	-0.1608	-0.1416	-0.1535	-0.1703
WC120	-0.1034	-0.1105	-0.1223	-0.1363	-0.1219	-0.1319	-0.1474
WC121	-0.1246	-0.1367	-0.1531	-0.1697	-0.1430	-0.1571	-0.1767
WC122	-0.1072	-0.1166	-0.1317	-0.1509	-0.1274	-0.1380	-0.1618
WC123	-0.1212	-0.1355	-0.1525	-0.1695	-0.1484	-0.1608	-0.1862
WC124	-0.0519	-0.0613	-0.0770	-0.1037	-0.0532	-0.0628	-0.0823
WC125	-0.0468	-0.0579	-0.0763	-0.1148	-0.0548	-0.0672	-0.0890
WC126	-0.0475	-0.0552	-0.0739	-0.1080	-0.0514	-0.0596	-0.0782
WC127	-0.0395	-0.0456	-0.0591	-0.0799	-0.0446	-0.0515	-0.0644
WC128	-0.0433	-0.0482	-0.0587	-0.0731	-0.0477	-0.0550	-0.0648
WC129	-0.0451	-0.0495	-0.0579	-0.0655	-0.0506	-0.0571	-0.0646
WC130	-0.0537	-0.0579	-0.0666	-0.0733	-0.0587	-0.0646	-0.0726
WC131	-0.0678	-0.0713	-0.0811	-0.0873	-0.0755	-0.0811	-0.0909
WC132	-0.0467	-0.0537	-0.0704	-0.0920	-0.0533	-0.0639	-0.0844
WC133	-0.0497	-0.0580	-0.0778	-0.1156	-0.0540	-0.0648	-0.0869
WC134	-0.0515	-0.0597	-0.0765	-0.1084	-0.0552	-0.0629	-0.0821
WC135	-0.0412	-0.0471	-0.0587	-0.0801	-0.0456	-0.0526	-0.0654
WC136	-0.0462	-0.0518	-0.0603	-0.0748	-0.0500	-0.0552	-0.0659
WC137	-0.0485	-0.0557	-0.0605	-0.0686	-0.0532	-0.0597	-0.0672
WC138	-0.0294	-0.0316	-0.0354	-0.0432	-0.0438	-0.0469	-0.0543
WC139	-0.0615	-0.0683	-0.0742	-0.0804	-0.0719	-0.0775	-0.0878

TABLE 4. — Continued

(g) Trailing disk configuration,
wind-tunnel disk, x/D = 0.60

TP	W071	W072	W073	W074
M	0.30	0.50	0.71	0.82
α, deg	0.35	0.40	0.46	0.53
c_{D_b}	0.0901	0.0976	0.1112	0.1235
c_D	0.2024	0.1973	0.2085	0.2201
Re $\times 10^{-6}$	18.80	28.93	35.70	37.83
q, kPa	6.066	15.100	25.464	30.499
(lb/ft^2)	(126.7)	(315.4)	(531.8)	(637.0)
c_A	0.2021	0.1971	0.2080	0.2195
c_M	0.0144	0.0175	0.0210	0.0273
c_L	0.0547	0.0304	0.0601	0.0632
c_p at				
WC1	-0.1204	-0.1356	-0.1689	-0.1997
WC2	-0.1333	-0.1428	-0.1869	-0.2176
WC3	-0.1837	-0.1944	-0.2477	-0.2870
WC4	-0.2250	-0.2313	-0.2864	-0.3099
WC5	-0.2054	-0.2196	-0.2677	-0.2868
WC6	-0.1607	-0.1716	-0.2055	-0.2335
WC7	-0.0847	-0.0944	-0.1140	-0.1537
WC8	-0.1256	-0.1412	-0.1595	-0.2037
WC9	-0.1898	-0.1954	-0.2170	-0.2406
WC10	-0.2086	-0.2267	-0.2503	-0.2768
WC11	-0.1839	-0.2007	-0.2291	-0.2652
WC12	-0.1252	-0.1487	-0.1848	-0.2272
WC13	-0.2100	-0.2299	-0.2520	-0.2843
WC14	-0.2537	-0.2675	-0.2961	-0.3186
WC15	-0.2234	-0.2392	-0.2610	-0.2864
WC16	-0.1824	-0.2032	-0.2253	-0.2578
WC17	-0.1112	-0.1288	-0.1356	-0.1671
WC18	-0.1624	-0.1721	-0.1635	-0.1935
WC19	-0.1960	-0.2138	-0.2035	-0.2194
WC20	-0.2003	-0.2169	-0.2164	-0.2354
WC21	-0.1844	-0.2008	-0.2048	-0.2315
WC22	-0.1518	-0.1702	-0.1778	-0.2066
WC23	-0.0890	-0.1089	-0.1456	-0.1831
WC24	-0.1140	-0.1300	-0.1546	-0.1890
WC25	-0.1617	-0.1776	-0.1923	-0.2201
WC26	-0.1955	-0.2029	-0.2132	-0.2421
WC27	-0.0903	-0.1010	-0.1118	-0.1485
WC28	-0.1438	-0.1595	-0.1671	-0.1992

TABLE 4. — Continued

(g) Continued

TP	W071	W072	W073	W074
M	0.30	0.50	0.71	0.82
α, deg	0.35	0.40	0.46	0.53
C_{D_b}	0.0901	0.0976	0.1112	0.1235
C_D	0.2024	0.1973	0.2085	0.2201
Re $\times$ 10^{-6}	18.80	28.93	35.70	37.83
q, kPa	6.066	15.100	25.464	30.499
(lb/ft^2)	(126.7)	(315.4)	(531.8)	(637.0)
C_A	0.2021	0.1971	0.2080	0.2195
C_M	0.0144	0.0175	0.0210	0.0273
C_L	0.0547	0.0304	0.0601	0.0632
C_p at				
WC29	-0.1810	-0.1918	-0.2098	-0.2379
WC30	-0.0419	-0.0587	-0.0942	-0.1383
WC31	-0.1147	-0.1349	-0.1684	-0.2088
WC32	-0.1717	-0.1857	-0.2200	-0.2579
WC33	-0.1649	-0.1801	-0.2070	-0.2441
WC34	-0.1229	-0.1352	-0.1724	-0.2083
WC35	-0.1655	-0.1821	-0.2074	-0.2487
WC36	-0.1988	-0.2146	-0.2259	-0.2526
WC37	-0.2744	-0.2882	-0.3179	-0.3493
WC38	0.0090	0.0113	0.0021	-0.0094
WC39	0.0049	0.0061	-0.0056	-0.0137
WC40	-0.0045	-0.0043	-0.0128	-0.0212
WC41	-0.0162	-0.0156	-0.0220	-0.0290
WC42	-0.0167	-0.0172	-0.0252	-0.0325
WC43	-0.0010	-0.0007	-0.0140	-0.0198
WC44	-0.0104	-0.0121	-0.0232	-0.0286
WC45	-0.0167	-0.0183	-0.0279	-0.0321
WC46	-0.0089	-0.0111	-0.0237	-0.0306
WC47	0.0050	0.0053	0.0003	-0.0091
WC48	0.0013	0.0006	-0.0040	-0.0117
WC49	-0.0026	-0.0019	-0.0068	-0.0152
WC50	0.0065	0.0049	-0.0024	-0.0114
WC51	0.0065	0.0085	0.0017	-0.0037
WC52	-0.0016	-0.0011	-0.0067	-0.0083
WC53	-0.0063	-0.0060	-0.0147	-0.0127
WC54	0.0004	0.0000	-0.0106	-0.0138
WC55	-0.0239	-0.0273	-0.0264	-0.0235
WC56	-0.0204	-0.0235	-0.0235	-0.0209

TABLE 4. — Continued

(g) Continued

TP	W071	W072	W073	W074
M	0.30	0.50	0.71	0.82
α, deg	0.35	0.40	0.46	0.53
C_{D_b}	0.0901	0.0976	0.1112	0.1235
C_D	0.2024	0.1973	0.2085	0.2201
Re × 10^{-6}	18.80	28.93	35.70	37.83
q, kPa	6.066	15.100	25.464	30.499
(lb/ft^2)	(126.7)	(315.4)	(531.8)	(637.0)
C_A	0.2021	0.1971	0.2080	0.2195
C_M	0.0144	0.0175	0.0210	0.0273
C_L	0.0547	0.0304	0.0601	0.0632
C_p at				
WC57	-0.0276	-0.0300	-0.0301	-0.0271
WC58	-0.0282	-0.0307	-0.0308	-0.0275
WC59	-0.0184	-0.0204	-0.0189	-0.0155
WC60	-0.0160	-0.0188	-0.0160	-0.0116
WC61	-0.0104	-0.0117	-0.0079	-0.0010
WC62	-0.0158	-0.0182	-0.0146	-0.0064
WC63	-0.0136	-0.0149	-0.0119	-0.0052
WC64	-0.0140	-0.0161	-0.0132	-0.0073
WC65	-0.0039	-0.0041	0.0004	0.0064
WC66	-0.0024	-0.0030	0.0010	0.0093
WC67	-0.0102	-0.0120	-0.0083	-0.0016
WC68	-0.0208	-0.0242	-0.0226	-0.0148
WC69	-0.0158	-0.0184	-0.0145	-0.0090
WC70	-0.0142	-0.0161	-0.0120	-0.0056
WC71	-0.0077	-0.0070	-0.0030	0.0031
WC72	-0.0135	-0.0131	-0.0109	-0.0055
WC73	-0.0135	-0.0133	-0.0124	-0.0089
WC74	-0.0136	-0.0148	-0.0133	-0.0114
WC75	-0.0161	-0.0179	-0.0172	-0.0113
WC76	-0.0227	-0.0257	-0.0252	-0.0197
WC77	-0.0298	-0.0329	-0.0302	-0.0232
WC78	-0.0480	-0.0554	-0.0645	-0.0795
WC79	-0.0439	-0.0518	-0.0605	-0.0735
WC80	-0.0450	-0.0519	-0.0615	-0.0740
WC81	-0.0461	-0.0520	-0.0602	-0.0726
WC82	-0.0291	-0.0322	-0.0385	-0.0512
WC83	-0.0444	-0.0505	-0.0566	-0.0677
WC84	-0.0342	-0.0382	-0.0458	-0.0549

TABLE 4. — Continued

(g) Continued

TP	W071	W072	W073	W074
M	0.30	0.50	0.71	0.82
α, deg	0.35	0.40	0.46	0.53
c_{D_b}	0.0901	0.0976	0.1112	0.1235
c_D	0.2024	0.1973	0.2085	0.2201
Re $\times$ 10^{-6}	18.80	28.93	35.70	37.83
q, kPa	6.066	15.100	25.464	30.499
(lb/ft^2)	(126.7)	(315.4)	(531.8)	(637.0)
c_A	0.2021	0.1971	0.2080	0.2195
c_M	0.0144	0.0175	0.0210	0.0273
c_L	0.0547	0.0304	0.0601	0.0632
c_p at				
WC85	−0.0358	−0.0403	−0.0480	−0.0564
WC86	−0.0365	−0.0396	−0.0462	−0.0540
WC87	−0.0301	−0.0327	−0.0378	−0.0453
WC88	−0.0437	−0.0487	−0.0555	−0.0613
WC89	−0.0462	−0.0534	−0.0581	−0.0616
WC90	−0.0444	−0.0517	−0.0568	−0.0605
WC91	−0.0478	−0.0539	−0.0605	−0.0655
WC92	−0.0452	−0.0516	−0.0598	−0.0647
WC93	−0.0247	−0.0271	−0.0324	−0.0375
WC94	−0.0310	−0.0344	−0.0347	−0.0476
WC95	−0.0390	−0.0419	−0.0506	−0.0585
WC96	−0.0445	−0.0508	−0.0611	−0.0704
WC97	−0.0354	−0.0401	−0.0494	−0.0601
WC98	−0.0279	−0.0312	−0.0412	−0.0527
WC99	−0.0358	−0.0398	−0.0498	−0.0618
WC100	−0.0496	−0.0568	−0.0670	−0.0792
WC101	−0.1096	−0.1177	−0.1409	−0.1602
WC102	−0.1076	−0.1195	−0.1382	−0.1588
WC103	−0.1177	−0.1293	−0.1503	−0.1723
WC104	−0.1155	−0.1256	−0.1448	−0.1670
WC105	−0.1234	−0.1349	−0.1538	−0.1749
WC106	−0.1229	−0.1347	−0.1514	−0.1740
WC107	−0.1232	−0.1353	−0.1512	−0.1736
WC108	−0.1222	−0.1341	−0.1494	−0.1702
WC109	−0.1143	−0.1251	−0.1401	−0.1585
WC110	−0.1239	−0.1344	−0.1493	−0.1680
WC111	−0.1233	−0.1351	−0.1496	−0.1654
WC112	−0.0684	−0.0816	−0.0873	−0.0873

TABLE 4. — Continued

(g) Concluded

TP	W071	W072	W073	W074
M	0.30	0.50	0.71	0.82
α, deg	0.35	0.40	0.46	0.53
C_{D_b}	0.0901	0.0976	0.1112	0.1235
C_D	0.2024	0.1973	0.2085	0.2201
Re $\times$ 10^{-6}	18.80	28.93	35.70	37.83
q, kPa	6.066	15.100	25.464	30.499
(lb/ft^2)	(126.7)	(315.4)	(531.8)	(637.0)
C_A	0.2021	0.1971	0.2080	0.2195
C_M	0.0144	0.0175	0.0210	0.0273
C_L	0.0547	0.0304	0.0601	0.0632
C_p at				
WC113	-0.1248	-0.1376	-0.1495	-0.1639
WC114	-0.1235	-0.1353	-0.1455	-0.1589
WC115	-0.1317	-0.1460	-0.1574	-0.1715
WC116	-0.1229	-0.1350	-0.1436	-0.1607
WC117	-0.1220	-0.1334	-0.1414	-0.1571
WC118	-0.1166	-0.1266	-0.1345	-0.1529
WC119	-0.1134	-0.1236	-0.1340	-0.1506
WC120	-0.0943	-0.1000	-0.1106	-0.1300
WC121	-0.1126	-0.1242	-0.1376	-0.1591
WC122	-0.0963	-0.1034	-0.1184	-0.1387
WC123	-0.1072	-0.1210	-0.1395	-0.1584
WC124	-0.0523	-0.0630	-0.0794	-0.1058
WC125	-0.0460	-0.0566	-0.0752	-0.1149
WC126	-0.0469	-0.0567	-0.0743	-0.1110
WC127	-0.0391	-0.0468	-0.0606	-0.0843
WC128	-0.0426	-0.0494	-0.0593	-0.0761
WC129	-0.0453	-0.0514	-0.0578	-0.0692
WC130	-0.0519	-0.0574	-0.0638	-0.0753
WC131	-0.0629	-0.0692	-0.0792	-0.0898
WC132	-0.0466	-0.0551	-0.0718	-0.0958
WC133	-0.0497	-0.0600	-0.0799	-0.1190
WC134	-0.0508	-0.0603	-0.0765	-0.1115
WC135	-0.0409	-0.0483	-0.0607	-0.0848
WC136	-0.0435	-0.0492	-0.0587	-0.0756
WC137	-0.0474	-0.0534	-0.0610	-0.0725
WC138	-0.0290	-0.0300	-0.0367	-0.0476
WC139	-0.0591	-0.0643	-0.0738	-0.0835

TABLE 4. — Continued

(h) Trailing disk configuration, flight disk, x/D = 0.44

TP	W081	W082	W083	W084	W381	W382	W383
M	0.30	0.50	0.71	0.82	0.30	0.50	0.71
α, deg	0.29	0.32	0.39	0.46	3.25	3.32	3.44
C_{D_b}	0.0786	0.0865	0.1111	0.1474	0.1139	0.1216	0.1351
C_D	0.1724	0.1683	0.1893	0.2271	0.2011	0.1973	0.2047
$Re \times 10^{-6}$	20.53	31.13	38.33	40.57	20.17	30.87	38.07
q, kPa	6.168	15.385	17.494	31.161	6.170	15.342	25.860
(lb/ft^2)	(128.8)	(321.3)	(365.4)	(650.8)	(128.9)	(320.4)	(540.1)
C_A	0.1721	0.1680	0.1891	0.2268	0.1924	0.1884	0.1956
C_M	0.0102	0.0136	0.0185	0.0248	0.0302	0.0329	0.0385
C_L	0.0493	0.0469	0.0280	0.0335	0.1475	0.1472	0.1450
C_p at							
WC1	-0.1201	-0.1520	-0.1962	-0.2489	-0.1051	-0.1404	-0.1993
WC2	-0.1236	-0.1528	-0.1943	-0.2447	-0.1253	-0.1684	-0.2192
WC3	-0.2208	-0.2492	-0.2828	-0.3159	-0.2066	-0.2389	-0.2816
WC4	-0.3161	-0.3358	-0.3635	-0.3785	-0.2860	-0.3065	-0.3362
WC5	-0.3416	-0.3608	-0.3850	-0.3915	-0.3251	-0.3397	-0.3637
WC6	-0.2283	-0.2460	-0.2841	-0.3165	-0.2504	-0.2677	-0.3038
WC7	-0.0601	-0.1057	-0.1586	-0.2196	-0.1082	-0.1435	-0.2018
WC8	-0.1185	-0.1417	-0.1985	-0.2598	-0.1694	-0.1872	-0.2459
WC9	-0.2263	-0.2388	-0.2902	-0.3448	-0.2649	-0.2747	-0.3152
WC10	-0.3143	-0.3254	-0.3652	-0.4027	-0.3347	-0.3430	-0.3678
WC11	-0.2028	-0.2272	-0.2687	-0.3195	-0.2417	-0.2593	-0.3009
WC12	-0.0961	-0.1353	-0.1787	-0.2370	-0.1681	-0.1932	-0.2462
WC13	-0.2006	-0.2278	-0.2638	-0.3078	-0.2185	-0.2424	-0.2910
WC14	-0.3672	-0.3902	-0.4047	-0.4075	-0.3038	-0.3300	-0.3624
WC15	-0.3067	-0.3223	-0.3439	-0.3727	-0.2612	-0.2863	-0.3204
WC16	-0.2153	-0.2435	-0.2810	-0.3227	-0.1899	-0.2216	-0.2698
WC17	-0.1279	-0.1482	-0.2010	-0.2542	-0.1338	-0.1605	-0.2196
WC18	-0.1904	-0.2080	-0.2538	-0.2990	-0.2298	-0.2520	-0.2914
WC19	-0.2591	-0.2725	-0.3141	-0.3511	-0.3157	-0.3256	-0.3482
WC20	-0.3003	-0.3112	-0.3512	-0.3860	-0.3448	-0.3579	-0.3778
WC21	-0.2405	-0.2603	-0.3019	-0.3476	-0.2749	-0.3015	-0.3325
WC22	-0.1895	-0.2120	-0.2609	-0.3124	-0.2279	-0.2600	-0.3013
WC23	-0.1461	-0.1662	-0.2209	-0.2855	-0.1178	-0.1396	-0.2025
WC24	-0.1906	-0.2139	-0.2568	-0.3032	-0.1758	-0.2123	-0.2505
WC25	-0.2966	-0.3173	-0.3529	-0.3879	-0.2938	-0.3141	-0.3460
WC26	-0.2044	-0.2166	-0.2895	-0.3735	-0.1982	-0.2052	-0.2824
WC27	0.0269	0.0212	0.0026	-0.0369	0.0284	0.0194	0.0085
WC28	-0.1350	-0.1615	-0.2118	-0.2622	-0.1473	-0.1676	-0.2250
WC29	-0.2486	-0.2680	-0.3087	-0.3471	-0.2461	-0.2662	-0.3082
WC30	-0.3751	-0.4058	-0.4282	-0.4420	-0.3330	-0.3668	-0.4023
WC31	0.0393	0.0378	-0.0043	-0.0483	0.0143	0.0147	0.0002

TABLE 4. — Continued

(h) Continued

TP	W081	W082	W083	W084	W381	W382	W383
M	0.30	0.50	0.71	0.82	0.30	0.50	0.71
α, deg	0.29	0.32	0.39	0.46	3.25	3.32	3.44
c_{D_b}	0.0786	0.0865	0.1111	0.1474	0.1139	0.1216	0.1351
c_D	0.1724	0.1683	0.1893	0.2271	0.2011	0.1973	0.2047
Re × 10^{-6}	20.53	31.13	38.33	40.57	20.17	30.87	38.07
q, kPa	6.168	15.385	17.494	31.161	6.170	15.342	25.860
(lb/ft^2)	(128.8)	(321.3)	(365.4)	(650.8)	(128.9)	(320.4)	(540.1)
c_A	0.1721	0.1680	0.1891	0.2268	0.1924	0.1884	0.1956
c_M	0.0102	0.0136	0.0185	0.0248	0.0302	0.0329	0.0385
c_L	0.0493	0.0469	0.0280	0.0335	0.1475	0.1472	0.1450
c_p at							
WC32	0.0345	0.0287	0.0057	-0.0437	0.0156	0.0135	-0.0020
WC33	0.0251	0.0229	0.0081	-0.0547	0.0068	0.0082	-0.0071
WC34	0.0173	0.0192	0.0087	-0.0374	-0.0074	-0.0072	-0.0112
WC35	0.0248	0.0235	0.0087	-0.0239	-0.0057	-0.0020	-0.0103
WC36	0.0285	0.0297	-0.0072	-0.0403	-0.0002	-0.0009	-0.0054
WC37	0.0201	0.0211	-0.0096	-0.0498	-0.0077	-0.0069	-0.0126
WC38	0.0276	0.0264	0.0061	-0.0325	-0.0018	-0.0015	-0.0028
WC39	0.0233	0.0197	-0.0054	-0.0396	-0.0050	-0.0049	-0.0135
WC55	-0.0234	-0.0261	-0.0232	-0.0192	-0.0358	-0.0383	-0.0396
WC56	-0.0208	-0.0219	-0.0204	-0.0145	-0.0333	-0.0373	-0.0392
WC57	-0.0263	-0.0291	-0.0274	-0.0223	-0.0385	-0.0429	-0.0439
WC58	-0.0270	-0.0300	-0.0279	-0.0219	-0.0388	-0.0430	-0.0442
WC59	-0.0188	-0.0200	-0.0163	-0.0115	-0.0293	-0.0323	-0.0316
WC60	-0.0168	-0.0181	-0.0150	-0.0095	-0.0245	-0.0275	-0.0254
WC61	-0.0104	-0.0118	-0.0080	-0.0015	-0.0130	-0.0146	-0.0128
WC62	-0.0168	-0.0184	-0.0148	-0.0074	-0.0135	-0.0160	-0.0144
WC63	-0.0134	-0.0142	-0.0116	-0.0022	-0.0040	-0.0055	-0.0035
WC64	-0.0142	-0.0153	-0.0121	-0.0023	0.0011	0.0009	0.0051
WC65	-0.0041	-0.0042	-0.0000	0.0104	0.0172	0.0177	0.0238
WC66	-0.0032	-0.0037	0.0003	0.0104	0.0196	0.0200	0.0256
WC67	-0.0108	-0.0120	-0.0081	0.0001	0.0104	0.0091	0.0157
WC68	-0.0223	-0.0250	-0.0220	-0.0134	-0.0057	-0.0074	-0.0027
WC69	-0.0165	-0.0181	-0.0152	-0.0060	-0.0058	-0.0074	-0.0027
WC70	-0.0149	-0.0168	-0.0122	-0.0032	-0.0110	-0.0111	-0.0088
WC71	-0.0072	-0.0075	-0.0034	0.0060	-0.0086	-0.0090	-0.0063
WC72	-0.0135	-0.0139	-0.0114	-0.0030	-0.0224	-0.0234	-0.0228
WC73	-0.0129	-0.0140	-0.0107	-0.0045	-0.0242	-0.0249	-0.0261
WC74	-0.0132	-0.0141	-0.0113	-0.0053	-0.0274	-0.0292	-0.0300
WC75	-0.0150	-0.0173	-0.0163	-0.0101	-0.0318	-0.0345	-0.0360
WC76	-0.0218	-0.0244	-0.0239	-0.0169	-0.0373	-0.0401	-0.0412
WC77	-0.0286	-0.0325	-0.0306	-0.0240	-0.0423	-0.0445	-0.0472

TABLE 4. — Continued

(h)   Continued

TP	W081	W082	W083	W084	W381	W382	W383
M	0.30	0.50	0.71	0.82	0.30	0.50	0.71
α, deg	0.29	0.32	0.39	0.46	3.25	3.32	3.44
c_{D_b}	0.0786	0.0865	0.1111	0.1474	0.1139	0.1216	0.1351
c_D	0.1724	0.1683	0.1893	0.2271	0.2011	0.1973	0.2047
$Re \times 10^{-6}$	20.53	31.13	38.33	40.57	20.17	30.87	38.07
q, kPa	6.168	15.385	17.494	31.161	6.170	15.342	25.860
(lb/ft^2)	(128.8)	(321.3)	(365.4)	(650.8)	(128.9)	(320.4)	(540.1)
c_A	0.1721	0.1680	0.1891	0.2268	0.1924	0.1884	0.1956
c_M	0.0102	0.0136	0.0185	0.0248	0.0302	0.0329	0.0385
c_L	0.0493	0.0469	0.0280	0.0335	0.1475	0.1472	0.1450
c_p at							
WC78	-0.0489	-0.0556	-0.0644	-0.0758	-0.0440	-0.0514	-0.0615
WC79	-0.0449	-0.0511	-0.0600	-0.0705	-0.0437	-0.0492	-0.0601
WC80	-0.0464	-0.0525	-0.0619	-0.0705	-0.0467	-0.0539	-0.0629
WC81	-0.0474	-0.0530	-0.0611	-0.0703	-0.0503	-0.0586	-0.0668
WC82	-0.0294	-0.0315	-0.0381	-0.0467	-0.0356	-0.0401	-0.0485
WC83	-0.0459	-0.0522	-0.0592	-0.0658	-0.0562	-0.0647	-0.0724
WC84	-0.0355	-0.0398	-0.0453	-0.0509	-0.0449	-0.0499	-0.0556
WC85	-0.0370	-0.0428	-0.0478	-0.0548	-0.0472	-0.0521	-0.0588
WC86	-0.0374	-0.0419	-0.0473	-0.0528	-0.0394	-0.0429	-0.0489
WC87	-0.0314	-0.0350	-0.0402	-0.0443	-0.0302	-0.0318	-0.0375
WC88	-0.0468	-0.0512	-0.0569	-0.0583	-0.0415	-0.0475	-0.0511
WC89	-0.0464	-0.0538	-0.0581	-0.0570	-0.0409	-0.0500	-0.0525
WC90	-0.0464	-0.0534	-0.0582	-0.0563	-0.0389	-0.0469	-0.0507
WC91	-0.0475	-0.0533	-0.0584	-0.0603	-0.0448	-0.0513	-0.0550
WC92	-0.0456	-0.0515	-0.0564	-0.0624	-0.0479	-0.0546	-0.0596
WC93	-0.0240	-0.0268	-0.0300	-0.0348	-0.0246	-0.0257	-0.0300
WC94	-0.0320	-0.0348	-0.0386	-0.0443	-0.0392	-0.0401	-0.0455
WC95	-0.0387	-0.0409	-0.0466	-0.0536	-0.0467	-0.0490	-0.0573
WC96	-0.0468	-0.0524	-0.0595	-0.0662	-0.0537	-0.0591	-0.0692
WC97	-0.0361	-0.0406	-0.0474	-0.0569	-0.0416	-0.0454	-0.0550
WC98	-0.0273	-0.0306	-0.0372	-0.0467	-0.0321	-0.0348	-0.0445
WC99	-0.0349	-0.0395	-0.0465	-0.0563	-0.0360	-0.0402	-0.0506
WC100	-0.0512	-0.0576	-0.0649	-0.0759	-0.0461	-0.0523	-0.0634
WC101	-0.1423	-0.1569	-0.1774	-0.1911	-0.1462	-0.1603	-0.1842
WC102	-0.1397	-0.1527	-0.1713	-0.1894	-0.1381	-0.1547	-0.1780
WC103	-0.1443	-0.1566	-0.1774	-0.1966	-0.1419	-0.1570	-0.1822
WC104	-0.1391	-0.1509	-0.1718	-0.1912	-0.1437	-0.1551	-0.1784
WC105	-0.1444	-0.1569	-0.1781	-0.1979	-0.1537	-0.1648	-0.1886
WC106	-0.1426	-0.1550	-0.1758	-0.1986	-0.1578	-0.1691	-0.1902
WC107	-0.1432	-0.1552	-0.1763	-0.1984	-0.1565	-0.1659	-0.1846
WC108	-0.1411	-0.1560	-0.1754	-0.1962	-0.1533	-0.1648	-0.1848

TABLE 4. — Continued

(h) Concluded

TP	W081	W082	W083	W084	W381	W382	W383
M	0.30	0.50	0.71	0.82	0.30	0.50	0.71
α, deg	0.29	0.32	0.39	0.46	3.25	3.32	3.44
C_{D_b}	0.0786	0.0865	0.1111	0.1474	0.1139	0.1216	0.1351
C_D	0.1724	0.1683	0.1893	0.2271	0.2011	0.1973	0.2047
Re $\times$ 10^{-6}	20.53	31.13	38.33	40.57	20.17	30.87	38.07
q, kPa	6.168	15.385	17.494	31.161	6.170	15.342	25.860
(lb/ft^2)	(128.8)	(321.3)	(365.4)	(650.8)	(128.9)	(320.4)	(540.1)
C_A	0.1721	0.1680	0.1891	0.2268	0.1924	0.1884	0.1956
C_M	0.0102	0.0136	0.0185	0.0248	0.0302	0.0329	0.0385
C_L	0.0493	0.0469	0.0280	0.0335	0.1475	0.1472	0.1450
C_p at							
WC109	-0.1350	-0.1472	-0.1660	-0.1844	-0.1407	-0.1521	-0.1715
WC110	-0.1434	-0.1562	-0.1760	-0.1909	-0.1439	-0.1577	-0.1777
WC111	-0.1433	-0.1566	-0.1757	-0.1898	-0.1380	-0.1523	-0.1713
WC112	-0.0857	-0.0985	-0.1048	-0.1032	-0.0708	-0.0865	-0.0976
WC113	-0.1460	-0.1614	-0.1789	-0.1889	-0.1313	-0.1463	-0.1658
WC114	-0.1439	-0.1582	-0.1739	-0.1846	-0.1277	-0.1419	-0.1589
WC115	-0.1546	-0.1699	-0.1866	-0.1979	-0.1456	-0.1590	-0.1770
WC116	-0.1450	-0.1583	-0.1758	-0.1865	-0.1445	-0.1557	-0.1733
WC117	-0.1448	-0.1582	-0.1752	-0.1891	-0.1532	-0.1651	-0.1832
WC118	-0.1393	-0.1518	-0.1724	-0.1872	-0.1541	-0.1691	-0.1882
WC119	-0.1380	-0.1507	-0.1731	-0.1893	-0.1563	-0.1717	-0.1925
WC120	-0.1161	-0.1239	-0.1444	-0.1638	-0.1360	-0.1454	-0.1654
WC121	-0.1396	-0.1533	-0.1765	-0.1946	-0.1566	-0.1720	-0.1936
WC122	-0.1208	-0.1317	-0.1539	-0.1727	-0.1404	-0.1532	-0.1745
WC123	-0.1364	-0.1537	-0.1728	-0.1851	-0.1337	-0.1538	-0.1746
WC124	-0.0513	-0.0614	-0.0768	-0.1014	-0.0493	-0.0575	-0.0797
WC125	-0.0473	-0.0573	-0.0775	-0.1153	-0.0514	-0.0631	-0.0863
WC126	-0.0473	-0.0553	-0.0734	-0.1075	-0.0486	-0.0561	-0.0756
WC127	-0.0393	-0.0461	-0.0598	-0.0798	-0.0407	-0.0487	-0.0615
WC128	-0.0432	-0.0495	-0.0594	-0.0729	-0.0431	-0.0517	-0.0619
WC129	-0.0471	-0.0523	-0.0592	-0.0665	-0.0467	-0.0537	-0.0624
WC130	-0.0555	-0.0610	-0.0684	-0.0753	-0.0561	-0.0637	-0.0720
WC131	-0.0719	-0.0786	-0.0869	-0.0938	-0.0743	-0.0825	-0.0849
WC132	-0.0457	-0.0551	-0.0690	-0.0932	-0.0499	-0.0595	-0.0802
WC133	-0.0477	-0.0585	-0.0776	-0.1155	-0.0511	-0.0621	-0.0840
WC134	-0.0508	-0.0607	-0.0767	-0.1091	-0.0524	-0.0621	-0.0800
WC135	-0.0404	-0.0479	-0.0598	-0.0798	-0.0430	-0.0513	-0.0616
WC136	-0.0443	-0.0510	-0.0599	-0.0729	-0.0456	-0.0529	-0.0620
WC137	-0.0500	-0.0562	-0.0632	-0.0690	-0.0508	-0.0578	-0.0654
WC138	-0.0351	-0.0359	-0.0416	-0.0487	-0.0418	-0.0450	-0.0515
WC139	-0.0669	-0.0718	-0.0793	-0.0885	-0.0722	-0.0785	-0.0874

TABLE 4. — Continued

(i) Trailing disk configuration, flight disk, x/D = 0.50

TP	W091	W092	W093	W094	W391	W392	W393
M	0.30	0.50	0.71	0.82	0.30	0.50	0.71
α, deg	0.29	0.32	0.39	0.43	3.34	3.41	3.50
c_{D_b}	0.0819	0.0898	0.1076	0.1345	0.1212	0.1292	0.1550
c_D	0.1826	0.1773	0.1884	0.2179	0.2129	0.2075	0.2252
Re × 10^{-6}	20.17	30.63	38.03	40.30	20.50	31.13	38.27
q, kPa	6.174	15.423	25.953	31.154	6.146	15.335	25.865
(lb/ft^2)	(128.9)	(322.1)	(542.0)	(650.7)	(128.4)	(320.3)	(540.2)
c_A	0.1824	0.1771	0.1882	0.2178	0.2040	0.1985	0.2158
c_M	0.0132	0.0160	0.0204	0.0264	0.0307	0.0330	0.0359
c_L	0.0372	0.0329	0.0277	0.0143	0.1467	0.1457	0.1476
c_p at							
WC1	-0.1229	-0.1484	-0.1713	-0.2169	-0.0779	-0.1193	-0.1968
WC2	-0.1230	-0.1430	-0.1718	-0.2112	-0.1052	-0.1497	-0.2493
WC3	-0.2136	-0.2284	-0.2545	-0.2735	-0.1625	-0.2008	-0.3332
WC4	-0.2785	-0.2914	-0.3100	-0.3256	-0.2218	-0.2507	-0.3646
WC5	-0.2817	-0.2914	-0.3165	-0.3329	-0.2580	-0.2776	-0.3506
WC6	-0.1868	-0.2022	-0.2370	-0.2719	-0.2138	-0.2376	-0.2858
WC7	-0.0926	-0.1090	-0.1609	-0.2147	-0.1273	-0.1347	-0.1423
WC8	-0.1107	-0.1421	-0.1972	-0.2510	-0.1775	-0.1943	-0.2046
WC9	-0.1851	-0.2119	-0.2762	-0.3277	-0.2779	-0.2858	-0.2647
WC10	-0.2322	-0.2653	-0.3168	-0.3556	-0.3195	-0.3216	-0.3006
WC11	-0.1918	-0.2101	-0.2507	-0.2889	-0.2118	-0.2296	-0.2559
WC12	-0.1356	-0.1537	-0.1859	-0.2209	-0.1308	-0.1567	-0.2062
WC13	-0.2237	-0.2417	-0.2611	-0.2854	-0.1670	-0.1956	-0.2696
WC14	-0.3135	-0.3290	-0.3363	-0.3485	-0.2455	-0.2670	-0.3369
WC15	-0.2647	-0.2743	-0.2999	-0.3295	-0.2235	-0.2473	-0.2838
WC16	-0.2119	-0.2233	-0.2553	-0.2917	-0.1668	-0.1948	-0.2365
WC17	-0.1074	-0.1298	-0.1668	-0.2215	-0.1393	-0.1767	-0.1990
WC18	-0.1604	-0.1815	-0.2138	-0.2609	-0.2375	-0.2557	-0.2550
WC19	-0.2054	-0.2331	-0.2639	-0.3029	-0.2960	-0.3120	-0.2876
WC20	-0.2274	-0.2503	-0.2878	-0.3237	-0.3044	-0.3136	-0.2997
WC21	-0.1971	-0.2214	-0.2509	-0.2920	-0.2333	-0.2554	-0.2815
WC22	-0.1583	-0.1853	-0.2207	-0.2654	-0.1974	-0.2232	-0.2531
WC23	-0.1228	-0.1369	-0.1801	-0.2295	-0.0716	-0.1003	-0.1324
WC24	-0.1658	-0.1847	-0.2116	-0.2640	-0.1403	-0.1720	-0.2197
WC25	-0.2280	-0.2492	-0.2852	-0.3273	-0.2492	-0.2684	-0.2820
WC26	-0.1074	-0.1483	-0.2107	-0.2908	-0.1647	-0.1714	-0.0941
WC27	-0.0010	0.0004	-0.0041	-0.0373	-0.0020	-0.0087	-0.0455
WC28	-0.1034	-0.1334	-0.1693	-0.2203	-0.1238	-0.1454	-0.1733
WC29	-0.2037	-0.2209	-0.2594	-0.2939	-0.2143	-0.2299	-0.2625
WC30	-0.3321	-0.3363	-0.3519	-0.3572	-0.2234	-0.2625	-0.3655
WC31	0.0271	0.0270	0.0090	-0.0201	-0.0039	-0.0070	-0.0078

TABLE 4. — Continued

TP	W091	W092	W093	W094	W391	W392	W393
M	0.30	0.50	0.71	0.82	0.30	0.50	0.71
α, deg	0.29	0.32	0.39	0.43	3.34	3.41	3.50
C_{D_b}	0.0819	0.0898	0.1076	0.1345	0.1212	0.1292	0.1550
C_D	0.1826	0.1773	0.1884	0.2179	0.2129	0.2075	0.2252
Re $\times$ 10^{-6}	20.17	30.63	38.03	40.30	20.50	31.13	38.27
q, kPa	6.174	15.423	25.953	31.154	6.146	15.335	25.865
(lb/ft^2)	(128.9)	(322.1)	(542.0)	(650.7)	(128.4)	(320.3)	(540.2)
C_A	0.1824	0.1771	0.1882	0.2178	0.2040	0.1985	0.2158
C_M	0.0132	0.0160	0.0204	0.0264	0.0307	0.0330	0.0359
C_L	0.0372	0.0329	0.0277	0.0143	0.1467	0.1457	0.1476
C_p at							
WC32	0.0241	0.0226	0.0143	-0.0232	-0.0090	-0.0095	-0.0146
WC33	0.0160	0.0163	0.0026	-0.0179	-0.0182	-0.0192	-0.0257
WC34	0.0081	0.0066	-0.0018	-0.0171	-0.0277	-0.0264	-0.0425
WC35	0.0140	0.0136	0.0072	-0.0212	-0.0262	-0.0253	-0.0394
WC36	0.0169	0.0163	0.0009	-0.0218	-0.0150	-0.0190	-0.0237
WC37	0.0088	0.0077	-0.0018	-0.0312	-0.0187	-0.0198	-0.0321
WC38	0.0135	0.0110	0.0035	-0.0323	-0.0118	-0.0123	-0.0276
WC39	0.0035	0.0083	-0.0051	-0.0433	-0.0153	-0.0153	-0.0318
WC55	-0.0195	-0.0203	-0.0207	-0.0156	-0.0360	-0.0380	-0.0388
WC56	-0.0158	-0.0170	-0.0174	-0.0123	-0.0337	-0.0359	-0.0371
WC57	-0.0222	-0.0252	-0.0247	-0.0184	-0.0384	-0.0410	-0.0432
WC58	-0.0224	-0.0258	-0.0252	-0.0185	-0.0378	-0.0413	-0.0429
WC59	-0.0139	-0.0131	-0.0142	-0.0072	-0.0292	-0.0315	-0.0328
WC60	-0.0121	-0.0112	-0.0120	-0.0032	-0.0250	-0.0264	-0.0269
WC61	-0.0068	-0.0050	-0.0046	0.0040	-0.0128	-0.0134	-0.0135
WC62	-0.0124	-0.0135	-0.0108	-0.0036	-0.0129	-0.0140	-0.0143
WC63	-0.0097	-0.0105	-0.0072	0.0018	-0.0033	-0.0031	-0.0019
WC64	-0.0100	-0.0114	-0.0075	-0.0000	0.0026	0.0012	0.0059
WC65	-0.0000	-0.0004	0.0034	0.0124	0.0182	0.0189	0.0244
WC66	0.0013	0.0004	0.0049	0.0126	0.0205	0.0208	0.0253
WC67	-0.0070	-0.0081	-0.0044	0.0037	0.0113	0.0101	0.0167
WC68	-0.0183	-0.0191	-0.0169	-0.0104	-0.0044	-0.0066	-0.0027
WC69	-0.0123	-0.0136	-0.0092	-0.0029	-0.0046	-0.0060	-0.0011
WC70	-0.0113	-0.0124	-0.0077	-0.0017	-0.0109	-0.0109	-0.0089
WC71	-0.0035	-0.0042	0.0016	0.0079	-0.0086	-0.0070	-0.0063
WC72	-0.0085	-0.0098	-0.0048	0.0004	-0.0221	-0.0242	-0.0229
WC73	-0.0088	-0.0097	-0.0065	-0.0009	-0.0237	-0.0263	-0.0263
WC74	-0.0089	-0.0096	-0.0069	-0.0022	-0.0268	-0.0300	-0.0292
WC75	-0.0105	-0.0134	-0.0104	-0.0055	-0.0307	-0.0355	-0.0355
WC76	-0.0181	-0.0216	-0.0179	-0.0129	-0.0359	-0.0406	-0.0416
WC77	-0.0246	-0.0280	-0.0246	-0.0186	-0.0415	-0.0460	-0.0468

TABLE 4. — Continued

(i)   Continued

TP	W091	W092	W093	W094	W391	W392	W393
M	0.30	0.50	0.71	0.82	0.30	0.50	0.71
α, deg	0.29	0.32	0.39	0.43	3.34	3.41	3.50
C_{D_b}	0.0819	0.0898	0.1076	0.1345	0.1212	0.1292	0.1550
C_D	0.1826	0.1773	0.1884	0.2179	0.2129	0.2075	0.2252
Re × 10^{-6}	20.17	30.63	38.03	40.30	20.50	31.13	38.27
q, kPa	6.174	15.423	25.953	31.154	6.146	15.335	25.865
(lb/ft^2)	(128.9)	(322.1)	(542.0)	(650.7)	(128.4)	(320.3)	(540.2)
C_A	0.1824	0.1771	0.1882	0.2178	0.2040	0.1985	0.2158
C_M	0.0132	0.0160	0.0204	0.0264	0.0307	0.0330	0.0359
C_L	0.0372	0.0329	0.0277	0.0143	0.1467	0.1457	0.1476
C_p at							
WC78	-0.0433	-0.0519	-0.0582	-0.0702	-0.0435	-0.0515	-0.0606
WC79	-0.0404	-0.0474	-0.0548	-0.0678	-0.0419	-0.0496	-0.0581
WC80	-0.0415	-0.0483	-0.0552	-0.0689	-0.0455	-0.0533	-0.0619
WC81	-0.0426	-0.0494	-0.0563	-0.0672	-0.0503	-0.0573	-0.0657
WC82	-0.0242	-0.0290	-0.0343	-0.0439	-0.0356	-0.0392	-0.0466
WC83	-0.0419	-0.0492	-0.0546	-0.0621	-0.0562	-0.0634	-0.0711
WC84	-0.0316	-0.0358	-0.0392	-0.0475	-0.0447	-0.0493	-0.0557
WC85	-0.0327	-0.0389	-0.0419	-0.0515	-0.0464	-0.0517	-0.0569
WC86	-0.0332	-0.0371	-0.0421	-0.0479	-0.0390	-0.0418	-0.0463
WC87	-0.0275	-0.0309	-0.0348	-0.0411	-0.0275	-0.0288	-0.0345
WC88	-0.0416	-0.0476	-0.0521	-0.0560	-0.0396	-0.0/.51	-0.0509
WC89	-0.0422	-0.0516	-0.0540	-0.0557	-0.0404	-0.0481	-0.0521
WC90	-0.0406	-0.0501	-0.0533	-0.0558	-0.0380	-0.0450	-0.0484
WC91	-0.0431	-0.0533	-0.0537	-0.0590	-0.0450	-0.0499	-0.0536
WC92	-0.0408	-0.0508	-0.0520	-0.0567	-0.0478	-0.0542	-0.0586
WC93	-0.0195	-0.0242	-0.0240	-0.0303	-0.0243	-0.0253	-0.0292
WC94	-0.0283	-0.0328	-0.0343	-0.0418	-0.0379	-0.0391	-0.0453
WC95	-0.0349	-0.0395	-0.0425	-0.0508	-0.0458	-0.0481	-0.0565
WC96	-0.0421	-0.0507	-0.0546	-0.0630	-0.0532	-0.0590	-0.0681
WC97	-0.0329	-0.0386	-0.0438	-0.0534	-0.0402	-0.0456	-0.0552
WC98	-0.0235	-0.0272	-0.0339	-0.0450	-0.0304	-0.0347	-0.0450
WC99	-0.0315	-0.0375	-0.0429	-0.0536	-0.0349	-0.0400	-0.0502
WC100	-0.0460	-0.0550	-0.0617	-0.0728	-0.0452	-0.0520	-0.0617
WC101	-0.1221	-0.1373	-0.1556	-0.1748	-0.1297	-0.1454	-0.1722
WC102	-0.1187	-0.1304	-0.1510	-0.1706	-0.1290	-0.1422	-0.1682
WC103	-0.1230	-0.1353	-0.1583	-0.1789	-0.1332	-0.1464	-0.1703
WC104	-0.1208	-0.1332	-0.1528	-0.1743	-0.1349	-0.1448	-0.1649
WC105	-0.1272	-0.1409	-0.1619	-0.1823	-0.1437	-0.1557	-0.1695
WC106	-0.1276	-0.1380	-0.1619	-0.1813	-0.1474	-0.1588	-0.1723
WC107	-0.1283	-0.1379	-0.1620	-0.1800	-0.1456	-0.1527	-0.1660
WC108	-0.1279	-0.1381	-0.1607	-0.1789	-0.1401	-0.1501	-0.1646

TABLE 4. — Concluded

(i) Concluded

TP	W091	W092	W093	W094	W391	W392	W393
M	0.30	0.50	0.71	0.82	0.30	0.50	0.71
α, deg	0.29	0.32	0.39	0.43	3.34	3.41	3.50
c_{D_b}	0.0819	0.0898	0.1076	0.1345	0.1212	0.1292	0.1550
c_D	0.1826	0.1773	0.1884	0.2179	0.2129	0.2075	0.2252
$Re \times 10^{-6}$	20.17	30.63	38.03	40.30	20.50	31.13	38.27
q, kPa	6.174	15.423	25.953	31.154	6.146	15.335	25.865
(lb/ft^2)	(128.9)	(322.1)	(542.0)	(650.7)	(128.4)	(320.3)	(540.2)
c_A	0.1824	0.1771	0.1882	0.2178	0.2040	0.1985	0.2158
c_M	0.0132	0.0160	0.0204	0.0264	0.0307	0.0330	0.0359
c_L	0.0372	0.0329	0.0277	0.0143	0.1467	0.1457	0.1476
c_p at							
WC109	-0.1218	-0.1326	-0.1501	-0.1683	-0.1291	-0.1362	-0.1502
WC110	-0.1313	-0.1428	-0.1611	-0.1775	-0.1314	-0.1420	-0.1563
WC111	-0.1309	-0.1440	-0.1611	-0.1769	-0.1244	-0.1383	-0.1517
WC112	-0.0770	-0.0893	-0.0986	-0.0969	-0.0658	-0.0793	-0.0881
WC113	-0.1365	-0.1484	-0.1625	-0.1751	-0.1199	-0.1344	-0.1495
WC114	-0.1343	-0.1451	-0.1583	-0.1686	-0.1157	-0.1306	-0.1427
WC115	-0.1419	-0.1533	-0.1663	-0.1813	-0.1317	-0.1465	-0.1589
WC116	-0.1311	-0.1430	-0.1536	-0.1700	-0.1287	-0.1424	-0.1523
WC117	-0.1302	-0.1415	-0.1544	-0.1720	-0.1364	-0.1495	-0.1616
WC118	-0.1223	-0.1363	-0.1499	-0.1699	-0.1375	-0.1504	-0.1663
WC119	-0.1203	-0.1348	-0.1500	-0.1711	-0.1400	-0.1563	-0.1722
WC120	-0.1002	-0.1082	-0.1243	-0.1444	-0.1201	-0.1328	-0.1482
WC121	-0.1201	-0.1343	-0.1539	-0.1745	-0.1399	-0.1574	-0.1777
WC122	-0.1025	-0.1132	-0.1315	-0.1519	-0.1235	-0.1389	-0.1607
WC123	-0.1156	-0.1322	-0.1489	-0.1654	-0.1230	-0.1435	-0.1671
WC124	-0.0471	-0.0576	-0.0714	-0.0975	-0.0482	-0.0588	-0.0786
WC125	-0.0465	-0.0582	-0.0765	-0.1142	-0.0514	-0.0640	-0.0860
WC126	-0.0431	-0.0518	-0.0679	-0.1051	-0.0471	-0.0570	-0.0740
WC127	-0.0350	-0.0424	-0.0534	-0.0786	-0.0399	-0.0484	-0.0609
WC128	-0.0386	-0.0462	-0.0549	-0.0700	-0.0430	-0.0508	-0.0610
WC129	-0.0406	-0.0480	-0.0537	-0.0624	-0.0458	-0.0524	-0.0603
WC130	-0.0503	-0.0569	-0.0625	-0.0705	-0.0548	-0.0613	-0.0697
WC131	-0.0648	-0.0711	-0.0774	-0.0874	-0.0716	-0.0793	-0.0884
WC132	-0.0424	-0.0527	-0.0617	-0.0904	-0.0488	-0.0596	-0.0788
WC133	-0.0448	-0.0556	-0.0676	-0.1110	-0.0509	-0.0614	-0.0822
WC134	-0.0474	-0.0577	-0.0677	-0.1052	-0.0503	-0.0599	-0.0779
WC135	-0.0365	-0.0454	-0.0477	-0.0767	-0.0412	-0.0489	-0.0617
WC136	-0.0395	-0.0476	-0.0600	-0.0699	-0.0443	-0.0509	-0.0610
WC137	-0.0441	-0.0526	-0.0579	-0.0669	-0.0491	-0.0558	-0.0630
WC138	-0.0292	-0.0339	-0.0348	-0.0462	-0.0401	-0.0423	-0.0486
WC139	-0.0582	-0.0672	-0.0710	-0.0796	-0.0683	-0.0745	-0.0829
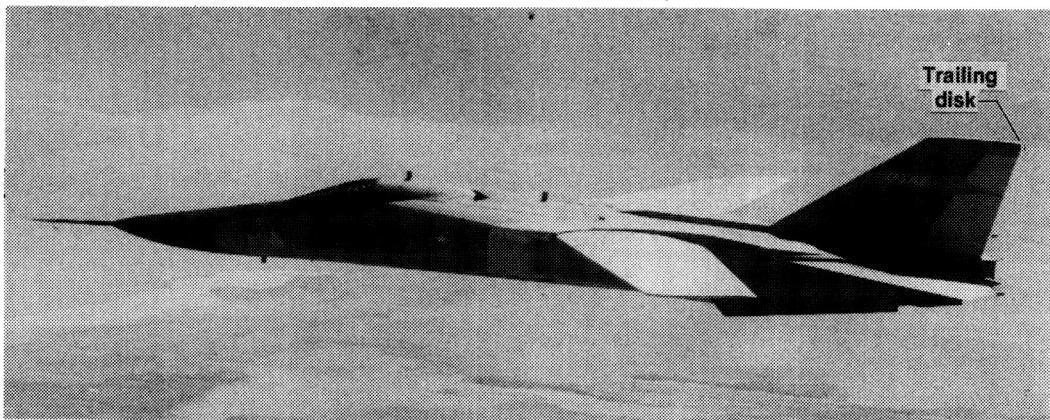
E 32727

Figure 1. F-111 airplane during flight. (Trailing disk location is indicated on body of revolution.)
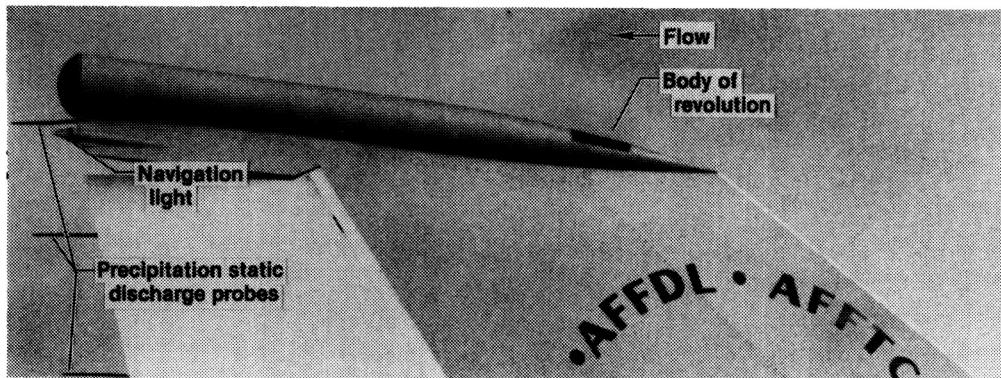
E 25493
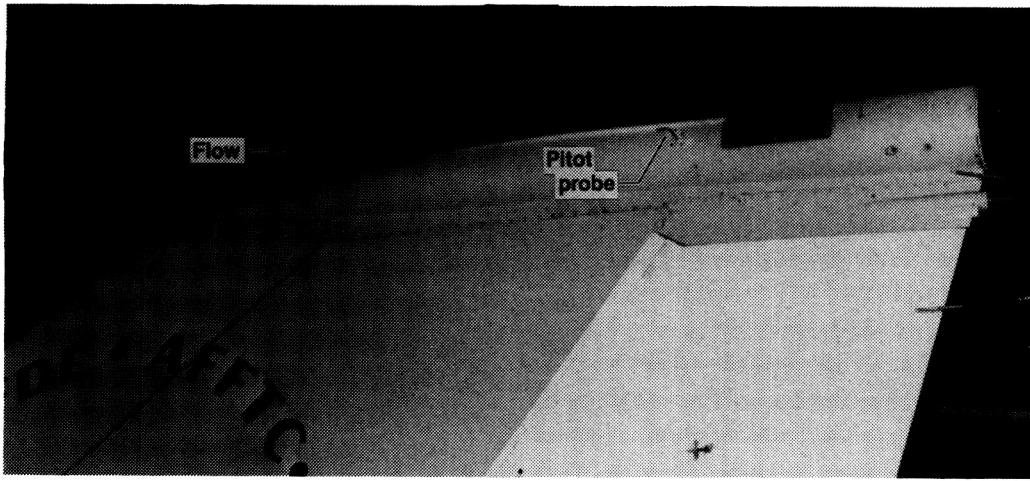
E 29321

Figure 2. Side view of body of revolution and portion of vertical tail. (Hemispherical base is installed. Dog-leg pitot probe is shown in lower photo.)

E 27969
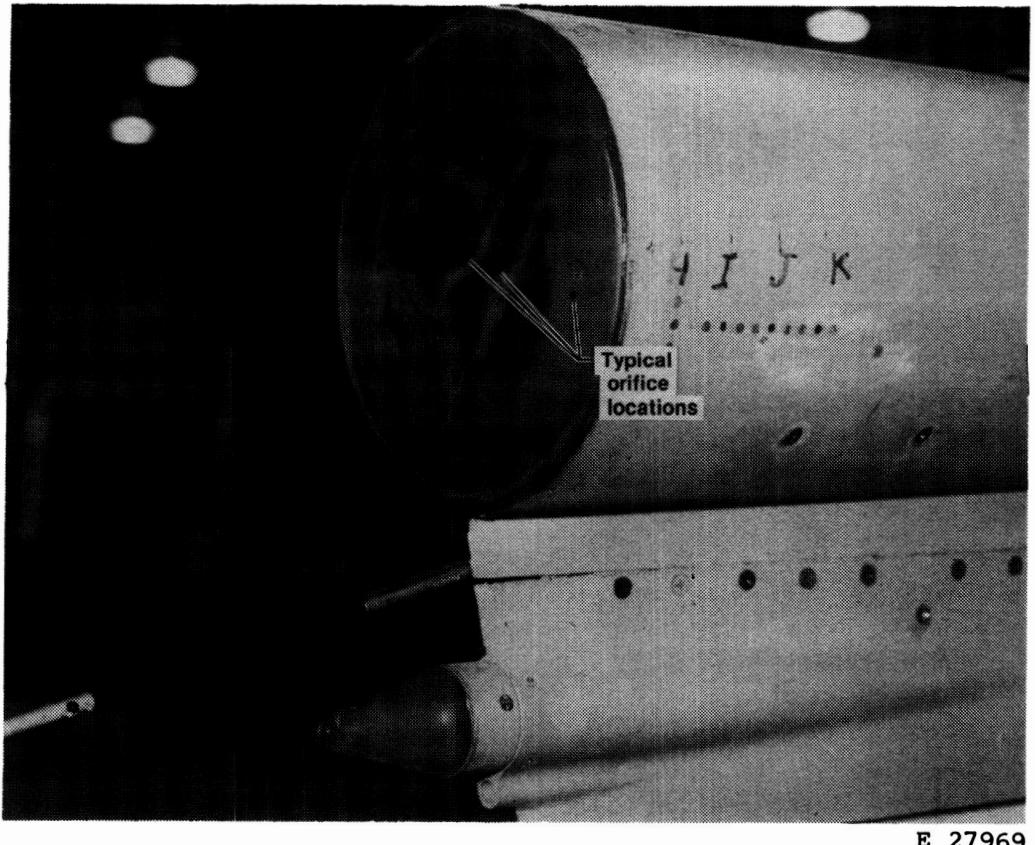
(a) Blunt base.

Figure 3. Base configurations tested in flight. (Numbers and letters were used for instrumentation identification.)
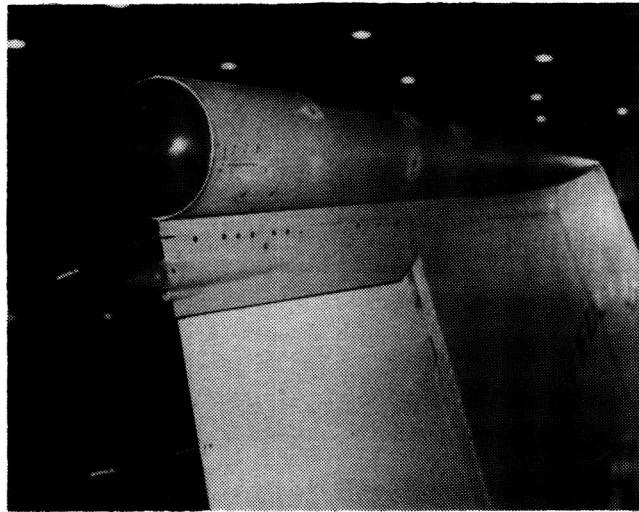
E 29322

(b) Hemispherical base.
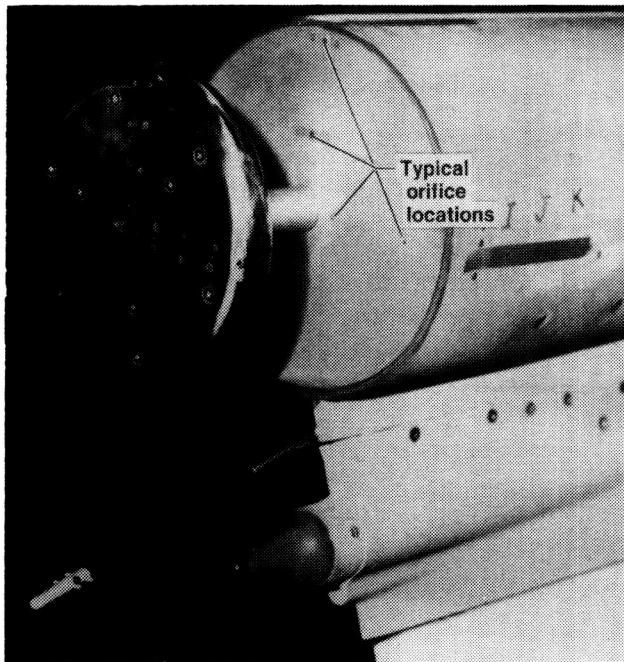
E 28011

(c) Trailing disk.

Figure 3. Concluded.
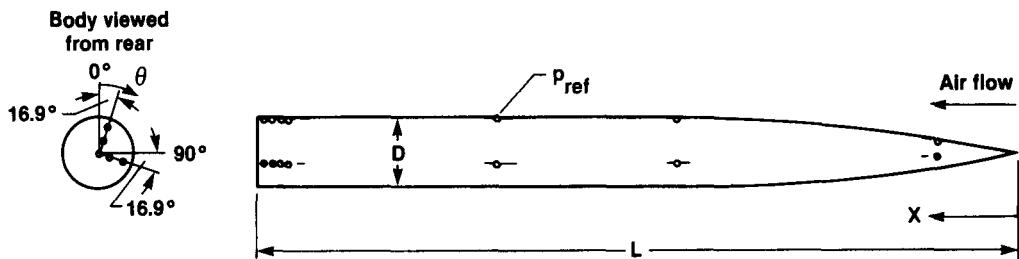
(a) Blunt and hemispherical configurations.
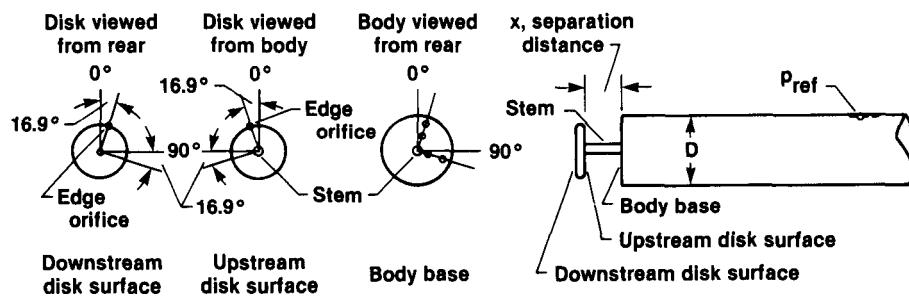
(b) Trailing disk configuration. (Only edge orifice of disk and center orifice of downstream disk surface are shown for disk surfaces.)

Figure 4. Schematic of orifice locations for flight configurations and nomenclature for both flight and wind-tunnel configurations. (Body dimensions and orifice locations are given in tables 1 and 2, respectively.)
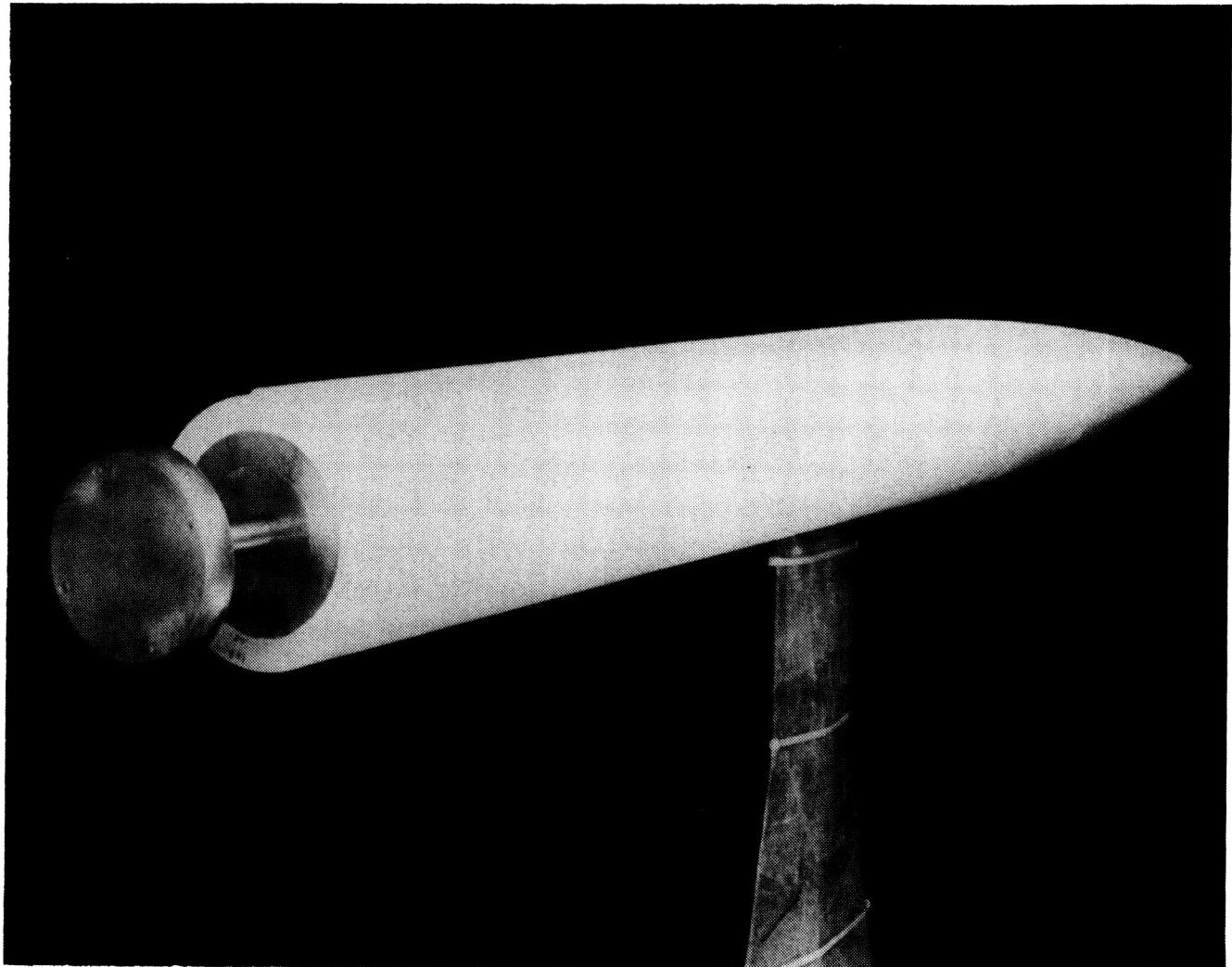
L 78-7515

(a) Body of revolution with wind-tunnel trailing disk installed.

Figure 5. Wind-tunnel body of revolution installed in Langley High-Speed 7- by 10-Foot Tunnel.
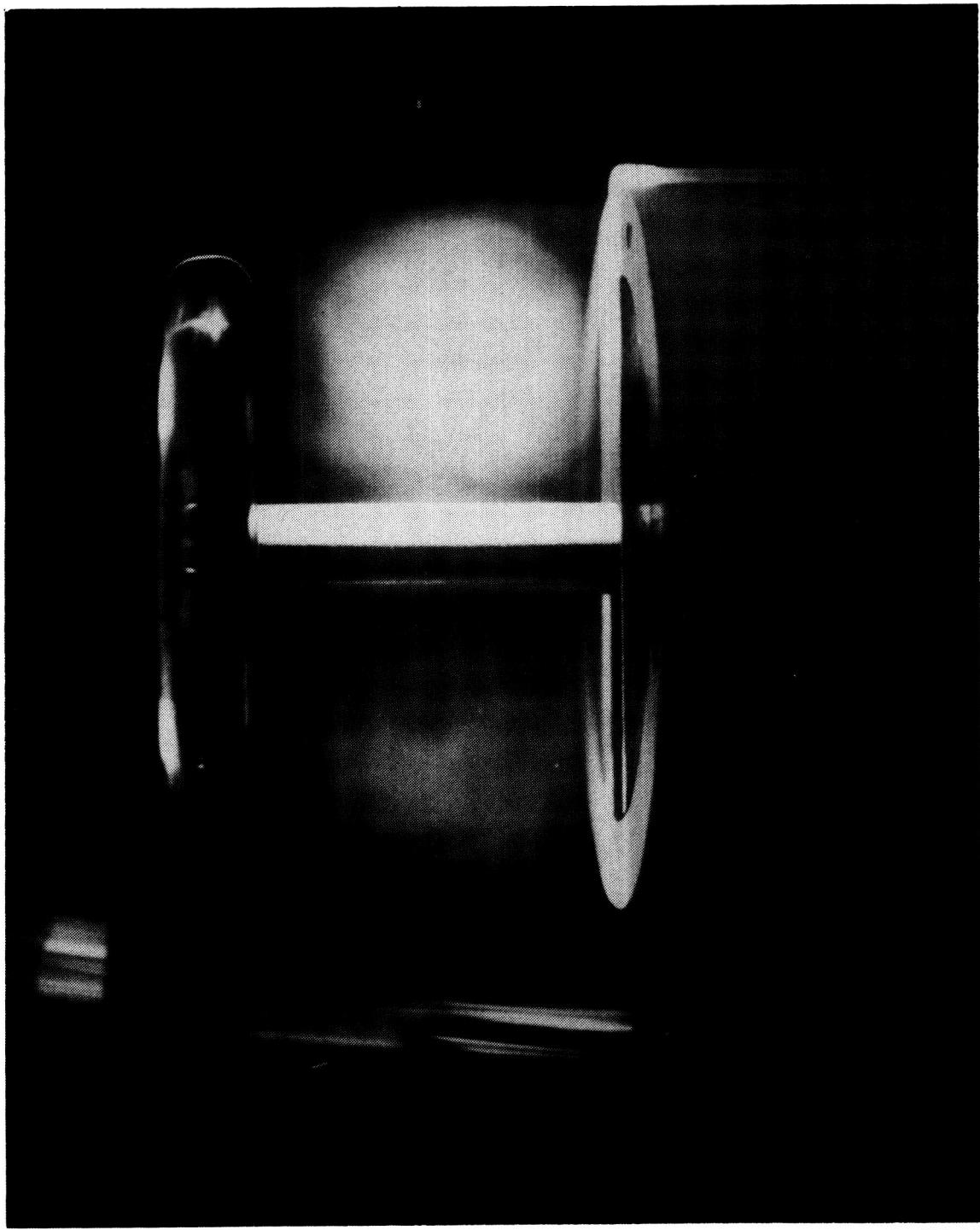
E 40349

(b) Toroidal vortices observed between body base and upstream surface of disk during flow visualization tests. (Flight trailing disk is installed.)
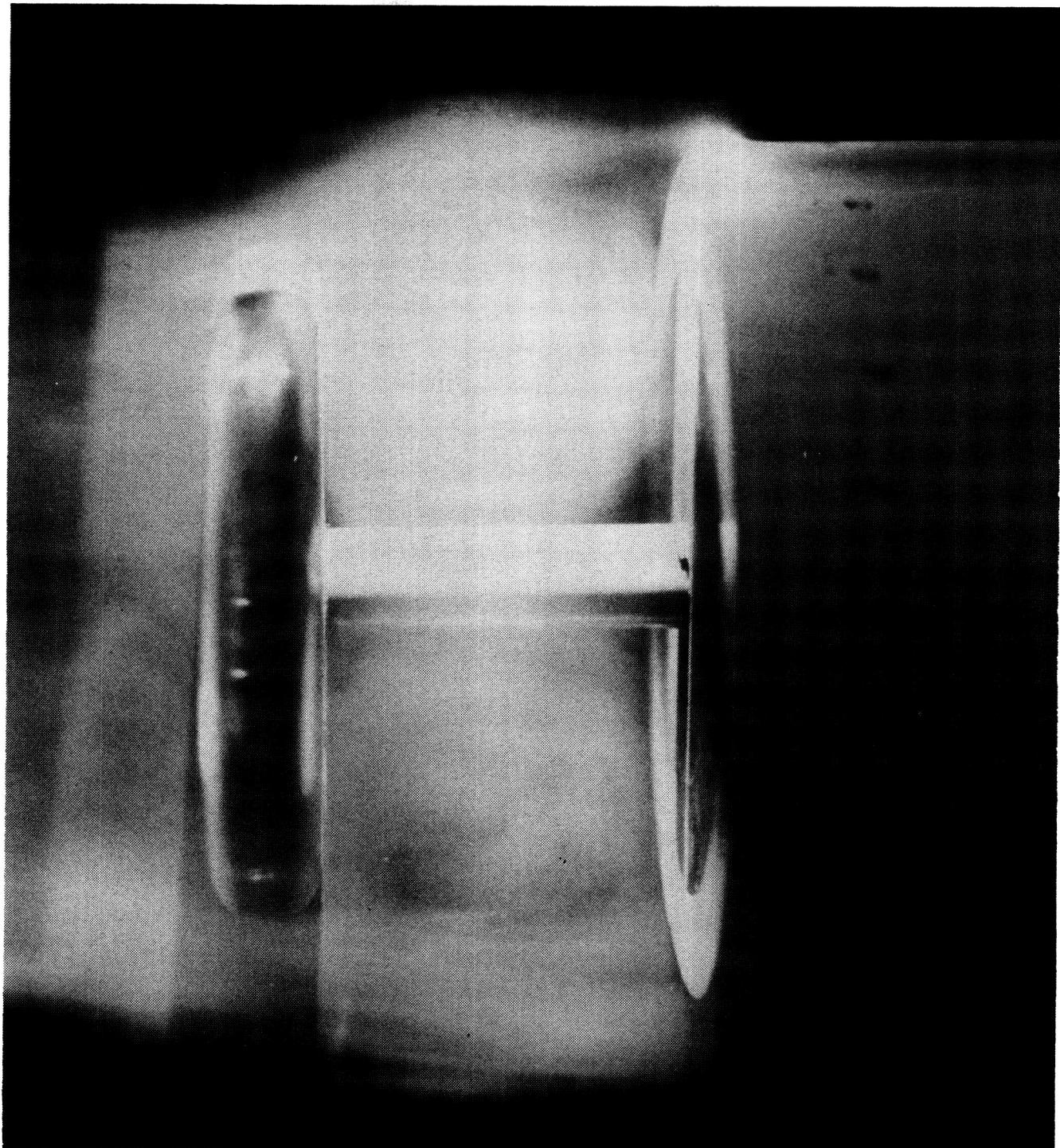
Figure 5. Continued.

E 40350

*(c) Streamlines and toroidal vortices formed during flow visualization tests.
(Flight trailing disk is installed.)*

Figure 5. Continued.
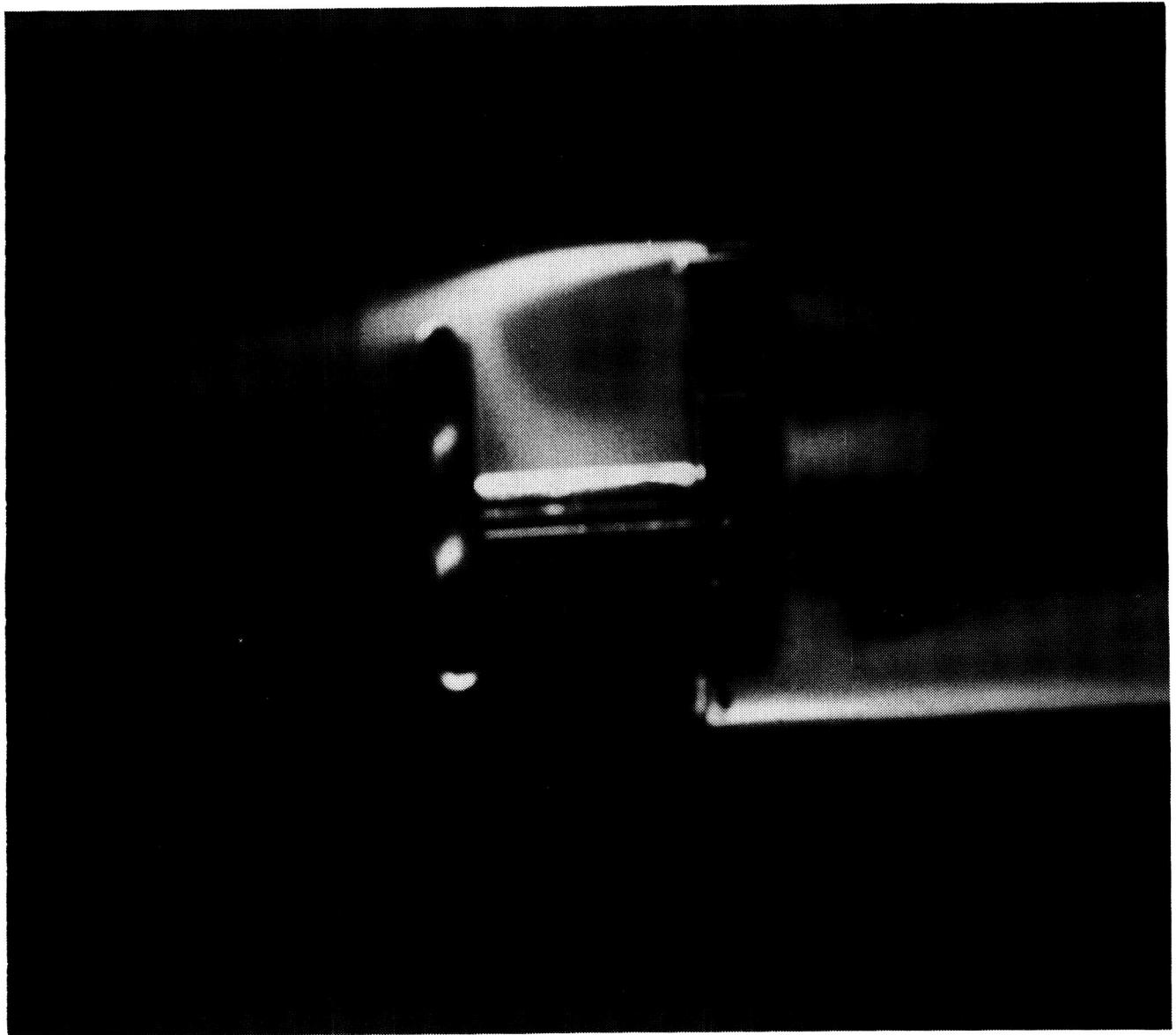
(d) Boattail shape formed by streamlines during flow visualization tests. (Wind-tunnel trailing disk is installed.)

Figure 5. Concluded.
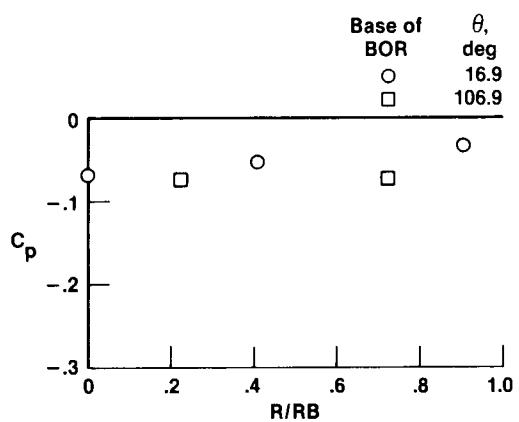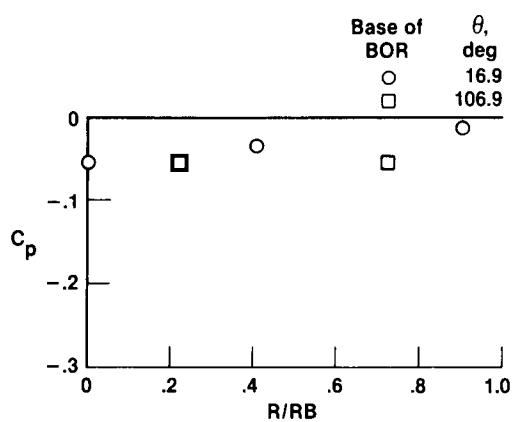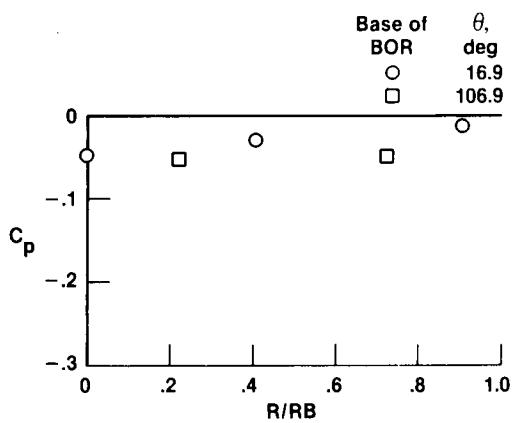
(a) Mach 0.70.
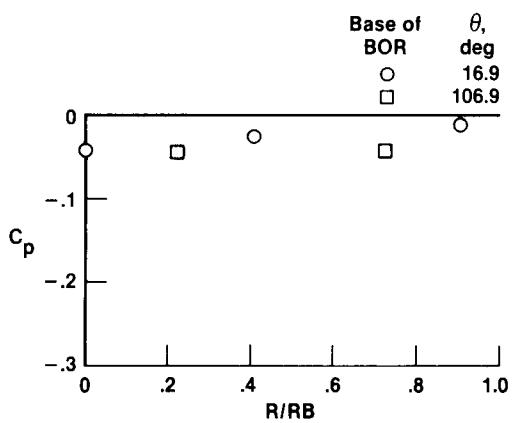
(b) Mach 0.79.
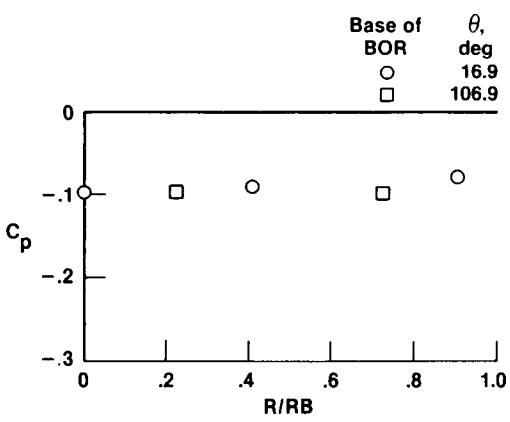
(c) Mach 0.89.
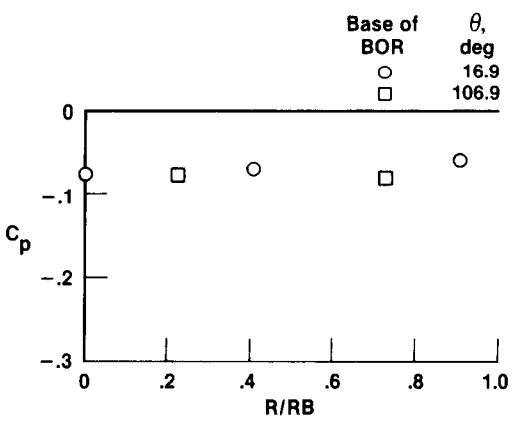
(d) Mach 0.93.

(e) Mach 1.21.

(f) Mach 1.23.

*Figure 6. Pressure coefficient in base region as a function of radial distance for blunt base configuration, flight data.*
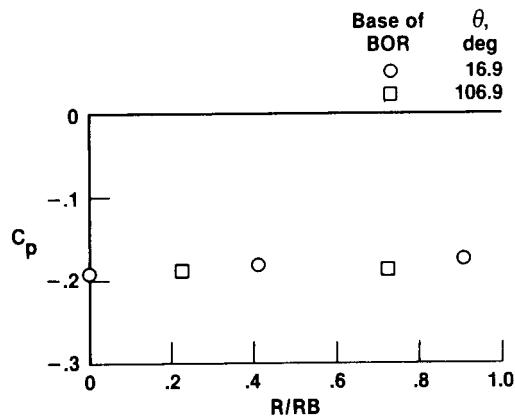
(g) Mach 1.39.
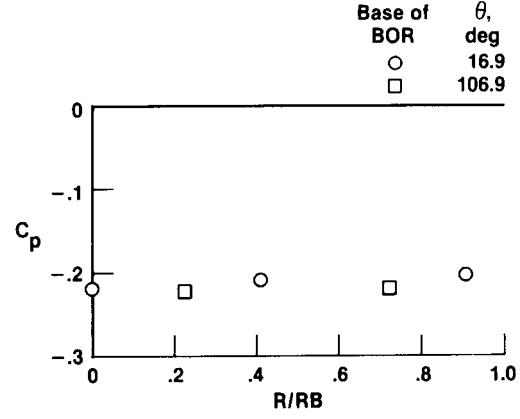
(h) Mach 1.57.

Figure 6. Concluded.
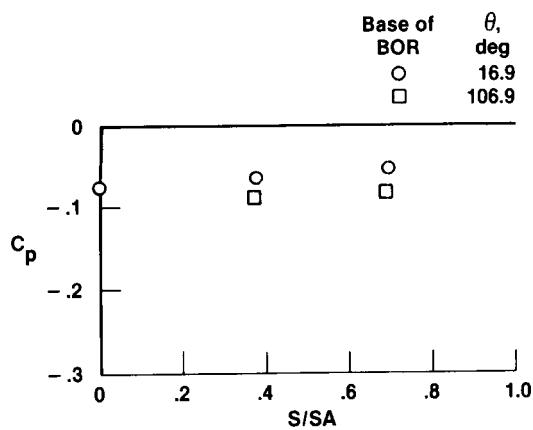
(a) Mach 0.70.
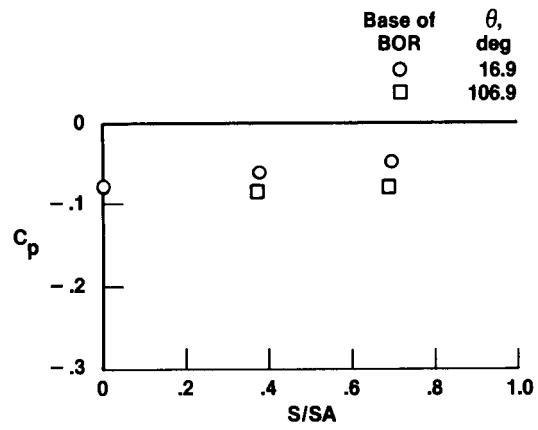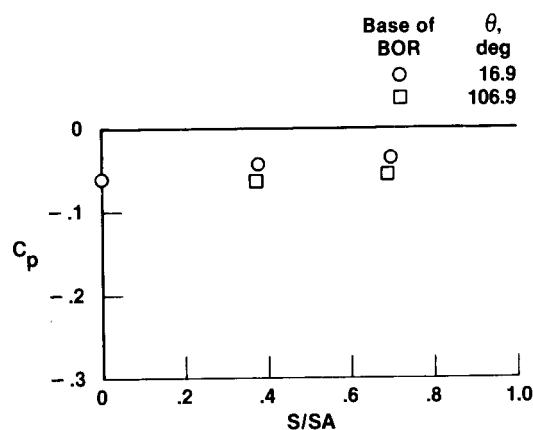
(b) Mach 0.79.

(c) Mach 0.89.
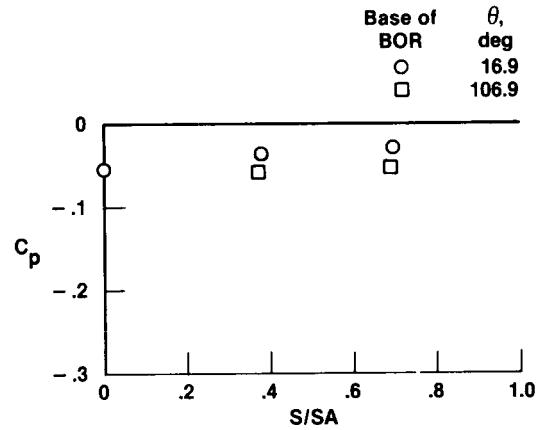
(d) Mach 0.93.

Figure 7. Pressure coefficient in base region as a function of surface distance for hemispherical base configuration, flight data.

C-2
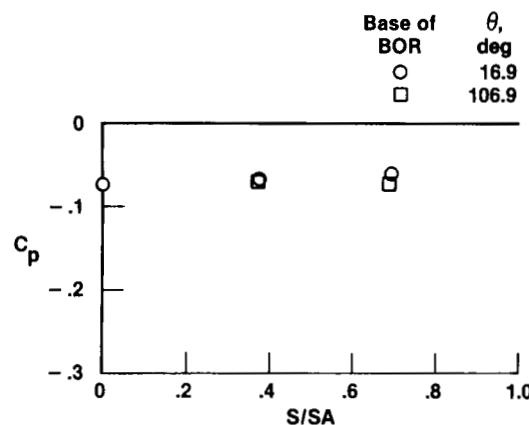
(e)   Mach 1.23.

Figure 7.   Concluded.
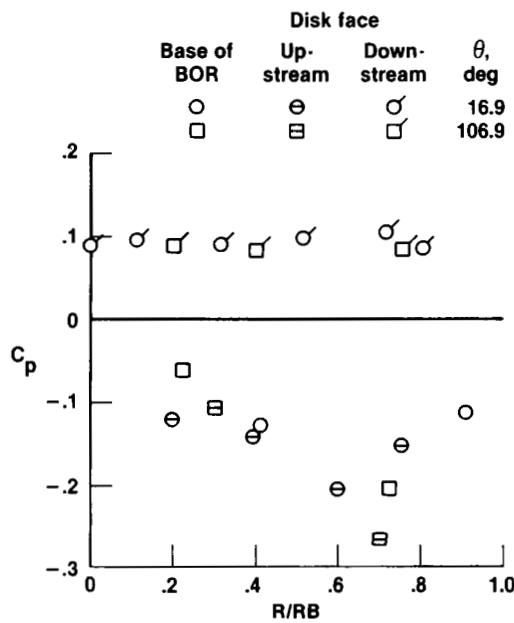
(a)   Mach 0.70.
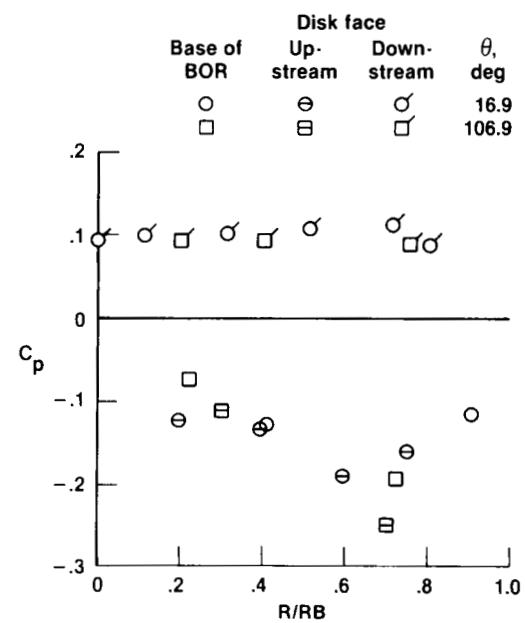
(b)   Mach 0.79.

Figure 8.   Pressure coefficient in base region as a function of radial distance for flight disk, x/D = 0.44, flight data.
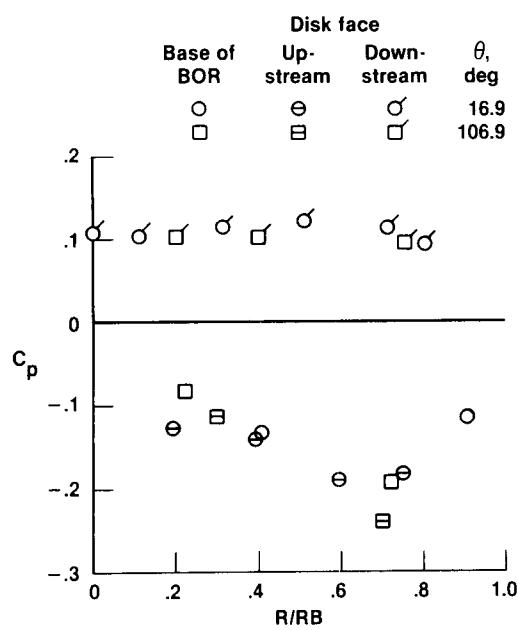
(c) Mach 0.89.
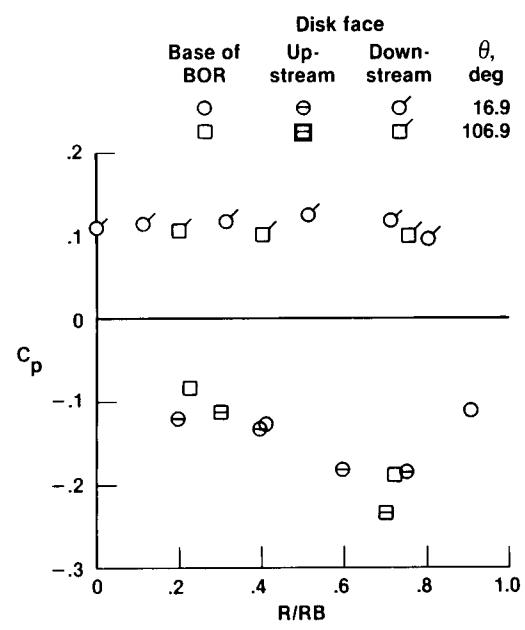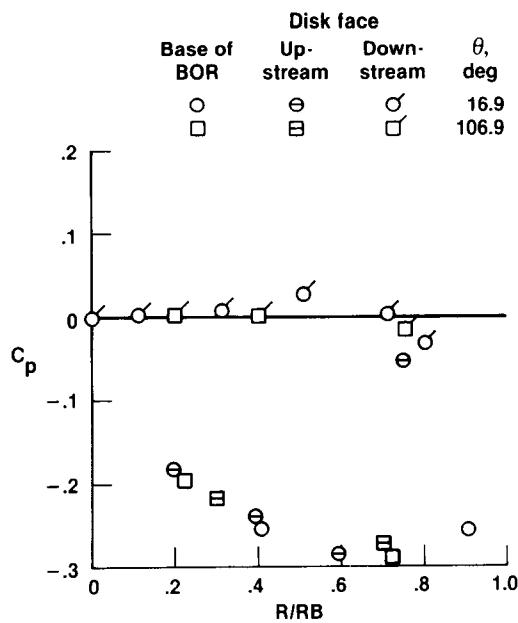
(d) Mach 0.93.

(e) Mach 1.24.
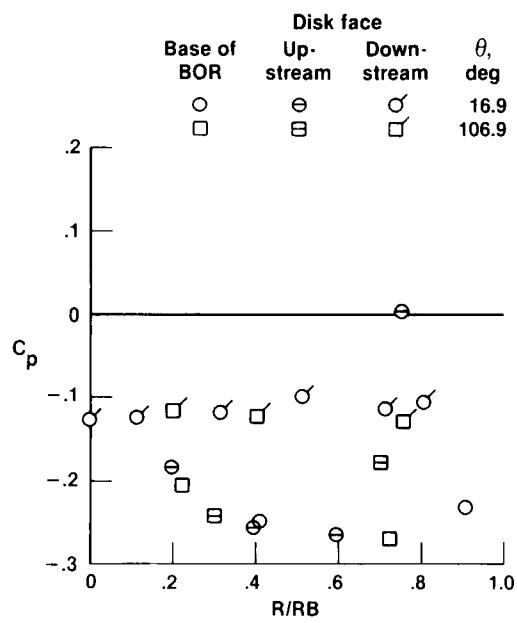
(f) Mach 1.40.

Figure 8. Continued.
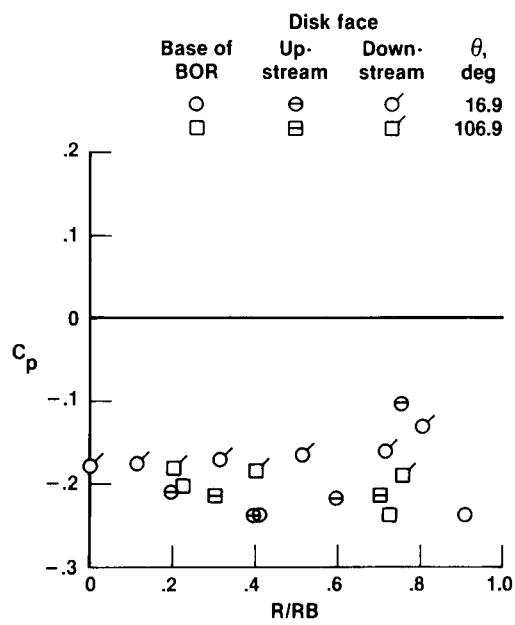
(g) Mach 1.57.

Figure 8. Concluded.
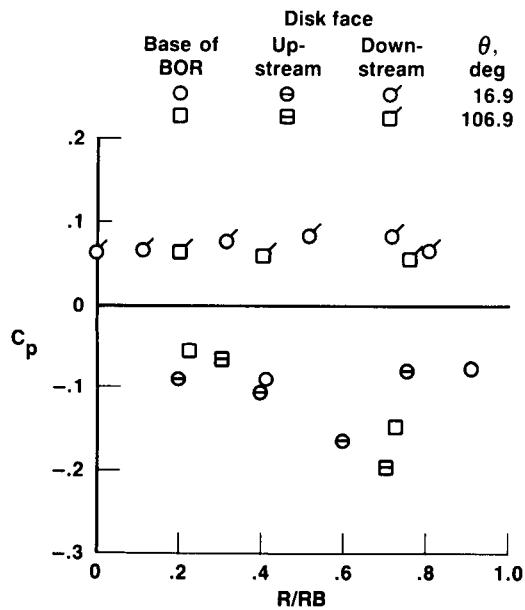
(a) Mach 0.69.
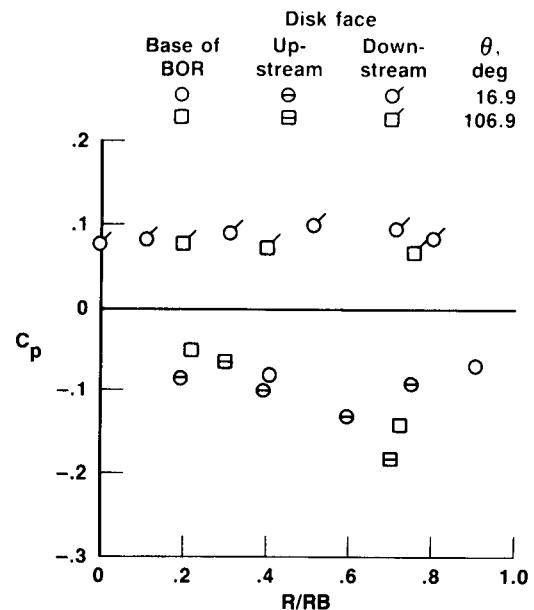
(b) Mach 0.79.

Figure 9. Pressure coefficient in base region as a function of radial
distance for flight disk, x/D = 0.50, flight data.
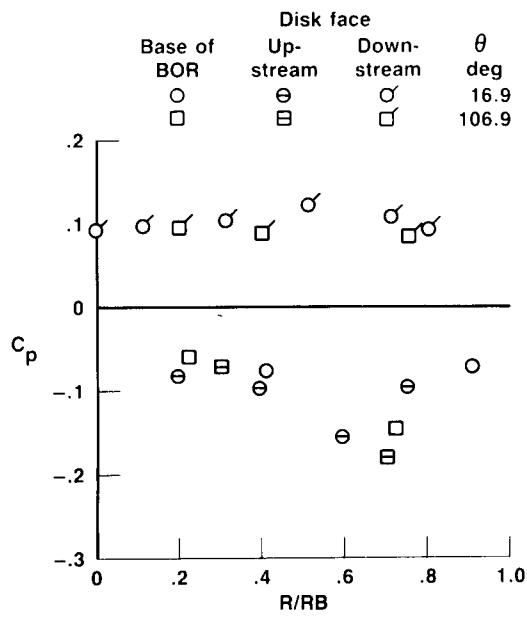
(c) Mach 0.89.
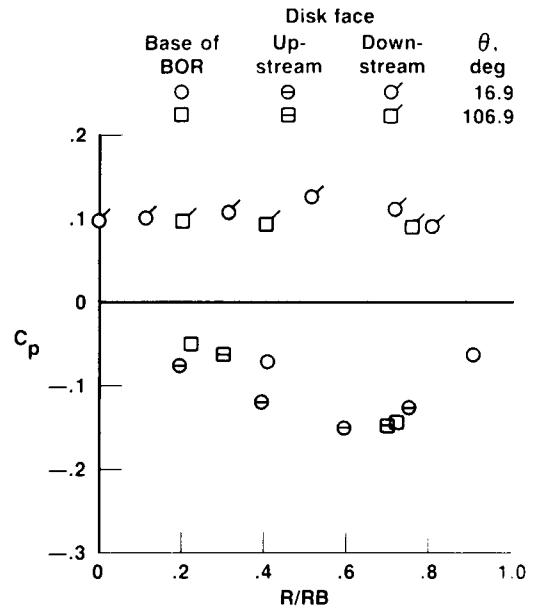
(d) Mach 0.93.
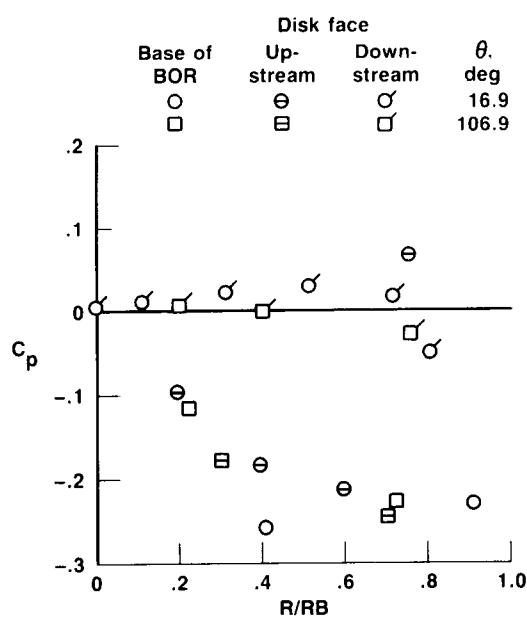
(e) Mach 1.23.
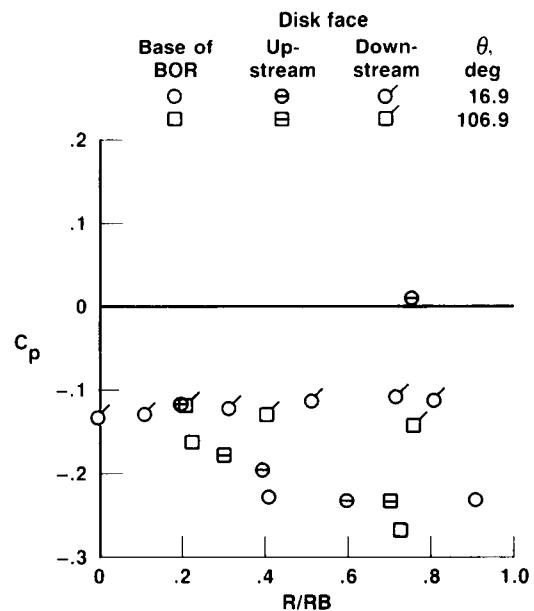
(f) Mach 1.40.

Figure 9. Concluded.
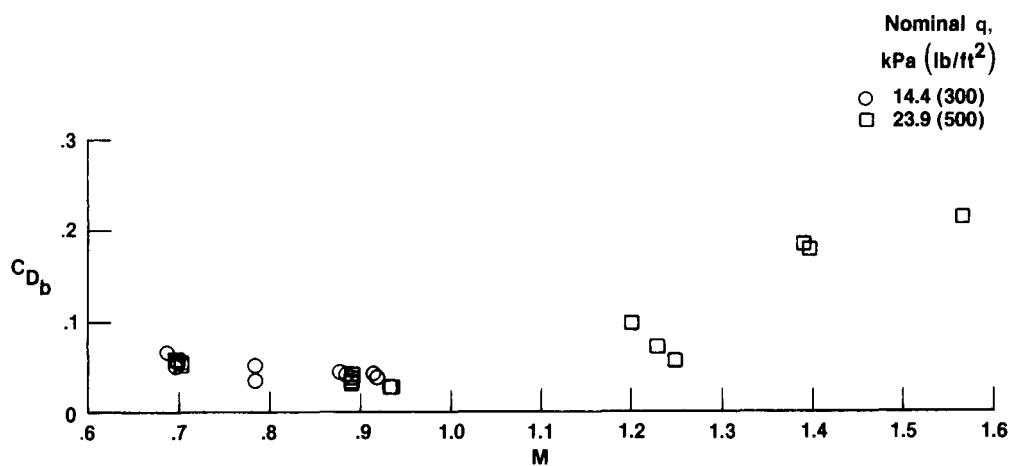
Figure 10. Base drag coefficient as a function of Mach number for blunt base configuration, Re = 1.5 × 10^7 to 2.7 × 10^7, flight data.
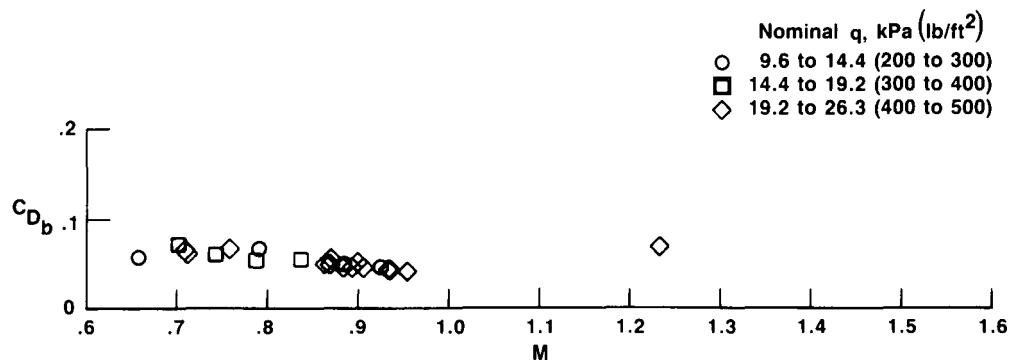
Figure 11. Base drag coefficient as a function of Mach number for hemispherical base configuration, Re = 1.5 × 10^7 to 2.6 × 10^7, flight data.

(a)   x/D = 0.44.

(b)   x/D = 0.50.
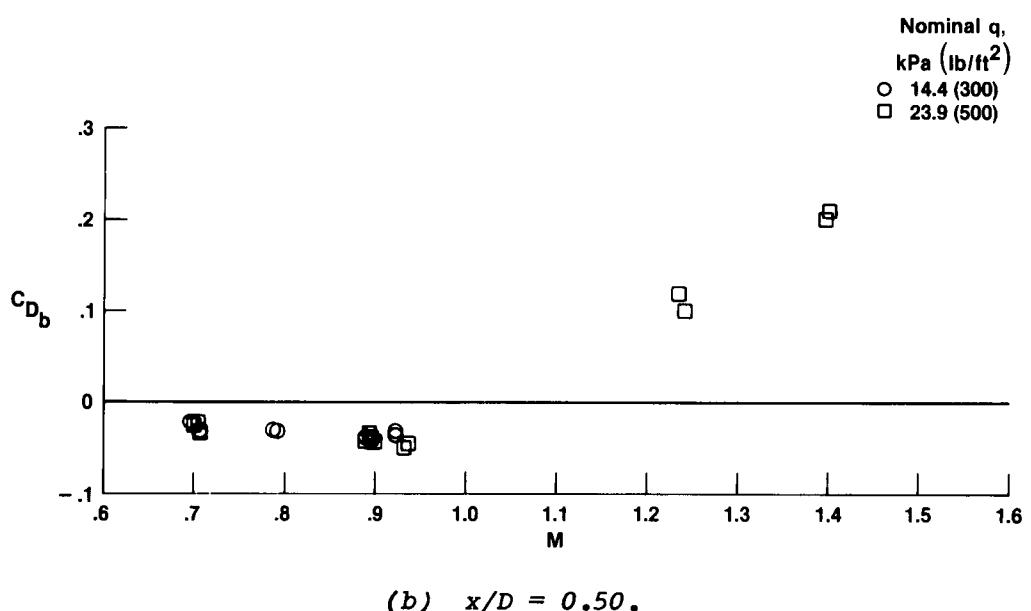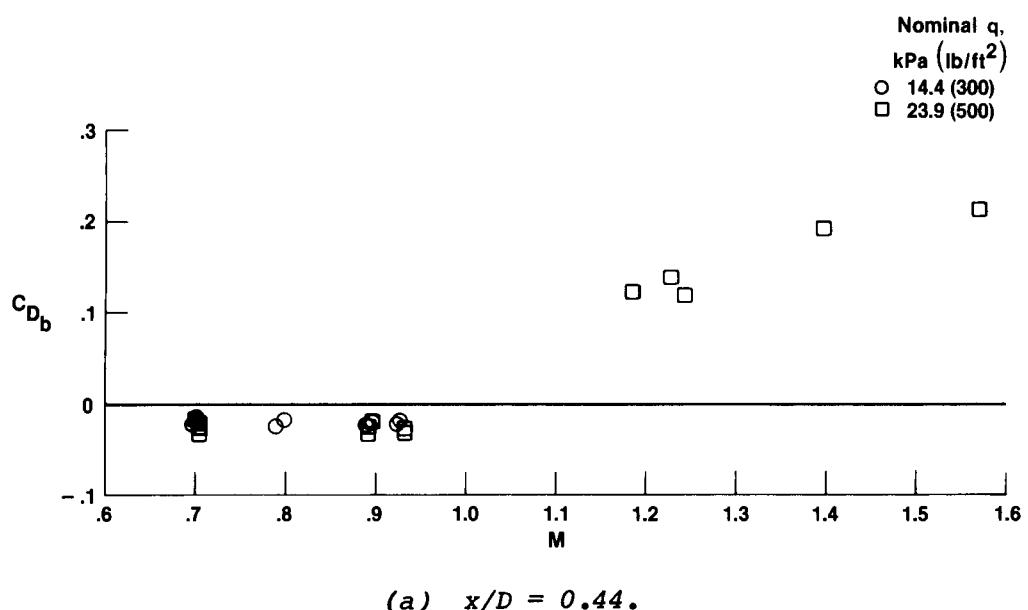
Figure 12.   Base drag coefficient as a function of Mach number for trailing disk configurations, Re = 1.5 × 10^{7} to 2.7 × 10^{7}, flight data.

(a) Base drag coefficient.
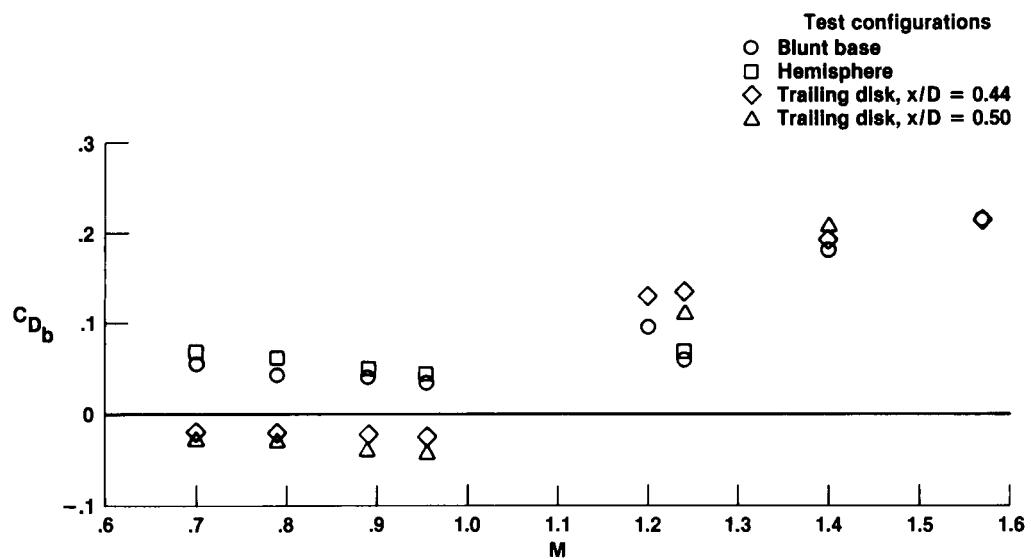
$$\Delta c_{D_b} = \left(c_{D_b}\right)_{Configuration} - \left(c_{D_b}\right)_{Blunt}$$
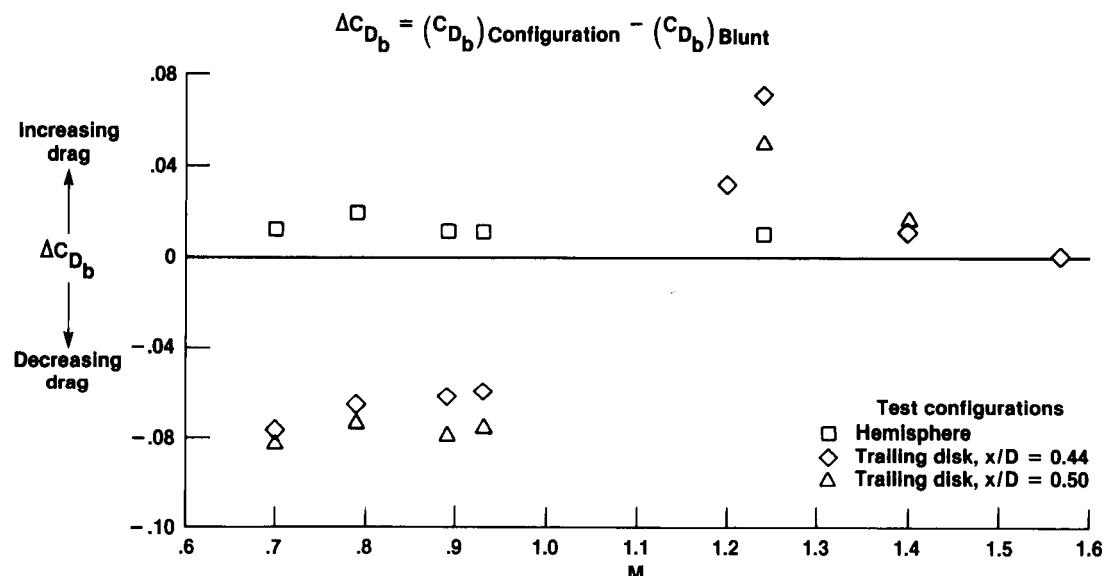
(b) Incremental difference in base drag coefficient between given configuration and blunt base. (Negative means base drag was less than blunt base drag.)

Figure 13. Average base drag as a function of Mach number.
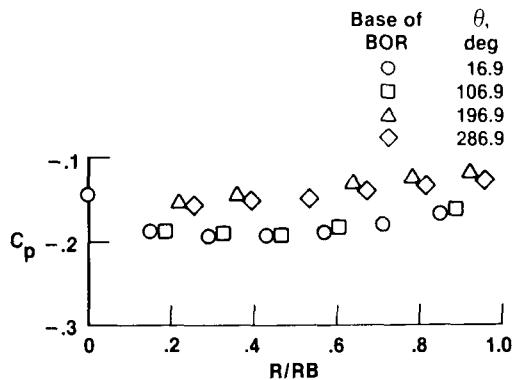
(a) Mach 0.30.
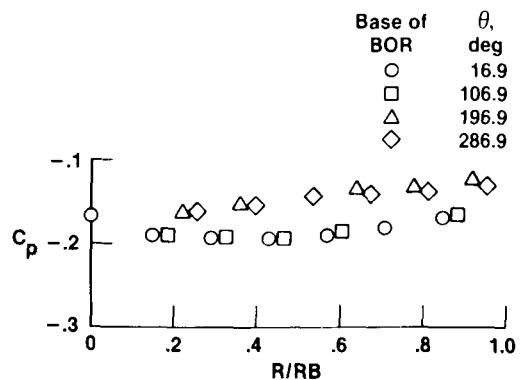
(b) Mach 0.50.
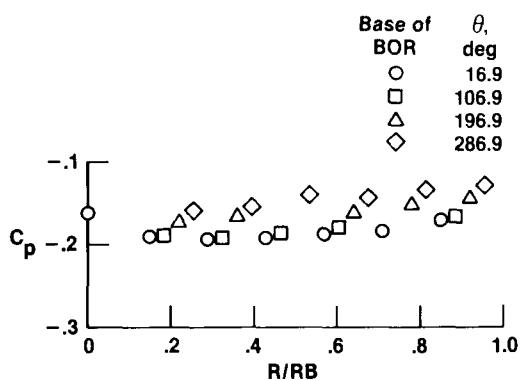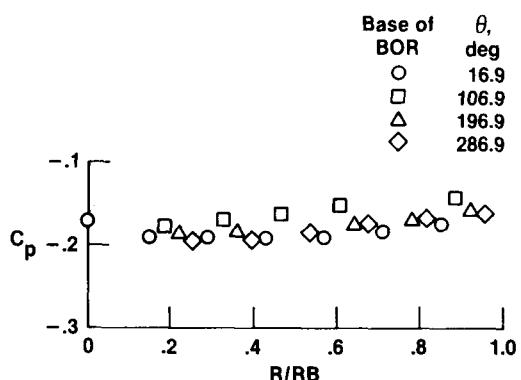
(c) Mach 0.71.

(d) Mach 0.82.

Figure 14. Pressure coefficient in base region as a function of radial distance for blunt base configuration, α ≈ 0°, wind-tunnel data.
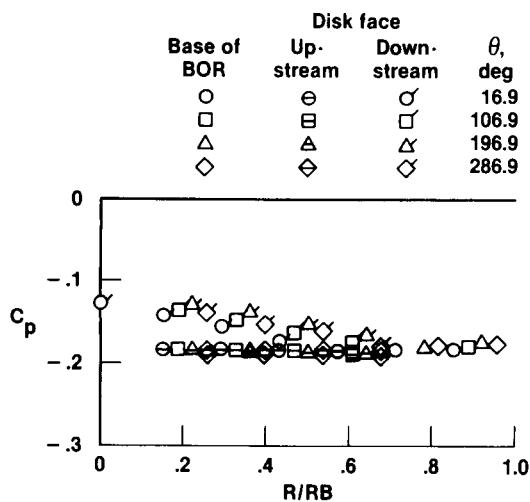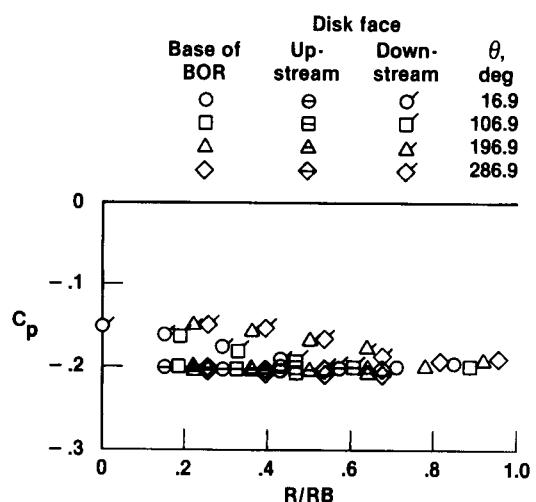
Figure 15. Pressure coefficient in base region as a function of radial distance for wind-tunnel disk, x/D = 0.20, α ≈ 0°, wind-tunnel data.
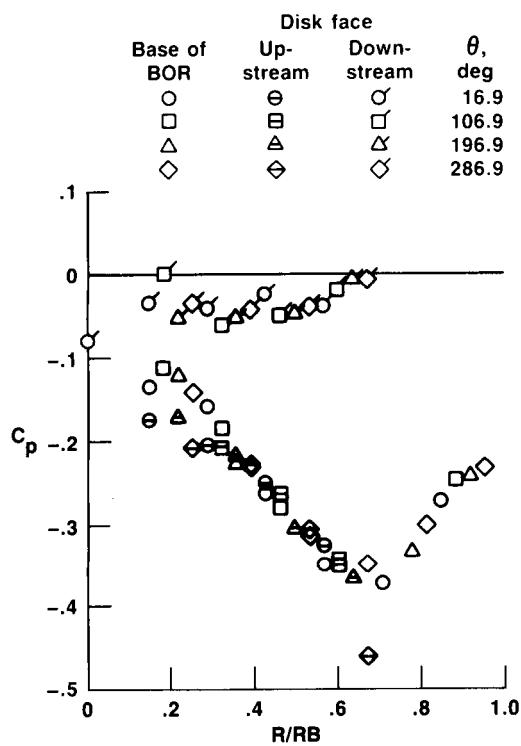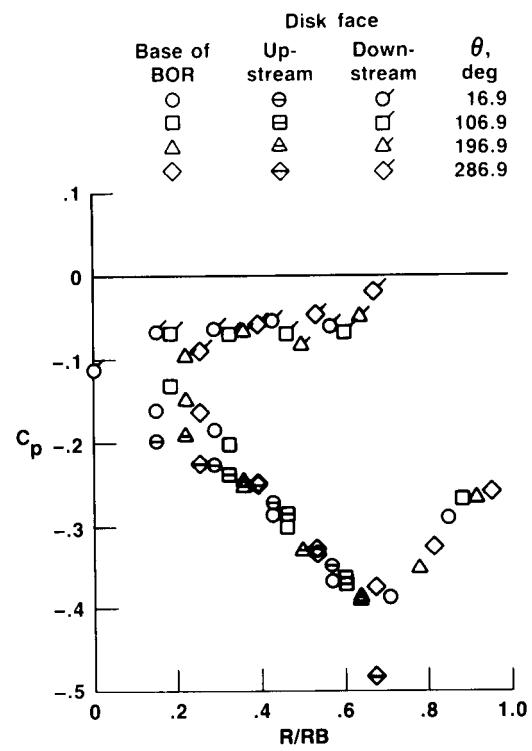
Figure 16. *Pressure coefficient in base region as a function of radial distance for wind-tunnel disk, x/D = 0.40, α ≈ 0°, wind-tunnel data.*
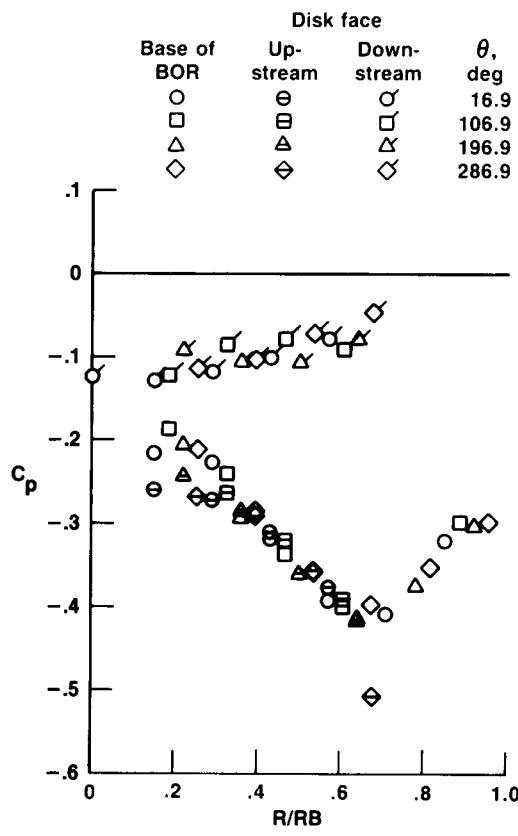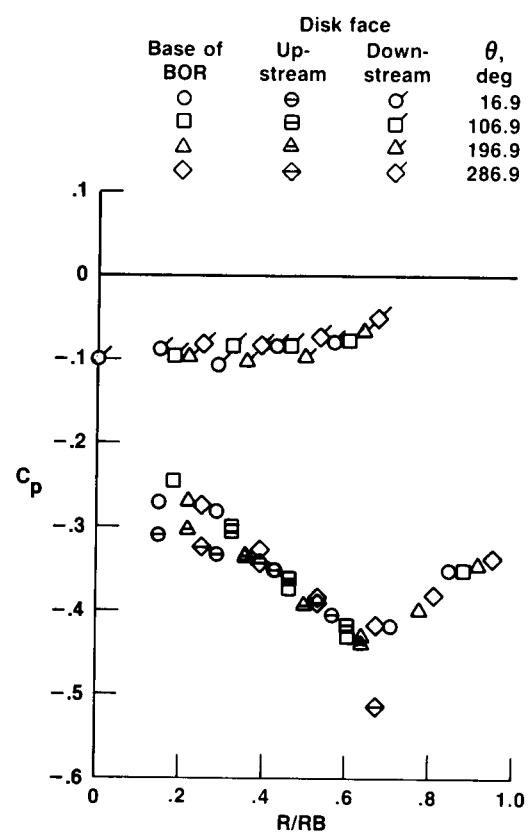
(c) Mach 0.71.   (d) Mach 0.82.

Figure 16. Concluded.

	Disk face		
Base of BOR	Up-stream	Down-stream	θ, deg
○	⊖	♂	16.9
□	⊟	�♂	106.9
△	△	⚠	196.9
◇	◈	◇	286.9

c_p

(a) *Mach 0.30.*

	Disk face		
Base of BOR	Up-stream	Down-stream	θ, deg
○	⊖	♂	16.9
□	⊟	�♂	106.9
△	△	⚠	196.9
◇	◈	◇	286.9

c_p
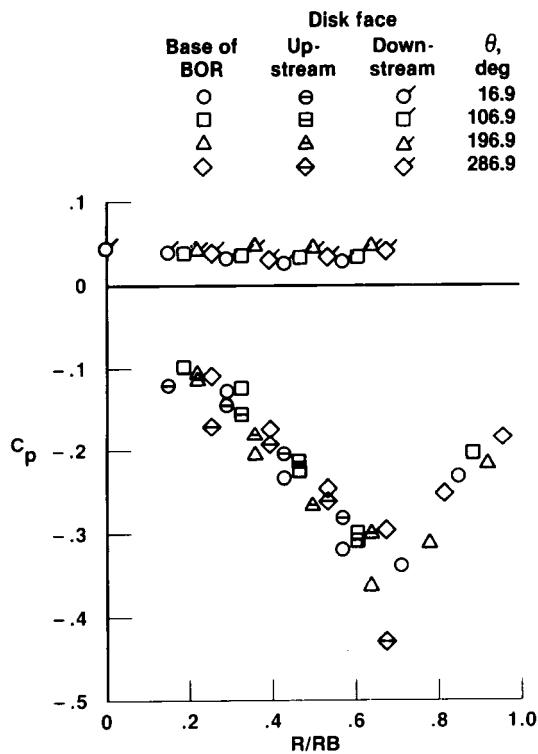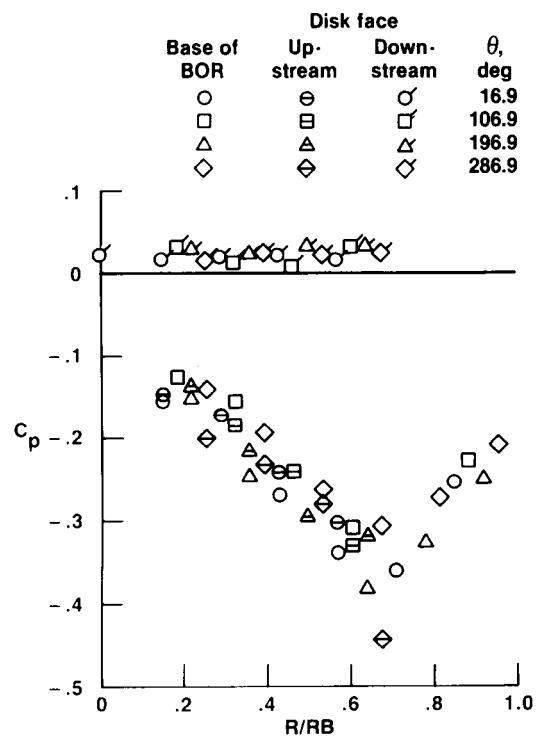
(b) *Mach 0.50.*

Figure 17. Pressure coefficient in base region as a function of radial distance for wind-tunnel disk, x/D = 0.45, α ≈ 0°, wind-tunnel data.
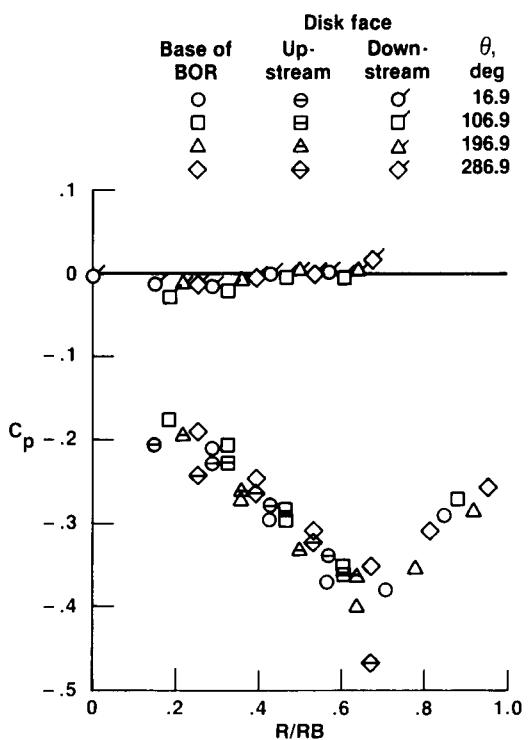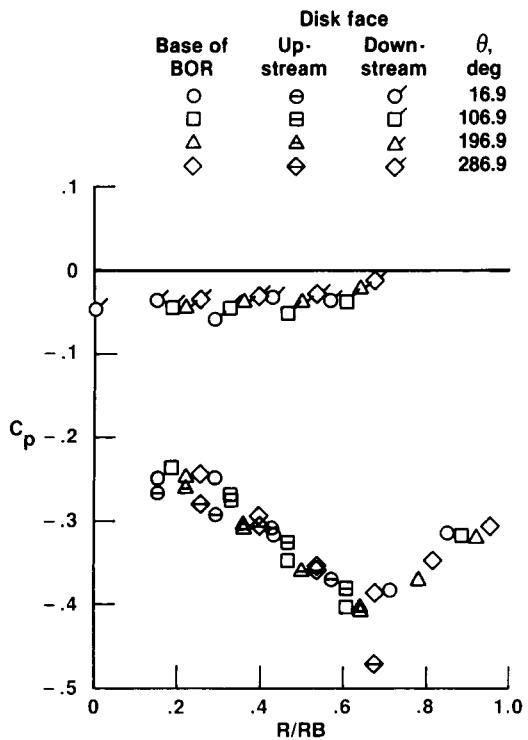
(c) Mach 0.71.

(d) Mach 0.82.

Figure 17. Concluded.
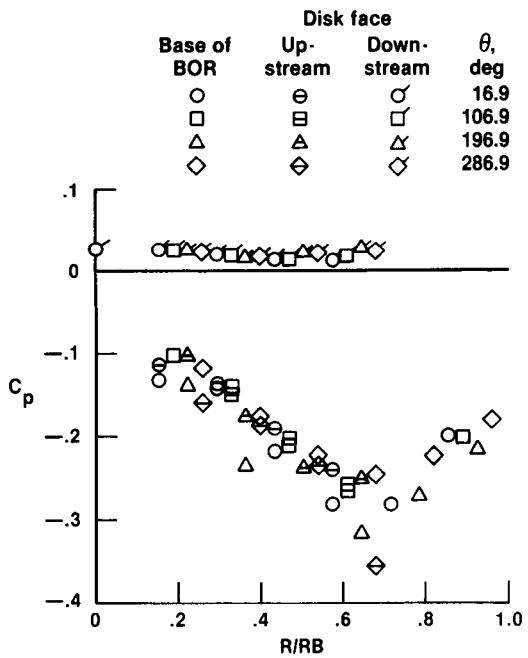
(a) Mach 0.30.
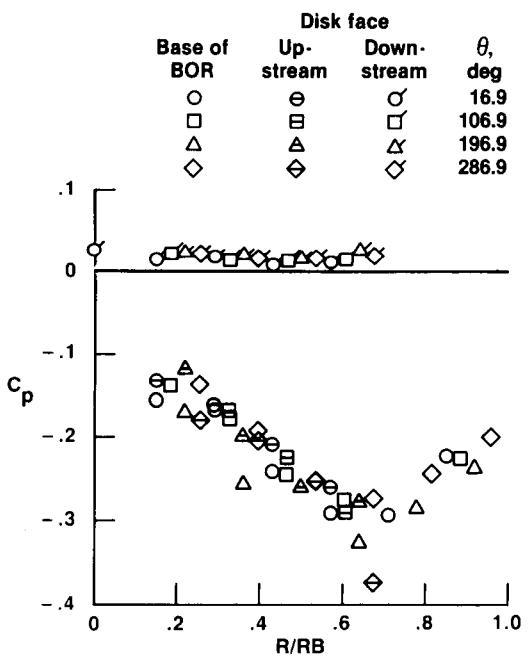
(b) Mach 0.50.

Figure 18. Pressure coefficient in base region as a function of radial distance for wind-tunnel disk, x/D = 0.50, α ≈ 0°, wind-tunnel data.
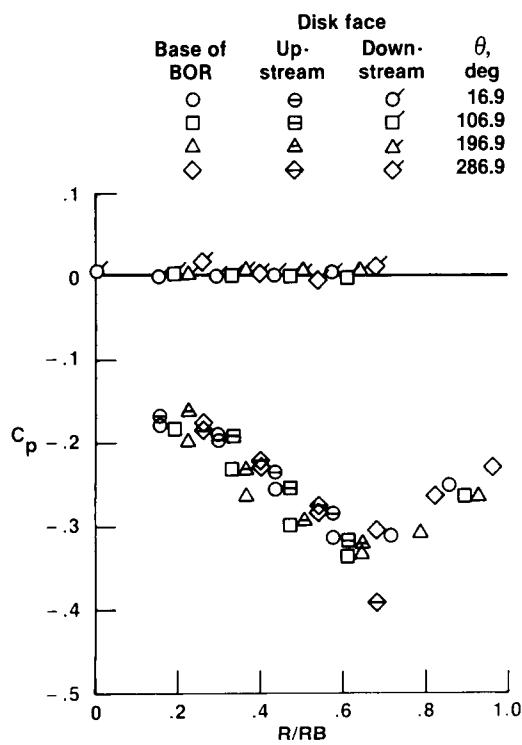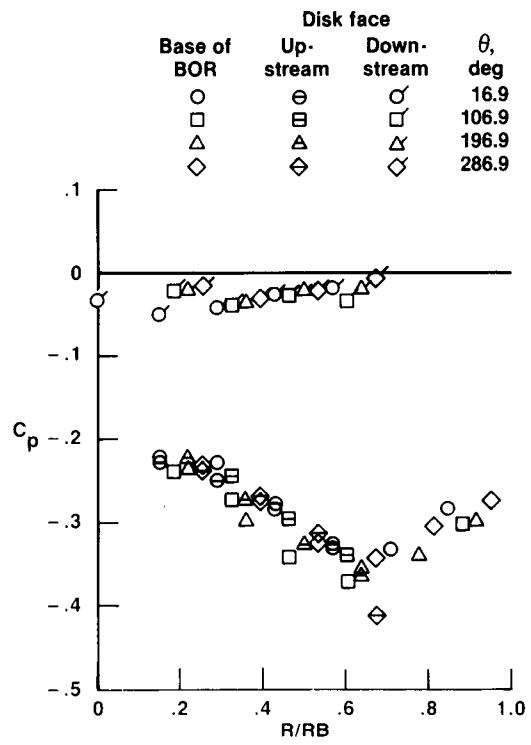
(c) Mach 0.71.

(d) Mach 0.82.

Figure 18. Concluded.
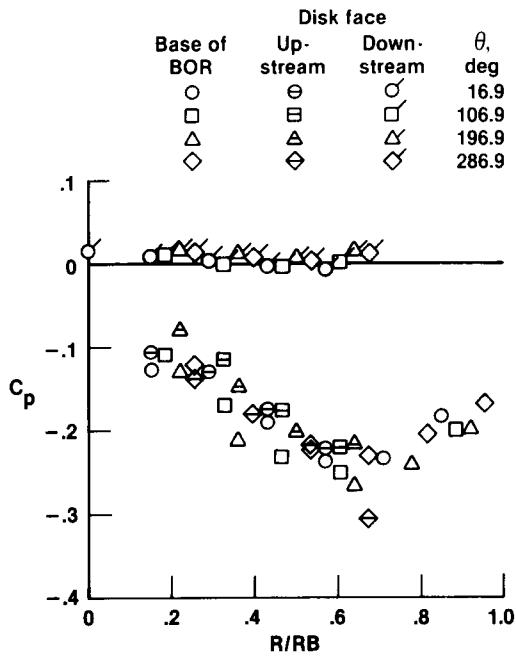
(a) Mach 0.30.
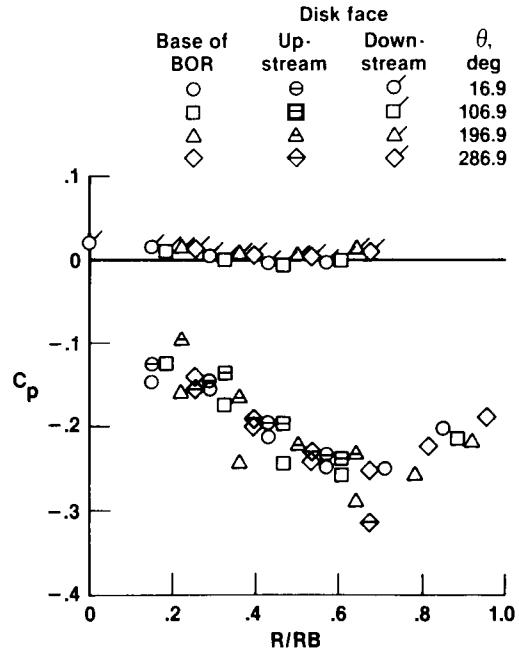
(b) Mach 0.50.

Figure 19. Pressure coefficient in base region as a function of radial distance for wind-tunnel disk, x/D = 0.55, α ≈ 0°, wind-tunnel data.
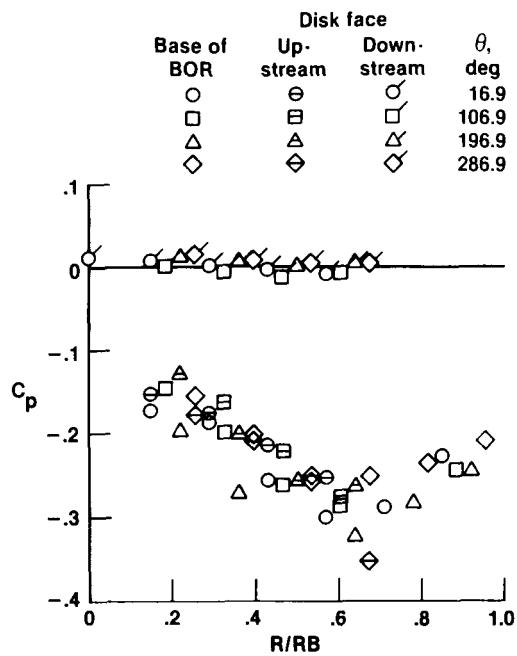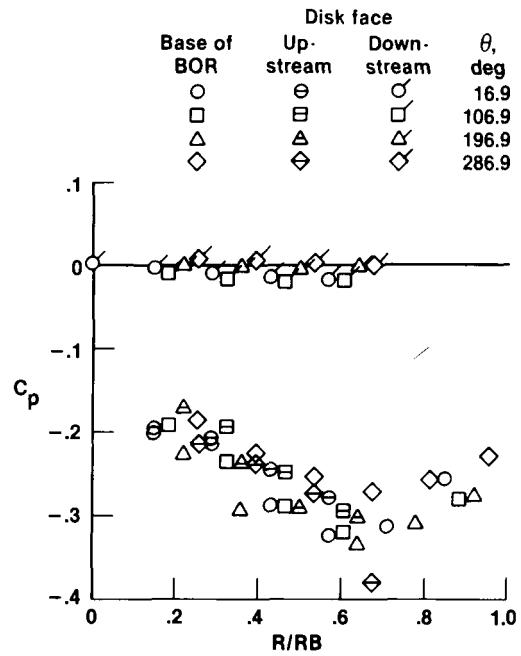
(c) Mach 0.71.

(d) Mach 0.82.

Figure 19. Concluded.
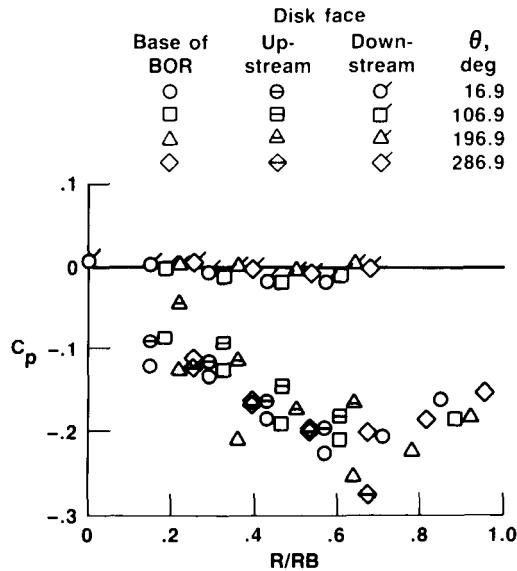
(a) Mach 0.30.
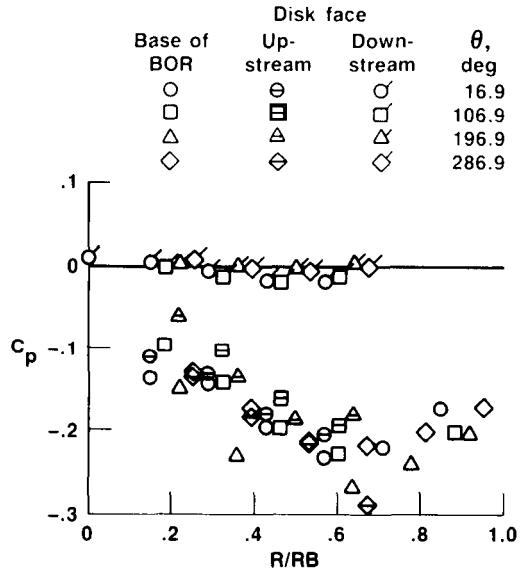
(b) Mach 0.50.

Figure 20. Pressure coefficient in base region as a function of radial distance for wind-tunnel disk, x/D = 0.60, α ≈ 0°, wind-tunnel data.

111
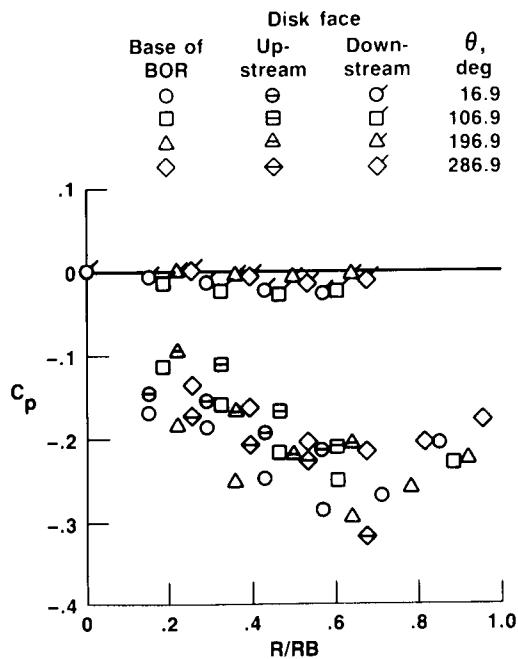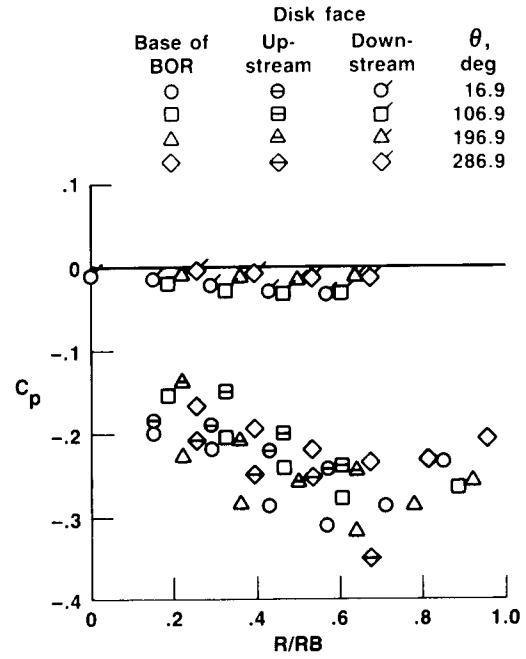
(c) Mach 0.71.

(d) Mach 0.82.

Figure 20. Concluded.
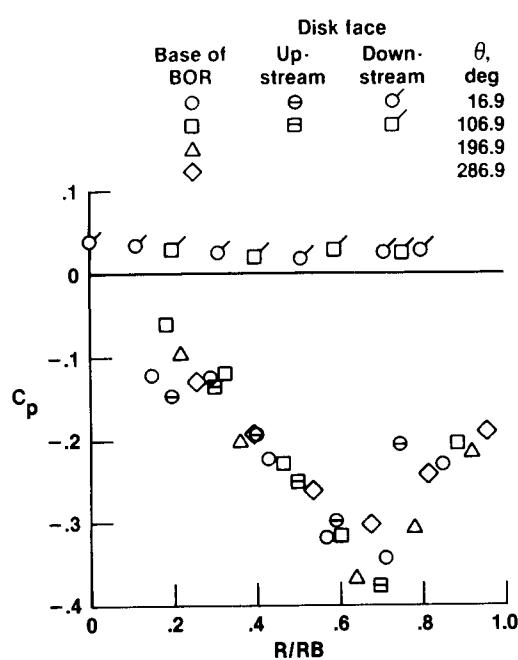
(a) Mach 0.30.
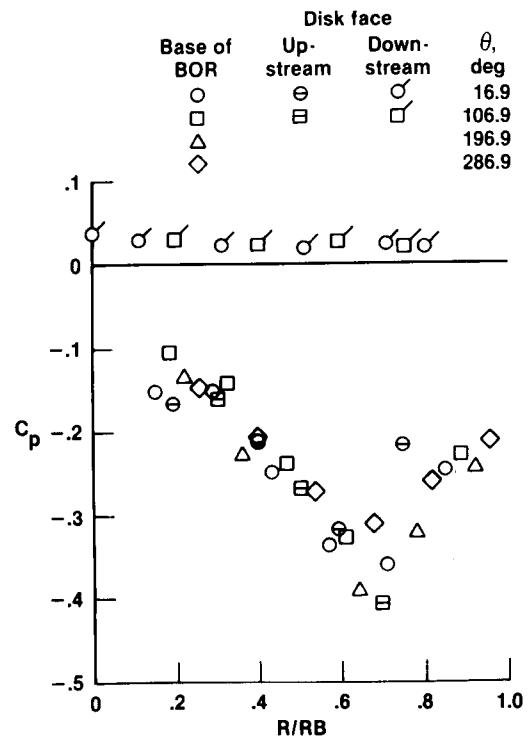
(b) Mach 0.50.

Figure 21. Pressure coefficient in base region as a function of radial distance for flight disk, x/D = 0.44, α ≈ 0°, wind-tunnel data.
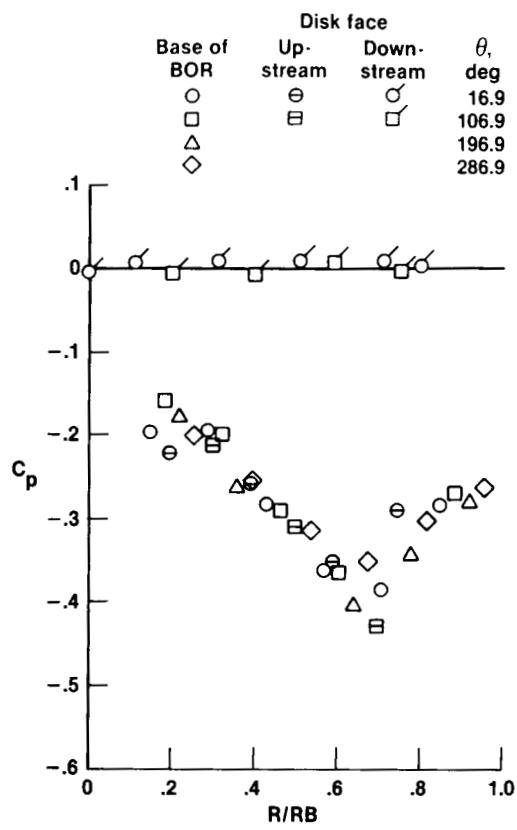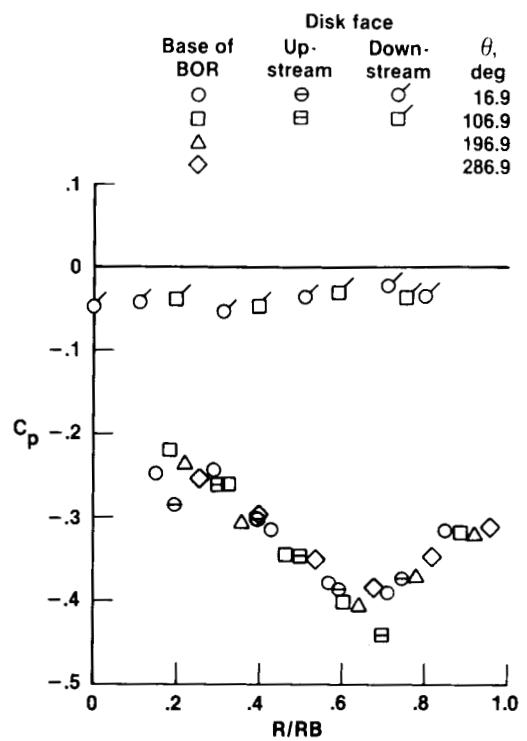
(c) Mach 0.71.

(d) Mach 0.82.

Figure 21. Concluded.
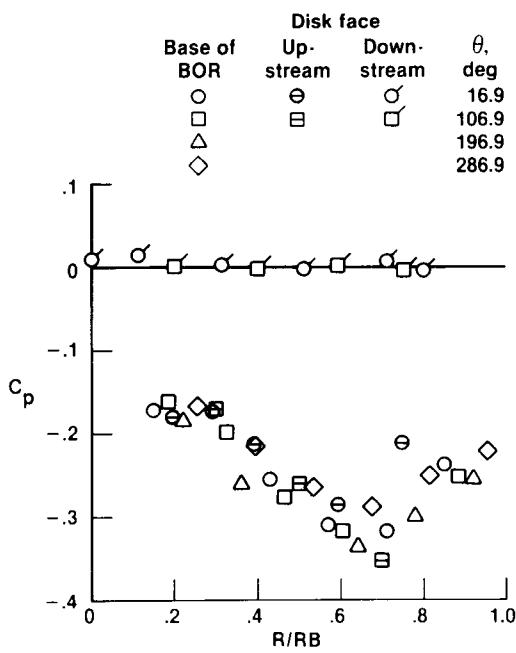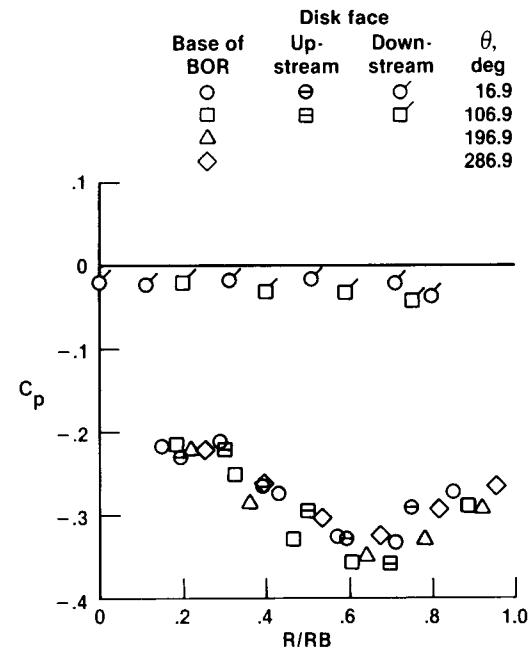
Figure 22. Pressure coefficient in base region as a function of radial distance for flight disk, x/D = 0.50, α ≈ 0°, wind-tunnel data.
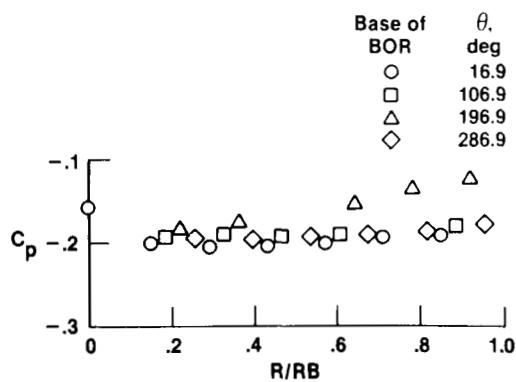
(a) Mach 0.30.
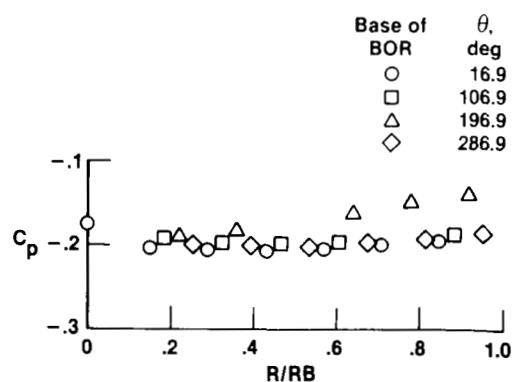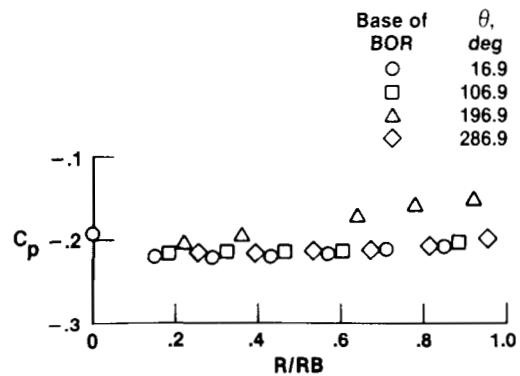
(b) Mach 0.50.

(c) Mach 0.71.

Figure 23. Pressure coefficient in base region as a function of radial distance for blunt base configuration, α ≈ 3°, wind-tunnel data.

(a) Mach 0.30.
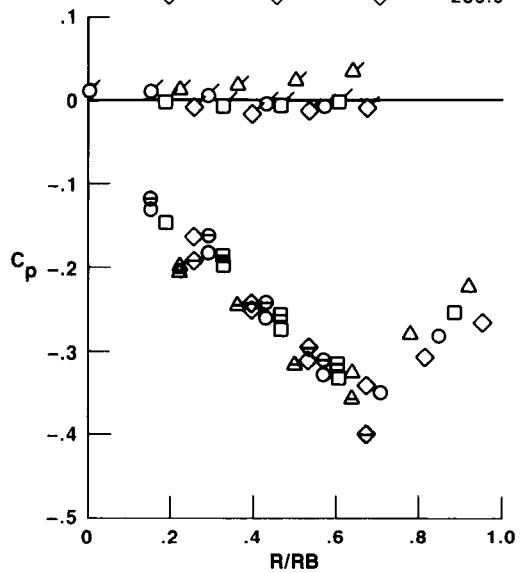
(b) Mach 0.50.

(c) Mach 0.71.

Figure 24. Pressure coefficient in base region as a function of radial distance for wind-tunnel disk, x/D = 0.45, α ≈ 3°, wind-tunnel data.

(a) Mach 0.30.
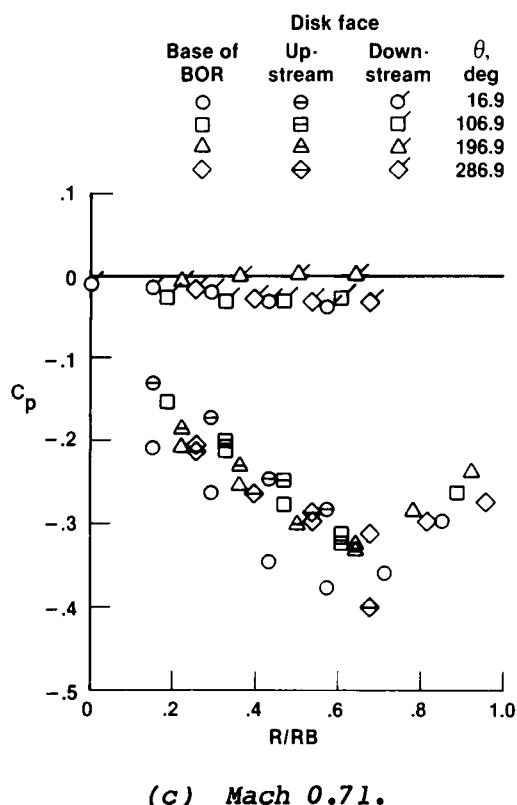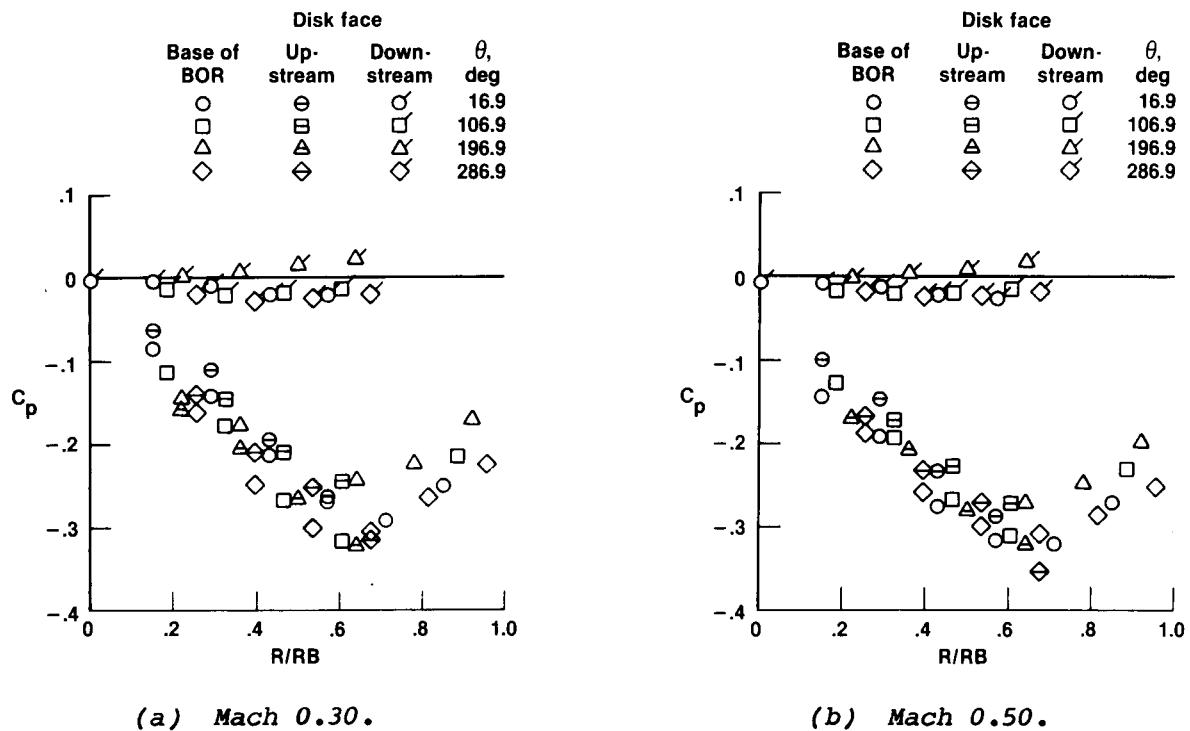
(b) Mach 0.50.

(c) Mach 0.71.

Figure 25. Pressure coefficient in base region as a function of radial distance for wind-tunnel disk, x/D = 0.50, α ≈ 3°, wind-tunnel data.
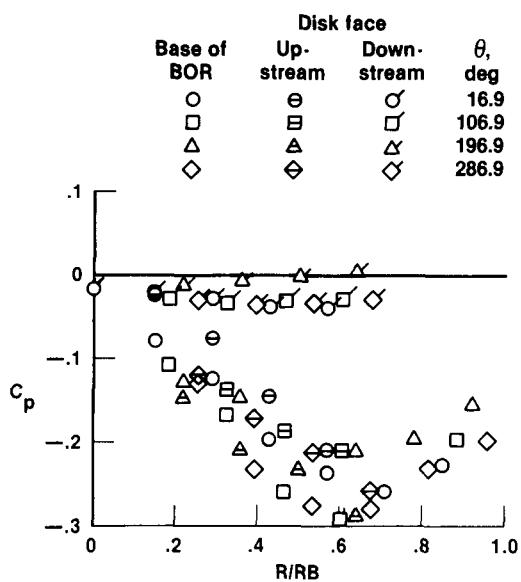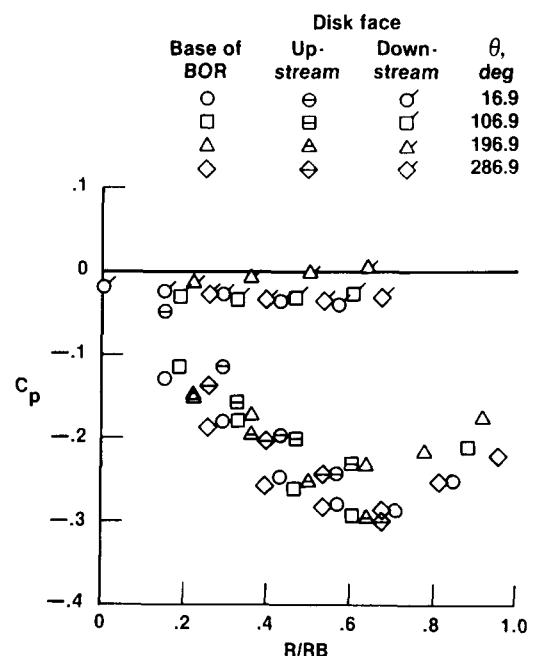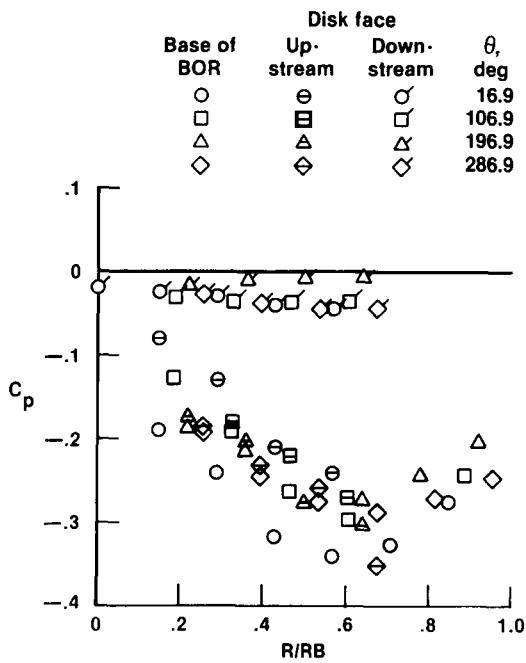
(a) Mach 0.30.

(b) Mach 0.50.

(c) Mach 0.71.

Figure 26. Pressure coefficient in base region as a function of radial distance for wind-tunnel disk, x/D = 0.55, α ≈ 3°, wind-tunnel data.
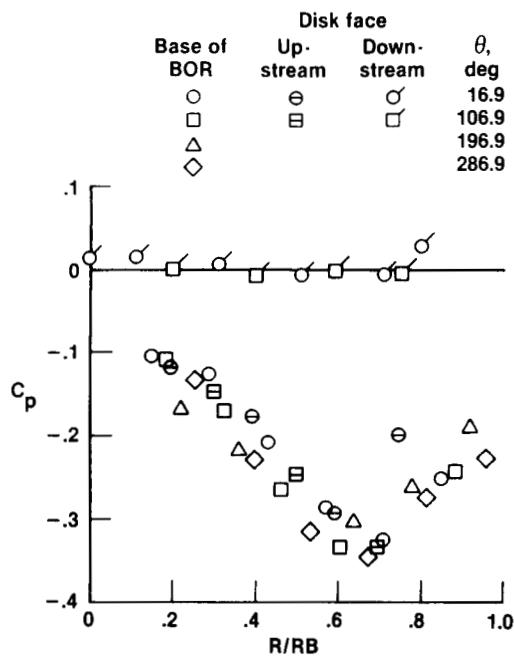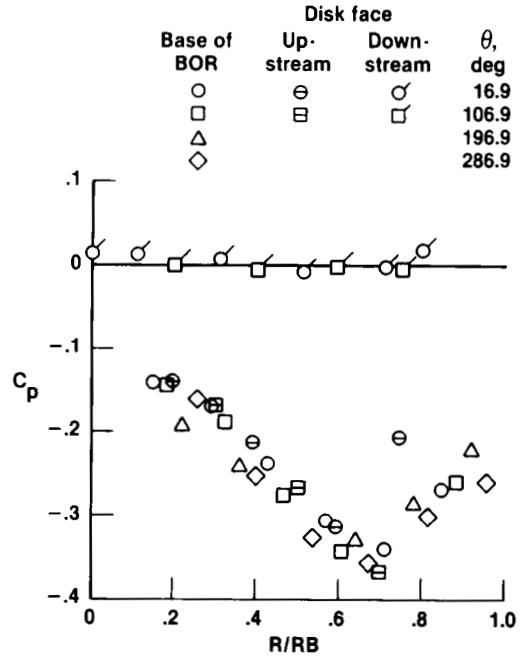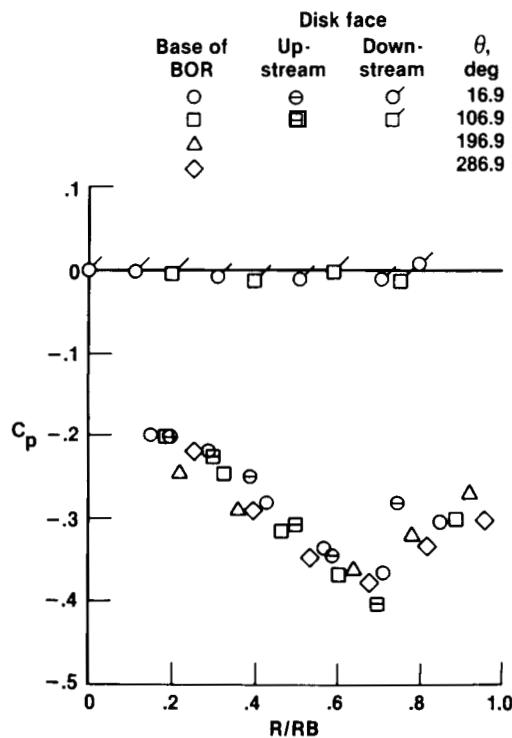
(a) Mach 0.30.

(b) Mach 0.50.

(c) Mach 0.71.

Figure 27. Pressure coefficient in base region as a function of radial distance for flight disk, x/D = 0.44, α ≈ 3°, wind-tunnel data.
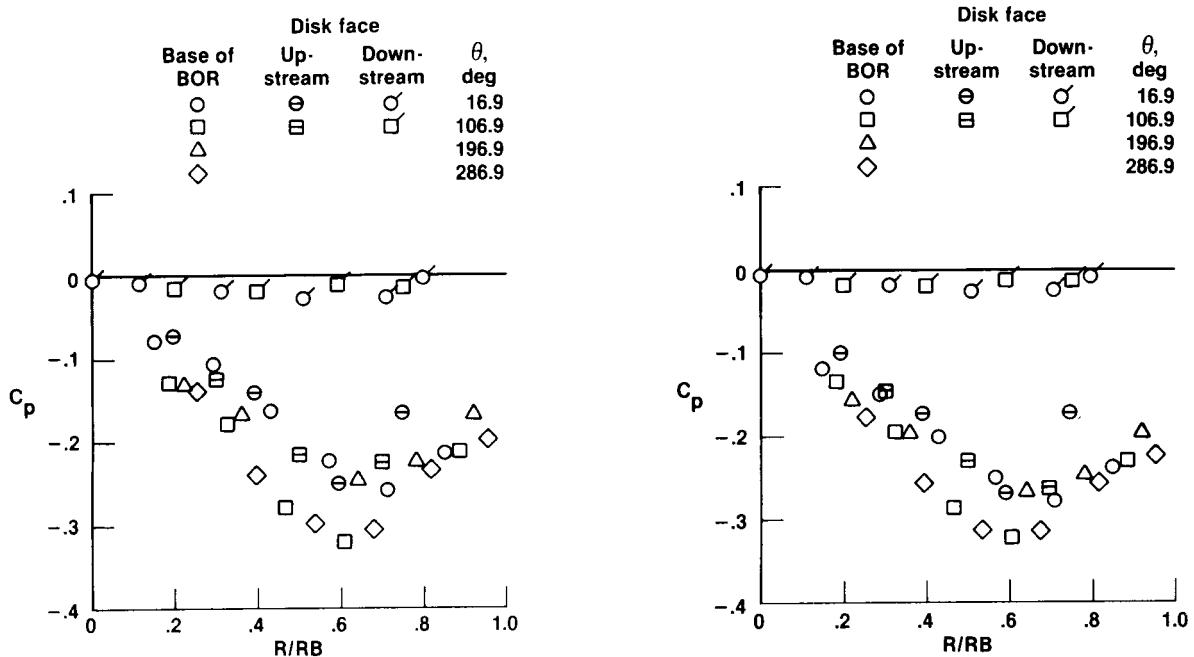
(a) Mach 0.30.
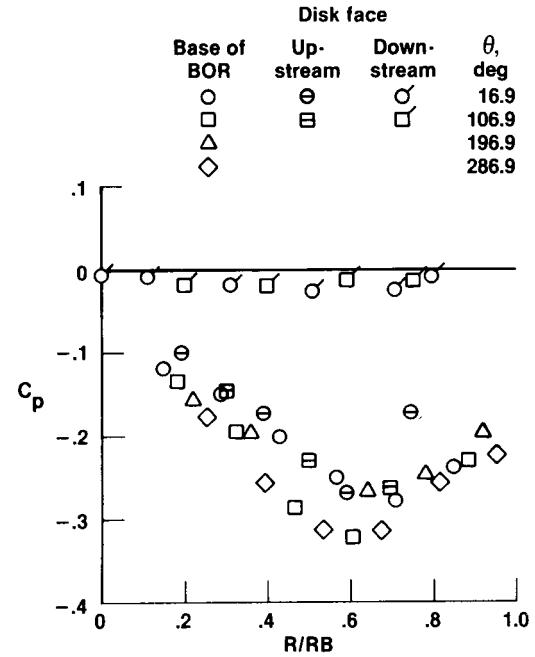
(b) Mach 0.50.
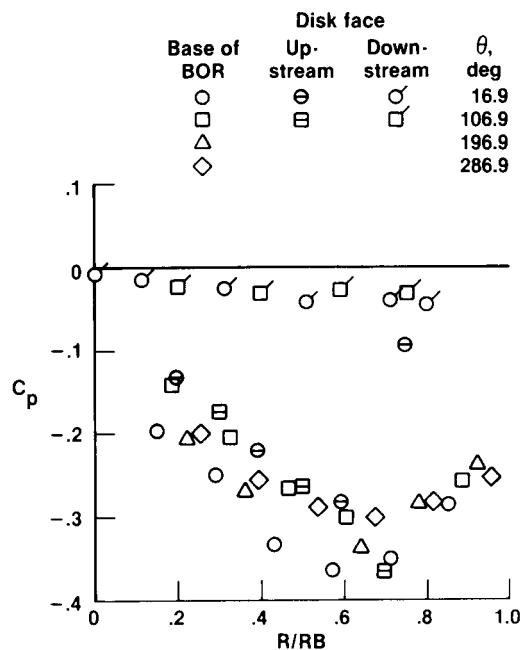
(c) Mach 0.71.

Figure 28. *Pressure coefficient in base region as a function of radial distance for flight disk, x/D = 0.50, α ≈ 3°, wind-tunnel data.*
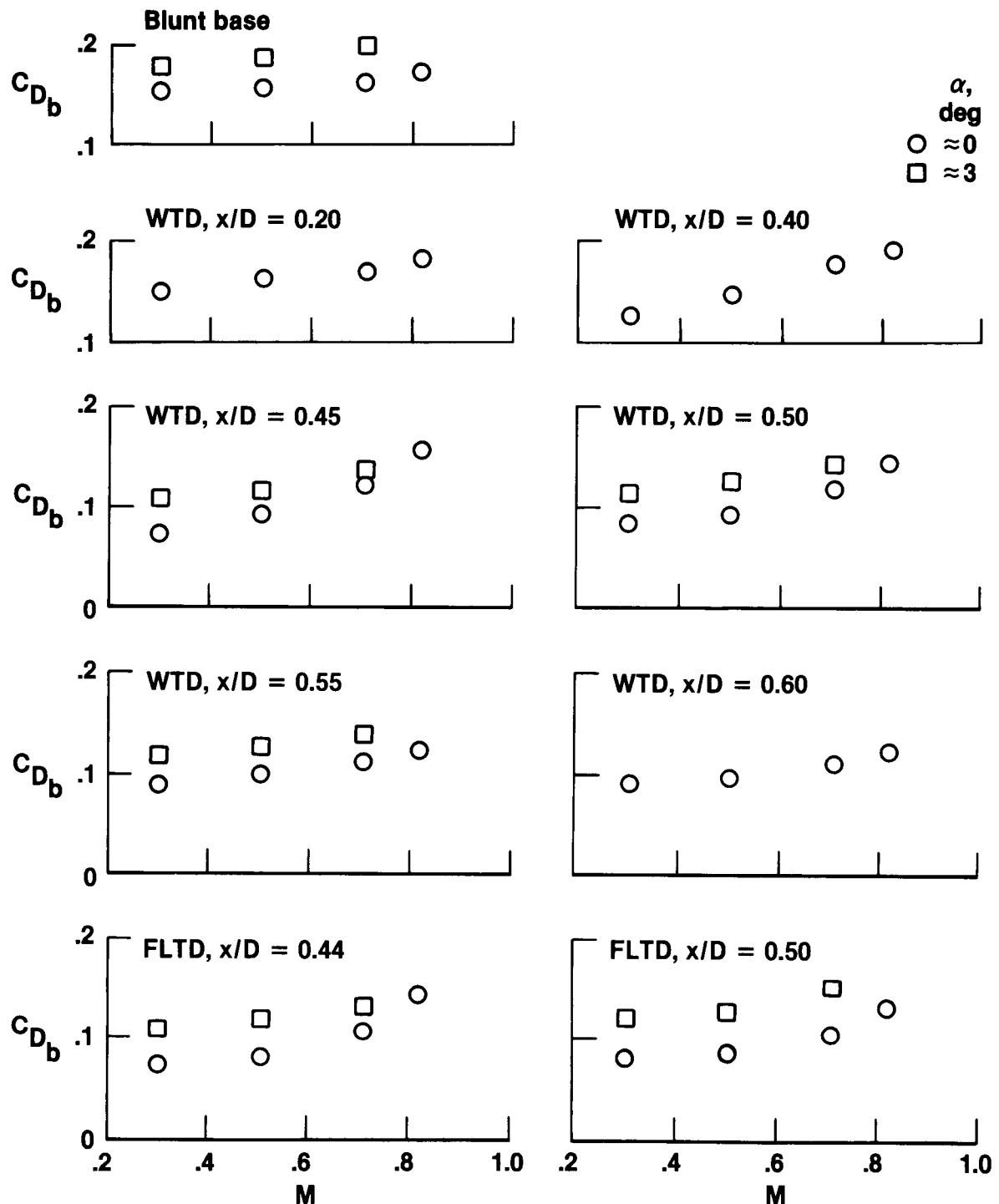
(a)   Base drag coefficient from pressure data.

Figure 29.   Drag coefficient as a function of Mach number, wind-tunnel data.
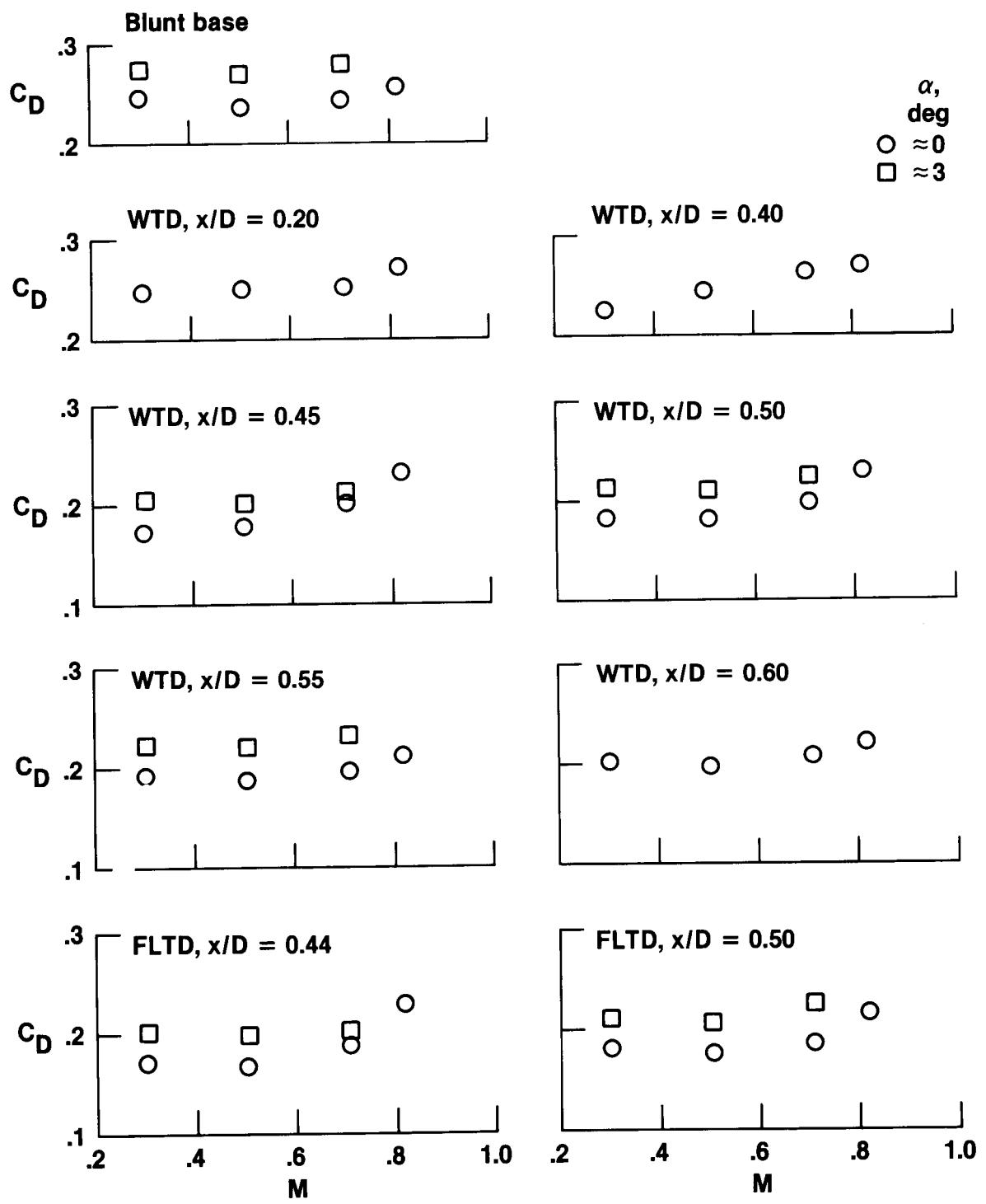
(b) *Total drag coefficient from force data.*

Figure 29. *Concluded.*
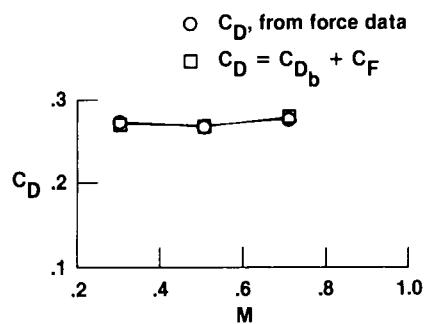
(a) *Blunt base,* α ≈ *3°.*
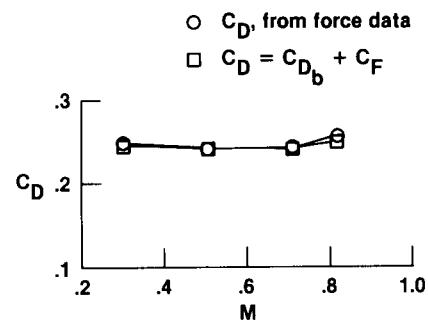
(b) *Blunt base,* α ≈ *0°.*
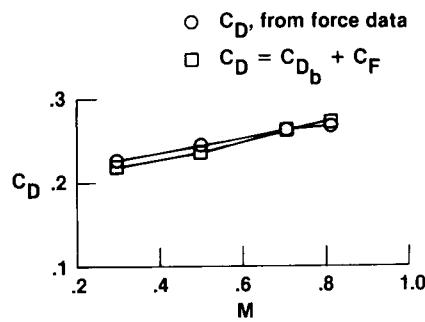
(c) *Wind-tunnel disk,*
x/D = 0.40, α ≈ *0°.*
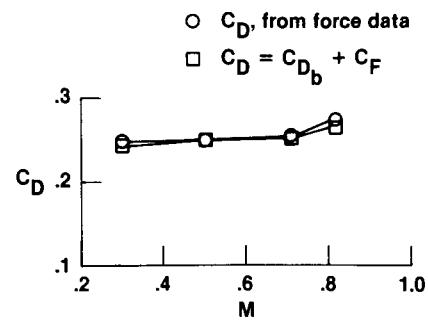
(d) *Wind-tunnel disk,*
x/D = 0.20, α ≈ *0°.*
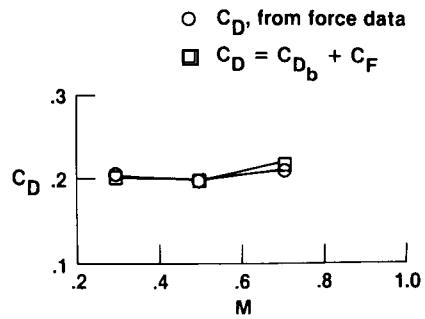
(e) *Wind-tunnel disk,*
x/D = 0.45, α ≈ *3°.*
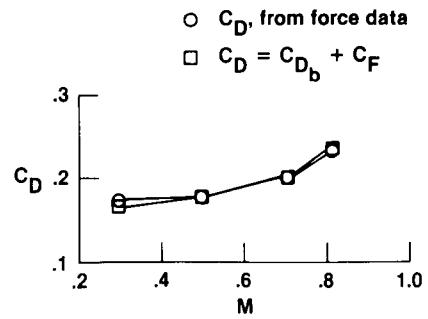
(f) *Wind-tunnel disk,*
x/D = 0.45, α ≈ *0°.*

Figure 30. Comparison of total drag coefficient with sum of base drag coefficient and predicted skin friction drag coefficient, wind-tunnel data.
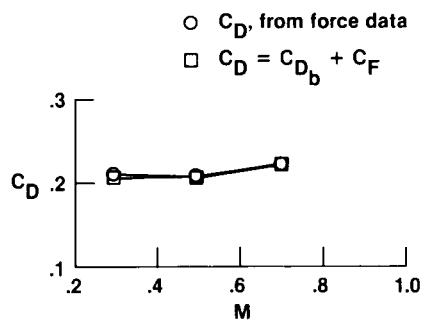
(g) Wind-tunnel disk,
x/D = 0.50, α ≈ 3°.
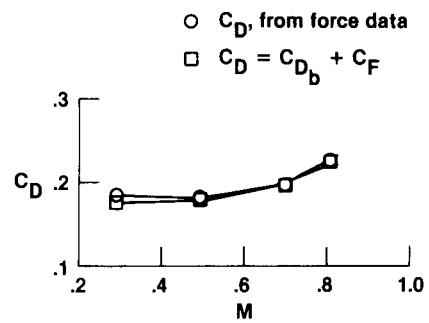
(h) Wind-tunnel disk,
x/D = 0.50, α ≈ 0°.
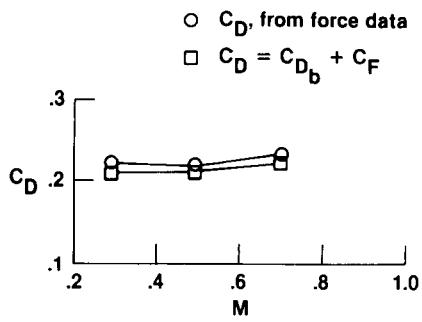
(i) Wind-tunnel disk,
x/D = 0.55, α ≈ 3°.
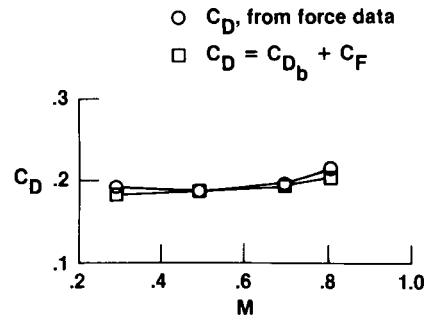
(j) Wind-tunnel disk,
x/D = 0.55, α ≈ 0°.
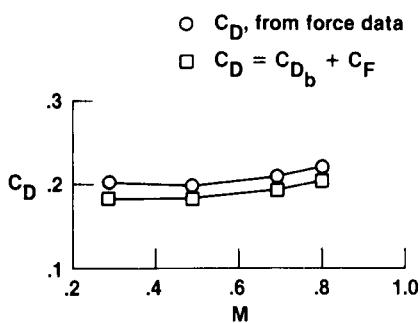
(k) Flight disk, x/D =
0.60, α ≈ 0°.
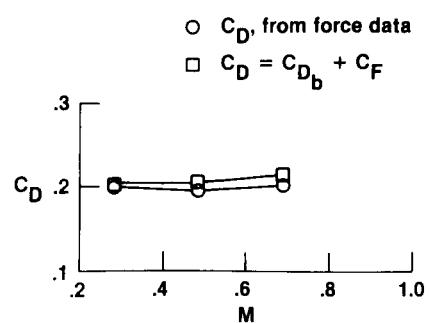
(l) Flight disk, x/D =
0.44, α ≈ 3°.

Figure 30. Continued.

○ C_D, from force data

□ $C_D = C_{D_b} + C_F$

.3

C_D .2

.1

.2 .4 .6 .8 1.0

M

(m) Flight disk, x/D = 0.44, α ≈ 0°.

○ C_D, from force data

□ $C_D = C_{D_b} + C_F$

.3

C_D .2

.1

.2 .4 .6 .8 1.0

M

(n) Flight disk, x/D = 0.50, α ≈ 3°.

○ C_D, from force data

□ $C_D = C_{D_b} + C_F$

.3

C_D .2

.1

.2 .4 .6 .8 1.0

M
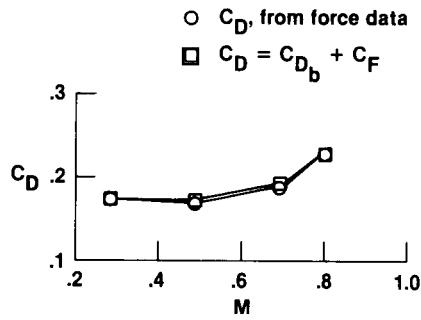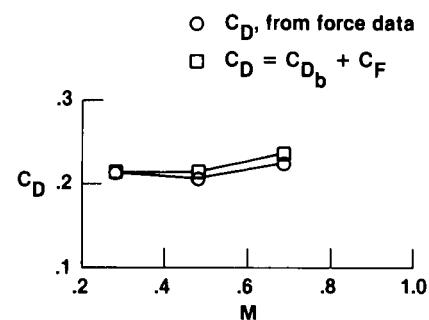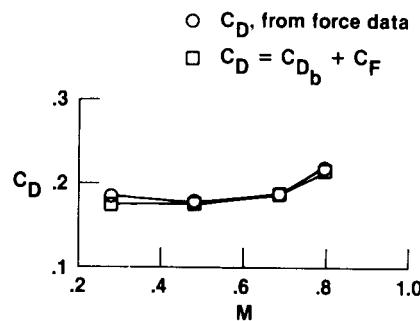
(o) Flight disk, x/D = 0.50, α ≈ 0°.

Figure 30. Concluded.
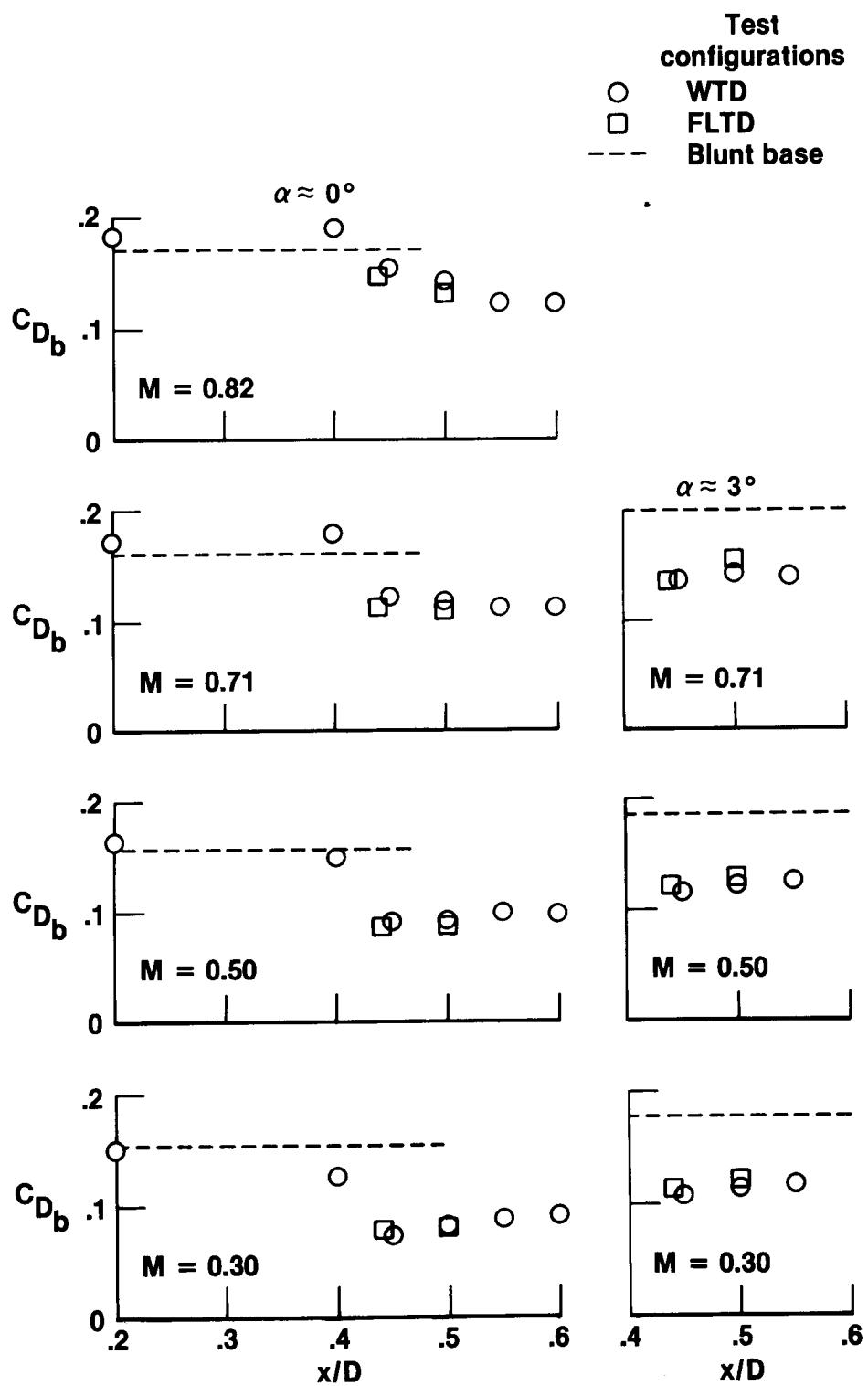
(a) Base drag coefficient from pressure data.

Figure 31. Drag coefficient as a function of x/D, wind-tunnel data.
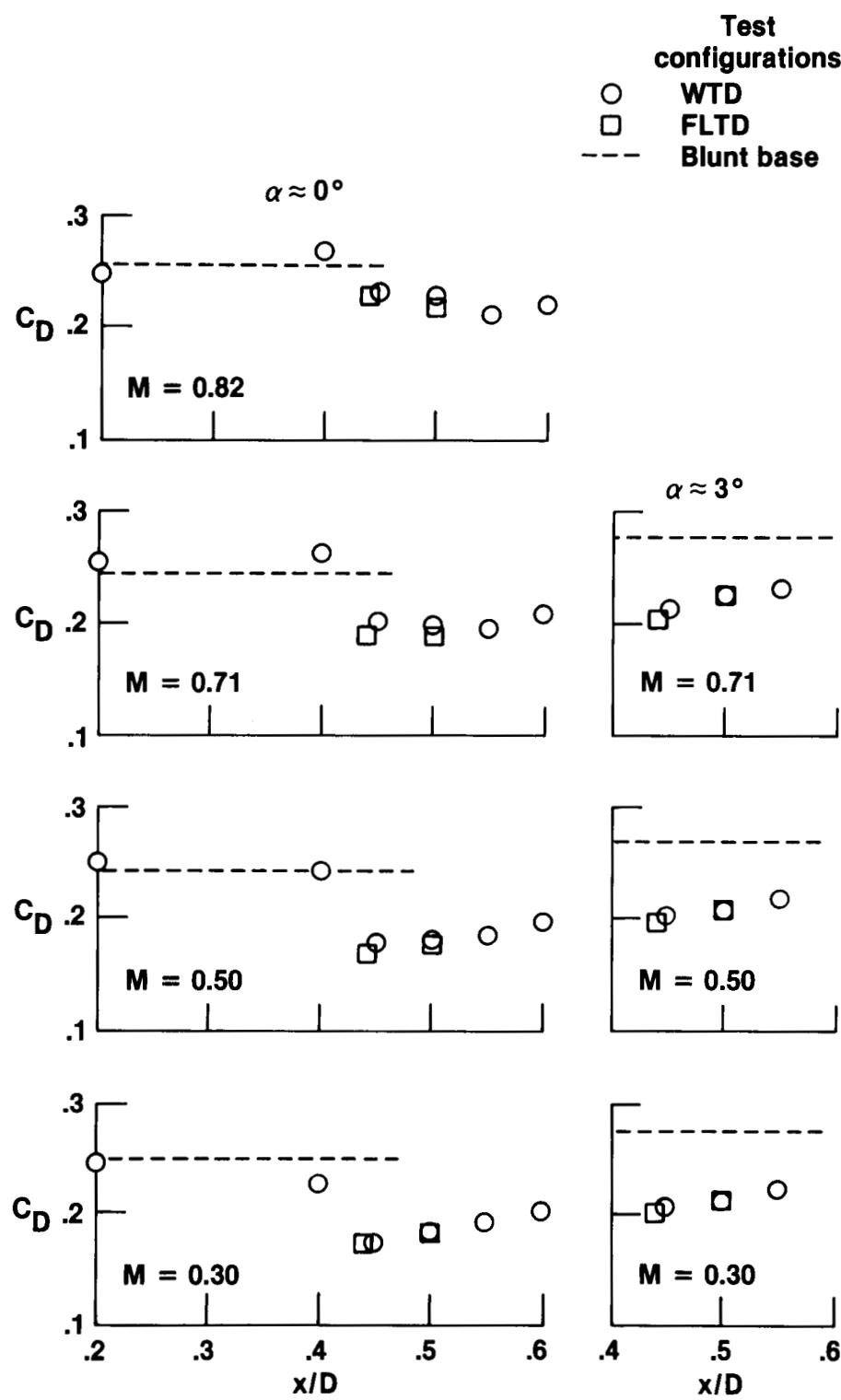
(b) Total drag coefficient from force data.

Figure 31. Concluded.

$$\Delta C_{D_b} = \left(C_{D_b}\right)_{\text{Trailing disk}} - \left(C_{D_b}\right)_{\text{Blunt}}$$
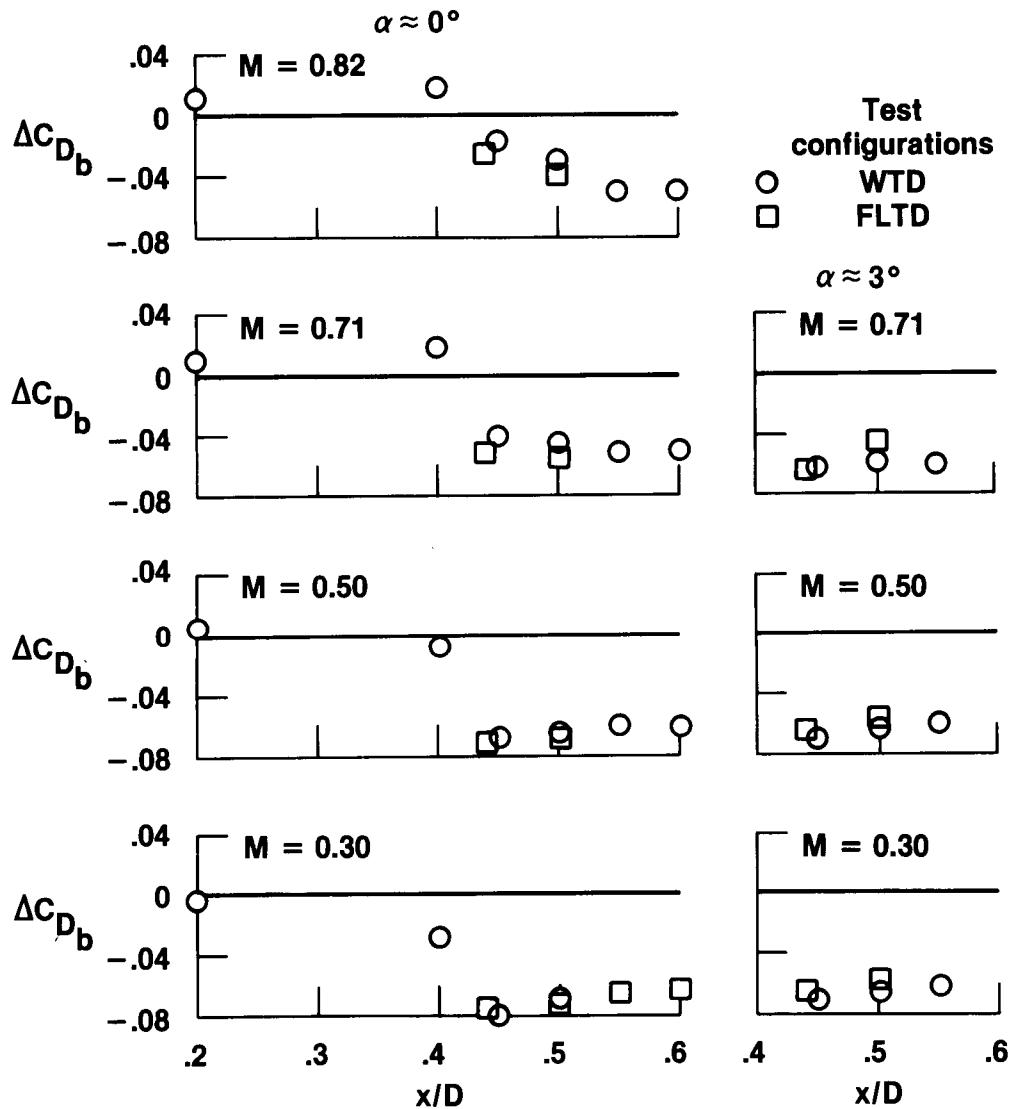
(a) Increment in base drag coefficient. (Negative means base drag was less than blunt base drag.)

Figure 32. Drag coefficient increment between given trailing disk configuration and blunt base as a function of x/D, wind-tunnel data.

$$\Delta c_D = \left(c_D\right)_{\text{Trailing disk}} - \left(c_D\right)_{\text{Blunt}}$$

$\alpha \approx 0°$

M = 0.82

M = 0.71

$\alpha \approx 3°$

M = 0.71

M = 0.50

M = 0.50

M = 0.30

M = 0.30

Test configuration

○   WTD
□   FLTD

x/D

x/D
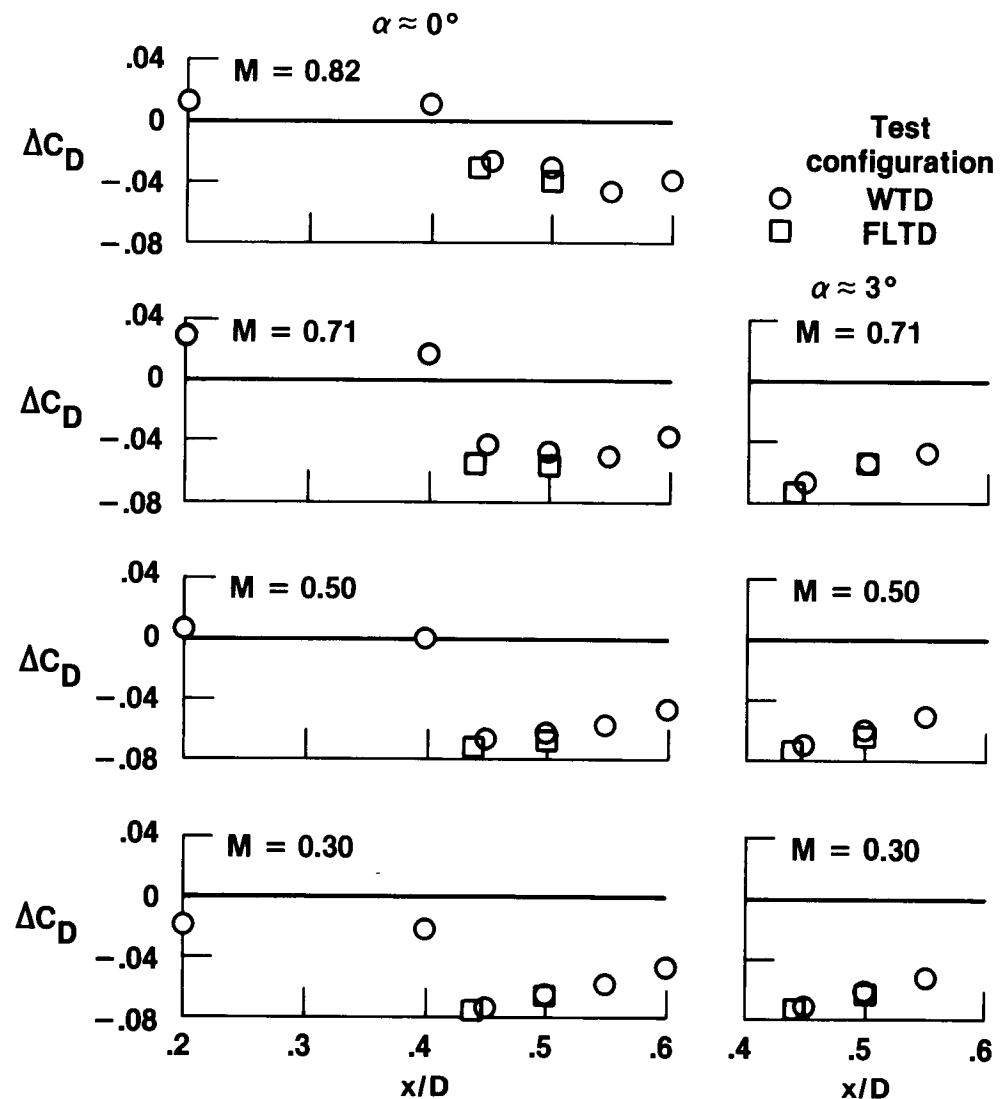
(b)   Increment in total drag coefficient. (Negative means BOR with trailing disk had less total drag than BOR with blunt base.)

Figure 32. Concluded.

129
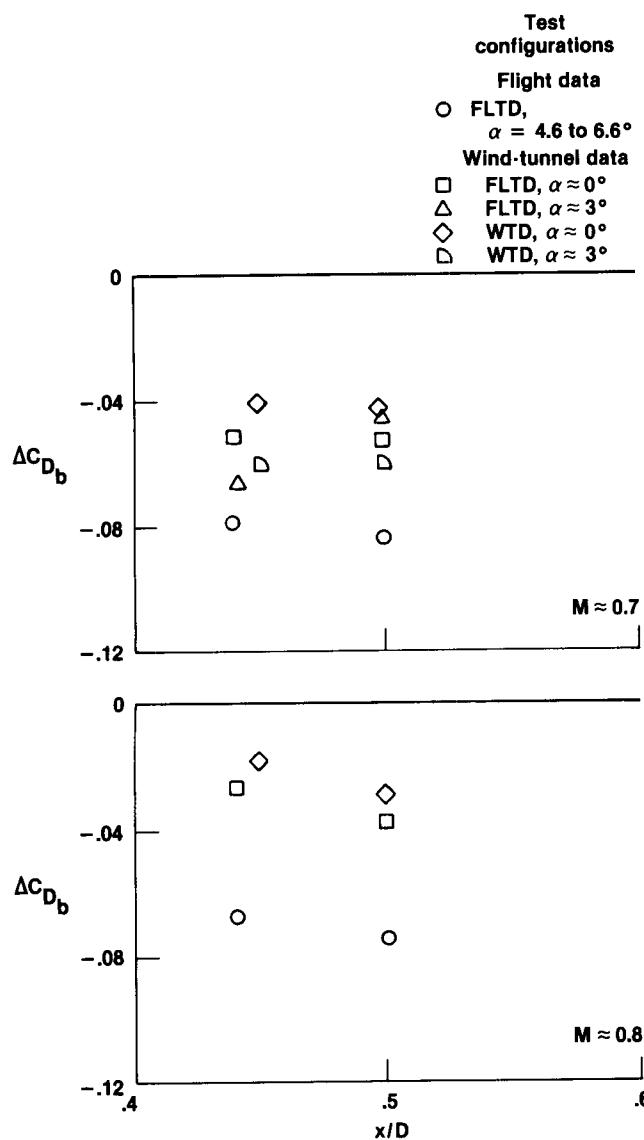
(a) Increment in base drag coefficient as a function of x/D.
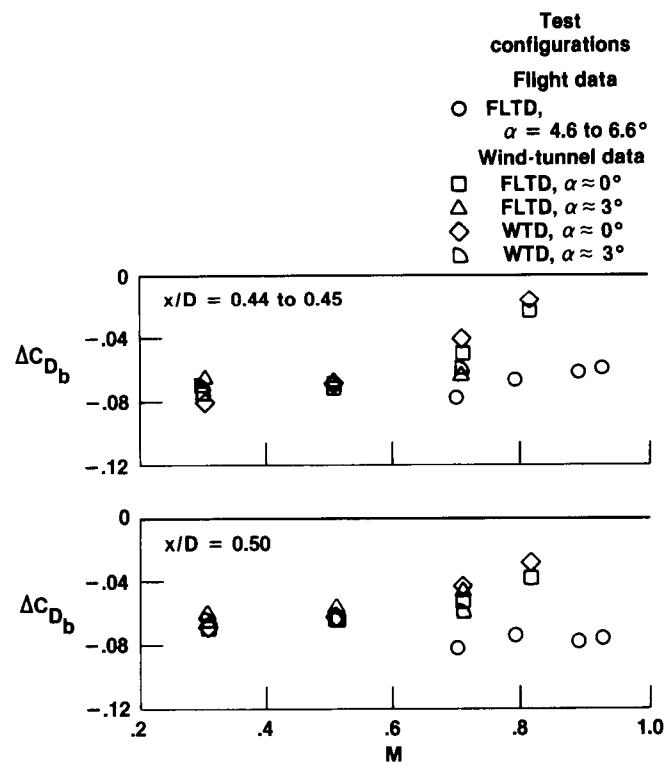
(b) Increment in base drag coefficient as a function of Mach number.

Figure 33. Comparison of data from present study, x/D = 0.44 to 0.50. (Flight data α is aircraft angle of attack.)

$$\Delta[\ ] = ([\ ])_{\text{Trailing disk}} - ([\ ])_{\text{Blunt}}$$

Test configurations

Present studies	Previous studies

Flight data,
L/D = 10.9

○ FLTD, α = 4.6 to 6.6

Wind-tunnel data, L/D = 10.9	Wind-tunnel data, $\alpha = 0°$
□ FLTD, $\alpha \approx 0°$	△ Ref. 7, L/D = 6.0
◻ FLTD, $\alpha \approx 3°$	◺ Ref. 7, L/D = 10.0
◇ WTD, $\alpha \approx 0°$	◹ Ref. 8, L/D = 11.3
◈ WTD, $\alpha \approx 3°$	◺ Ref. 9
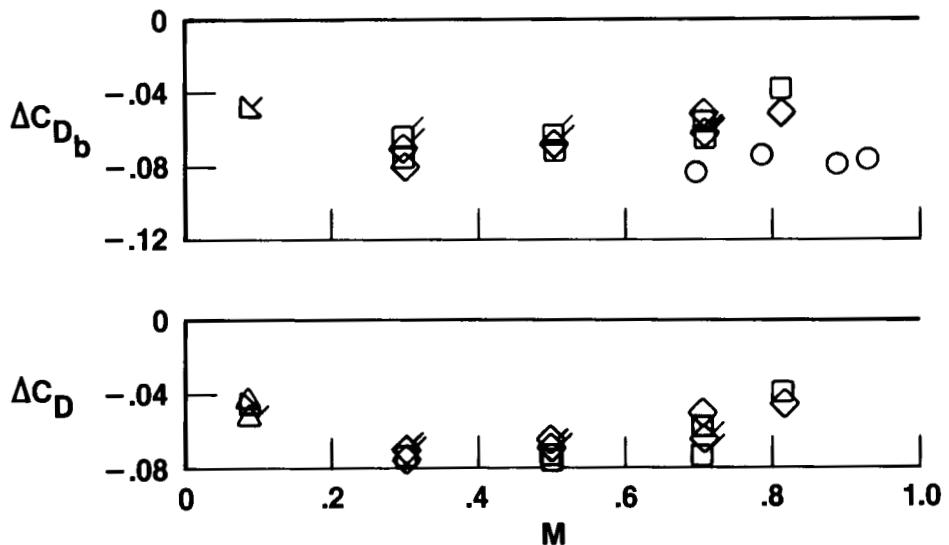
Figure 34. Comparison of maximum drag coefficient reduction for flight and wind-tunnel data of present study and previous wind-tunnel studies. (Flight data α is aircraft angle of attack.)
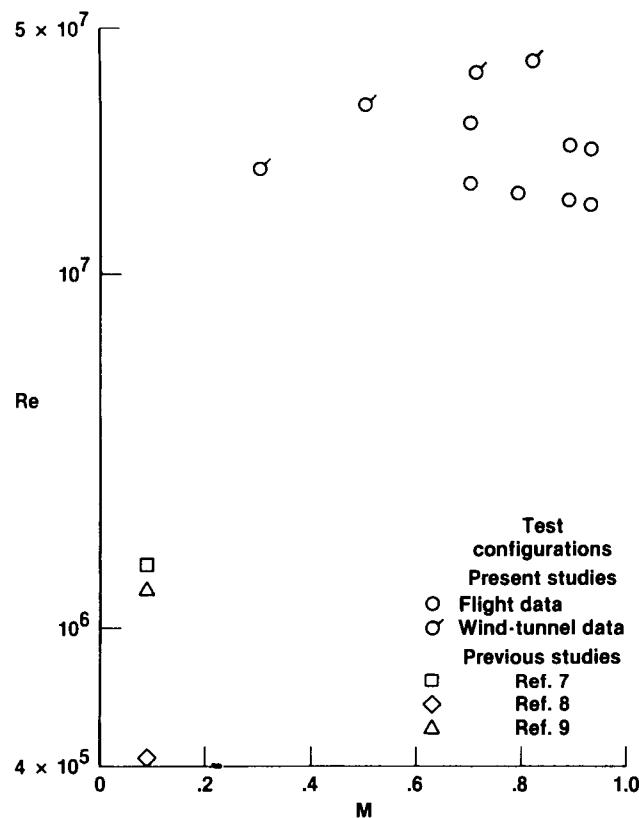
Figure 35. *Reynolds number as a function of Mach number for present flight and wind-tunnel study and previous wind-tunnel studies.*
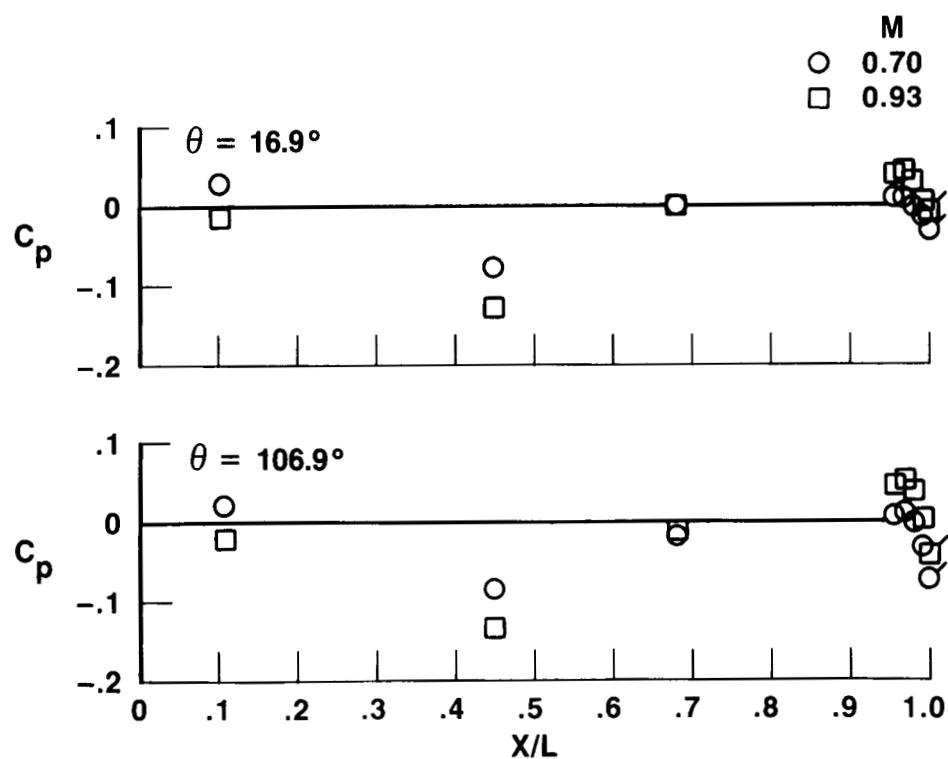
(a) Subsonic data.

Figure 36. Surface pressure coefficient as a function of body length for blunt base configuration, flight data. (Flagged symbols denote base surface data.)
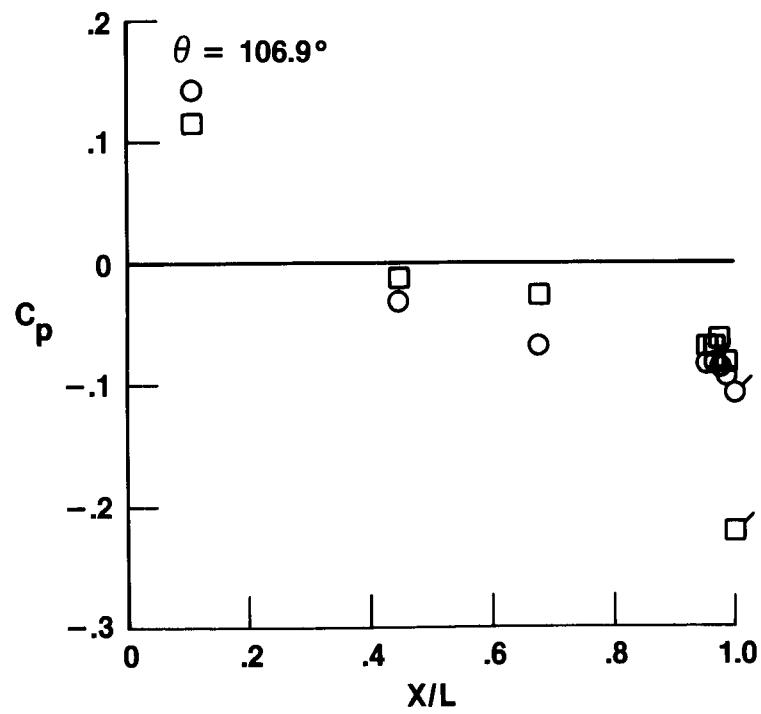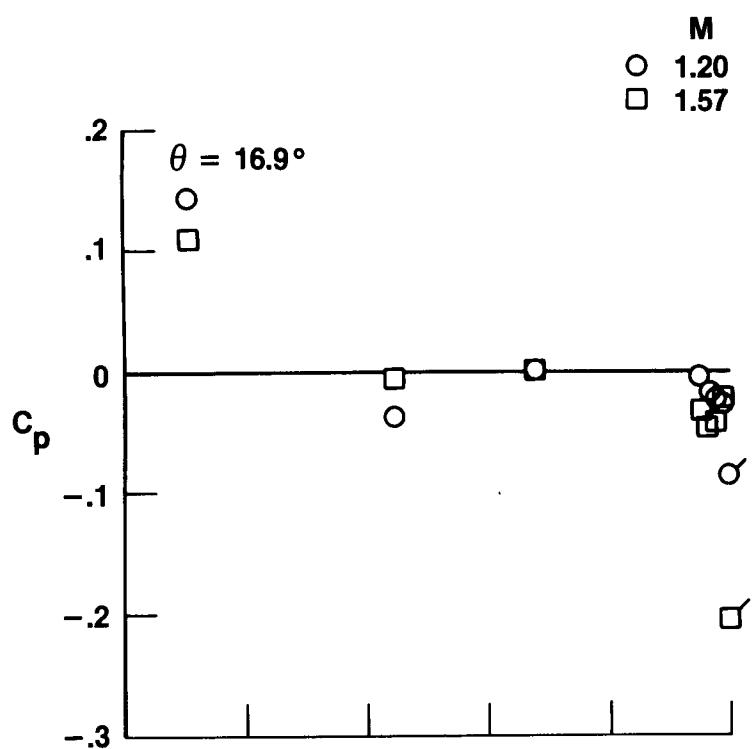
(b) Supersonic data.

Figure 36. Concluded.
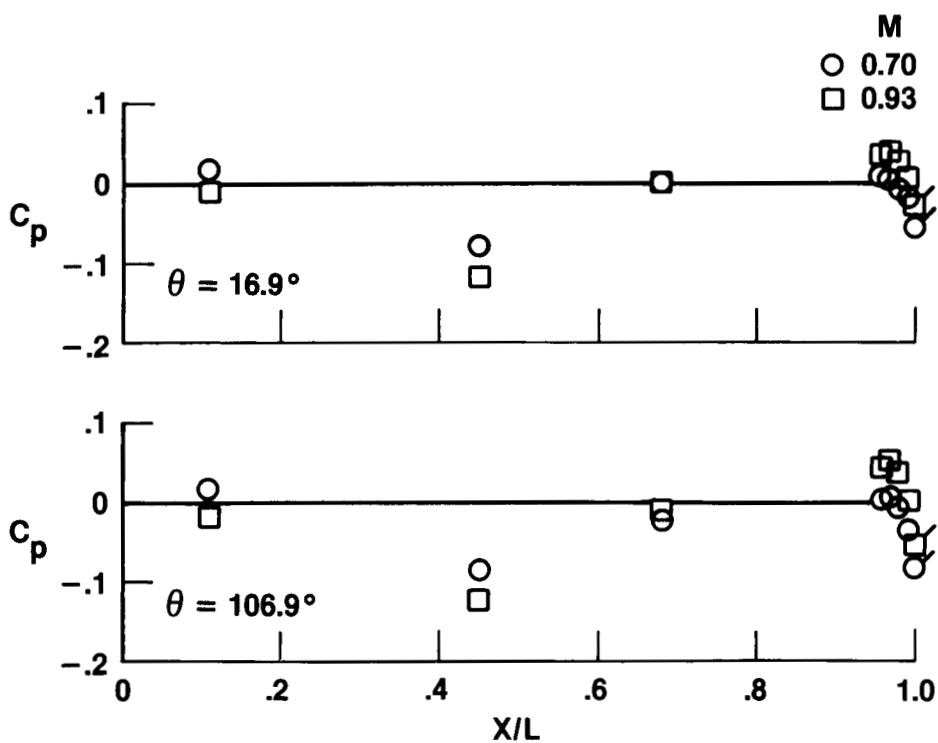
(a) Subsonic data.
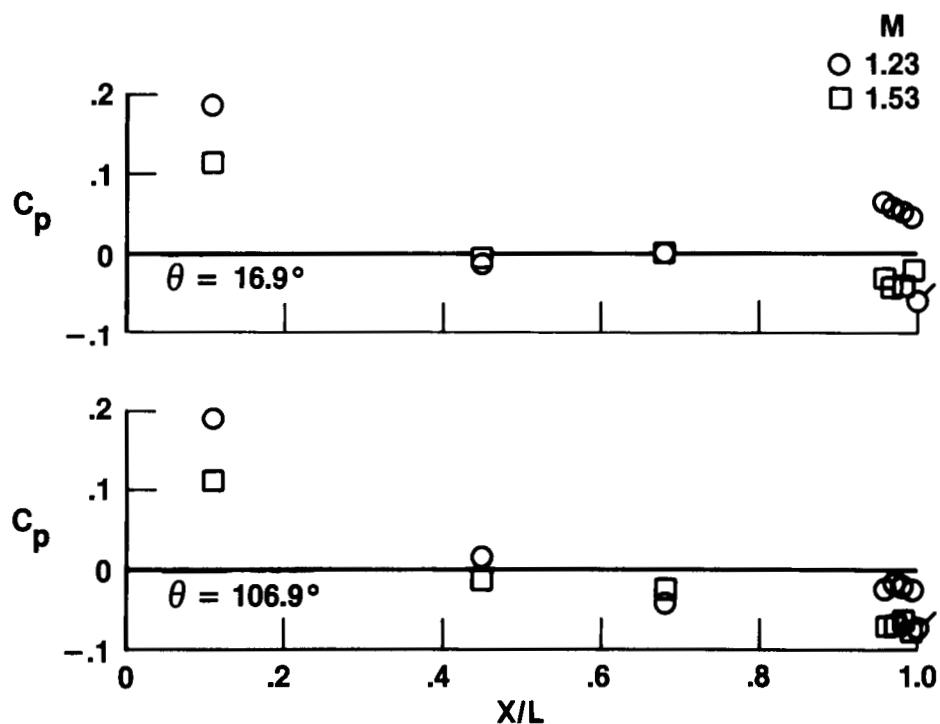
(b) Supersonic data.

Figure 37. Surface pressure coefficient as a function of body length for hemispherical configuration, flight data. (Flagged symbols denote base surface data.)
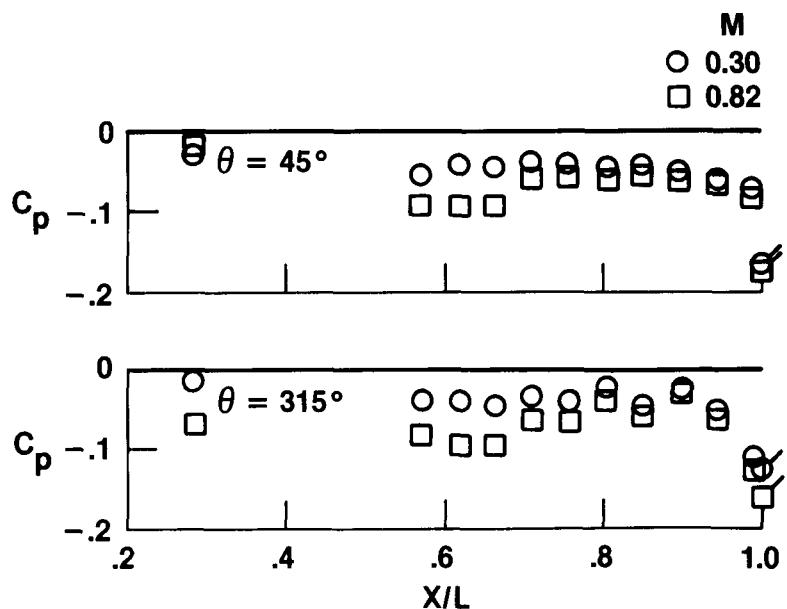
(a) C_p as a function of X/L.
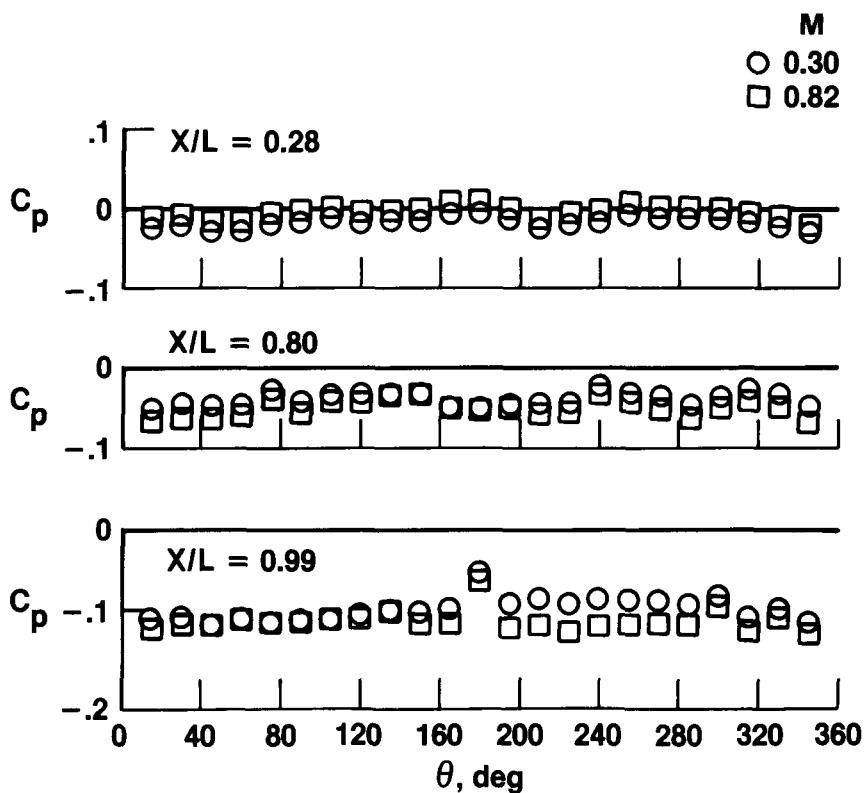
(b) C_p as a function of θ.

Figure 38. Surface pressure coefficient as a function of body length or angular location for blunt base configuration, $\alpha \approx 0°$, wind-tunnel data. (Flagged symbols are on base surface data.)
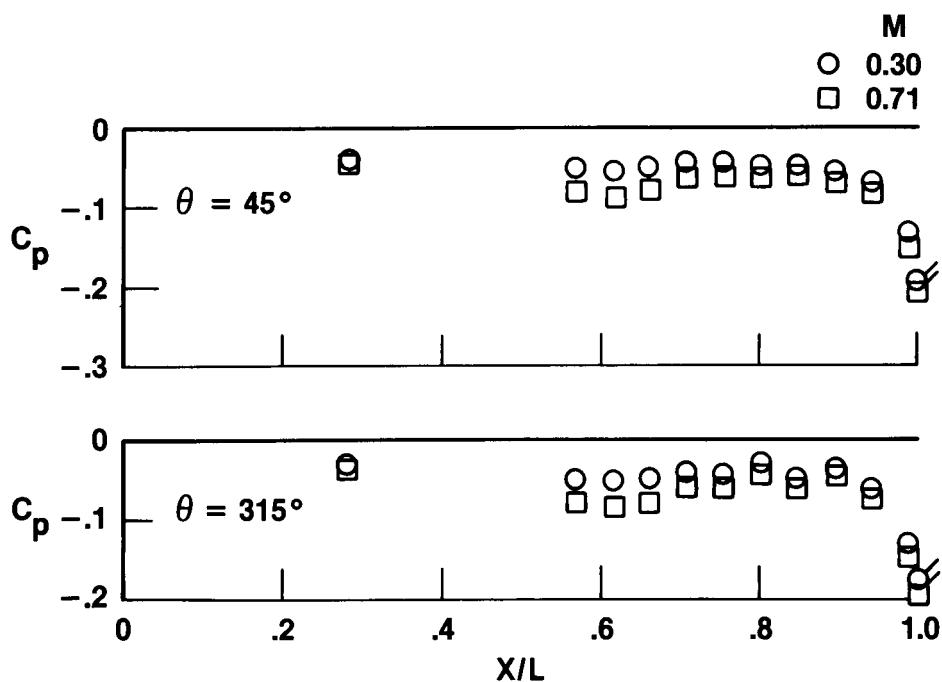
(a) C_p as a function of X/L.
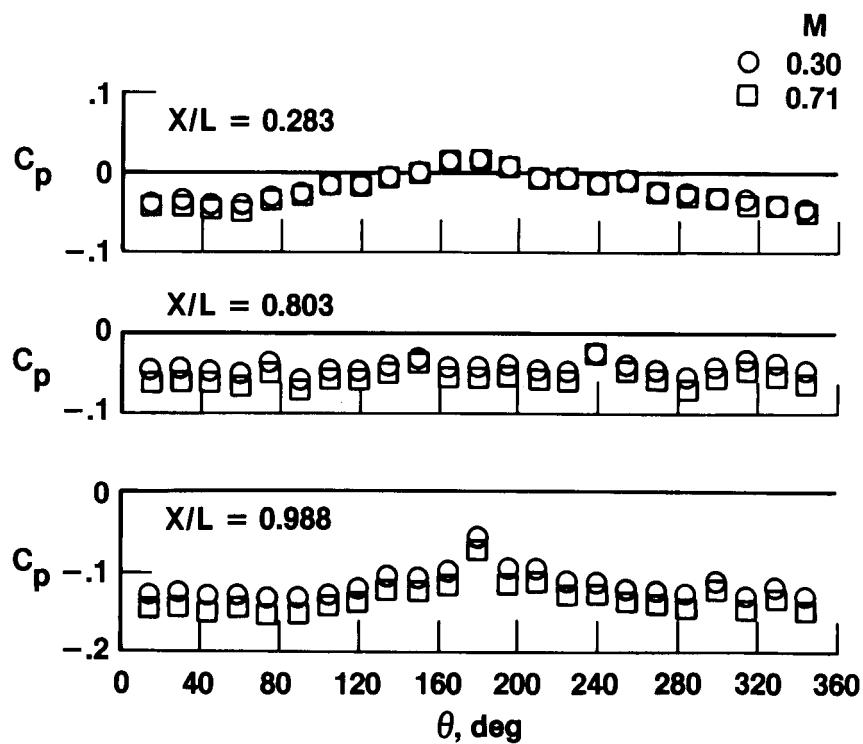
(b) C_p as a function of θ .

Figure 39. Surface pressure coefficient as a function of body length or angular location for blunt base configuration, $\alpha \approx 3°$, wind-tunnel data. (Flagged symbols denote base surface data.)

$$\Delta C_p = \left(C_{p_{\text{trailing disk}}} - C_{p_{\text{blunt}}}\right)_{X/L \,=\, .988,\ \theta \,=\, 315°}$$

(a) $\alpha \approx 0°$.
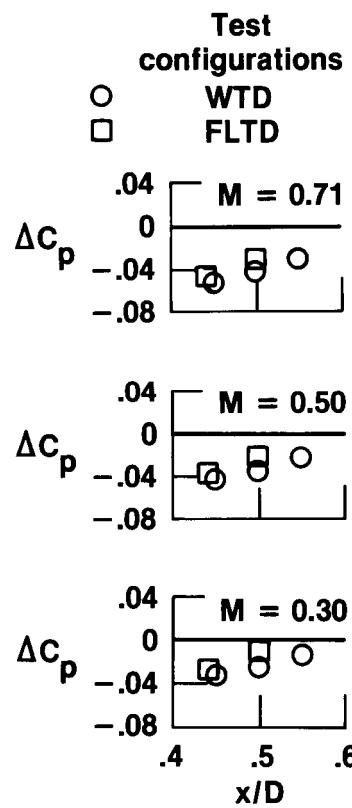
(b) $\alpha \approx 3°$.

Figure 40. Increment in surface pressure coefficients for disk configurations from blunt configuration as a function of x/D for X/L = 0.99, wind-tunnel data. (Negative means surface pressure coefficient with disk was more negative than for blunt base.)

138
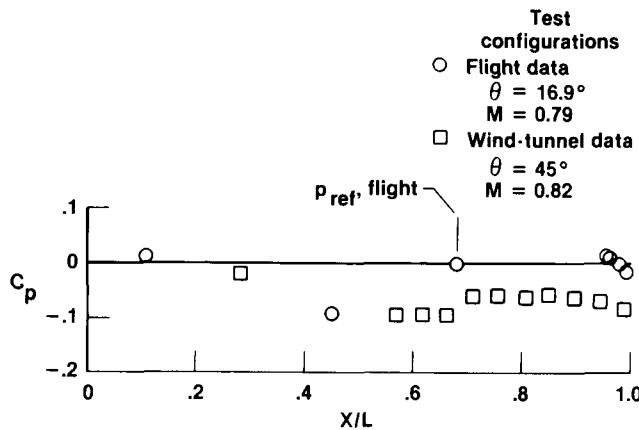
Figure 41. Comparison of surface pressure coefficients for flight and wind-tunnel data of present study as a function of body length.
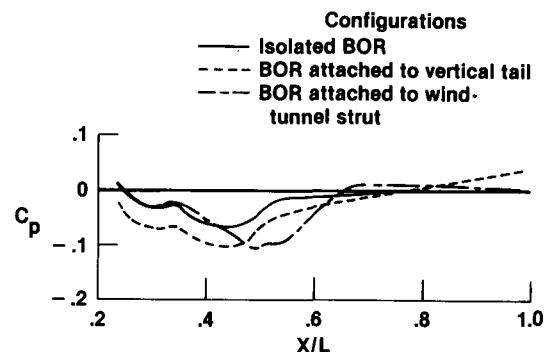
*Figure 42. Comparison of surface pressure coefficients calculated from Woodward-Carmichael method (ref. 10) for Mach 0.82, $\alpha = 0°$, and $\theta \approx 45°$.*
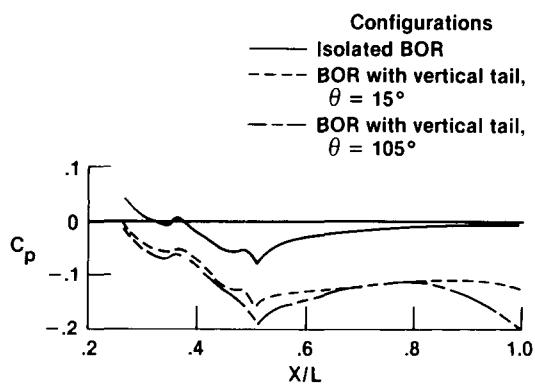
(a) Mach 1.20.
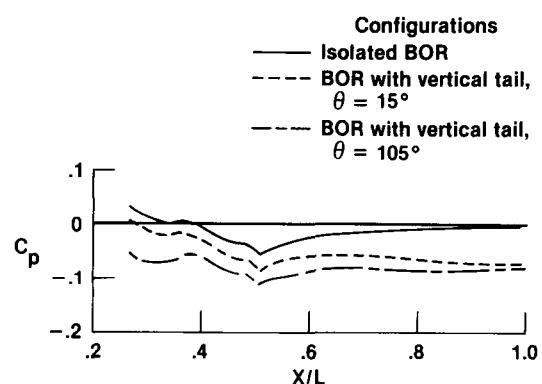
(b) Mach 1.53.

Figure 43. Comparison of surface pressure coefficients calculated from Woodward-Carmichael method (ref. 10) for supersonic Mach numbers, $\alpha = 0°$.

1. Report No. NASA TP-2638	2. Government Accession No.	3. Recipient's Catalog No.
4. Title and Subtitle Flight and Wind-Tunnel Measurements Showing Base Drag Reduction Provided by a Trailing Disk for High Reynolds Number Turbulent Flow for Subsonic and Transonic Mach Numbers		5. Report Date November 1986
		6. Performing Organization Code
7. Author(s) Sheryll Goecke Powers, Jarrett K. Huffman, and Charles H. Fox, Jr.		8. Performing Organization Report No. H-1281
9. Performing Organization Name and Address Dryden Flight Research Facility P.O. Box 273 Edwards, CA 93523-5000		10. Work Unit No. RTOP 505-31-21
		11. Contract or Grant No.
12. Sponsoring Agency Name and Address National Aeronautics and Space Administration Washington, D.C. 20546		13. Type of Report and Period Covered Technical Paper
		14. Sponsoring Agency Code

15. Supplementary Notes

Sheryll Goecke Powers is affiliated with Ames-Dryden Flight Research Facility.
Jarrett K. Huffman and Charles H. Fox, Jr., are affiliated with Langley Research Center.

16. Abstract

   The effectiveness of a trailing disk, or trapped vortex concept, in reducing the base drag of a large body of revolution, about 20-cm (8-in) diameter, was studied from measurements made both in flight and in a wind tunnel. Pressure data were obtained for the flight experiment, and both pressure and force-balance data were obtained for the wind-tunnel experiment. The flight study also included data obtained from a hemispherical base. Reynolds number, based on the length of the body of revolution, ranged from 1.5×10^7 to 2.7×10^7 for the flight data and from 1.9×10^7 to 4.1×10^7 for the wind-tunnel data. Primary Mach numbers for the flight data were from 0.70 to 0.93 with a limited amount of data obtained for Mach 1.20 to 1.60. Mach numbers for the wind-tunnel study ranged from 0.30 to 0.82.

   The present experiment demonstrated the significant base drag reduction capability of the trailing disk to Mach 0.93 and to Reynolds numbers (based on body length) up to 80 times greater than for the earlier pioneering studies performed at incompressible speeds. For the trailing disk data from the flight experiment, the maximum decrease in base drag ranged from 0.08 to 0.07 as Mach number increased from 0.70 to 0.93. Aircraft angles of attack ranged from 3.9° to 6.6° for the flight data. For the trailing disk data from the wind-tunnel experiment, the maximum decrease in base drag and total drag ranged from 0.08 to 0.05 for the approximately 0° angle-of-attack data as Mach number increased from 0.30 to 0.82. For the approximately 3° angle-of-attack data, the maximum decrease was 0.07 to 0.06 for the base drag and remained a constant 0.07 for the total drag as Mach number increased from 0.30 to 0.71. For the flight data, the trailing disk caused a drag penalty near Mach 1.20, but this penalty decreased rapidly as Mach number increased to 1.40 and appeared to be eliminated as Mach number increased from 1.40 to 1.60. The hemispherical base had an almost constant drag increase of approximately 0.01 for data from Mach 0.70 to 0.93 and 1.24.

17. Key Words (Suggested by Author(s)) Base drag reduction, Blunt bodies, Bodies of revolution, Trailing disk, Trapped vortex, Turbulent flow	18. Distribution Statement Unclassified — Unlimited STAR category 34	
19. Security Classif. (of this report) Unclassified	20. Security Classif. (of this page) Unclassified	21. No. of Pages 140	22. Price* A07